Public

Report

Document ID	Version	Status	Reg no	Page
1434744	2.0	Approved		1 (131)
Author Ulf Ronneteg Thomas Grybäck			Date 2015-02-04	
Reviewed by Lisette Åkerman (QA)			Reviewed date 2015-02-26	
Approved by Jan Sarnet			Approved date 2015-02-26	

Non-destructive testing of canister components and welds

Summary

This report summarises the development, during the period of 2009-2013, of non-destructive testing (NDT) techniques for inspecting canister components and welds. The basis for the development is the experiences from the manufacturing processes, the acceptance criteria defined in the design premises (SKB 2009) and the damage tolerance analyses as presented in the canister production report (SKB 2010) and its references. The acceptance criteria have in the beginning of 2014 been further refined (SKBdoc 1414374, 1414760, 1415307).

This report describes the current phase in the development of NDT which has the long-term objective to develop the inspection techniques for production of canisters. In the current phase, close interaction with the test production is crucial to acquire inspection experiences, information about defect characteristics and information of component quality as input to the development of the manufacturing and welding processes.

A strategy for inspecting the components in different stages of the manufacturing process line is presented. Inspection practices are proposed to be conducted at a stage in which component geometry favours NDT techniques.

Three ultrasonic phased array techniques (normal incidence, angular and transmission inspection) were developed for inspection of the insert. The developmental process was conducted by practical trials in combination with sound field simulations. The developed techniques were evaluated by probability of detection (POD) calculations for artificial defects and by metallographic and computed tomography inspection of indicated defects. The results generally showed high inspection sensitivity. Full-size inserts were inspected by the developed ultrasonic techniques, and the results were used as input to the development of the manufacturing processes.

Several techniques (for example eddy current and magnetic particle inspection) for inspection of insert surfaces were tested, and the results show that the techniques can be applied for inspection of inserts.

For inspection of copper tubes and lids, the phased array ultrasonic techniques were further developed to achieve a higher and more uniform sensitivity and to make the techniques more robust to variations in grain size. The techniques were used for inspection of several full-size copper tubes and copper lids. The pre-machined lid design was modified to facilitate ultrasonic inspection. In addition to being inspected by ultrasonic techniques, the copper lids were inspected by penetrant testing, which indicated that forging laps occurred in several lids.

Three inspection techniques were developed for inspection of friction stir welds: phased array ultrasonics, digital X-ray and eddy current testing. NDT reliability is introduced as an important tool

Svensk Kärnbränslehantering AB
Swedish Nuclear Fuel and Waste Management Co
PO Box 925, SE-572 29 Oskarshamn
Visiting address Gröndalsgatan 15
Phone +46-491-76 79 00 Fax +46-491-76 79 30
www.skb.se
556175-2014 Seat Stockholm

in developing NDT techniques. The probability of detection for several of the inspection techniques was calculated. For more complex cases, a multi-parameter POD methodology was developed and applied, for example, to calculate POD curves for the ultrasonic inspection of copper tube materials with different levels of ultrasonic attenuation. In addition, human factor perspectives are also introduced into the mechanised inspection process.

A preliminary qualification process that considered the method applied for in-service inspection in the nuclear industry, when applicable, was developed. Because the acceptance criteria and their application differ for the case of in-service inspection, a slightly different approach is proposed.

The developed and/or tested inspection techniques were evaluated based on the extent to which the acceptance criteria for NDT could be assessed to be fulfilled, and some shortcomings in the acceptance criteria were identified.

Sammanfattning

Denna rapport sammanfattar utvecklingen av oförstörande provning (OFP) utförd under perioden 2009-2013 av kapselkomponenter och svetsar. Utvecklingen har baserats på erfarenheter från tillverkningsprocesserna, kunskap om defekter samt de acceptanskriterier (definierade utifrån skadetålighetsanalyser) och OFP-tekniker som presenteras i produktionsrapporten med referenser för kapseln (SKB 2010). Acceptanskriterierna har reviderats i början av 2014 (SKBdoc 1414374, 1414760, 1415307).

Rapporten redovisar nuvarande status avseende utveckling av OFP som har det långsiktiga målet att utveckla inspektionsteknik för produktion av kapslar. I nuvarande skede har växelverkan med provtillverkningen en avgörande betydelse för att bygga upp erfarenheter, erhålla information om defekters karakteristik samt återmata information om komponenternas kvalitet för vidare utveckling av tillverknings- och svetsprocesserna.

En strategi för provning av komponenterna i olika stadier av tillverkningsprocessen presenteras. Det föreslås att provningarna lämpligen utförs i ett skede när komponenternas geometri är gynnsam ur ett provningsperspektiv.

Tre phased array ultraljudtekniker (normalt infall, vinklat infall och transmissionsprovning) har utvecklats för provning av insatsen. Utvecklingen har genomförts genom praktiska försök i kombination med ljudfältssimuleringar. Utvärdering av de utvecklade teknikerna, med POD-beräkningar (Probability of Detection) på artificiella defekter, metallografiska och datortomografiinspektioner av defekter, har generellt visat på en hög känslighet. Fullstora insatser har provats med de utvecklade ultraljudsteknikerna och resultaten har återmatats till tillverkningsprocessen.

Flera tekniker (t ex virvelström och magnetpulverprovning) har testats och visat sig lämpliga för provning av insatsens yta.

För provning av kopparrör och lock har phased array ultraljudtekniken utvecklats ytterligare för att nå en högre och jämnare känslighet och för att bättre tolerera kornstorleksvariationer. Tekniken har använts för provning av flera fullstora kopparrör och kopparlock. Designen av ”pre-machined”-utförandet av lock har modifierats för att underlätta ultraljudprovningen. Förutom ultraljudprovning har kopparlock även provats med penetrantprovning som indikerat förekomst av smidesveck i flera lock.

För provning av friktionsomrörningssvetsen har tre provningstekniker utvecklats, ultraljud phased array, digital röntgen och virvelströmsteknik.

Tillförlitlighet hos OFP har införts som ett viktigt verktyg vid utvecklingen av OFP-tekniken. Sannolikheten för detektering (POD) har beräknats för flera av inspektionsteknikerna. För mer komplicerade fall har en multi-parameter POD metodik utvecklats som till exempel har tillämpats för beräkning av POD-kurvor för ultraljudprovning av kopparrörmaterial med olika grad av ultraljuddämpning. Dessutom har inverkan av den mänskliga faktorn i samband med mekaniserad provning studerats.

En preliminär kvalificeringsprocess har definierats. Processen beaktar den metodik som tillämpas för återkommande provning inom kärnkraftsindustrin när så är tillämpligt. Men då provningskrav och dess tillämpning skiljer sig från fallet för återkommande provning, är delvis en annan metodik föreslagen.

De utvecklade och/eller utprovade provningsteknikerna har utvärderats i vilken utsträckning OFP kraven kan anses vara uppfyllda och dessutom har vissa brister i kraven identifierats.

Table of Contents

1 Background

SKB Canister Laboratory has been in operation in Oskarshamn since 1998 and has continuously worked to develop non-destructive testing (NDT) techniques for canisters. In the first years, the work was focussed on developing NDT techniques for the copper sealing welds; however, since 2005, NDT techniques for the canister components (cast iron insert, copper tube, lid and base) have also been developed.

In 2011 SKB handed in the application to build the final repository and the encapsulation plant. As part of this application, the status of the development of copper canisters was summarised in the canister production report (SKB 2010). In the report and its references, basic acceptance criteria, knowledge of the relevant manufacturing processes (including defect formation) and the inspection techniques developed up to that point were described. The canister production report was used as the basis for the development of the non-destructive testing techniques described in this report.

2 Introduction

The objective of this report is to present the status of the NDT techniques developed for inspection of canister components and welds. This report presents the current status of NDT development up to the end of 2013, and thereby, this report replaces the previous NDT report (SKBdoc 1179633).

The report is structured as follows:

- **Chapter 3** describes the canister components including an overview of the corresponding manufacturing processes and component geometries.
- **Chapter 4** presents defect specifications and acceptance criteria
- **Chapter 5** presents an inspection strategy applied throughout the canister process line.
- **Chapter 6** presents the development of the NDT techniques at the Canister Laboratory, supported by simulations and practical trials, the used NDT equipment and the inspection techniques currently used at the Canister Laboratory and at the supplier.
- **Chapter 7** presents the results and experiences obtained from the development process, from inspecting full-size components and welds and from inspections of cut-out samples. The results regarding both indications of defects and practical aspects of inspection are considered.
- **Chapter 8** presents work concerning NDT reliability, which considers both the technical reliability (detectability) and human factors associated with mechanised inspection.
- **Chapter 9** presents the qualification process of the NDT techniques throughout the entire process line.
- **Chapter 10** presents motives for the development process, a reasoning to which level the acceptance criteria are met and the identification of the limitations in the acceptance criteria.
- **Chapter 11** presents the conclusions of this work.

NDT techniques are developed with both long-term and short-term objectives. In the long term, the final techniques are developed for conducting inspections in the canister factory and in the encapsulation plant; however, the techniques are also designed to be used for inspection at the supplier. In the short term, the techniques are developed with the goal of being used for inspection of manufactured components and welds in the developmental phase of manufacturing and welding processes. At this stage of development, the latter objective is crucial to enabling the development of reliable manufacturing and welding processes as well as to increase the knowledge of defects. In support of the development of reliable manufacturing processes, a significant amount of resources was dedicated to performing full-scale inspections of manufactured components.

NDT development was conducted iteratively. In the first step some basic or well-known techniques were applied for full-scale inspections. Based on the results obtained from these inspections, either the techniques were further developed or the need for additional techniques was identified. In the next step, the new or optimised techniques were further tested, and the performance was analysed with respect to the techniques' applicability, the results achieved and the techniques' reliability. In this manner, enhanced knowledge of, for example, possible defects and general material quality, was obtained from both inspection and manufacturing point of view.

The knowledge of possible defects and the acceptance criteria for NDT are crucial for developing suitable NDT techniques. At the beginning of NDT development, the specifications for the detection of possible defects and the acceptance criteria for NDT were limited, which emphasised the need to use NDT to further understand the characteristics and occurrence of defects; therefore, focus has been placed on full-scale component inspections. The installation of welding equipment in the Canister Laboratory has allowed for the possibility of carrying out large numbers of welding trials and combined with a close collaboration with NDT, adequate knowledge of defect characteristics has been obtained. For canister components, however, the number of full-scale trials has been more limited.

Some factors have contributed to the complexity of obtaining information regarding defect characteristics:

- The input originating from the materials and manufacturing processes has been insufficient.
- The number of defect indications has been limited.
- The verification of indicated defects has not always been successful.
- In parallel with the development of NDT techniques, the casting process for manufacturing inserts has been improved. This improved quality has resulted in a limited number of relevant defect indications identified by the improved inspection techniques.

The foregoing factors, together with the iterative damage tolerance analysis of the long-term integrity of the canister, resulted in the fact that only limited acceptance criteria (section 4.1) were defined as perquisites for the NDT development. The current acceptance criteria (section 4.2) were established first after the NDT development efforts described in this report were completed. In other words, the development of the NDT techniques was primarily conducted to satisfy the short-term objective of supporting the development of manufacturing processes as well as increasing the knowledge of the properties of the components.

Inspection with regards to handling defects, like indentations and cold work, of the copper shell is covered by a separate project (SKB 2013) and therefore not covered by this report.

3 Canister

In this chapter, an overview of the canister according to the reference design (SKB 2010) is provided. The canister consists of a load-bearing insert made of nodular cast iron and a tight copper corrosion barrier, as shown in Figure 3-1. The main canister components (insert, copper tube, copper lid and base) are machined in two steps, the “pre-machined” step for volumetric NDT and the “machined” step in which the final dimensions for surface inspection are achieved.

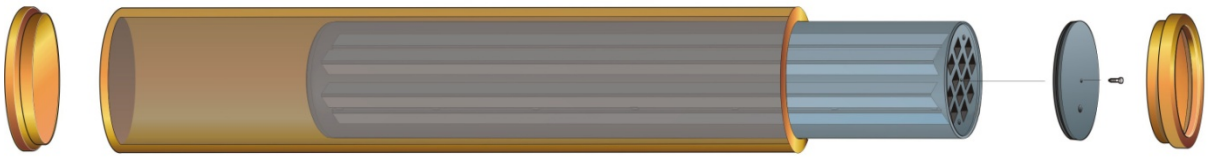

Figure 3-1. *SKB reference canister with an outer corrosion barrier made of copper and an insert made of nodular cast iron.*

3.1 Insert

In this section, an overview of the insert is described; a more detailed description is found in SKBdoc 1432361.

The insert comprises two different designs, one for 12 boiling water reactor (BWR) fuel assemblies and one for four pressure water reactor (PWR) fuel assemblies. Figure 3-2 shows the differences between the two. The insert is manufactured using nodular cast iron with steel channel tubes, which are used to position the fuel assemblies. The channel tubes are made from square steel tubes, which are welded together to form a steel tube cassette, which is placed in the casting mould.

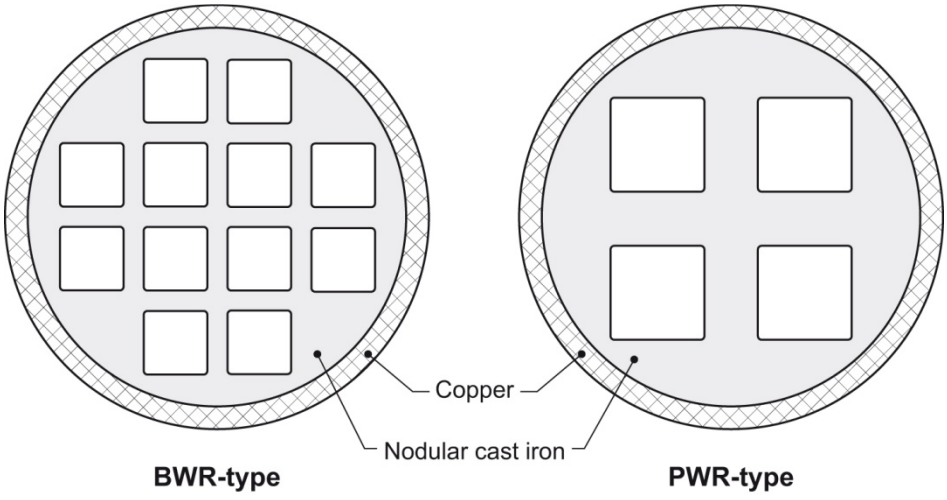

Figure 3-2. *Basic differences between the BWR and PWR canister designs.*

3.1.1 Steel tube cassette

The steel tube cassette (Figure 3-3) is formed by square steel tubes with thicknesses of 10 mm (BWR) and 12.5 mm (PWR) welded together. The distance between the fuel channels tubes, 30 mm for the BWR and 110 mm for the PWR, is maintained by steel plates (called support plates) positioned equidistantly vertically along the insert.

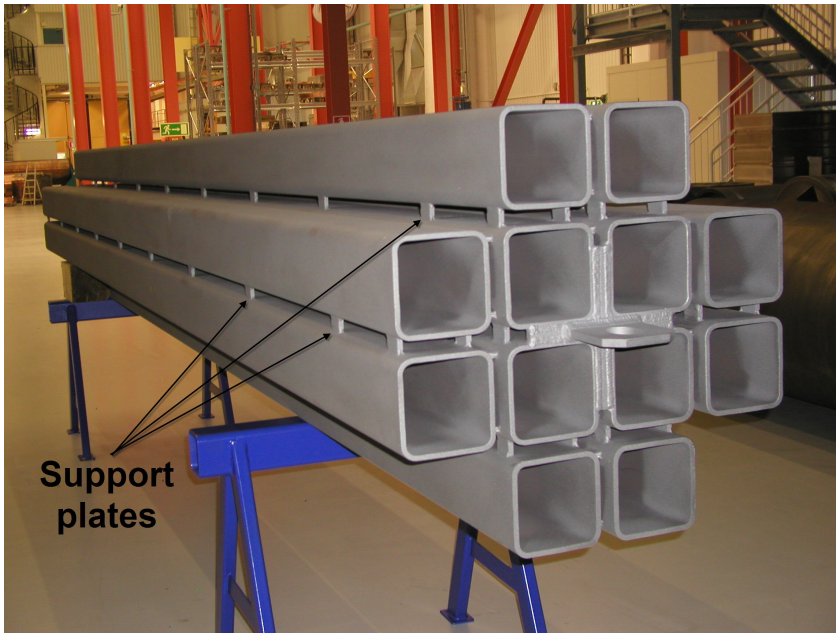

Figure 3-3. *Steel cassette for the BWR insert.*

3.1.2 Cast iron insert

The insert is manufactured from nodular cast iron, for which the formwork and method of casting can vary between foundries. Before casting, the cassette is placed in a mould made from either sand or metal, and the channel tubes are filled with compacted sand. Casting is performed either by filling the molten metal from the top, referred to as top pouring, or by bottom pouring, whereby the molten metal is led via a channel down into the bottom of the mould (SKBdoc 1432361).

After the insert has cooled, it is machined to the pre-machined state (Figure 3-4), on which the majority of inspections are performed, and finally, the insert is machined to its final dimensions. In Table 3-1, the nominal dimensions of the BWR and PWR inserts are summarised.

Table 3-1. Nominal dimensions of the BWR and PWR inserts (SKB 2010, SKBdoc 1203875, 1175208). Values in parentheses refer to the pre-machined state.

Parameter	Nominal value [mm], BWR	Nominal value [mm], PWR
Length of insert	4573 (4595)	4573 (4595)
Insert diameter	949 (960)	949 (960)
Edge distance	33.3 (38.8)	37.3 (42.8)
Thickness of bottom (excl. steel plate)	50 (57)	60 (66)
Bottom steel plate thickness	10	20
Ext. channel tube cross-section	180	260
Distance between channel tubes	30	110
Support plate height	50	100
Number of axial support plates	7	8

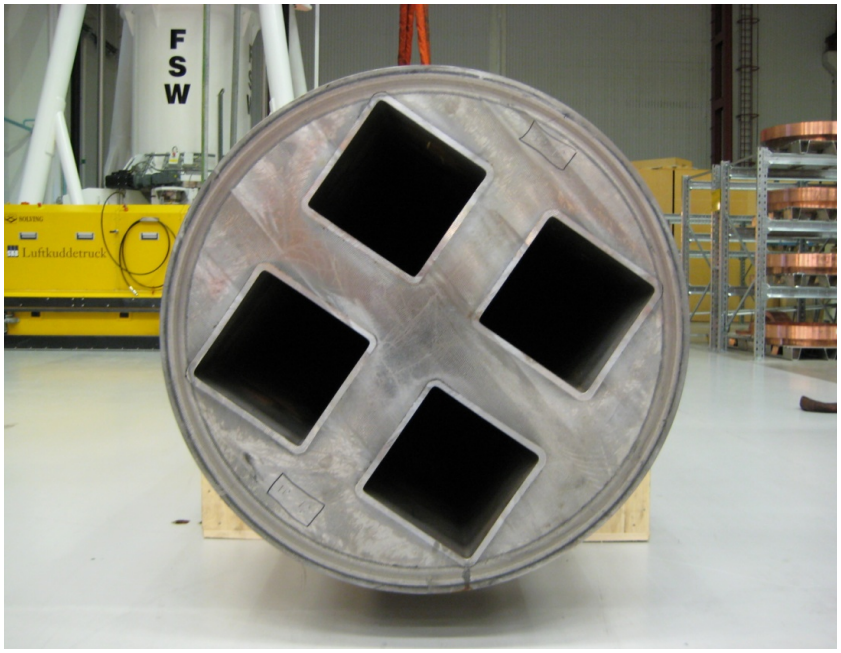

Figure 3-4. *Pre-machined PWR insert.*

3.1.3 Steel lid

The steel lid (Figure 3-5) is manufactured from a conventional steel plate, which includes some associated parts such as the screw, gasket and valve for atmosphere replacement. The lid has a nominal thickness of 50 mm and a diameter of 910 mm (SKB 2010).

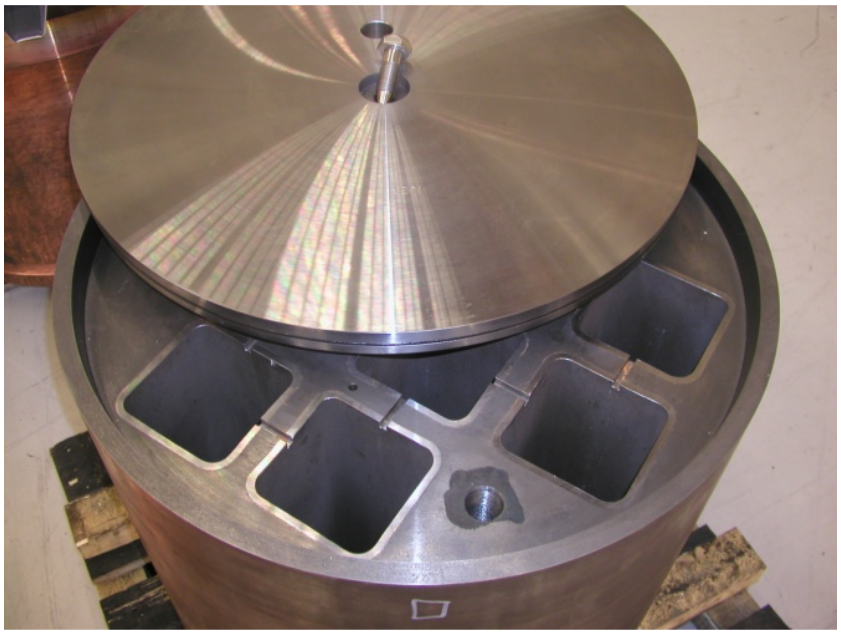

Figure 3-5. *BWR insert with steel lid.*

3.2 Copper tube

In this section, an overview of the copper tube is provided; a more detailed description is found in SKBdoc 1432038.

The copper tube is manufactured using highly pure copper (>99.99%); the process begins with casting a homogeneous copper ingot that is used in the subsequent hot-forming steps.

3.2.1 Copper tube ingot

The copper ingots are manufactured via semi-continuous casting, which creates cylindrical and solid ingots, as shown in Figure 3-6. After casting, the ingot is machined to a nominal diameter of 850 mm and a nominal weight of 12.4 tons for tube extrusion or 13.4 tons for the manufacture of tubes with an integrated base by the pierce-and-draw process.

Figure 3-6. *Ingot used to manufacture tubes.*

3.2.2 Copper tube

The reference method used to manufacture copper tubes is extrusion (SKBdoc 1432038). The extrusion is conducted in two separate steps (Figure 3-7), manufacturing of the blocker and extrusion of the tube. The ingot is heated to the desired temperature, pressed in several steps and finally pierced to form a thick-walled cylinder (blocker). After the blocker has cooled, it is machined. Finally, the blocker is heated, and tube extrusion is performed in a single step. The dimensions after the machining of the blocker and the extruded tube are summarised in Table 3-2.

For copper tube manufacturing, an alternative method, the pierce-and-draw method, was developed. The operating principle of this technique is similar to that of the extrusion technique. Manufacturing is performed in two hot-forming steps with intermediate machining. In the first step, the ingot is compressed and pierced, and in the second step, several sub-sequent drawing steps are performed until the desired diameter and wall thickness are achieved. A more detailed description is presented in SKBdoc 1432038.

Table 3-2. Nominal dimensions of the copper blocker and the copper tube (values in parentheses refer to the pre-machined state).

Parameter	Nominal value [mm]
Blocker length	1300-1500
Blocker outer diameter	1300-1500
Blocker wall thickness	200-300
Tube length	4740 (4900)
Tube outer diameter	1050 (1060)
Tube wall thickness	49 (54)

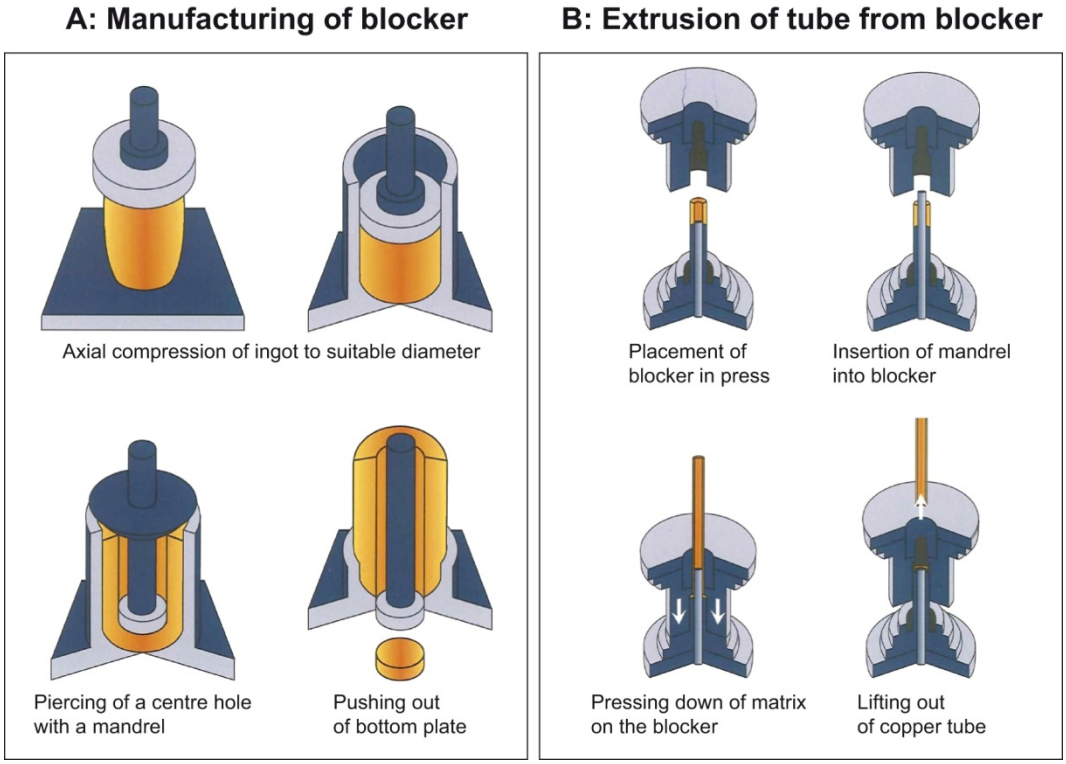

Figure 3-7. *Schematic illustration of the extrusion process, including how the blocker is manufactured and how the tube is extruded.*

3.3 Copper lid/base

In this section, an overview of the copper lid/base is described; a more detailed description can be found in SKBdoc 1432038. From an inspection point of view, the lid and base have similar geometry, and therefore, only the lid will be mentioned further on.

The copper lid/base is manufactured using highly pure copper (>99.99%); the process begins with casting a homogeneous copper billet that is cut into ingots that is used in the subsequent forging process.

3.3.1 Copper lid ingot

Copper ingots for the lids are manufactured by continuous casting; from a single individual batch of molten metal, a large number of ingots are obtained when the main billet, after casting, is cut to required sizes. After cutting, the ingots are machined to a nominal diameter of 500 mm and a nominal weight of about 1 300 kg.

3.3.2 Copper lid

The reference method for manufacturing the copper lid is forging (SKBdoc 1432038). The ingot is heated to the desired temperature and forged in several different steps until it completely fills the cavity in the lower forging tool to form a lid. After the blank has cooled, it is machined to the pre-machined state with a simplified geometry suitable for ultrasonic inspection. From that state it is further machined to the final lid dimensions prior to welding. The copper lid dimensions are summarised in Table 3-3 (SKB 2010).

Table 3-3. Nominal dimensions of the copper lid (values in parentheses refer to the pre-machined state).

Parameter	Nominal value [mm]
Lid thickness	50 (54)
Lid outer diameter	1060 (1064)
Lid height	190 (194)
Flange inner diameter	821 (817)
Lid inner diameter	850 (817)

3.4 Friction stir welding

In this section, an overview of the friction stir welding is provided; a more detailed description is found in SKBdoc 1435653.

The copper lid and base are welded on to the copper tube by friction stir welding. The welding is performed by a rotating tool, which consists of a probe and shoulder, which is forced down into the joint to be welded and moved along the joint around the entire circumference of the canister, as shown in Figure 3-8. The function of the probe is to heat the metal by friction and, through its shape and rotation, force the metal to stir and create a weld. The function of the shoulder is to heat the metal through friction and to prevent the metal from being forced out of the weld zone. The dimensions of the weld are presented in Table 3-4.

Table 3-4. Dimensions of the friction stir weld.

Weld Dimension	Value [mm]
Outer diameter	1050 [1)]
Axial width	50 [2)]
Radial depth	49 [1)]
Centre position from lid top	58 [2)]

1) Nominal values obtained from drawing (SKBdoc 1203875).
2) Values obtained from measurements.

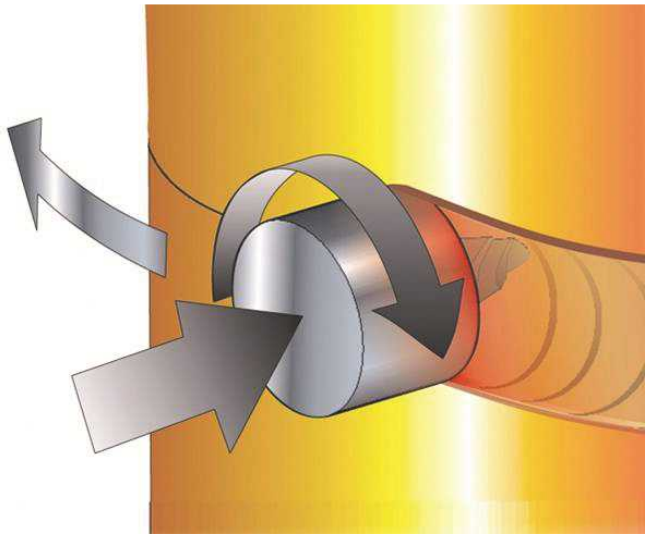

Figure 3-8. *Illustration of the welding process.*

4 Defects and acceptance criteria

In the canister production report (SKB 2010) and its references, possible canister defects as well as acceptable defect sizes from damage tolerance analyses of the insert, were presented. During the last years the knowledge of canister defects has increased and complementary damage tolerance analyses have been conducted. In the beginning of 2014 acceptance criteria for the cast iron insert (SKBdoc 1414760), copper components (SKBdoc 1414374) and friction stir welds (SKBdoc 1415307) were released.

Based on the above, the NDT development, in this specific project, was mainly conducted aiming towards the original acceptance criteria, compiled in section 4.1. The acceptance criteria presented in section 4.2 then formed the basis for the assessment of the developed techniques presented in chapter 10. The process flow in this specific project is shown in Figure 4-1.

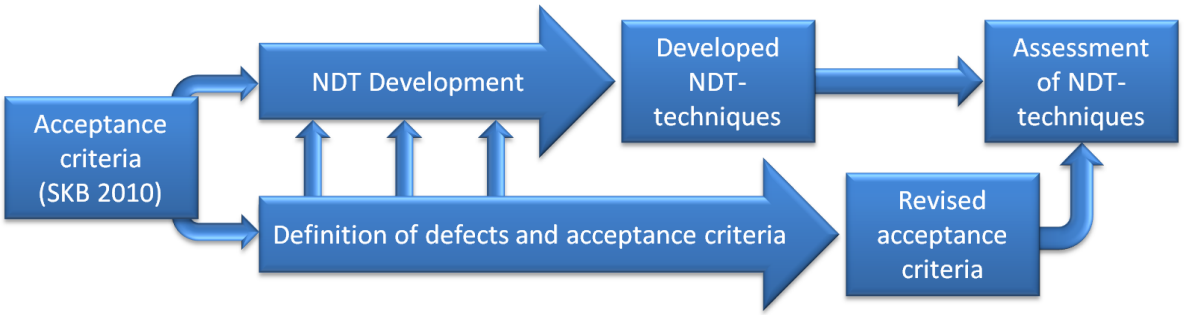

Figure 4-1. *Process for continuous development of NDT-techniques and acceptance criteria.*

4.1 Acceptance criteria TR-10-14 (prerequisites for the NDT development)

In this section the information of possible defects and acceptable defect sizes defined in the canister production report (SKB 2010) and its references is compiled.

4.1.1 Cast iron insert

In SKBdoc 1175208 a number of possible manufacturing defect types such as shrinkage, shrinkage pores, blowhole, chaplet blowhole, cracks, sand- and slag inclusion were presented for the insert. The defects were all, except cracks, defined as volumetric (hole) defects in the canister production report (SKB 2010).

The canister production report (SKB 2010) presented acceptance criteria for the isostatic and shear load case respectively. For the isostatic load case the BWR and PWR inserts were divided into different zones (Figure 4-2). Based on these zones, acceptance criteria for defects were created, see Table 4-1 and 4-2. For the shear load case acceptance criteria were defined for surface and internal defects, see Table 4-3.

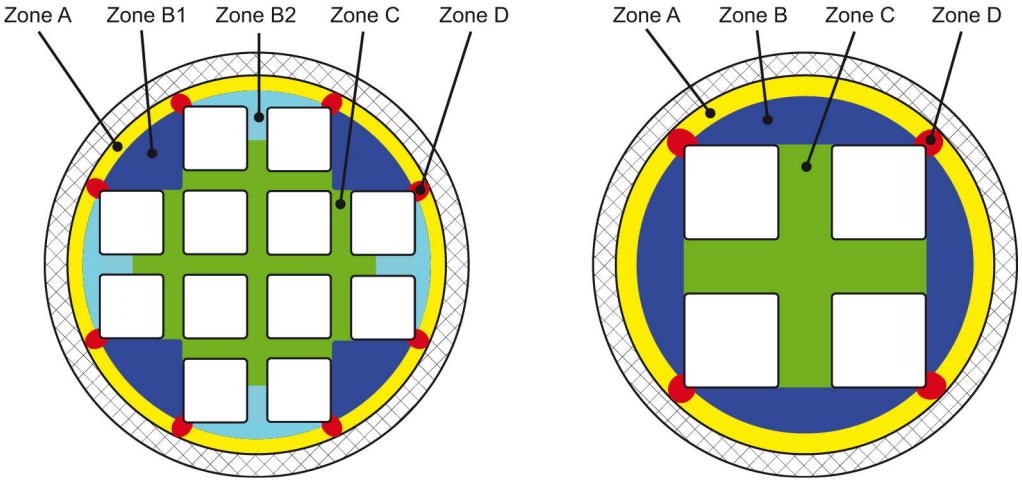

Figure 4-2. *Zones in the inserts used for damage tolerance analysis.*

Table 4-1. Maximum acceptable sizes for axial defects (isostatic load).

Zone (Figure 4-2)	Defect depth/height (axial length in parenthesis), [mm]	
	BWR-insert	PWR-insert
A	37 (222)	53 (318)
B	NA	112 (672)
B1	65 (390)	NA
B2	50 (300)	NA
C	24 (144)	104 (624)
D	32 (192)	31 (186)

Table 4-2. Maximum acceptable sizes for volumetric defects (isostatic load).

Zone (Figure 4-2)	Defect size (diameter) [1], [mm]	
	BWR-insert	PWR-insert
A	40	80
B	NA	100
B1	60	NA
B2	20	NA
C	20	100
D	20	20

1) All calculations were based on cylinders with length equal to the insert length and no other limiting axial size was considered, and therefore no requirements were set for axial size.

Table 4-3. Maximum acceptable sizes for postulated defects[1] (shear load case, 5 cm shearing), BWR insert.

Postulated defect geometry	Depth/height [mm]	Length [mm]
Internal elliptical defects[2]	>10	>60
Internal circular defects[2]	>10	>10
Semi-elliptical surface defects	4.5	27.0
Semi-circular surface defects	8.2	16.4

1) The definition of the postulated defects originates from the damage tolerance analysis.
2) Acceptable defect sizes were only calculated for defects in zone A, B, B1, B2 and D.

4.1.2 Copper tube

In SKBdoc 1175208, slag inclusions, oxidised and foreign particles were identified as possible defects in the copper tube. In the canister production report (SKB 2010) no acceptance criteria for defects were specified. However, in the initial state chapter, it was stated that the maximum local reduction of the copper wall thickness was estimated to be less than 10 mm for 99.9% of the canisters. Thereby a maximum wall thickness reduction of 10 mm was used as an assumption for the NDT development.

4.1.3 Copper lid

In SKBdoc 1175208 forging laps, slag inclusions, oxidised and foreign particles were identified as possible defects in the copper lid. In the same way as for the copper tube (section 4.1.2) no acceptance criteria was stated and thereby a maximum wall thickness reduction of 10 mm, was applied as an assumption for the NDT development.

4.1.4 Friction stir weld

In SKBdoc 1175208, cavity and joint line hooking were presented as possible defects in the weld. In the same way as for the copper tube (section 4.1.2) no acceptance criteria was stated and thereby a maximum wall thickness reduction of 10 mm, was applied as an assumption for the NDT development.

4.2 Defect specifications and acceptance criteria for NDT

Based on the information presented in the canister production report (SKB 2010) and systematic analyses of the manufacturing processes, more detailed defect specifications and acceptance criteria for NDT were established. This work was conducted iteratively, which means that some information was available during the NDT development while the acceptance criteria were first established after the NDT development presented in this report was completed.

4.2.1 Cast iron insert

Description of defects and acceptance criteria for NDT has been specified for the insert (SKBdoc 1414760, 1432361). These documents only consider the cast iron in the insert. This means that no acceptance criteria are specified so far for NDT of the steel tube cassette, steel lid etc.

Defects

For the insert, a number of manufacturing defect types have been presented (SKBdoc 1414760, 1432361), which are summarised in Table 4-4.

Table 4-4. Defects in the cast iron insert[1].

Defect	Description	Occurrence
Shrinkage	Volumetric irregular defect with dendritic walls.	Not found.
Shrinkage pores	Clusters of small volumetric defects with dendritic walls.	Identified in several inserts.
Chaplet blowhole	Irregular volumetric defect in connection to the cassette.	Identified in some inserts.
Blowhole	Volumetric defect with smooth surfaces.	Identified in some inserts.
Hot tear	Axial crack from the outer corner of the outer fuel channels.	Not found.
Sand inclusion	Sand particles embedded in the cast iron.	Identified in some early manufactured inserts.
Slag inclusion	Particles or films with irregular surfaces.	Frequently occurring.

1) The cold crack type defect is excluded as being a non-manufacturing related defect requiring high loads at freezing temperatures to occur.

Acceptance criteria for NDT

The primary inspection acceptance criteria for NDT concern defect detection. However, one geometric measure, the edge distance, was identified as a measurement requirement for NDT. The acceptance criteria were derived from the compilation of the results of damage tolerance analysis (SKBdoc 1288292, Dillström and Bolinder 2010) and from the acceptance criteria (SKBdoc 1414760, 1432361). The BWR and PWR inserts were divided into different zones (Figure 4-2), and based on these zones, acceptance criteria were created, which are compiled in Table 4-6 to Table 4-12.

Table 4-6. Maximum acceptable sizes for volumetric defects, BWR insert.

Defect	Diameter[1] [mm]				
	A	B1	B2	C	D
Shrinkage	40	60	20	20	20
Shrinkage pores	40	60	20	20	20
Chaplet blowhole	40[2]	60	20	20	20
Blowhole	40	60	20	20	20

1) All calculations were based on cylinders with length equal to the insert length and no other limiting axial size was considered, and therefore no requirements were set for axial size.
2) The chaplet blowhole only occurs in connection with the cassette structure, not in this region.

Table 4-7. Maximum acceptable sizes for axial defects, BWR insert.

Defect	Depth/height (axial length in parenthesis), [mm]					
	A, 0-2 mm from surface	A, >2 mm from surface	B1	B2	C	D
Slag inclusion	37 (222)	37 (222)	65 (393)	50 (300)	24 (144)	32 (196)
Sand inclusion[1]	37 (222)	37 (222)	65 (393)	50 (300)	24 (144)	32 (196)
Hot tear	37 (222)[2]	37 (222)[2]	65 (393)[2]	50 (300)[2]	24 (144)[2]	32 (196)

1) Sand inclusion has been considered to have the same appearance as slag inclusion.
2) The probability that the hot tear defect type occurs in this volume of the insert is considered to be very low. The necessity of this requirement is to be further investigated.

Table 4-8. Maximum acceptable sizes for circumferential defects, BWR insert.

Defect	Radial depth/height (circumferential length in parenthesis), [mm]					
	A, 0-2 mm from surface[1)]	A, >2 mm from surface	B1	B2	C	D
Slag inclusion	4.5 (27) 8.2 (16.4)	>10 (>60)	>10 (>60)	>10 (>60)	>10 (>60)	>10 (>60)
Sand inclusion[2)]	4.5 (27) 8.2 (16.4)	>10 (>60)	>10 (>60)	>10 (>60)	>10 (>60)	>10 (>60)

1) Calculations were performed for two combinations of depth length ratio, originating from the postulated semi-circular and half-elliptical defect geometries.
2) Sand inclusion has been considered to have the same appearance as slag inclusion.

Table 4-9. Maximum acceptable sizes for volumetric defects, PWR insert.

Defect	Diameter[1)] [mm]			
	A	B	C	D
Shrinkage	80	100	100	20
Shrinkage pores	80	100	100	20
Chaplet blowhole	80[2)]	100	100	20
Blowhole	80	100	100	20

1) All calculations were based on cylinders with length equal to the insert length and no other limiting axial size was considered, and therefore no requirements were set for axial size.
2) The chaplet blowhole only occurs in connection with the cassette structure, not in this region.

Table 4-10. Maximum acceptable sizes for axial defects, PWR insert.

Defect	Depth/height (axial length in parenthesis), [mm]				
	A, 0-2 mm from surface	A, >2 mm from surface	B	C	D
Slag inclusion	53 (318)	53 (318)	112 (672)	104 (624)	31(186)
Sand inclusion[1)]	53 (318)	53 (318)	112 (672)	104 (624)	31(186)
Hot tear	53 (318)[2)]	53 (318)[2)]	112 (672)[2)]	104 (624)[2)]	31 (186)

1) Sand inclusion has been considered to have the same appearance as slag inclusion.
2) The probability that the hot tear defect type occurs in this volume of the insert is considered to be very low. The necessity of this requirement is to be further investigated.

Table 4-11. Maximum acceptable sizes for circumferential defects, PWR insert.

Defect	Radial depth/height (circumferential length in parenthesis), [mm]				
	A, 0-2 mm from surface[1)]	A, >2 mm from surface	B[1)]	C	D
Slag inclusion	4.1 (24.6) 7.5 (15)	>10 (>60)	>10 (>60) >20 (>20)[2)]	No values available	>10 (>60)
Sand inclusion[3)]	4.1 (24.6) 7.5 (15)	>10 (>60)	>10 (>60) >20 (>20)[2)]	No values available	>10 (>60)

1) Calculations were performed for two combinations of depth length ratio, originating from the postulated semi-circular and half-elliptical defect geometries.
2) This defect size is only acceptable for the inner region of this zone.
3) Sand inclusion has been considered to have the same appearance as slag inclusion.

Table 4-12. Acceptance criteria for edge distance in the BWR and PWR inserts (SKB 2010, SKBdoc 1175208).

Insert	Edge distance pre-machined [mm]	Edge distance machined [mm]
BWR	28.8-48.8	23.3-43.3
PWR	32.8-52.8	27.3-47.3

4.2.2 Copper tube

Description of defects and acceptance criteria for NDT has been specified for the copper tube (SKBdoc 1414374, 1432038). These documents consider the whole manufacturing chain, that is manufacturing the copper ingot, copper blocker, and the copper tube.

Defects

From the manufacture of copper tubes, different defect types have been presented (SKBdoc 1414374, 1432038) for the ingot (Table 4-13), the blocker (Table 4-14) and for the copper tube (Table 4-15).

Table 4-13. Defects in the copper tube ingot.

Defect	Description	Occurrence
Foreign particles	Particles pressed into the ingot surface.	Identified in some ingots.
Cold laps	Laminar copper of the ingot surface.	Identified in some ingots.
Cracks	Axial or circumferential surface cracks.	Identified in some ingots.
Indentation	Handling damages on the surface.	Identified in some ingots.
Spider cracks	Radial/axial cracks in the centre of the end faces.	Identified in some ingots.
Exogenous slag	Impurities from the manufacturing process.	Not found.

Table 4-14. Defects in the copper blocker.

Defect	Description	Occurrence
Foreign particles	Particles pressed into the blocker surface.	Identified in some blockers.
Indentation	Handling damages on the surface.	Identified in some blockers.
Exogenous slag	Impurities from the manufacturing process.	Not found.

Table 4-15. Defects in the copper tube.

Defect	Description	Occurrence
Foreign particles	Particles pressed into the tube surface.	Identified in some tubes.
Indentation	Handling damages on the surface.	Identified in some tubes.
Axial scratch	Oxidised axial scratch caused by damaged extrusion die.	Identified in one tube.

Acceptance criteria for NDT

The acceptance criteria for NDT are described (SKBdoc 1414374, 1432038) and summarised in Table 4-16 (ingot), Table 4-17 (blocker) and Table 4-18 (copper tube) including updated acceptable depths for handling defects (indentation and foreign particles).

Table 4-16. Maximum acceptable defect sizes for the copper tube ingot[1)].

Defect[2)]	Acceptable depth/height [mm][3)] envelope surface	Acceptable depth/height [mm][3)] end surfaces
Foreign particles	25	18
Cold laps	10	[4)]
Cracks	10	[4)]
Indentation	25	18
Spider cracks	[4)]	18

1) The preliminary detectability criterion for NDT is that defects with half of the acceptable depth shall be detected.
2) Exogenous slag can first be inspected in the blocker stage and therefore no acceptance criteria were set for the ingot inspection.
3) Currently, acceptance criteria have not been defined for any other direction than the depth direction.
4) Acceptance criteria are only set for positions where the defects can occur.

Table 4-17. Maximum acceptable defect sizes for the copper blocker[1)].

Defect	Acceptable depth/height [mm][2)] envelope surface	Acceptable depth/height [mm][2)] end surfaces
Foreign particles	10	10
Indentation	18	10
Exogenous slag	10[3)]	10[3)]

1) The preliminary detectability criterion for NDT is that defects with half of the acceptable depth shall be detected.
2) Currently, acceptance criteria have not been defined for any direction other than the depth direction.
3) The acceptance criterion for exogenous slag is also valid for internal defects. The acceptable depth refers to the radial defect size.

Table 4-18. Maximum acceptable defect sizes for the copper tube[1)].

Defect	Acceptable depth/height [mm][2)] envelope surface	Acceptable depth/height [mm][2)] end surfaces
Foreign particles	10	[3)]
Indentation	10	[3)]
Axial scratch	10[4)]	[5)]

1) The preliminary detectability criterion for NDT is that defects with half of the acceptable depth shall be detected.
2) Currently, acceptance criteria have not been defined for any direction other than the depth direction.
3) Currently, no acceptance criteria have been defined for the weld joint surfaces.
4) The criterion is valid for both inner and outer tube surfaces.
5) Acceptance criteria are only set for positions where the defects can occur.

4.2.3 Copper lid

Description of defects and acceptance criteria for NDT has been specified for the copper lid (SKBdoc 1414374, 1432038). These documents consider the whole manufacturing chain, that is manufacturing the copper ingot and the copper lid.

Defects

From the manufacture of copper lids, different defect types have been presented (SKBdoc 1414374, 1432038) for the ingot (Table 4-19) and for the copper lid (Table 4-20).

Table 4-19. Defects in the copper lid ingot.

Defect	Description	Occurrence
Foreign particles	Particles pressed into the ingot surface.	Identified in some ingots.
Cold laps	Laminar copper of the ingot surface.	Not found.
Cracks	Radial/axial or circumferential surface cracks.	Identified in some ingots.
Indentation	Handling damages on the surface.	Identified in some ingots.

Table 4-20. Defects in the copper lid.

Defect	Description	Occurrence
Foreign particles	Particles pressed into the surface.	Identified in some lids.
Oxidised strings	Oxidised strings caused by damaged forging tool.	Not found.
Forging lap	Laps caused by overlapping surfaces during forging.	Identified in some lids.
Indentation	Handling damages on the surface.	Identified in some lids.
Exogenous slag	Impurities from the manufacturing process.	Not found.

Acceptance criteria for NDT

The acceptance criteria for NDT are described in (SKBdoc 1414374, 1432038) and summarised in Table 4-21 (ingot) and Table 4-22 (copper lid) including updated acceptable depths for handling defects (indentation and foreign particles).

Table 4-21. Maximum acceptable defect sizes for the copper lid ingot[1)].

Defect	Acceptable depth/height [mm][2)] envelope surface	Acceptable depth/height [mm][2)] end surfaces
Foreign particles	6.5	10
Cold laps	6.5	[3)]
Cracks	6.5	[3)]
Indentation	6.5	10

1) The preliminary detectability criterion for NDT is that defects with half of the acceptable depth shall be detected.
2) Currently, no acceptance criteria have been defined for the size along the surface.
3) Acceptance criteria are only set for positions where the defects can occur.

Table 4-22. Maximum acceptable defect sizes for the copper lid[1)].

Defect	Acceptable depth/height [mm][2)] envelope surface	Acceptable depth/height [mm][2)] end surfaces
Foreign particles	10	10
Oxidised strings	10	10
Forging lap	[3)]	10
Indentation	10	10
Exogenous slag	10[4)]	10

1) The preliminary detectability criterion for NDT is that defects with half of the acceptable depth shall be detected.
2) Currently, no acceptance criteria have been defined for the size along the surface.
3) Acceptance criteria are only set for the positions where the defects can occur.
4) The acceptance criterion for exogenous slag is also valid for internal defects. The acceptable depth refers to the defect size in the direction of the corrosion barrier.

4.2.4 Friction stir weld

Description of defects and acceptance criteria for NDT has been specified for the friction stir weld (SKBdoc 1415307, 1435653).

Defects

In friction stir welds, a number of defect types have been presented (SKBdoc 1415307, 1435653), which are summarised in Table 4-23.

Table 4-23. Defects in friction stir welds.

Defect	Description	Occurrence
Cavity	Irregularly shaped voids in the outer regions of the weld.	Identified in welds performed at excessively low temperature.
Joint line hooking	Bent joint in the weld root due to the tool penetrating too far.	Frequently occuring.
Remaining joint	Horizontal joint in the weld root due to the tool not penetrating far enough.	Identified in some welds.

Acceptance criteria for NDT

The acceptance criteria for NDT (SKBdoc 1415307, 1435653) are summarised in Table 4-24.

Table 4-24. Maximum acceptable defect sizes for friction stir welds.

Defect	Acceptable radial size [mm][1)]
Cavity	5
Joint line hooking	5
Remaining joint	5

1) Currently, there are no acceptance criteria for the size along the circumference or in the axial direction.

5 Inspection strategy

SKB shall inspect the canister to ensure that the acceptance criteria are fulfilled. For inspection of the canister components and welds, it has been concluded that inspecting the final component is not always the optimum method, and therefore, another strategy has been developed. This strategy has evolved over the years after performing a large number of inspection trials at the Canister Laboratory. Depending on future canister production optimisation and logistics as well as development of the inspection requirements, further changes in the inspection strategy can be foreseen.

The present inspection strategy is based on two corner-stones:

- Inspection should, if possible, be conducted at a stage when an NDT inspection is favoured by the geometry.
- Inspection should be conducted in successive steps to minimise the risk of rejection in later stages.

Based on these corner-stones and the process line defined for canister production, a preliminary inspection scheme was created, as shown in Figure 5-1. In this inspection scheme, the manufacturing and inspection steps are grouped as follows:

- **Supplier level 2**: Suppliers that delivers pre-fabricated components such as the welded steel cassette and copper ingots that are used to manufacture the main components (copper tube, lid and base, and cast iron insert) to supplier level 1. Inspections are primarily performed to minimise the risk of rejection in the following production steps, though the inspections might also be performed to ensure that the acceptance criteria for post closure safety are fulfilled.
- **Supplier level 1**: Supplier that delivers components to SKB. Inspections are performed either to verify the final quality of less critical components (for example the steel lid and steel screw) or as part of the procurement of individual components or to reduce the risk of rejection in the canister factory.
- **Canister factory**: The final production steps (for example machining, welding and inspection) of the canister components are conducted to ensure that acceptance criteria for post closure safety are fulfilled. This step requires the highest degree of reliability.
- **Encapsulation plant**: Final sealing and inspection are conducted in a nuclear environment to ensure that acceptance criteria for post closure safety are fulfilled. This step requires the highest degree of safety and reliability.

The pre-fabricated components (such as the welded steel cassette and copper ingots) are, depending on the specified requirements, inspected by either qualified or proven techniques. The less critical components (such as the steel lid and steel screw), which are manufactured by proven technology and/or have a minor effect on post closure safety, are inspected by proven technology.

Inspections of the main components (copper tube, lid and base, and cast iron insert) are conducted in several steps. The first inspection is performed on the supplier's premises to reduce the risk of rejection in later production steps. These inspections are performed using the suppliers' instructions approved by SKB. The instructions are based on industrial standards combined with additional requirements such as acceptance levels, mechanised inspection and increased level of documentation. To reduce the risk of rejection caused by damages incurred during handling and reduce the effect of the limitations of the ultrasonic technique near the surface, inspections are conducted on components machined to the pre-machined state with excess material thickness.

In the next step, the components are transported to the canister factory, where inspections are conducted to ensure that the acceptance criteria for post closure safety are fulfilled. At the canister factory, inspections are conducted in two steps. During the first inspections, performed by ultrasonic techniques, the components remain in the pre-machined state with an excess material thickness. In this manner, the entire volume of the final component is inspected without being affected by ultrasonic

limitations, the so-called dead zone, near the inspection surface. Finally, after being machined to the final dimensions, the component surfaces are inspected by specific surface inspection techniques.

The final machined components are then assembled, and in the first step, the base and tube are welded by FSW; after machining, the weld is inspected. Then, the insert is installed in the tube and transported (together with the steel and copper lid) to the encapsulation plant. At the encapsulation plant, the canister is filled with spent fuel and then sealed by FSW, and finally, after machining, the weld is inspected by remotely controlled inspection techniques.

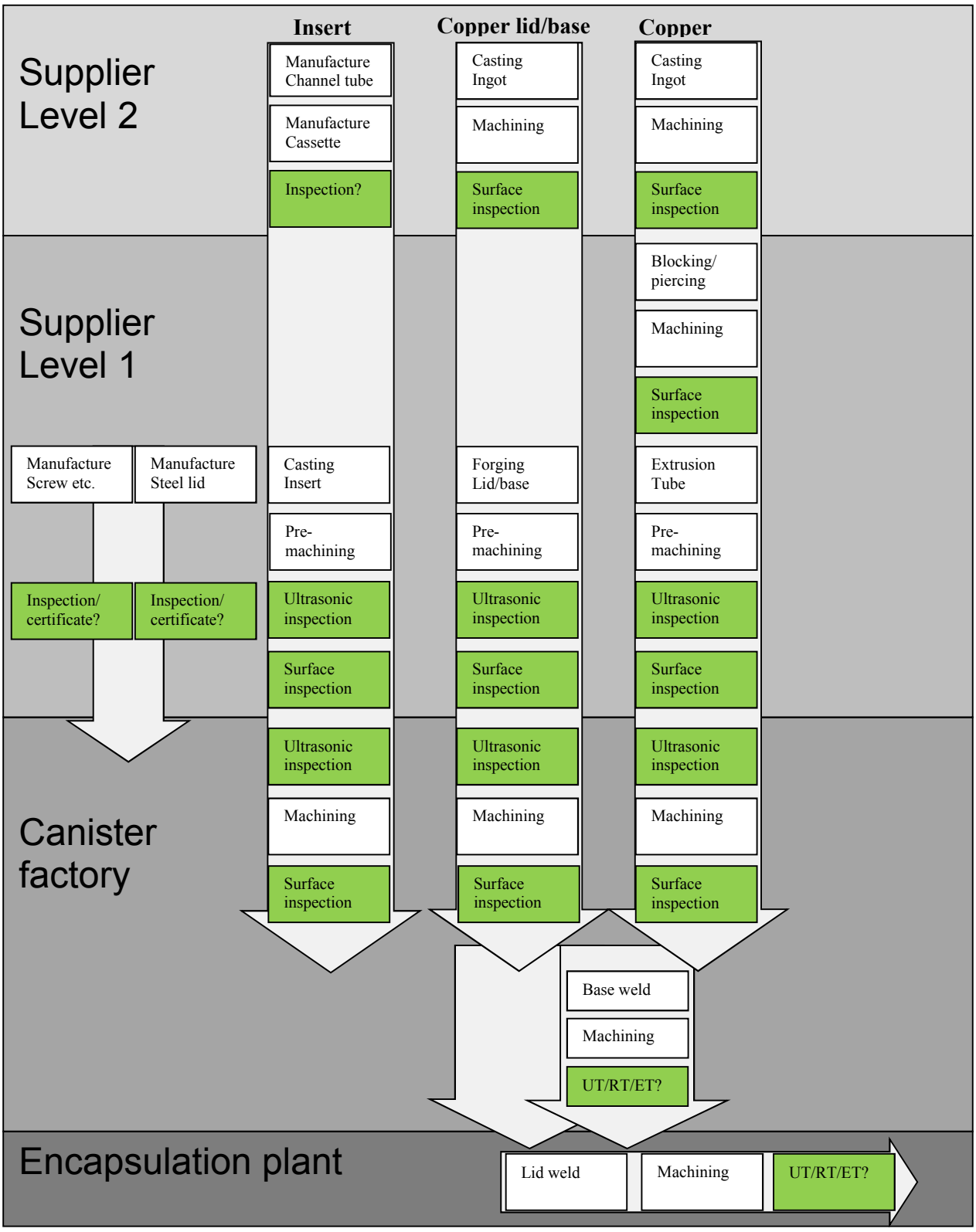

Figure 5-1. *Preliminary inspection scheme for canister components and welds.*

6 Non-destructive testing techniques

In this chapter, the equipment, the developmental process of the NDT techniques and the developed techniques are described. The description is derived from the framework of the canister production line report (SKB 2010) and the corresponding NDT reference report (SKBdoc 1179633).

6.1 Equipment

At the Canister Laboratory in Oskarshamn, equipment for full-scale inspections have been developed and installed for inspection of the cast iron insert, copper tube, copper lid and base and the friction stir welds.

6.1.1 Manipulators

For inspection of the large components, the cast iron insert and the copper tube, SKB developed a manipulator, as shown in Figure 6-1. The manipulator consists of two separate parts, one in which a reference object with the same geometry as the component is attached and one for the component itself. The manipulator was built to be flexible in several respects. For example, the manipulator can be used to inspect cast iron inserts, copper tubes and, in special cases, copper blockers as well. Both short segments and full-scale components can be inspected, and different types of NDT equipment can be used. During inspection, a number of manipulation sequences can be used by rotating the object or the reference object and through linear movement of the NDT equipment in the axial direction.

For inspection of copper lids and bases, a manipulator with an immersion tank has been developed, as shown in Figure 6-2. This manipulator can be used for one-dimensional scans and for two-dimensional scans of, for example, the entire lid end surfaces.

Friction stir welds are inspected either by the integrated manipulator in the X-ray system or by the rotary table used, for example, for ultrasonic and eddy current inspection. Both manipulators (Figure 6-3) rotate the welded component during inspection, and for the X-ray manipulator, an inspection angle of 5°-40° can be used.

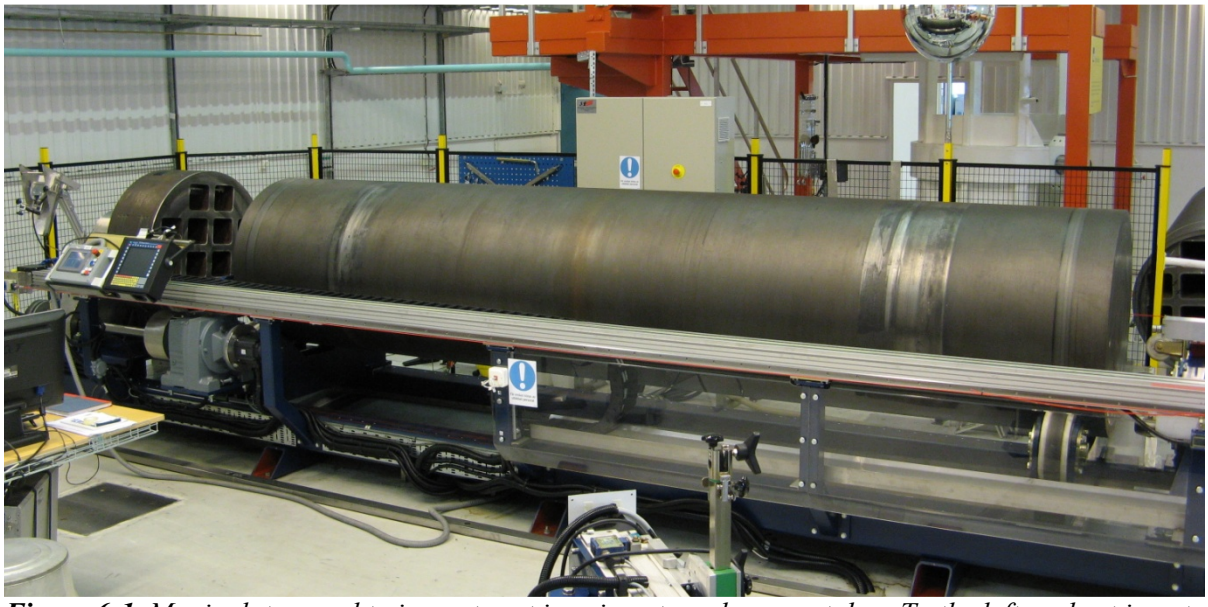

Figure 6-1. *Manipulator used to inspect cast iron inserts and copper tubes. To the left, a short insert segment, used as a reference object, is attached.*

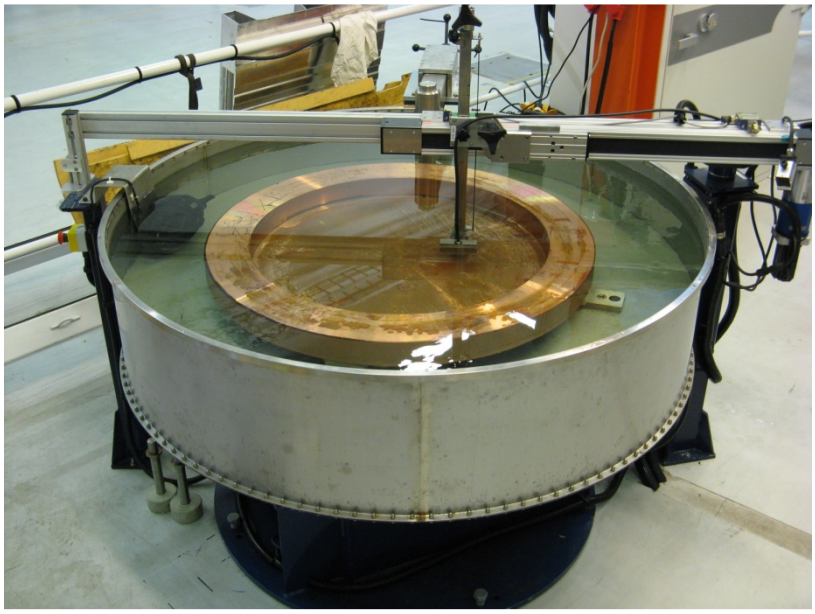

Figure 6-2. *Manipulator for inspection of copper lids and bases.*

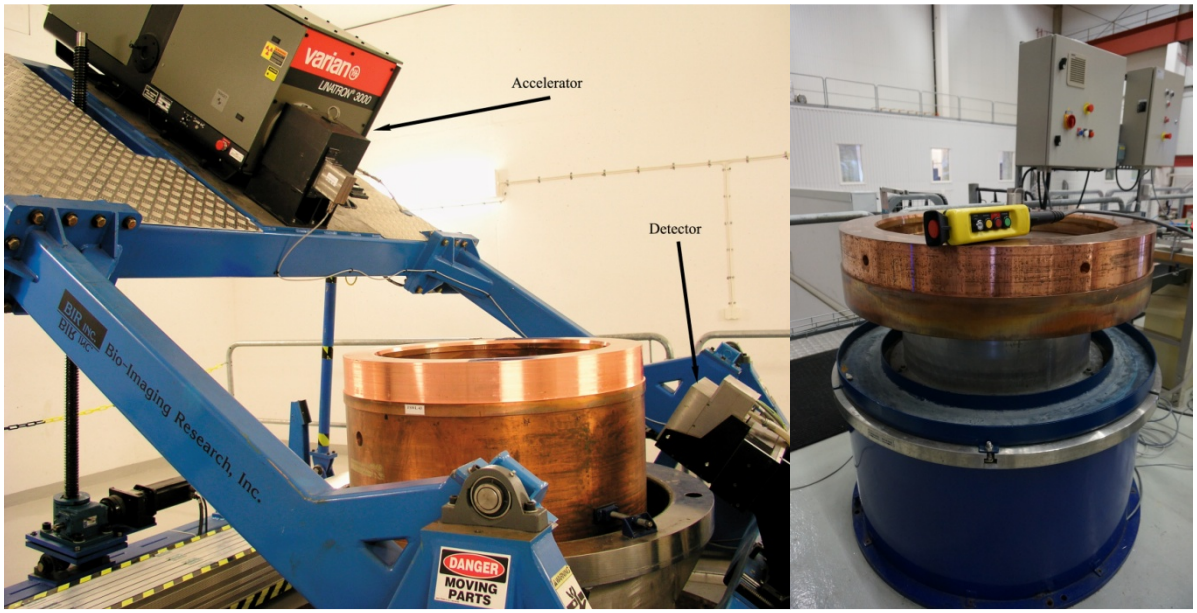

Figure 6-3. *X-ray manipulator (left) and rotary table (right) for ultrasonic and eddy current inspection of welds.*

6.1.2 NDT equipment

At the Canister Laboratory, NDT equipment for ultrasonic, eddy current and X-ray inspection are used. In addition, the laboratory has resources for performing magnetic particle and penetrant inspections.

Ultrasonic equipment

Ultrasonic equipment used in the development and inspection of canister components and welds include a high-performance, 128-channel phased array instrument (Zetec - Dynaray) used together with the software programme UltraVision, as shown in Figure 6-4. The equipment can be used with different numbers of array probes or with up to 16 conventional probes. The instrument collects the full wave-forms with 16-bit resolution, and the data can then be analysed by A-, B-, C- and D-scans and in different types of three-dimensional visualisations.

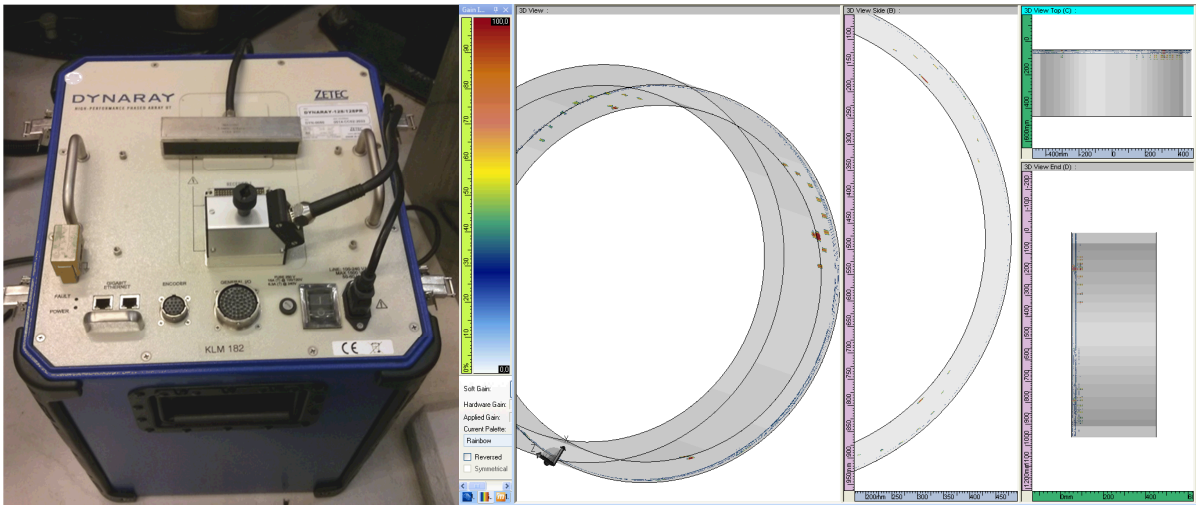

Figure 6-4. *Ultrasonic phased array equipment with a linear array probe to the left and three-dimensional visualisation of ultrasonic data in UltraVision to the right.*

X-ray equipment

The high-energy X-ray system shown in Figure 6-3 consists of a 9-MeV linear accelerator (Varian Linatron 3000), a collimated linear array detector and a manipulator system. The accelerator generates a maximum dose rate of 30 Gy/min with an average energy of approximately 3.5 MeV. The total vertical height of the detector (scintillator elements) is approximately 100 mm, and the detector array is composed of 2048 lines with a width 0.05 mm, and in the horizontal direction, the beam is collimated by a slit with a width of 0.4 mm.

Eddy current equipment

The eddy current equipment used in the development and inspection of canister components and welds is a high-performance, 64-channel array instrument (Eddyfi - Ectane) used together with the software programme Magnifi, as shown in Figure 6-5. The equipment can be used with different numbers of array probes with several array topologies and with conventional probes.

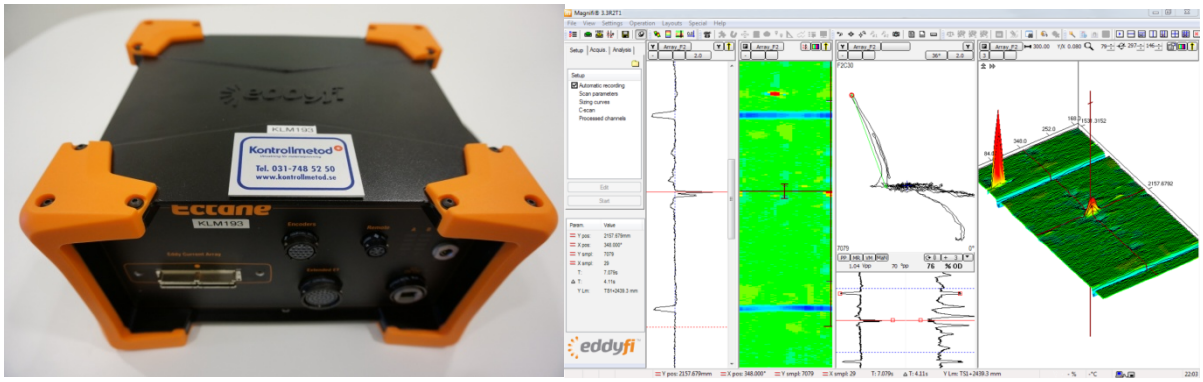

Figure 6-5. *Eddy current array equipment to the left and visualisation of eddy current data in Magnifi to the right.*

6.2 NDT techniques for the insert

In this section, the development process and the actual status of the developed NDT techniques are described for each part of the insert.

6.2.1 Steel tube cassette

Currently, there are no explicit acceptance criteria for NDT established for steel cassette sub-parts or the welded assembly, and therefore, no activities regarding developing or applying NDT techniques have been performed. However, such acceptance criteria are anticipated in the future.

6.2.2 Cast iron insert

The cast iron insert is inspected in several steps, as described in Figure 5-1. The first inspections are performed by the supplier as part of an agreement to gain permission for delivery and to minimise the risk for rejection in any of the following inspections. The inspections by the supplier include both ultrasonic and magnetic particle inspections.

The final inspection of the insert, which is planned to be performed at the canister factory to verify that the insert fulfils the desired acceptance criteria, is performed in two steps. The ultrasonic inspections are performed in the first step, when the insert is machined to the pre-machined state with excess material thickness. In this manner, the entire volume will be inspected as the volume near the inspection surface, where the sensitivity of the ultrasonic techniques is limited, will be removed during final machining. Finally, the surface will be inspected by dedicated surface inspection techniques after being machined to its final dimensions. The ultrasonic inspection techniques were developed based on the different zones described in section 4.1.1, and for the primary volume, three inspection techniques, angle inspection, normal inspection and transmission inspection, were developed as shown in Figure 6-6.

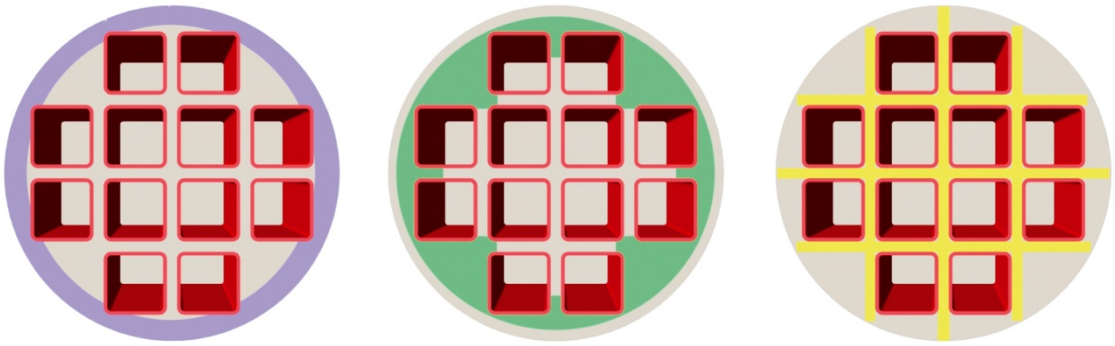

Figure 6-6. *Testing areas for BWR insert. The various techniques used to investigate the areas are angle inspection (lilac), normal inspection (green) and transmission inspection (yellow).*

In the following sections, the status of the inspections performed by suppliers and by using the developed ultrasonic and surface inspection techniques at the Canister Laboratory is described.

Inspections by the supplier

The inspections of the insert performed by the supplier as part of the acceptance process were further developed in terms of technical details, extent and managing documents. The NDT techniques include pulse-echo ultrasonics, fluorescent magnetic particle inspection with an AC yoke and visual inspection.

An attempt to mechanise ultrasonic inspection from the envelope surface was introduced, which replaced the previous manual inspection technique. Using a conventional turning machine, in which the cutter has been replaced by an ultrasonic transducer, the insert is scanned in a helical pattern. Because this alternative approach requires a new way to apply the necessary ultrasound couplant, a special transducer fixture with an integrated irrigation system was designed. Additionally, a final surface machining operation for the insert, optimised for ultrasonic inspection, was developed.

A video recording of the channel tube interior is used to verify the removal of the foundry sand and document the interior condition of the tubes.

The ultrasonic and magnetic particle inspections, as shown in Figure 6-7, are based on techniques and acceptance criteria that are commonly used by the foundry industry for large nodular cast iron components. Although international standard specifications are used, it is necessary to elaborate the extent of inspection and the technical details and to create a managing document supplementary regarding the referenced specifications.

Figure 6-7. *Ultrasonic and magnetic particle inspections of the inserts are performed by the supplier. The ultrasonic inspection (left) is automated using a turning machine as the manipulator; the cutting tool has been replaced with an ultrasonic probe that is fed with water as a couplant. The fluorescent magnetic particle inspection (right) is performed by magnetising each square decimetre of the insert in two orthogonal directions under UV lighting.*

Normal incidence ultrasonic inspection techniques (UT31)

The normal incidence (0°) ultrasonic inspection technique is the primary inspection technique for the cast iron insert and covers the volume from the insert envelope surface down to a depth of 200 millimetres. SKBdoc 1179633 describes the original inspection technique (UT31 version 2.0), which is performed using a 2-MHz linear array. The choice of the 2-MHz ultrasonic frequency was made by assuming that the cast iron was expected to be rather attenuating and that a higher frequency would increase the noise level and thereby decreases the sensitivity.

Based on the inspection results obtained for approximately 20 inserts, it was concluded that the cast iron is more homogeneous and less attenuating than expected and that a higher ultrasonic frequency could therefore be used.

With the foregoing factors as a starting point and because it was also discovered that the detection capabilities, analysed by the POD curves (probability of detection) obtained for the side-drilled holes (SDH), were strongly affected by the inspection depth, the need for further development was apparent. The primary focus of the development was to achieve a higher sensitivity and, in particular, more uniform sensitivity along the entire inspection depth.

To define a suitable ultrasonic frequency, several basic, practical trials were performed on test objects with simple geometries, and a reasonable balance between detectability and inspectability was attained at a frequency of 3.5 MHz. Thus, a 128-element linear array probe, as specified in Table 6-1, was obtained, with which the inspection parameters were developed.

Table 6-1. Probe specification for the 0° ultrasonic inspection technique (UT31).

Parameter	Value
Centre frequency	3.5 MHz
Number of elements	128
Pitch between elements	1.0 mm
Passive aperture size	16 mm

To limit the so-called dead zone near the inspection surface, it was determined to continue to use the local immersion technique (Figure 6-8), and by using a water path of approximately 65 mm, the risk of

disturbing the multiple surface echoes within the inspection range was avoided. The scan pattern, a semi-continuous helical scanning sequence, in which the array is moved in the axial direction after each turn of the insert, as shown in Figure 6-9, was retained from the original technique.

The definition of the inspection parameters such as the number of focus depths, focal depths, aperture size and gain settings, were developed by using the integrated simulation tool in the UltraVision software and by conducting practical trials on SDHs at different depths. From the simulation, it was observed that a reasonable uniform sensitivity along the entire inspection depth could be achieved using three different inspection channels with individual phased array settings. The preliminary phased array settings from the simulation were then further optimised by performing practical trials on SDHs at different depths; finally, to facilitate the evaluation of the collected data, individual TCG (Time Corrected Gain) settings were applied for the three different inspection channels. In Table 6-2, the primary phased array parameters for the developed technique (UT31 version 6.0) are summarised.

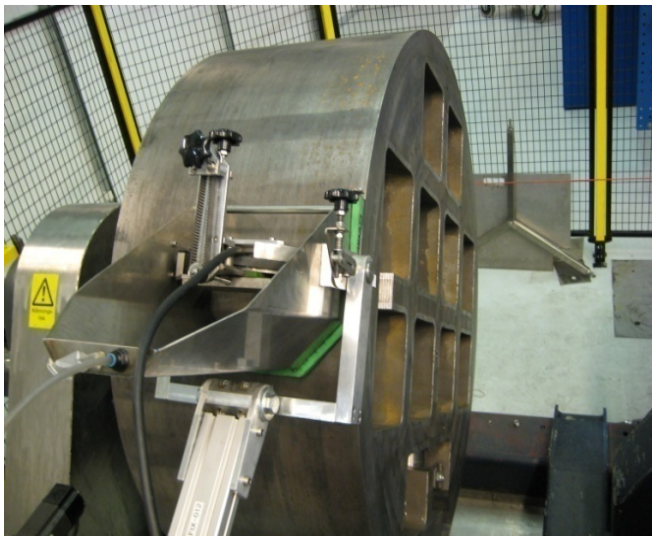

Figure 6-8. *Linear array for local immersion inspection of the cast iron insert.*

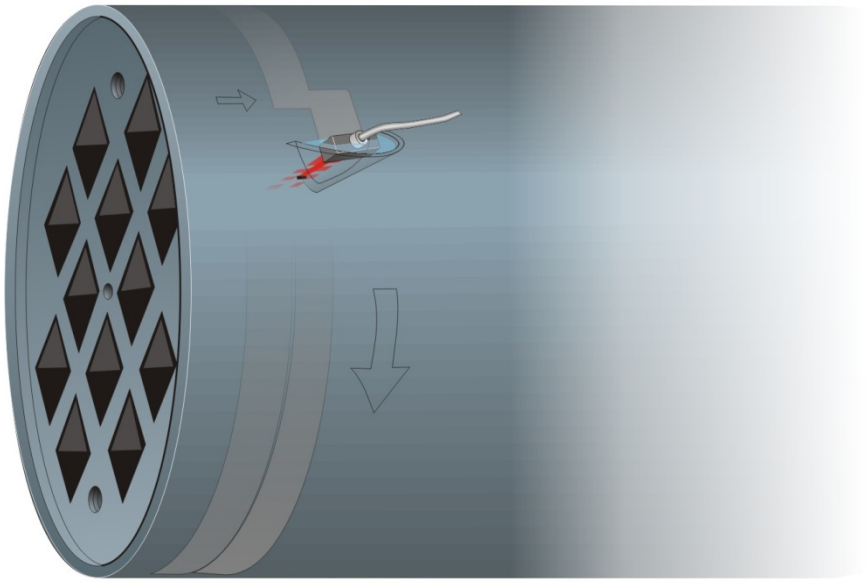

Figure 6-9. *Scan pattern for the normal incidence ultrasonic inspection technique (UT31).*

Table 6-2. Phased array parameters for the 0° ultrasonic inspection technique (UT31).

Inspection channel	Depth range [mm])	Aperture size [number of elements]	Focus depth [mm]
FD12 18elts	5-45	18	12
FD80 32elts	45-110	32	80
FD160 40elts	110-210	40	160

To investigate the effects of increasing the probe frequency from 2 MHz to 3.5 MHz and the effect of the optimised focus parameters on the sound field, simulations were performed (SKB 2013) using the Civa software programme. In the previous setup, two inspection channels with apertures with 24 and 32 elements with focal depths of 80 mm and 200 mm, respectively, were used, whereas in the new setup, three inspection channels are used with the settings listed to Table 6-2. In Figure 6-10 it is shown that the sound pressure is more uniform along the entire inspection depth and also that a narrower sound beam is achieved. The simulations also show that in the future, additional improvements in the developed technique are possible because the focussed beam is not at the middle of the depth of the different inspection channels.

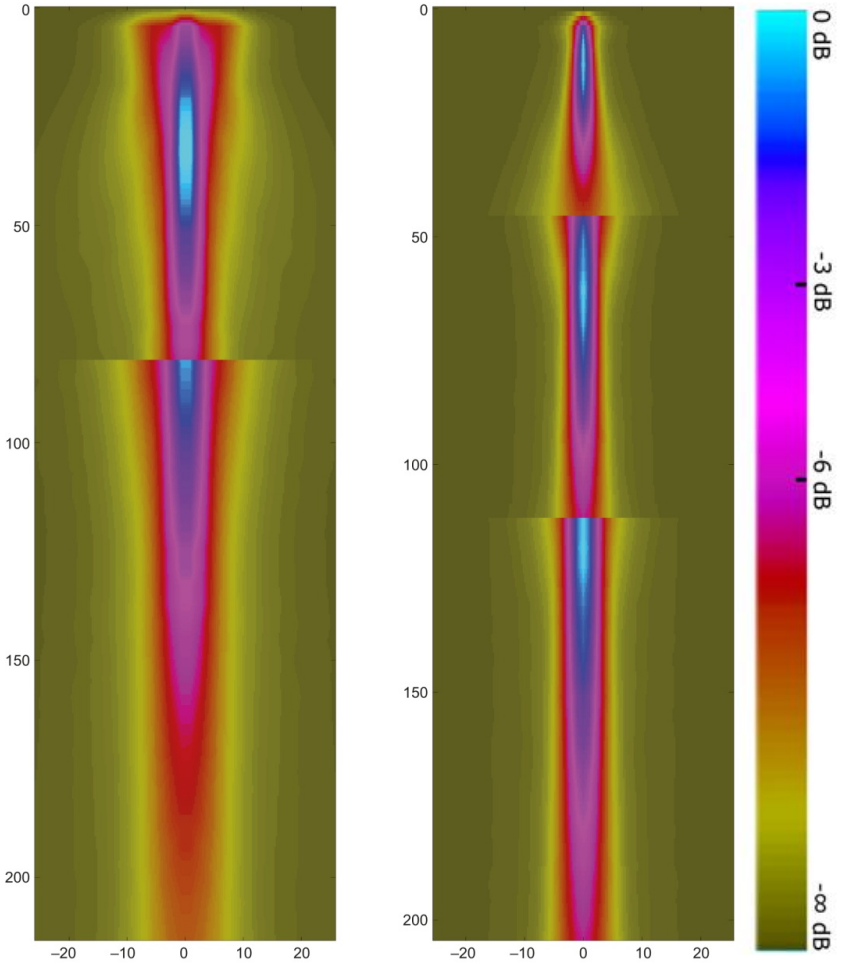

Figure 6-10. *Results from the ultrasonic simulation in Civa. The figures show, with a colour-coded signal amplitude, the width of the sound field in millimetres in the active direction of the array probe (x-axis) as a function of the inspection depth, which ranges from 0 to 200 millimetres (y-axis). The figure on the left shows the original phased array technique (2 MHz), and the figure on the right shows the developed technology (3.5 MHz). The developed technique, which is divided into three focal depths, shows a narrower sound field with more uniform amplitude along the entire inspection depth compared with that of the original technique, which is divided into only two focal depths. Note: the colour-scale is set to 0 dB (maximum amplitude) for each individual focal depth.*

The simulations of the beam for the developed technique in the active direction of the probe showed that improvements can still be made. Therefore, it was assumed that it was necessary to optimise the beam in the non-focussed passive probe direction. To obtain a quantitative measurement of how the probe and focussing could be further developed, a simulation study (SKBdoc 1411571) was initiated. The results showed that the sound field in the passive direction of the probe is clearly wider and less uniform along the depth than the sound field in the active direction. The simulated sound fields are presented in Figure 6-11, and the simulated beam widths are shown in Figure 6-12.

In the next step some possible optimisations of the probe and applied focussing were studied (SKBdoc 1411571). For the active direction, minor potentials to optimise the focus depths were identified, whereas for the passive direction considerable improvements of the sound field could be achieved. A reduction of the depth of the first channels from 0-45 mm to 0-30 mm would be beneficial. This would allow the inspection around the outer channel tube corners and the edge distance measurements to be performed using only one inspection channel (the second), which would clearly simplify the data analysis in this region.

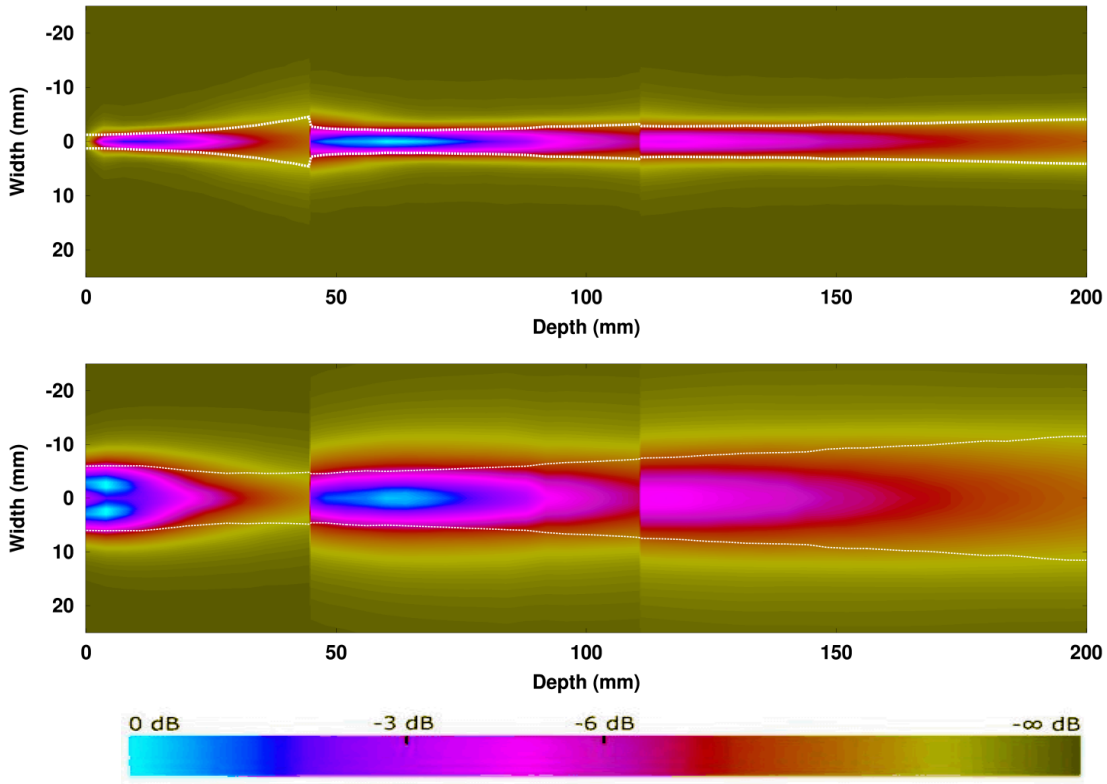

Figure 6-11. *Civa-simulated sound field in the active direction (top) and passive direction (bottom). Note: the colour-scale for each direction (active and passive) is set to 0 dB based on the maximum amplitude.*

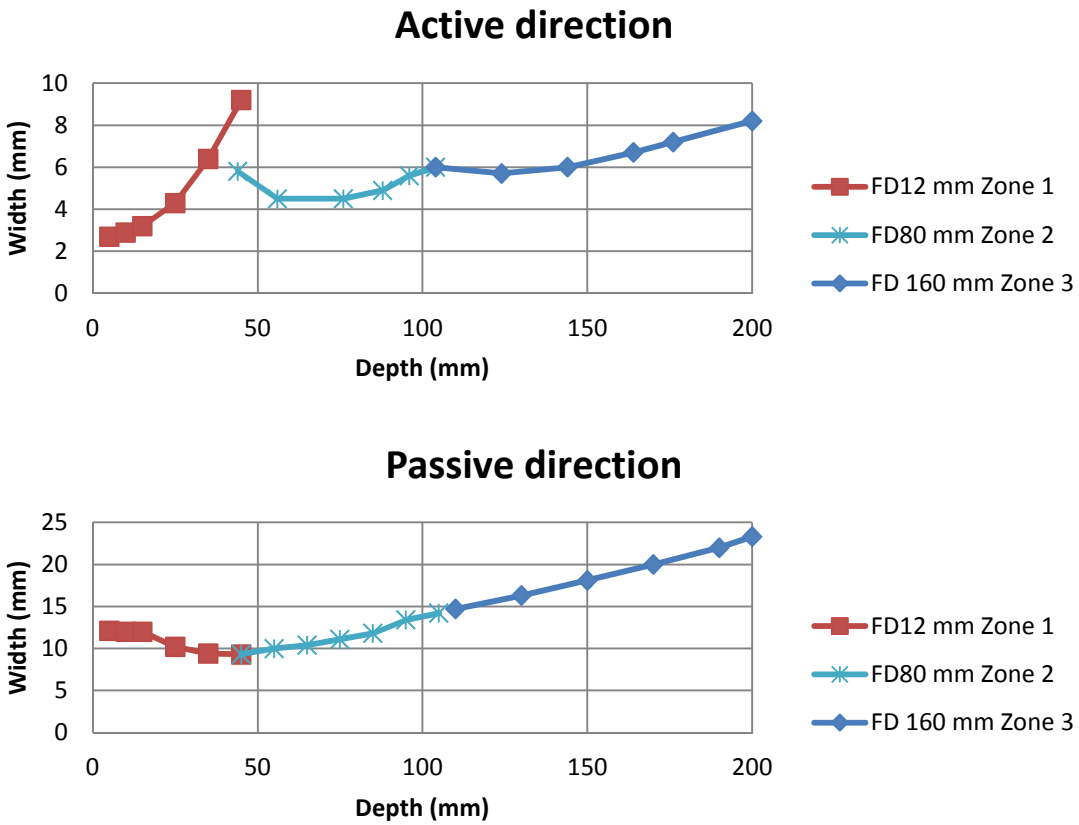

Figure 6-12. *Simulated beam width in the active direction (top) and passive direction (bottom).*

For the passive direction, which was identified as the direction with the most needed improvements, several options were studied (SKBdoc 1411571). The conventional way to achieve these improvements is to mechanically focus the probe; the simulations in Figure 6-13 show that a considerably better focussed beam can be achieved if the inspection is performed using at least two probes (instead of one) focussed at different depths (for example, the yellow and lilac line). In addition, two other focussing techniques were studied, the multi-point focussing technique and the Bessel focussing technique. The multi-point focussing technique uses the central part of the probe for a shallow focal point and the outer part of the probe for a deep focal point; in contrast, the Bessel focussing technique uses a pyramid-shaped probe. Both techniques result in uniform sound fields, even the Bessel focussing technique, which only uses one probe. However, the technique must be further evaluated for its applicability because the simulation showed a risk for side lobes and also because a more complex probe geometry must be considered.

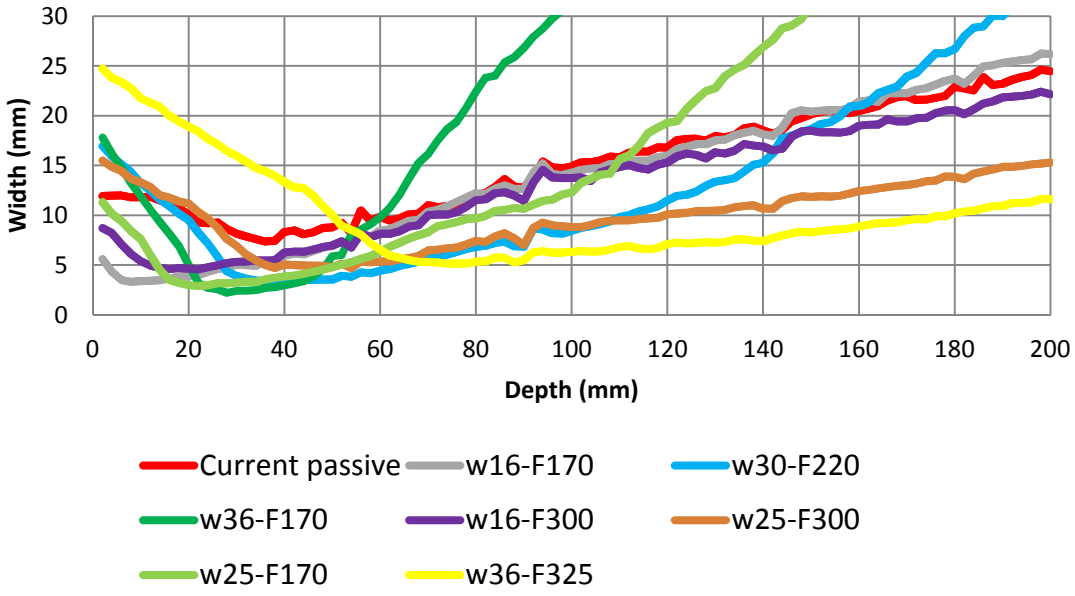

Figure 6-13. *Simulated beam widths, where w= probe width and F=focal distance in water (includes the water path of 65 mm).*

Angular shear wave ultrasonic inspection technique (UT34)

The angular incidence (70°) ultrasonic inspection technique is a complementary inspection technique for the cast iron insert and covers the volume from the insert envelope surface down to a depth of 50 mm. The primary objective of the technique is to detect defects, where the main axis is in the radial-circumferential plane. In earlier projects the TRL (Transmitter Receiver Longitudinal) technique was developed and investigated. SKBdoc 1179633 describes the original inspection technique (UT32 version 2.0), which uses four TRL probes at a frequency of 2 MHz. The TRL technique (UT32) was chosen because it is sensitive near the probe surface and the longitudinal waves are less sensitive to highly attenuating materials.

Experience gathered inspecting a number of inserts using the TRL technique has revealed that interpreting the signals in the region of the outer corner of the fuel channel is extremely difficult. The reason for this difficulty was identified because both longitudinal and transverse waves reflect at the channel tube walls. In Figure 6-14, the typical appearance of the channel tube corner in the B-scan for a TRL probe directed in the circumferential direction is shown. The red indication to the right of the blue line cursor corresponds to the longitudinal reflection at the actual depth of the channel tube corner; whereas the red indication between the red and blue line cursors corresponds to wave mode conversion that hide possible relevant indications in at least 10 mm of the inspection depth.

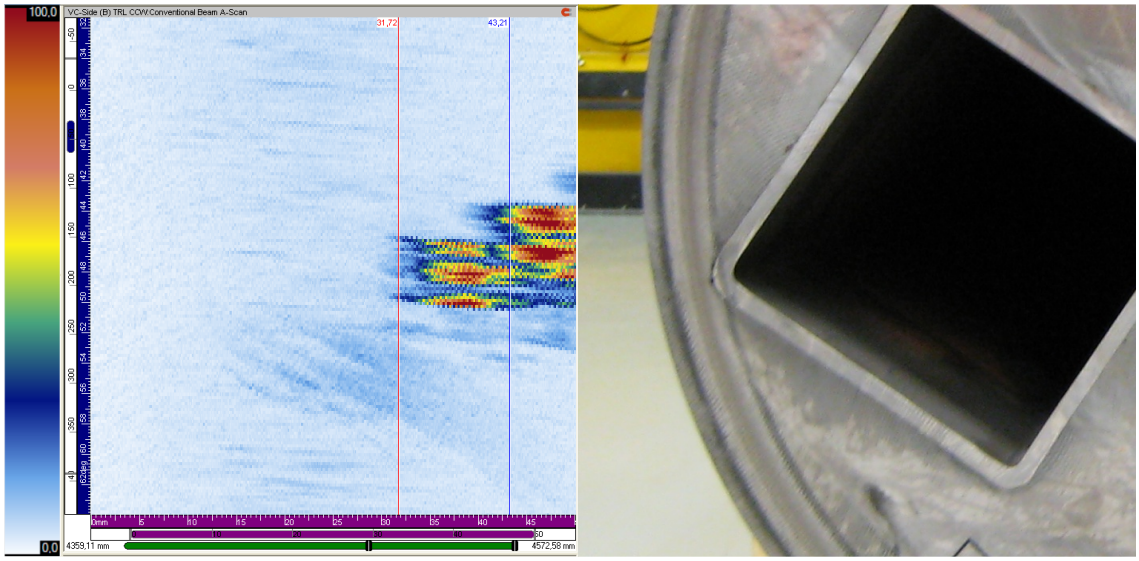

Figure 6-14. *Ultrasonic B-scan (left), where the y-axis represents approximately 30° of the circumference, and the x-axis represents the inspection depth between 0 and 50 mm. The cross-section of the PWR-insert (right) is shown to present an overview of the inspection area.*

Based on the aforementioned observations, a study was initiated to determine whether the inspection could be performed with the use of shear waves. In the first step, the TRL technique was simulated to obtain an understanding of the sensitivity along the inspection depth, and then, a number of different possible probe configurations were evaluated (SKBdoc 1437573). Based on this evaluation, a linear shear wave array was chosen for further analysis.

To define the required characteristics of the probe, a number of parameters were analysed (SKBdoc 1437573). For practical application, limited by the 128 ultrasonic channels in the existing Dynaray ultrasonic equipment, only probes with 32 elements were considered as the approach was, similar to the TRL-technique, to inspect in four directions simultaneously. In the first step, probe simulations were performed for frequencies between 1.5 to 2.15 MHz with active aperture sizes of 67 and 100 mm. Based on the design consideration of obtaining the highest signal-to-noise ratio (SNR) possible and the best focussed beam possible, a probe frequency of 1.7 MHz with an aperture size of 100 mm for 32 elements was chosen. In the next step, the effect of the curvature in the passive direction of the probe was simulated; as shown in Figure 6-15, a significantly better focussed beam is achieved with a curvature, and therefore, a radius of 150 mm was specified.

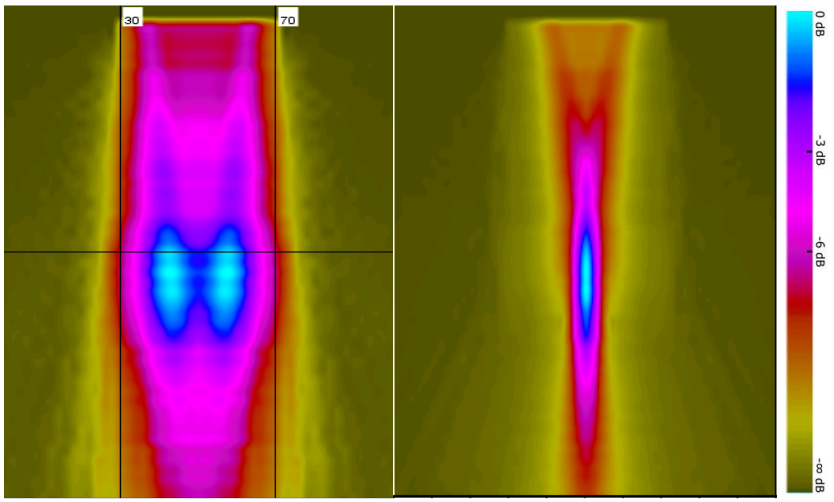

Figure 6-15. *Civa-simulated ultrasonic sound field in the passive direction without mechanical focussing (left) and with mechanical focussing by a radius of 150 mm (right).*

To obtain good inspection performance for the entire inspection depth, the setup was divided into two inspection channels, one for the depth from the outer surface down to a depth of 15 mm and the second for the depth range of 15-50 mm (Figure 6-16).

The defined probe characteristics and the developed focussing parameters were then simulated and compared to those of the original TRL technique. As shown in the simulations of the inspection of side-drilled holes in Figure 6-17, both the spatial resolution and the signal-to-noise ratio (Figure 6-18), particularly for holes at a large depth, clearly improved (holes 2 and 3). Moreover, the irrelevant (due to wave mode conversion) indications visible at the right in the top figure were eliminated by the use of shear waves.

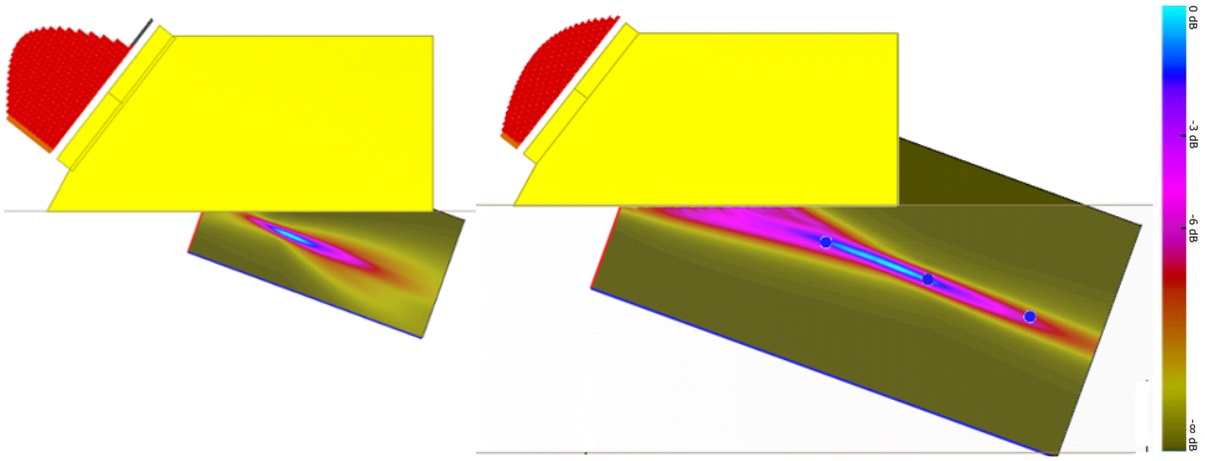

Figure 6-16. *Civa-simulated ultrasonic sound field in the active direction for a depth range of 0-15 mm (left) and for a depth range of 15-50 mm (right).*

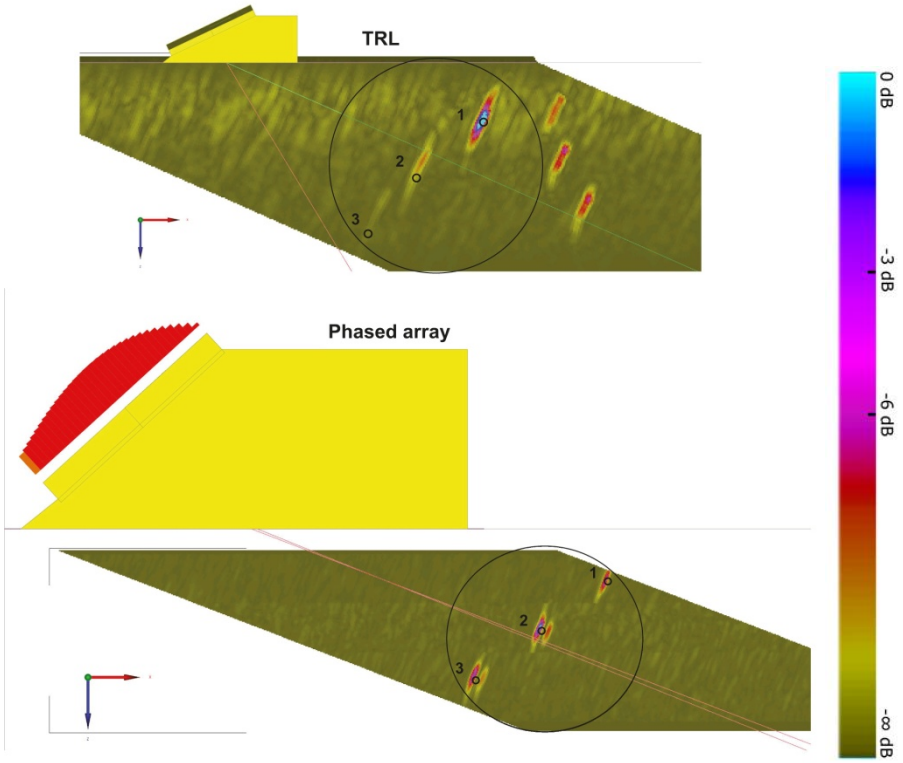

Figure 6-17. *Results from ultrasonic simulations performed in Civa of the inspection of side-drilled holes at depths of 15, 30 and 45 mm (marked 1, 2 and 3, respectively). The top image shows the TRL probe, and the bottom image shows the results obtained with the newly designed array probe.*

The next steps in the development of the inspection technique were to manufacture the curved linear arrays, two arrays adapted to the insert surface for inspection in the axial direction and two arrays for inspection in the circumferential direction, and to design and manufacture a fixture. The probes were manufactured with an integrated water irrigating system, for which the specifications are compiled in Table 6-3, and because the probes were rather heavy (half a kilo each), special attention was given to the design and manufacture of a rigid probe fixture (Figure 6-19).

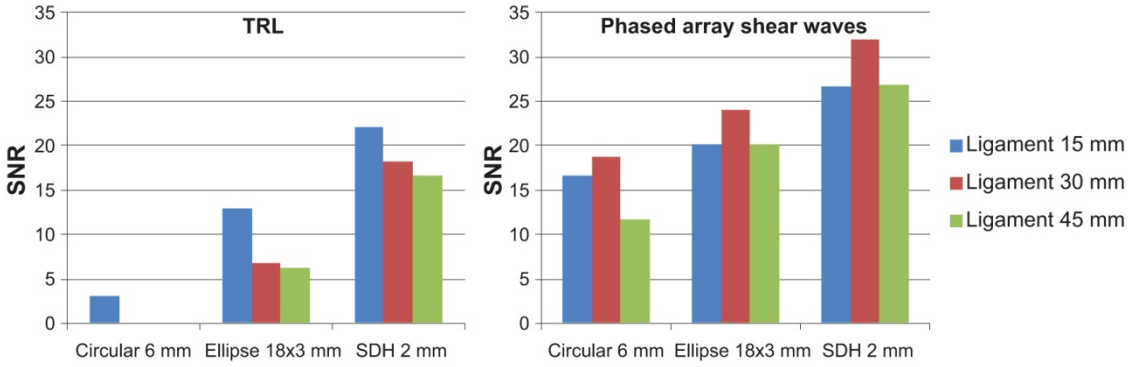

Figure 6-18. *Simulated signal-to-noise ratio (SNR) for different reflectors with phased array shear waves and TRL technique.*

Table 6-3. Probe specification for the angular ultrasonic inspection technique (UT34).

Parameter	Value
Centre frequency	1.7 MHz
Number of elements	32
Nominal angle	70° shear wave
Passive focus	R 150 mm
Pitch between elements	2.1 mm
Passive aperture size	40 mm

Figure 6-19. *Fixture with four 32-element linear arrays (1.7 MHz) for ultrasonic testing of the outer five centimetres with shear waves and approximately 70° incident angle.*

Finally, the inspection setup, which included the fine-tuned focal laws, gain (including TCG) and gate settings, the helical scanning sequence (Figure 6-20), etc., was defined; in addition, instructions for full-scale inspection, including data evaluation, were developed. In Table 6-4, the primary phased array parameters for the developed shear wave angular inspection technique (UT34 version 2.0) are summarised.

Table 6-4. Phased array parameters for the angular ultrasonic inspection technique (UT34).

Inspection channel	Inspection direction	Depth range [mm]	Aperture size [number of elements]	Focus depth [mm]
CCW 0-15	Counter-clockwise	0-16.5	22	10
CCW 15-50	Counter-clockwise	16.5-50	32	30
CW 0-15	Clockwise	0-16.5	22	10
CW 15-50	Clockwise	16.5-50	32	30
Front 0-15	Axial towards the top	0-16.5	22	7
Front 15-50	Axial towards the top	16.5-50	32	30
Back 0-15	Axial towards the base	0-16.5	22	7
Back 15-50	Axial towards the base	16.5-50	32	30

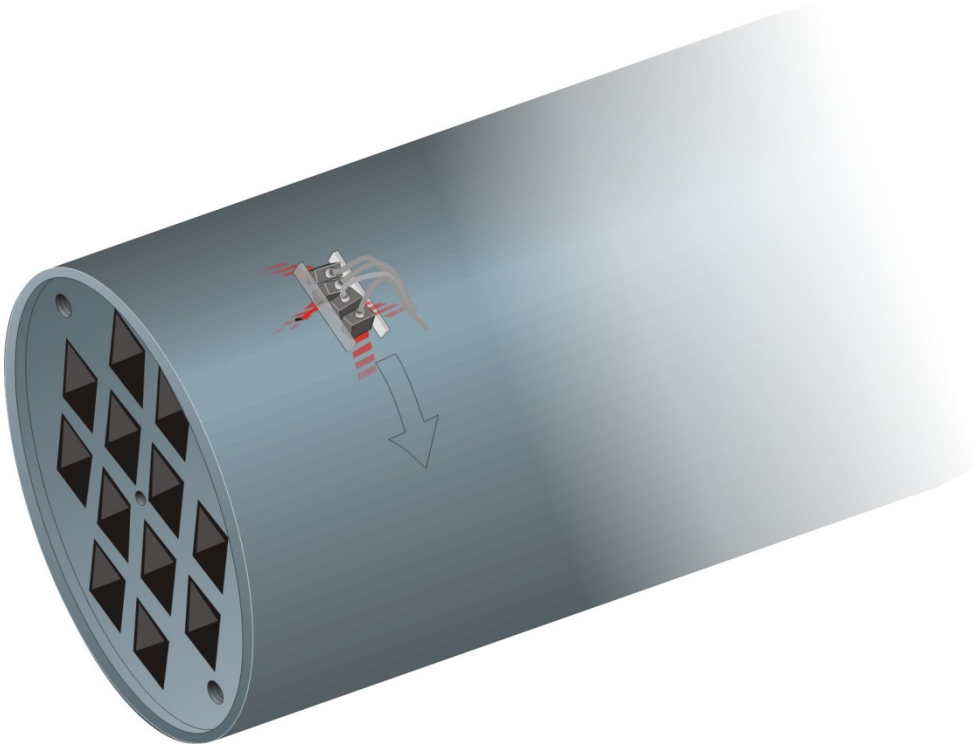

Figure 6-20. *Scan pattern for the angular incidence ultrasonic inspection.*

The majority of the development work of the shear wave angular inspection technique was conducted using ultrasonic Civa simulations. In parallel, also practical trials were conducted. Therefore, it is of special interest to investigate the correlation between the results obtained from the simulations and the actual data. In Figure 6-21, one correlation associated with the inspection simulations of the SDHs at different depths is shown; the results show that there is a good correlation between the simulation results and the actual inspection results.

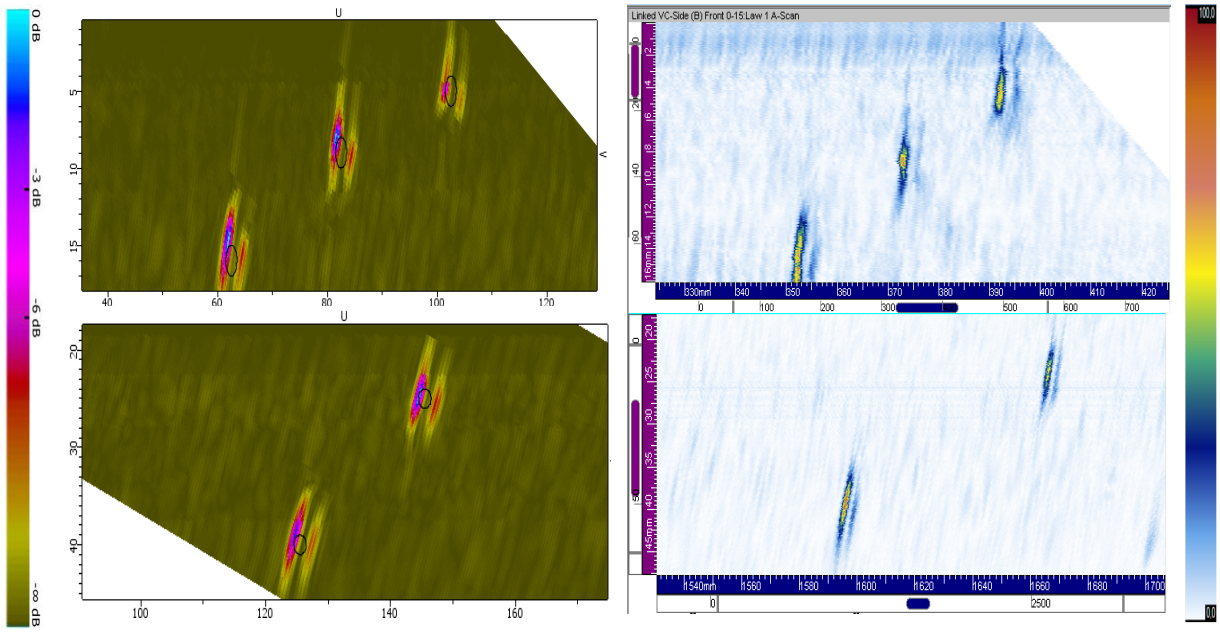

Figure 6-21. *Correlation of the simulated and collected data of side-drilled holes at different depths. The images on the left show the Civa-simulated B-scan, and the images on the right show the collected data. The top images show the results for the shallow inspection channel (SDHs at depths of 4 mm, 8 mm and 15 mm), and the bottom images show the results for the deep inspection channel (SDHs at depths of 24 mm and 39 mm).*

Ultrasonic inspection of the volume between the fuel channels (UT33)

The original ultrasonic inspection technique (UT33 draft version) for the central part of the insert is described briefly in SKBdoc 1179633; two 1-MHz arrays are used in both the pulse echo and in the transmission.

As mentioned previously, the insert material attenuates to a lower degree than expected. Therefore, it was concluded that a higher frequency could also be used for this inspection, and based on some practical trials, a frequency of 2 MHz was chosen.

The inspection of the central part of the insert is the only technique that clearly differs due to the different geometry between the BWR and the PWR inserts. Because the development of the manufacturing process for the PWR insert was the primary focus during this period, the development process began with the creation of an inspection technique for this type of insert. The basis for the development was that the entire volume between the fuel channels should be inspected, where a maximum of 64 ultrasonic channels could be used for each of the two probes.

The development of the inspection technique for the PWR insert was executed in several steps. First, simulations (SKBdoc 1435214) were performed to define the focussing parameters. As a starting point, the same concept used in the original technique was retained: two probes are placed on opposite sides of the insert, and each probe operates in both the pulse echo and transmission mode. The pulse echo channels were created as sector scans using all probe elements from -20° to +20° with a 0.4° step between the inspection angles, yielding a maximum distance between two adjacent inspection angles of 3.35 mm for the centre of the insert. The transmission channels were also created as sector scans. For transmission, all elements were used in a sequence from -3.1° to +3.1° with a 0.24° step between the inspection angles. The focus point is set beyond the centre of the insert to minimise beam spreading. In the receiving aperture, 12 elements adapted to each individual transmitted beam are used. In Figure 6-22, simulations of the pulse echo and transmission inspections of the PWR insert are shown.

The next steps in developing the inspection technique were to manufacture the two curved linear arrays adapted to the insert surface and to modify the Posiva probe fixture (Figure 6-23). The probes were manufactured with an integrated water irrigation system, the specifications of which are compiled in Table 6-5. Finally, the inspection setup, which includes the fine-tuned focal laws, gain and gate settings etc., was defined, and instructions for full-scale inspection, which included data evaluation, were developed (UT33-PWR version 2.0). In Table 6-6, the primary phased array parameters used to inspect the central part of the PWR insert are summarised.

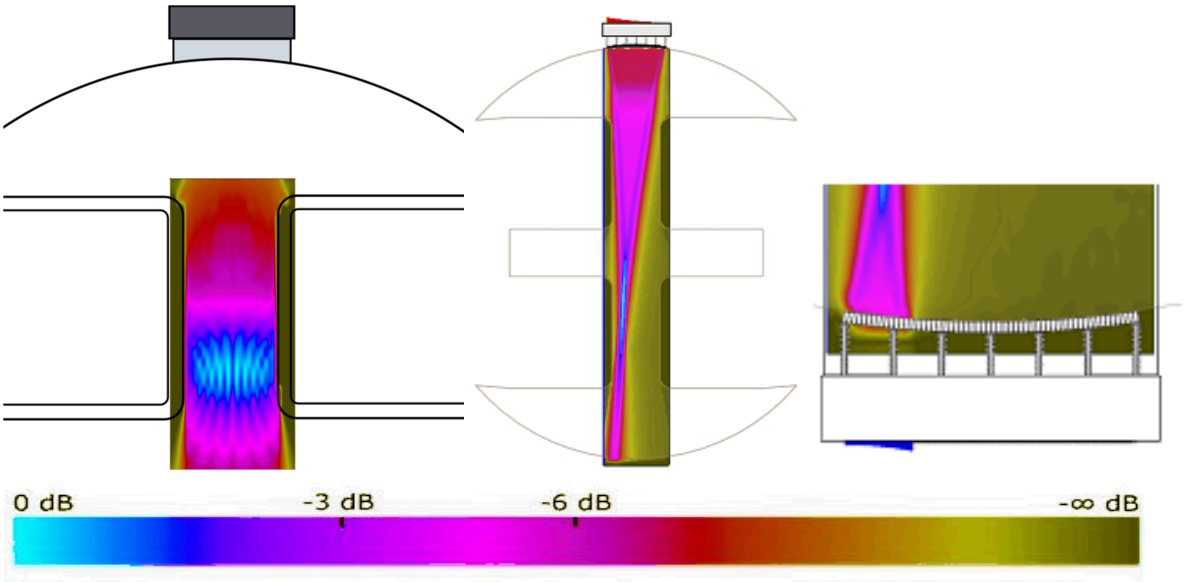

Figure 6-22. *Results from the ultrasonic simulations with Civa, presented with colour-coded signal amplitudes of the ultrasonic technique, for testing the central parts in the PWR insert. The figure on the left shows the pulse echo technique, the middle image shows the transmitted beam in the through-transmission technique and the right image shows the corresponding receiving aperture.*

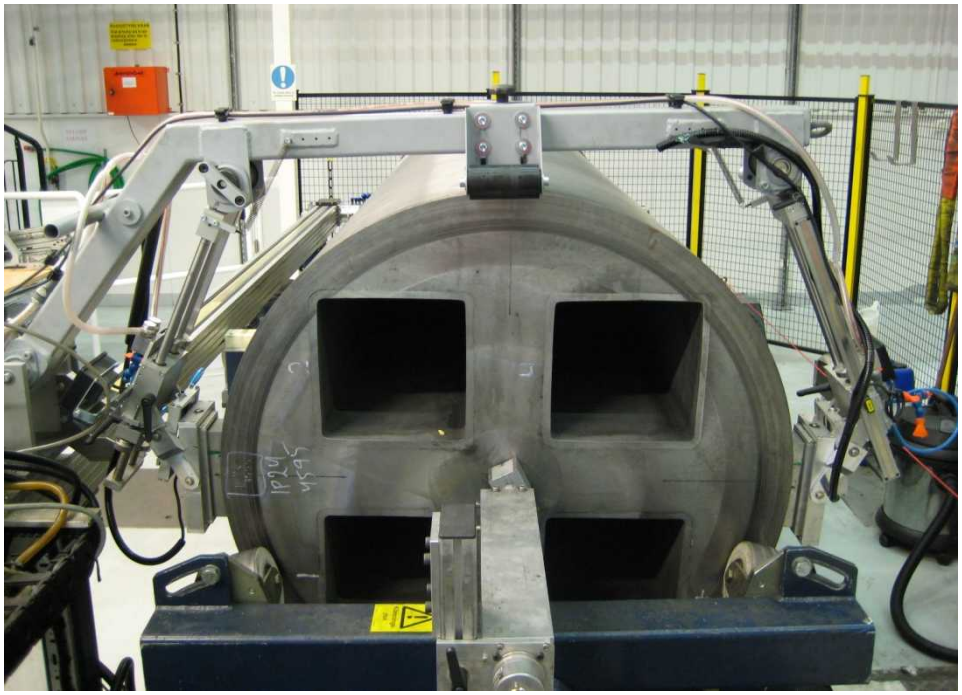

Figure 6-23. *Ultrasonic testing of the volume between the channel tubes in a PWR insert using the Posiva probe fixture.*

Table 6-5. Probe specifications for the inspection of the central part of the PWR insert (UT33).

Parameter	Value
Centre frequency	2 MHz
Number of elements	64
Pitch between elements	2.1 mm
Passive aperture size	40 mm

Table 6-6. Phased array parameters used to inspect the central part of the PWR insert (the index in the inspection channel corresponds to the probe used as the transmitter).

Inspection channel	Inspection angles [°]	Depth range [mm]	Aperture size [number of elements]	Focus depth [mm]
Sector1/ sector 2	±20, resolution 0.4	0-500	64	400
TTU1/TTU2 Transmitter	±3.1, resolution 0.24	0-960	64	600
TTU1/TTU2 Receiver	0	900-1000	12	100

The development of the inspection technique for the BWR insert is based on the technique developed for the PWR insert (UT33-PWR version 2.0). The general principles for the inspection are the same; the same probes and fixture are used, both probes are used as both transmitters and receivers and sector scans are used for the transmitter. The differences are caused by the geometrical differences between the two insert types; 12 channel tubes instead of 4 channel tubes are used and, more importantly, the distance between the channel tubes is 30 mm instead of 110 mm. The latter difference limits the possibility of steering the beam (SKBdoc 1435214), and therefore, the beam size at larger depths is equivalent to the distance between the fuel channels, see the simulation results shown in Figure 6-24. In addition, the BWR insert contains six pathways between the fuel channels, whereas the PWR insert contains two pathways; therefore, a specific set of ultrasonic channels dedicated to the off-centre pathways was created, as described in Figure 6-25. In Table 6-7, the primary phased array parameters developed (UT33-BWR version 1.0) to inspect the central part of the BWR insert are summarised.

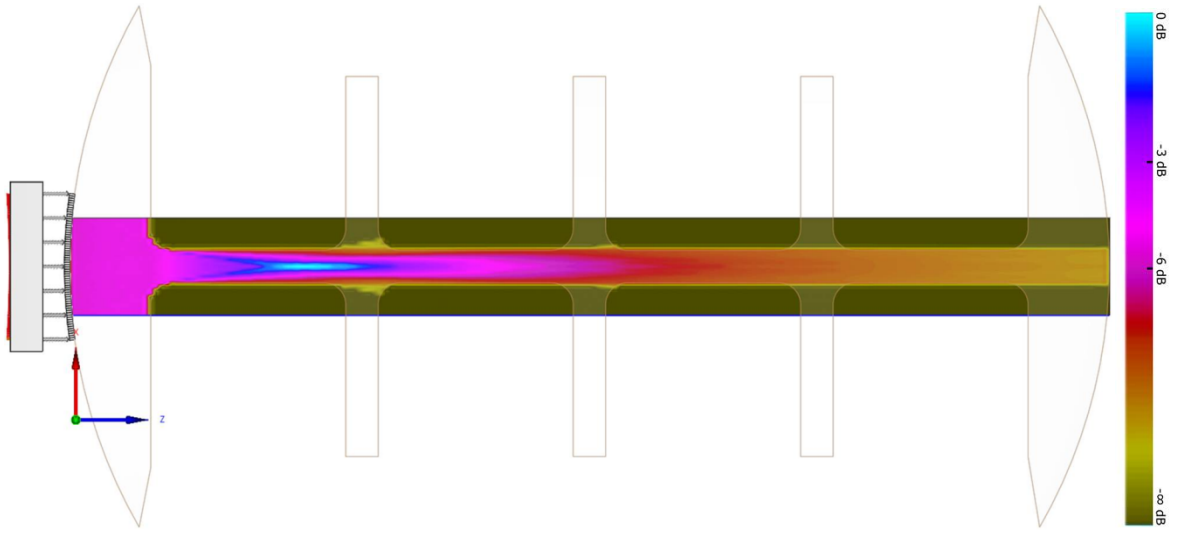

Figure 6-24. *Civa simulation of the sound field for the transmitter beam in the through-transmission inspection of the centre pathway of the BWR insert.*

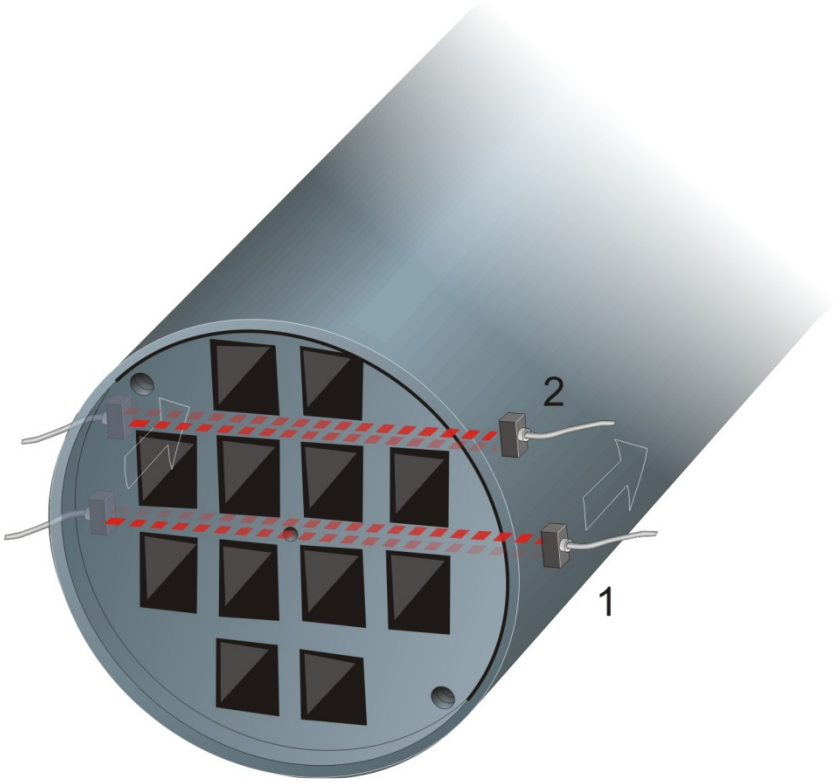

Figure 6-25. *Schematic view of the two different inspection positions for the BWR insert. For the inspection through the centre of the insert (1), two axial scans with a 90° separation are performed. For the off-centre inspection of the insert (2), four axial scans with a 90° separation are performed.*

Table 6-7. Phased array parameters used to inspect the central part of the BWR insert (the index in the inspection channel corresponds to the probe used as the transmitter).

Inspection channel	Inspection volume	Inspection angles [°]	Depth range [mm]	Aperture size [number of elements]	Focus depth [mm]
Sector1/ sector 2	Centre	±16, resolution 0.4	0-500	24	400
TTU1/TTU2 Transmitter	Centre	±3.1, resolution 0.24	0-960	64	600
TTU1/TTU2 Receiver	Centre	0	900-1000	12	100
Sector1/ sector 2	Off-centre	-32 - -16, resolution 0.4	0-500	24	300
TTU1/TTU2 Transmitter	Off-centre	-29 - -20, resolution 0.3	0-900	24	400
TTU1/TTU2 Receiver	Off-centre	-29 - -20, resolution 0.3	820-900	24	400

Surface inspection techniques

The methods developed for the inspection of insert surfaces primarily consist of eddy current inspection and magnetic particle inspection. The magnetic flux leakage method (MFL) has been evaluated to a limited extent on smaller reference parts.

Conventional manual yoke-based magnetic particle inspection with UV-fluorescent particles, similar to the inspection technique that is currently performed by the supplier, exhibits, among other advantages, good detectability for small, linear discontinuities. However, one disadvantage of this manual, arduous technique in inspecting larger components, such as inserts, is reduced efficiency in terms of the probability of detecting defects. The contamination of an insert with a particle suspension could also be a potential drawback of the technique in its subsequent use for insert inspection.

The magnetic flux leakage (MFL) method is an NDT technique that, when combined with mechanised inspection, does not demonstrate the aforementioned drawbacks. The method uses a sensor to detect any leakage of the magnetic field associated with a discontinuity while the adjacent material volume is being magnetised. To evaluate the potential of using the MFL technique for insert inspection, a pre-study was performed. The pre-study results showed that the MFL method could detect surface-breaking, rectangular EDM (Electrical Discharge Machined) notches with length of 8 mm, depth of 1 mm and with width of 0.35 mm. A drawing of the reference object with notches used in the study is shown in Figure 6-26, and some typical results are shown in Figure 6-27. Even notches with a ligament size of 1 mm were, to some extent, detected. One drawback of the MFL method that was identified was the so-called lift-off signal caused by a non-constant gap between the sensor and the component under investigation. Despite this and other drawbacks of the MFL technique, this method demonstrates clear potential for future use in inspecting insert surfaces, and therefore, the techniques development will be closely followed. However, currently, and especially compared with eddy current inspection, it was not judged as the most suitable technique to base a development of a mechanised inspection upon.

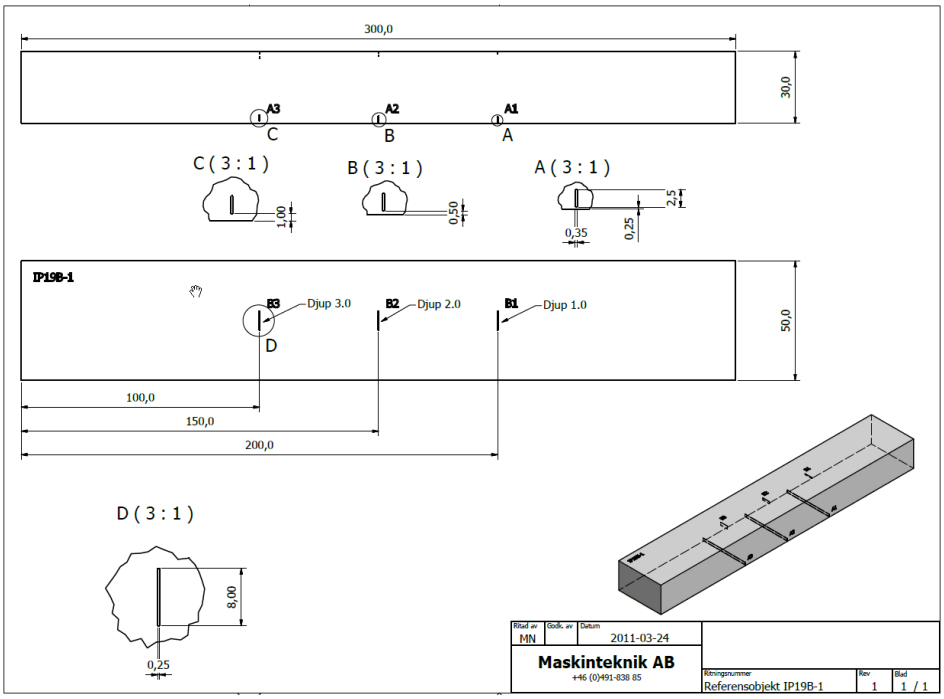

Figure 6-26. *Reference object IP19B-1 made out of nodular cast iron. The EDM-notches are both surface breaking and with ligament.*

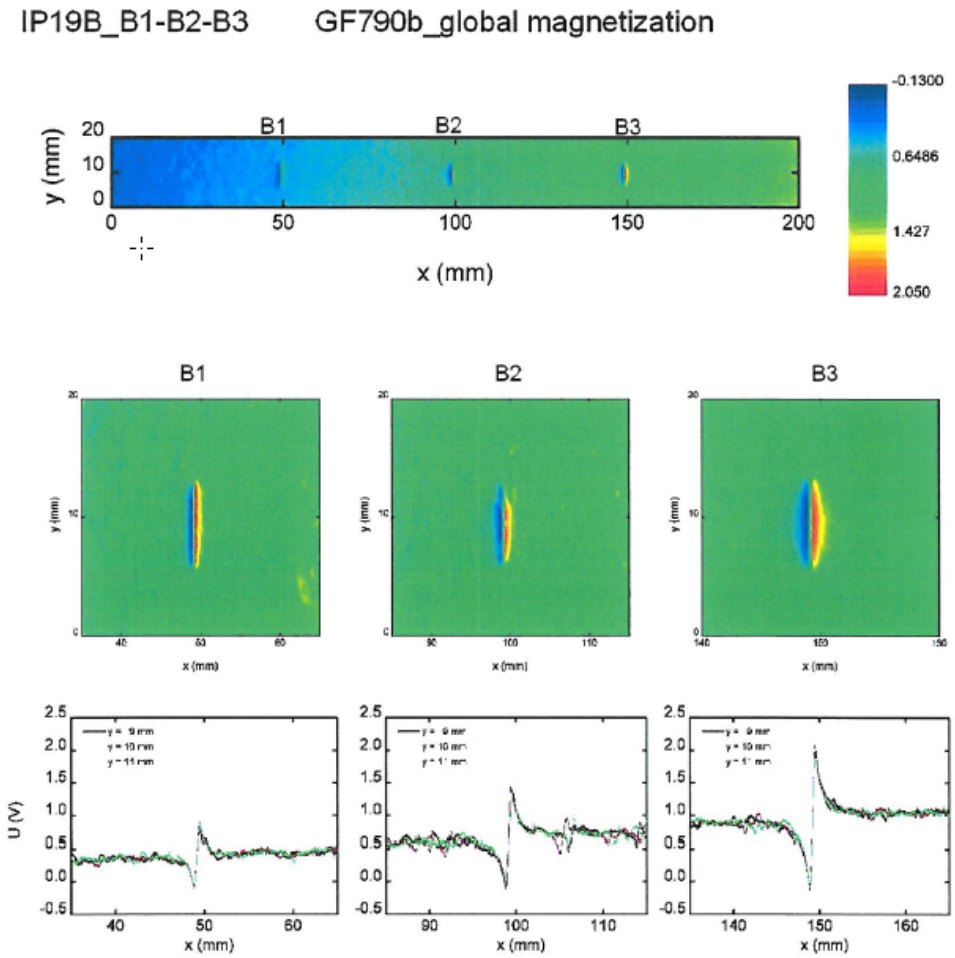

Figure 6-27. *Indications from the surface-breaking EDM-notches on reference object IP19B-1 obtained by the magnetic flux leakage technique (MFL).*

Eddy current inspection is a candidate for the mechanised inspection of insert surfaces. However, the magnetic and electrical properties and their local variations within the nodular cast iron component could pose drawbacks and obstacles, such as a penetration depth that is too shallow due to a high magnetic permeability and signal noise problems due to fluctuating magnetic permeability properties. Some initial trials were performed to select an eddy current probe with the most promising design. The selected probe was a surface probe with an extended sensitivity for sub-surface defects that operates as an absolute sensor with a half-transmission-type build with two adjacent coils in a send-receive circuit, as shown in Figure 6-28.

Initial tests with the eddy current technique on the reference object IP19B-1 (Figure 6-26) revealed that surface-breaking EDM notches and notches with a ligament size of up to approximately 0.5 millimetres can be detected. Figure 6-29 shows the results obtained for reference object IP19B-1. The left image shows the response on the three surface-breaking notches at an excitation frequency of 100 kHz, and the right images show the response on the three notches with ligaments at an excitation frequency of 2.9 kHz.

The next step was to perform a full-scale inspection of the envelope surface of an insert.
Prior to the insert inspection, the sensitivity settings were verified by scanning the reference object, KLM162, which contained surface-breaking elliptical EDM notches. The smallest notch that was detected was a notch with dimensions of 3 x 1.5 mm (length x depth), as shown in Figure 6-30.

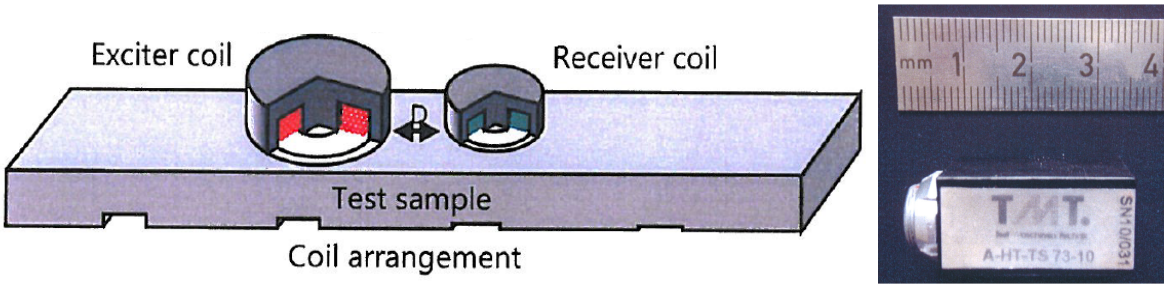

Figure 6-28. *Eddy current probe selected for inspection of insert surfaces. Design principle on the left and photograph on the right.*

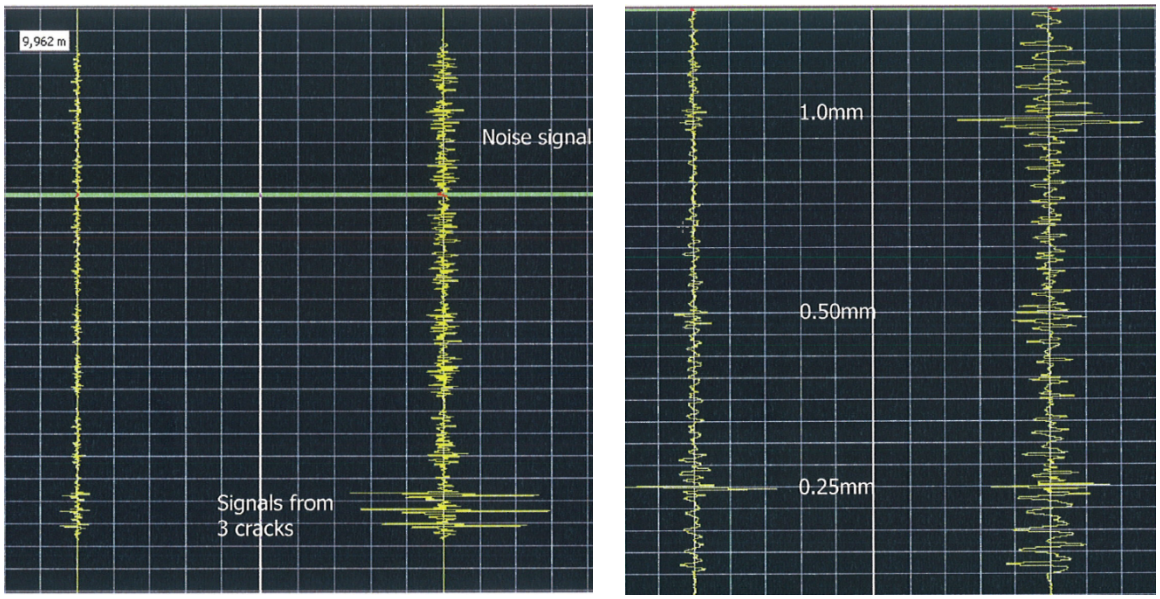

Figure 6-29. *Eddy current inspection results for notches on reference object IP19B-1. To the left, 3 surface-breaking notches detected at an excitation frequency of 100 kHz.*
To the right, 3 notches with ligaments of sizes 0.25, 0.50 and 1.0 mm detected at an excitation frequency of 2.9 kHz.

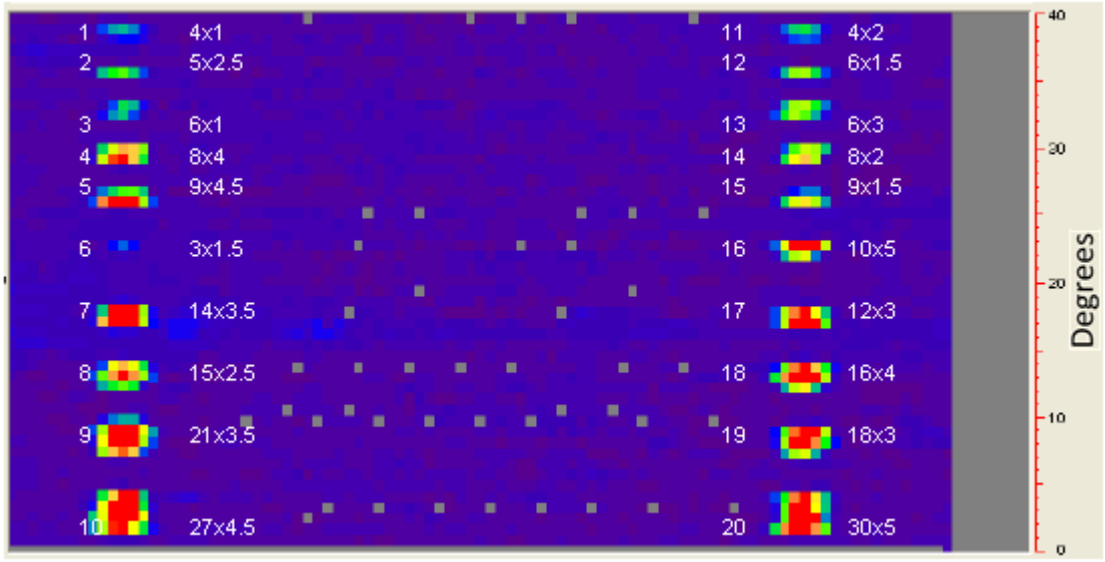

Figure 6-30. *Eddy current inspection result from scanning reference object KLM162 containing surface-breaking elliptical EDM notches. The dimensions are presented in terms of length x depth. The grey pixels correspond to missing data, which are likely due to an encoder issue.*

Several full-scale inspections were performed with the eddy current technique. The results indicated that the material's magnetic/electrical properties were uniform, which is a prerequisite for using the eddy current technique. Figure 6-31 shows an example of inspecting the envelope surface of a nearly 2.5-m-long insert section. The small variations shown were due to conditions such as wear of the probes protective foil (horizontal indications) and the surface conditions related to the support wheels (vertical bands). The narrower band type indications around the axial position 650 mm were due to slight variations in the surface condition. The red circle highlights an encoder-related false indication.

In addition to these indications, there were also periodic indications located approximately 200 mm apart in both directions. These indications, which become even clearer if the gain is increased, as shown in Figure 6-31, coincide with the position of the pole of the yoke used for the magnetic particle inspection of the insert during the acceptance test on the supplier's premises. To more clearly establish the relation, a section of an insert was further machined to remove any magnetic poles at the surface. Thereafter, a magnetic yoke was used to simulate the magnetisation of the insert. The following eddy current inspection could verify the expected effect: the residual magnetic field from the magnetic particle inspection could be observed by the eddy current inspection technique, as shown in Figure 6-32.

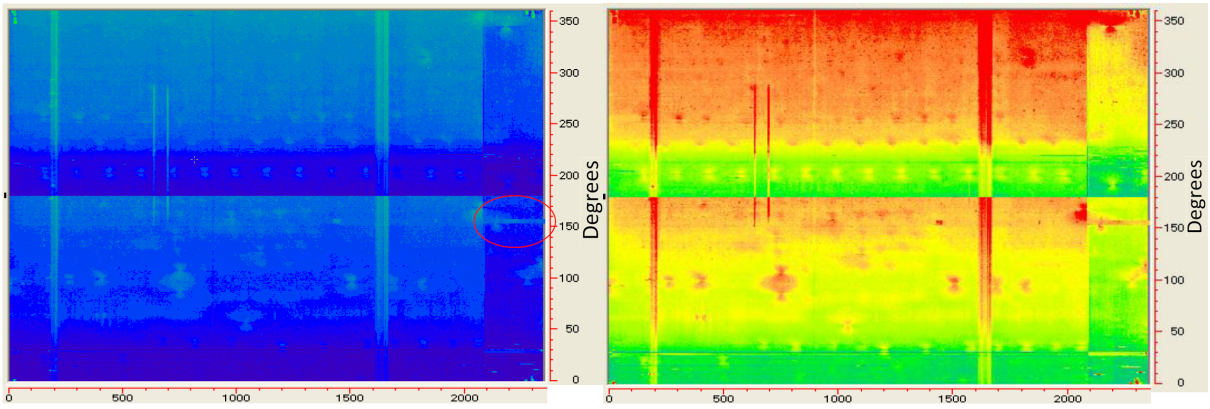

Figure 6-31. *Eddy current inspection results from scanning a nearly 2.5-m-long section of an insert. The results are presented for a low gain (left) and a high gain (right).*

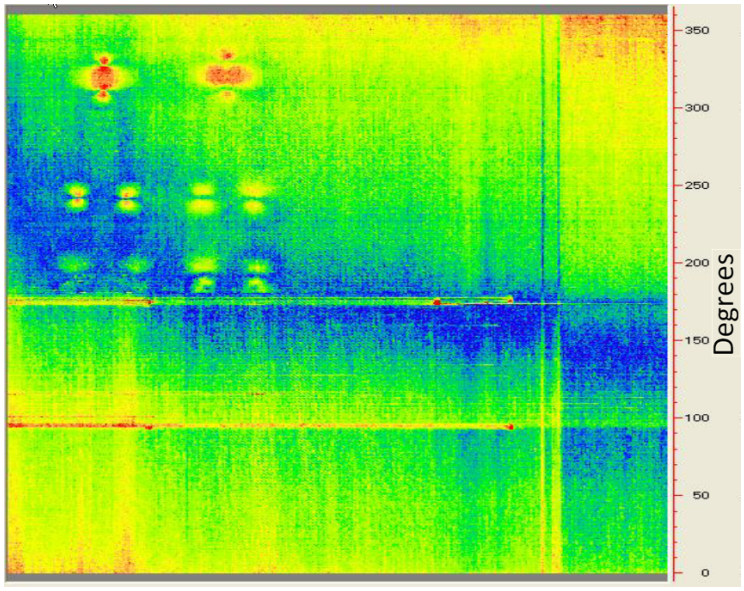

Figure 6-32. *Eddy current inspection results from scanning a section of an insert. The indications in the top left part of the image are verified to be related to residual magnetic fields originating from yoke magnetisation.*

The eddy current inspection of a large component such as an insert with a single probe would be an extremely time-consuming task. Using an eddy current probe with an array configuration, a considerably faster inspection can be achieved. A feasibility study using a primitive prototype eddy current array probe setup was performed. The results obtained from using reference object IP19B-1 are shown in Figure 6-33.

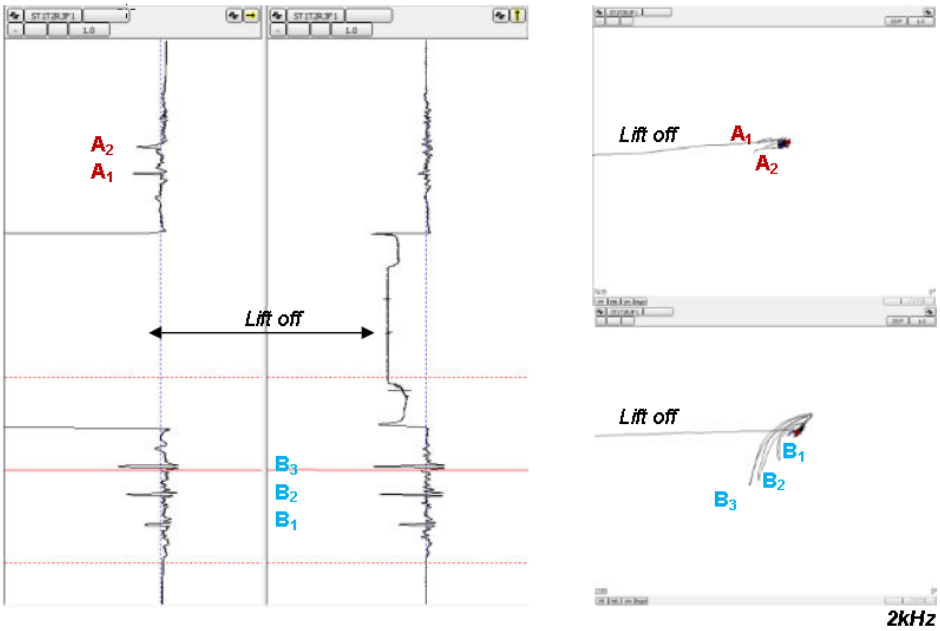

Figure 6-33. *Eddy current array probe inspection results for three surface-breaking notches (B1, B2 and B3) and notches with ligaments (A1 and A2) on reference object IP19B-1.*

6.2.3 Steel lid

Currently, there are no explicit acceptance criteria for NDT established for the steel lid because it is presumed to be manufactured from conventional hot-rolled plates, for which there already exists proven inspection systems that are based on acknowledged practical applications specified in standardised procedures. More precise acceptance criteria are anticipated for the associated lid components, such as the screw, gasket, and valve for atmosphere replacement.

6.3 NDT techniques for the copper tube

In this section, the development process and the actual status of the developed NDT techniques are described for each step in the manufacturing of the copper tube.

6.3.1 Copper tube ingot

The acceptance criteria for NDT of the copper ingot were defined late in this development phase and therefore limited efforts have been made on defining the desired inspections. Because the grain structure in the ingots is extremely coarse, with grain sizes on the centimetre scale and thicknesses of 850 mm, no volumetric inspection is considered.

Machined copper ingots, in addition to being visually inspected, are inspected using a dye penetrant according to international inspection procedures. Some sample results obtained from inspecting the envelope surface and end surface of a machined copper tube ingot are shown in Figures 6-34 and 6-35.

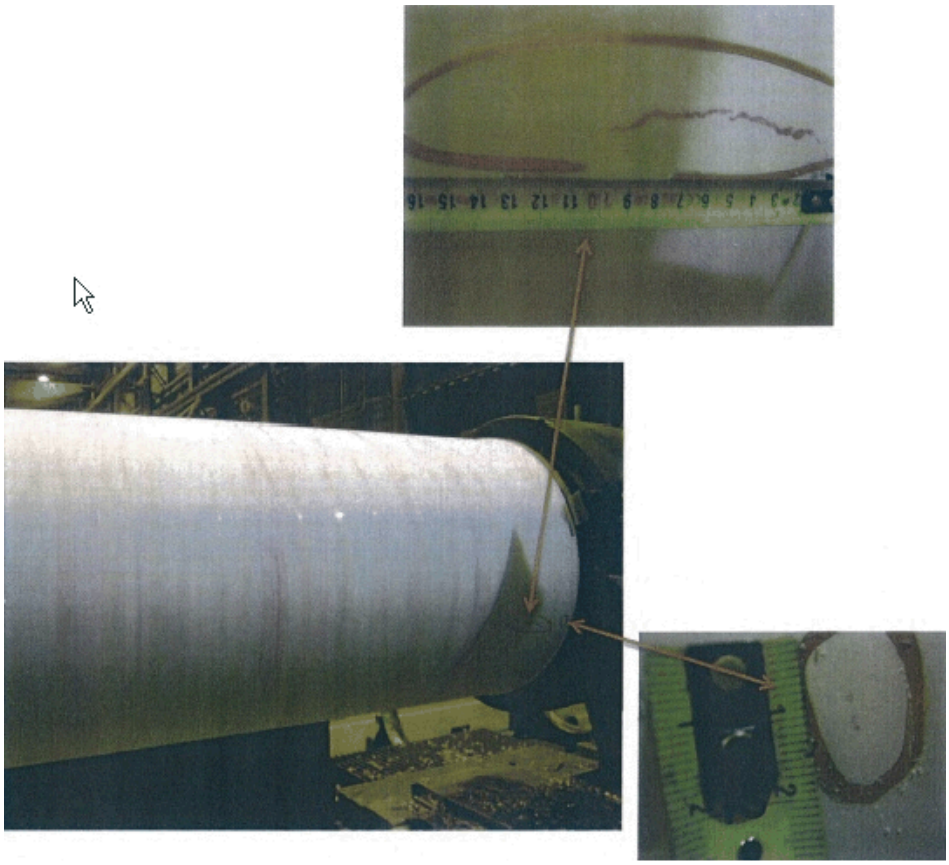

Figure 6-34. *Dye penetrant inspection results on the envelope surface of a machined copper tube ingot. At the top in the close-up photograph, a linear indication is circled.*

Figure 6-35. *Dye penetrant inspection results on the end surface of a machined copper tube ingot. In the centre, two penetrant indications are visible.*

6.3.2 Copper tube

The copper tube is inspected in several steps, as described in Figure 5-1. The first inspections are performed by the supplier as part of an agreement to grant permission for delivery and to minimise the risk for rejection in any of the following inspections. The inspections by the supplier are not currently defined, although they will likely include both ultrasonic and surface inspections.

The final inspection of the copper tube, which is planned to be performed in the canister factory to verify that the tube fulfils the acceptance criteria, is performed in two steps. The ultrasonic inspections are performed in the first step, when the tube is machined to the pre-machined state with excess material thickness. In this manner, the entire volume will be inspected as the volume near the inspection surface, where the sensitivity of the ultrasonic techniques is limited, will be removed in the final machining. Finally, the surface is inspected by dedicated surface inspection techniques after being machined to its final dimensions. In addition to the final inspection, the recently defined acceptance criteria for NDT of the tube (SKBdoc 1414374, 1432038) specify the need to inspect the tube between the hot-forming steps in the stage of the so-called blocker.

In the following sections, the status of the inspections performed by the suppliers and that of the ultrasonic and surface inspection techniques developed at the Canister Laboratory are described.

Inspections by the supplier

Currently, the suppliers do not perform any NDT on the manufactured tubes, one reason being that the extruded tube supplier does not have the resources to machine the tubes to the pre-machined state.

In the future, it is likely that SKB will require a general ultrasonic inspection and surface inspection to be performed by the supplier to permit delivery of each component.

Ultrasonic inspection techniques

The previous NDT report (SKBdoc 1179633) describes how the tube is originally inspected by both a normal incidence (0°) ultrasonic inspection technique (UT11 version 1.0) using a 5-MHz linear array and by an angular incidence (45°) ultrasonic inspection technique (UT12 version 1.0) using four conventional shear wave probes, two in the axial direction and two in the circumferential direction.

During the NDT development, surface defects were identified as to be the most probable occurring defects, while the presence of different kind of internal defects was assumed to be rare. This assumption has further been supported by the acceptance criteria presented in section 4.2.2 in which no internal defects is specified and thereby the primary purpose of the ultrasonic inspection is to detect unknown defects. Thus, it was determined that one ultrasonic inspection technique is adequate, and therefore, the angular inspection technique is excluded. The scan pattern, the semi-continuous helical scanning sequence through which the array is moved in the axial direction after each turn of the insert, as shown in Figure 6-36, was retained from the original normal incidence technique.

With the foregoing factors as a starting point and because it was discovered that the detection capabilities, analysed by the POD curves obtained for side-drilled holes, were affected by the inspection depth, the need for further development was verified. The primary objective in the development of the phased array technique was to achieve more uniform sensitivity along the entire inspection depth and to develop a technique that is less sensitive to variations in grain structure. To define a suitable ultrasonic frequency some basic, practical trials were performed on test objects with a simple geometry, and a reasonable balance between the detectability and inspectability was achieved at a frequency of 3.5 MHz. Thus, a 128-element linear array probe (see specification in Table 6-8) was used, with which the inspection parameters were developed.

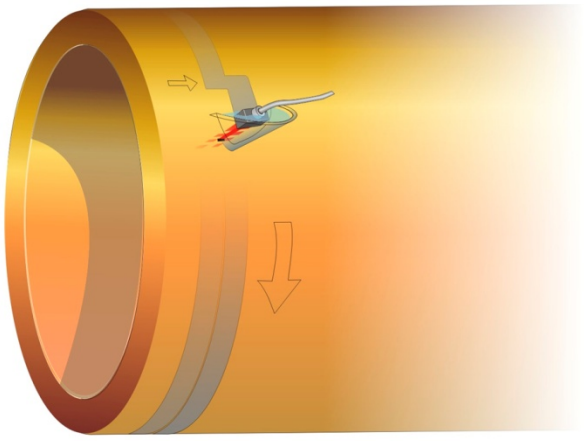

Figure 6-36. *Scan pattern for the normal incidence ultrasonic inspection.*

Table 6-8. Probe specification for the 0° ultrasonic inspection technique (UT11).

Parameter	Value
Centre frequency	3.5 MHz
Number of elements	128
Pitch between elements	1.0 mm
Passive aperture size	16 mm

To limit the so-called dead zone near the inspection surface, it was determined that the same local immersion technique described for the insert should continue to be used (Figure 6-8). By using a water path of approximately 30 mm, the risk of disturbing multiple surface echoes over the defined inspection range was excluded. The inspection parameters such as the number of focus depths, focal depths, aperture size and gain settings, were defined using the integrated simulation tool in the UltraVision software program and by performing practical trials on SDHs at different depths. From the simulation results, it was observed that reasonable, uniform sensitivity along the entire inspection depth could be achieved using two different inspection channels with individual phased array settings. The preliminary phased array settings from the simulation were then further optimised by performing practical trials on SDHs at different depths; finally, to facilitate the evaluation of the collected data, individual TCG settings were applied for the two different inspection channels.

Simulations were performed (SKB 2013) using the Civa software programme to investigate the effect of decreasing the probe frequency from 5 MHz to 3.5 MHz and the effect of the optimised focussing parameters on the sound field. In the original setup, one inspection channel, with apertures using 16 elements and focal depths of 55 mm, were used, whereas in the developed (UT11 version 2.0) setup, two inspection channels are used with the settings reported in Table 6-9. The results (Figure 6-37) show that the sound pressure is more uniform along the entire inspection depth.

Table 6-9. Phased array parameters for the 0° ultrasonic inspection technique (UT11).

Inspection channel	Depth range [mm]	Aperture size [number of elements]	Focus depth [mm]
FD10 12elts	0-20	12	10
FD40 16elts	20-55	16	40

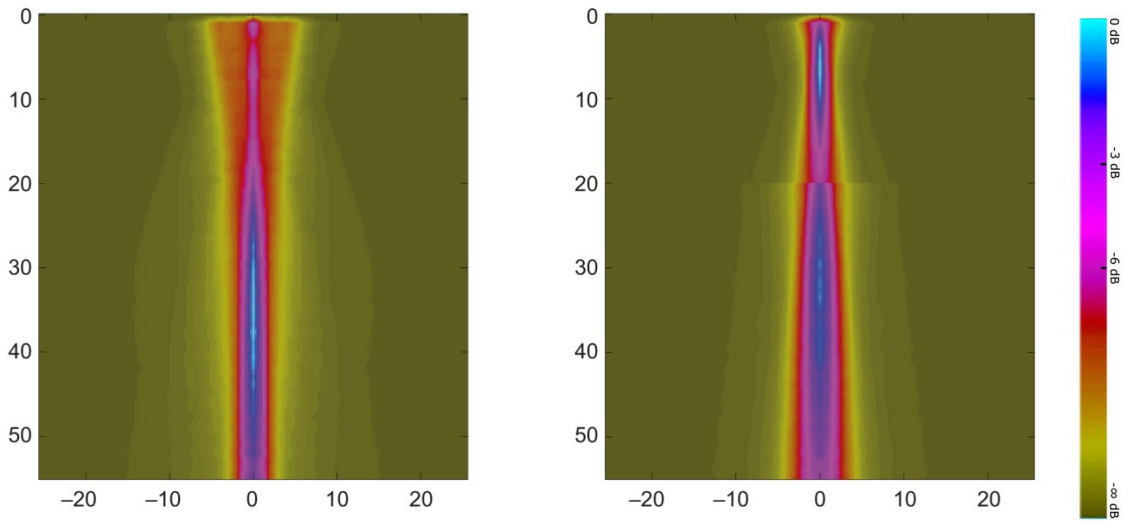

Figure 6-37. *Results from the ultrasonic simulations in Civa. The figures show, with a colour-coded signal amplitude, the width of the sound field in millimetres in the array probe's active direction (x-axis) as a function of the inspection depth, from 0 to 54 millimetres (y-axis). The left-hand figure shows the original phased array technique (5 MHz), and the right-hand figure shows the developed technique (3.5 MHz). The developed technique, which is divided into two focal depths, resulted in a more uniform sound field along the entire inspection depth compared with that of the original technology with only one focal depth.*

The recently defined requirement that the blocker must be inspected (SKBdoc 1414374), has so far resulted in that only few initial studies have been performed in this respect. In these studies, three blockers (for manufacturing copper tubes T65, T66 and T67) were inspected by a 5 MHz linear array. The results shown in Figure 6-38 indicate that the attenuation in the blockers is rather low and homogeneous, which allows for the possibility of developing ultrasonic inspection techniques.

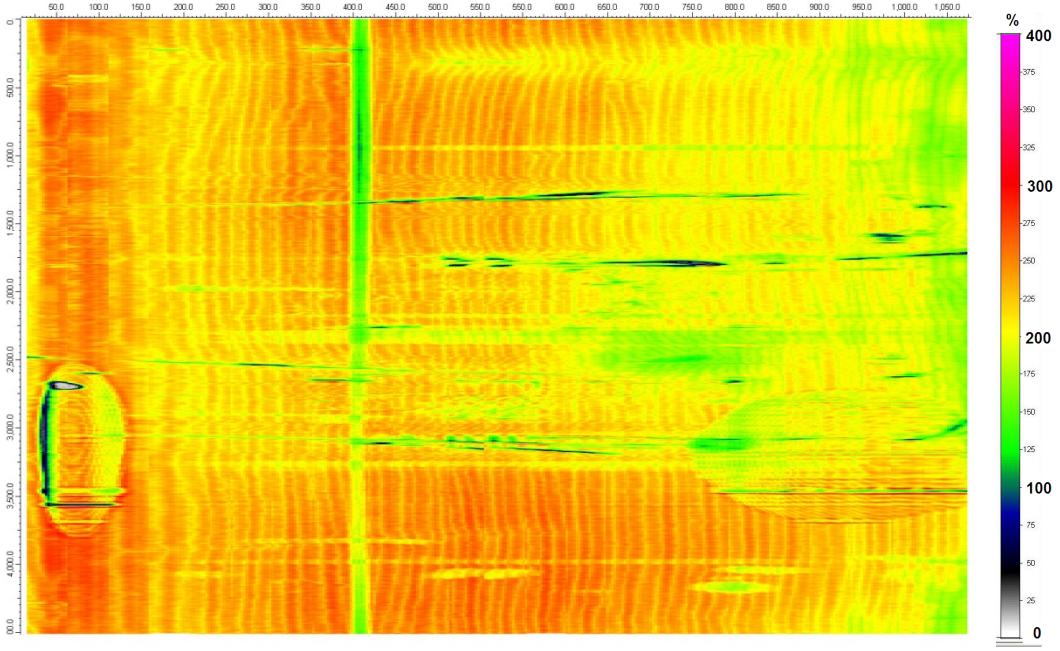

Figure 6-38. *C-scan of the back wall echo amplitudes from ultrasonic inspection of the blocker in the manufacturing of copper tube T67. The x-axis represents the axial direction, and the y-axis represents the circumferential direction of the blocker. The deviating areas are due to surface damages or areas that not have been machined.*

Surface inspection techniques

The technique for testing of the surfaces of the copper components with array technique for eddy currents will be further developed. As a basis for this development, the experiences from the development of the eddy current technique applied to the friction stir weld will be used.

6.4 NDT techniques for the copper lid/base

In this section, the development process and the status of the developed NDT techniques are described for each step in the manufacturing of the copper lid and base. The copper lid and base are inspected in several steps, as described in Figure 5-1, and as the inspections are performed in the same way, only the lid will be further discussed.

6.4.1 Copper lid ingot

Historically, no inspection other than a general visual inspection of billets and ingots used to forge the lid has been performed. However, it is assumed that some type of surface inspection of the billets/ingots will be applied. The results obtained up to this point indicate that to perform an adequate inspection, the component surfaces must be machined.

6.4.2 Copper lid

The first inspections are performed by the supplier as part of an agreement to obtain permission for delivery and to minimise the risk for rejection in any of the following inspections. The inspections by the supplier are not defined currently, although they will likely include both ultrasonic and surface inspections.

The final inspection of the copper lid, which is performed at the canister factory to verify that the lid fulfils the acceptance criteria, is performed at two stages. Ultrasonic inspections are performed in the first stage, which is when the lid is machined to the pre-machined state with excess material thickness. In this manner, the entire volume will be inspected as the volume near the inspection surface, where the sensitivity of the ultrasonic techniques is limited, will be removed in the final machining. Finally, the surface will be inspected using dedicated surface inspection techniques after it has been machined to its final dimensions.

In the following sections, the status of the inspections performed by the suppliers and that of the ultrasonic and surface inspection techniques developed at the Canister Laboratory are described.

Inspections by the supplier

No inspection other than a general visual inspection of the lid in its pre-machined stage is presently performed by the supplier. However, it is assumed that some type of ultrasonic and surface inspection is to be performed by the supplier on the lid in the component's pre-machined state.

Ultrasonic inspection techniques

The previous NDT report (SKBdoc 1179633) describes how the lid originally is inspected by six normal incidence (0°) ultrasonic immersion techniques (UT21-UT26 version 1.0), one for the inner thin part of the lid and five for the thick outer flange, using a 5-MHz linear array.

The basic evaluation and the further development of these inspection techniques were performed in the same way as those for the normal incidence (0°) ultrasonic inspection technique for the copper tube. For example, it was determined that the same probe (Table 6-8) should be used and that the same focussing parameters should be used for the inner thin part of the lid, which has the same thickness as the tube wall.

During the development of the inspection techniques, the ultrasonic settings were not the only factor considered. One important factor was that the design of the pre-machined state was re-designed to facilitate ultrasonic inspection. Figure 6-39 shows the previous and new design of the pre-machined lid. Another change that was made to facilitate ultrasonic inspection was that the primary inspections were applied from the bottom side of the lid (Figure 6-40) with the lid turned upside-down, which simplified access because all inspections in the axial direction could be performed from a flat surface.

Additionally, the use of a sealing plate that sealed the entire top surface of the lid during the inspection eliminated variations in the back wall echo caused earlier by areas that had water instead of air in contact with the back wall surface.

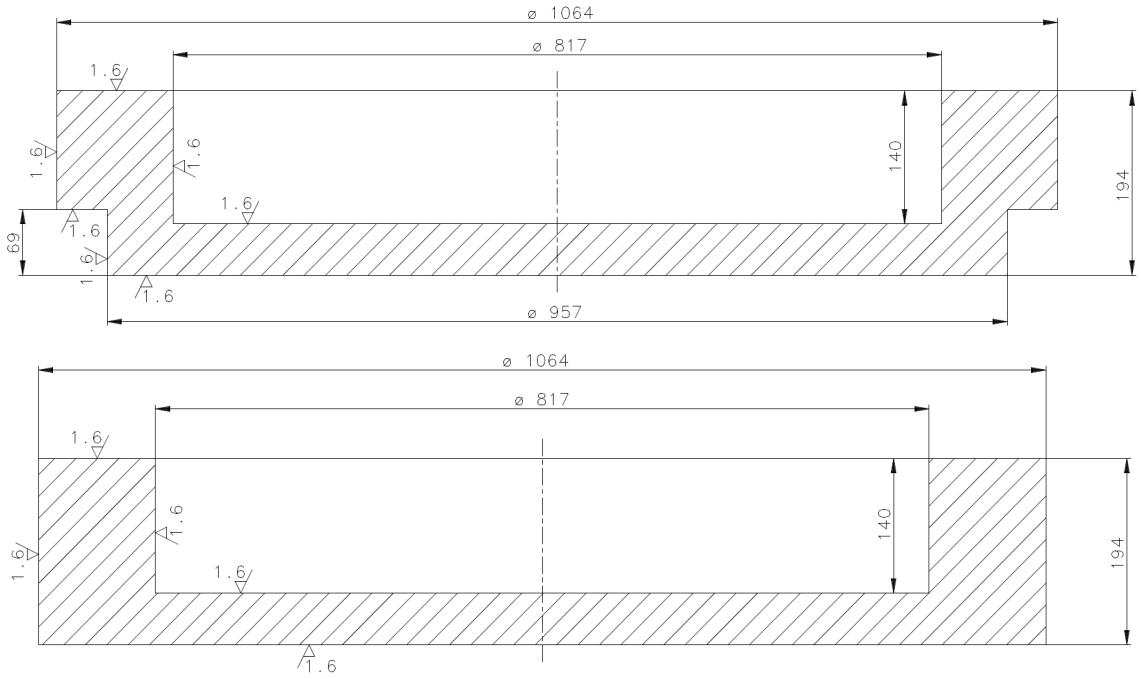

Figure 6-39. *Design of the pre-machined lid: the previous design (top) and the new design (bottom).*

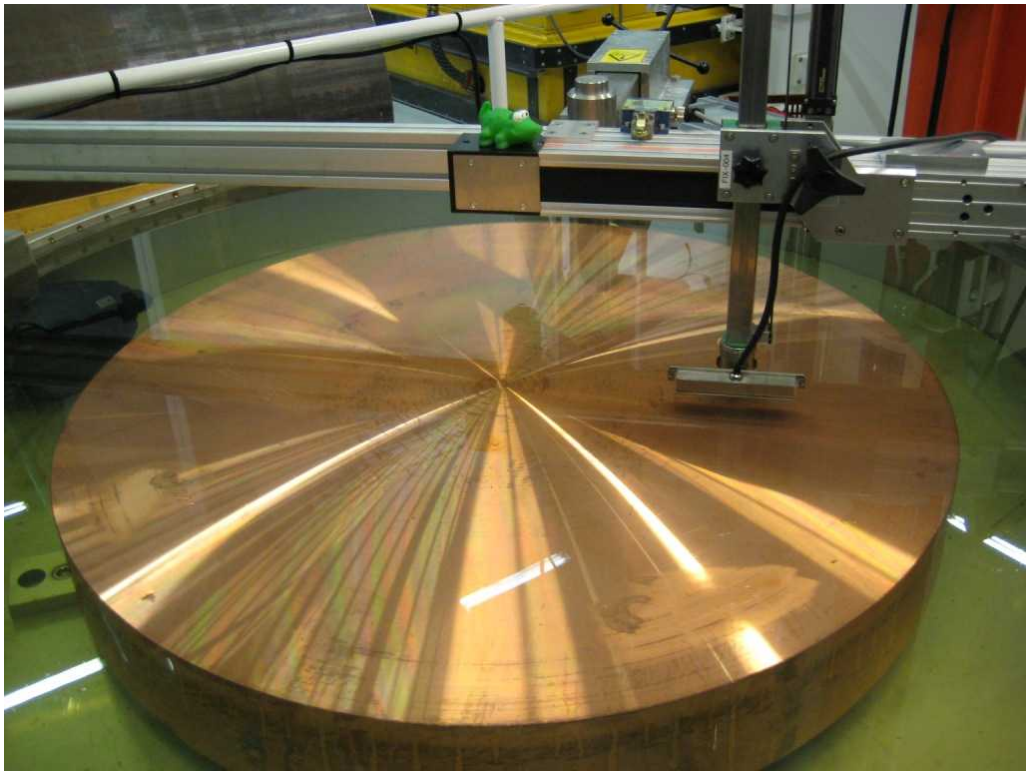

Figure 6-40. *Inspection of the copper lid from the bottom side.*

The first plan was to inspect the lid by three different setups using a normal (0°) incidence sound field, one in the axial direction for the thin inner part of the lid and one in both the axial and radial direction for the thick outer flange. However, it was discovered that because rather large apertures were used for inspections at larger depths, a significant portion of the volume near the flange surfaces was not covered. Therefore, two additional setups were defined with a slightly inclined sound field (±10°). Figure 6-41 shows a schematic view of the different setups.

The practical application of the ultrasonic inspection of the copper lid is controlled by an inspection instruction (UT27) and consists of three sequences: one for the central part (A) and two for the bottom (B, C) and side surfaces (D, E) of the thick outer flange. For all sequences, a semi-continuous helical scan pattern is used. To inspect from the bottom, the array is moved in the radial direction after each turn of the lid, whereas to inspect the from the outer envelope surface, the array is moved in the axial direction after each turn.

The inspection parameters, such as the number of focus depths, focal depths, aperture size and gain settings, were defined using the integrated simulation tool in the UltraVision software programme and by conducting practical trials. To inspect the thin central part of the lid, the same inspection parameters applied for the copper tube were used, and thereby, the same sound field was expected (Figure 6-37). The inspection of the thick outer flange was originally performed, both in contact and an with a water column, whereas the developed technique was only performed with a water column with a height of 65 mm. Figure 6-42 clearly shows that the sound field is much more uniform along its length with the developed technique. In Table 6-9, the primary phased array parameters for the developed technique (UT27 version 1.0) are summarised.

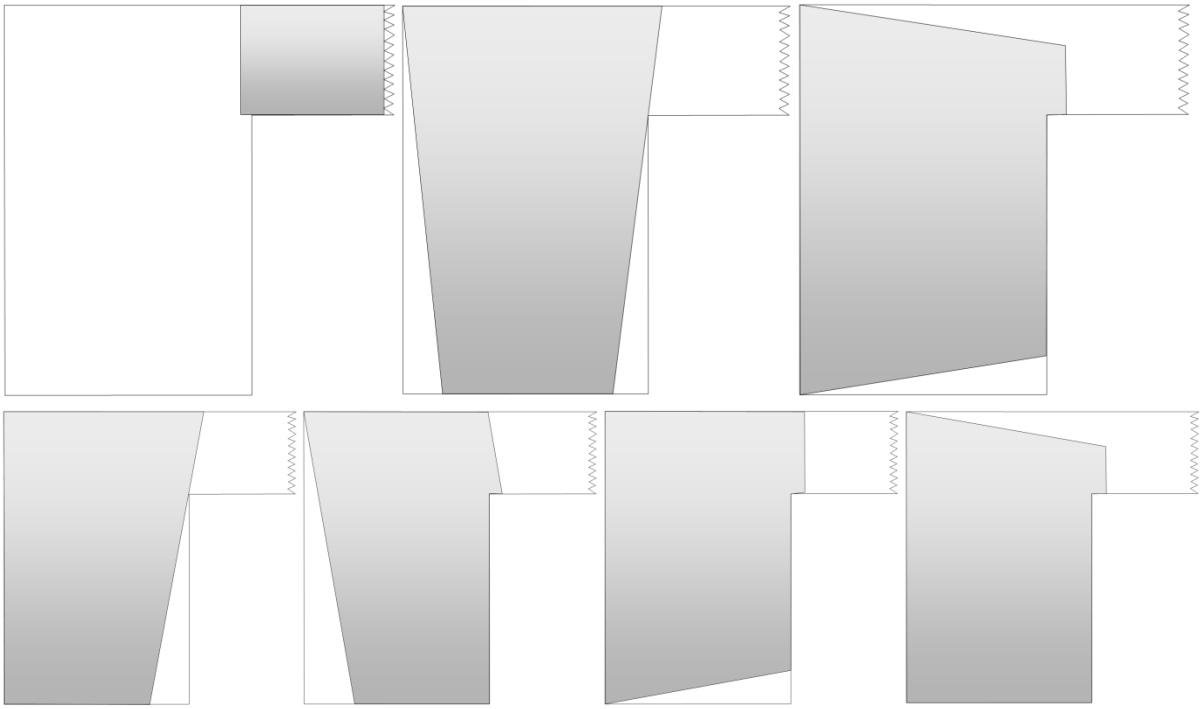

Figure 6-41. *Schematic view of the different setups for the copper lid. At the top, the three main setups are shown: A for the thin central part of the lid (left), B for the axial inspection of the outer flange (middle) and D for the radial inspection of the outer flange. At the bottom, the complementary setups to cover the edges of the flange are shown: C for the axial inspection of the outer flange with ±10° (the two images on the left) and E for the radial inspection of the outer flange with ±10° (the two images on the right).*

Table 6-9. Phased array parameters for the ultrasonic inspection of the lid (UT27).

Inspection sequence	Inspection channel	Inspection angle [°]	Depth range [mm]	Aperture size [number of elements]	Focus depth [mm]
A	FD10 12elts	0	0-20	12	10
A	FD40 16elts	0	20-55	16	40
B/D	FD20 16elts	0	0-45	16	20
B/D	FD100 26elts	0	45-105	26	100
B/D	FD180 40elts	0	105-200	40	180
C/E	FD180 40elts	-10	0-197	40	180
C/E	FD180 40elts	-10	0-197	40	180
C/E	FD180 40elts	+10	0-197	40	180
C/E	FD180 40elts	+10	0-197	40	180

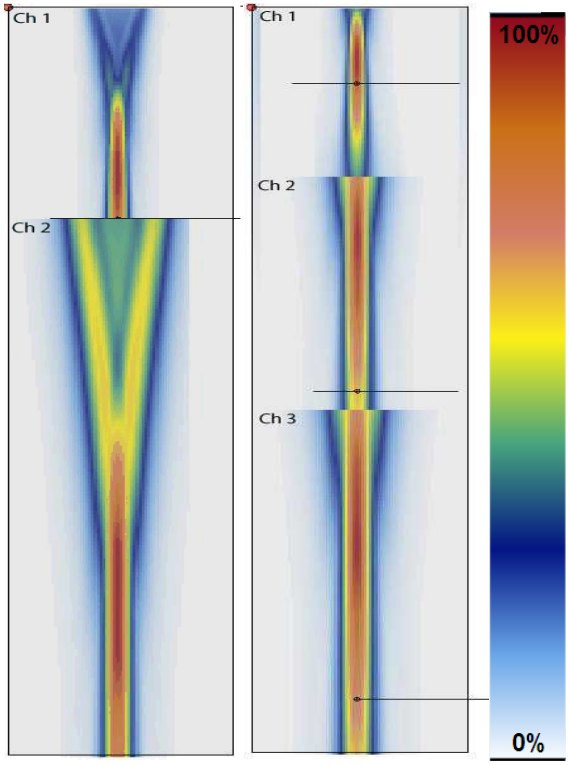

Figure 6-42. *Results from the ultrasonic simulations performed using UltraVision of the inspection in the axial direction of the outer flange. The image on the left shows the original setups with channel 1 used with a water column and channel 2 in contact. The image on the right shows the developed technique with all three channels used in the same setup using a water column.*

Surface inspection techniques

One type of defect that is known to form in forged copper lids is forging laps, which is one of the primary reasons why a method for the surface inspection of copper components is required. Different types of eddy current technology were studied, which resulted in the purchase of new equipment along with an array probe adapted for testing copper. The technique for testing the surfaces of copper components with the array technique for eddy currents will be further developed.

The fluorescent penetrant inspection technique was used to inspect a number of forged lids in the pre-machined state, whereas no inspections were performed on the lids machined to its final dimension.

6.5 NDT techniques for the friction stir welds

The friction stir welds, the base and the lid welds, are inspected separately in the canister factory and the encapsulation plant, as described in Figure 5-1. The current approach is that the inspection from a NDT point of view will be performed in the same way for both welds even though the inspection of the lid weld in the encapsulation plant will require fully remote inspection, whereas manual access is possible during the inspection of the base weld in the canister factory. Thus, the description provided in this section is valid for both types of welds.

To inspect the friction stir welds, ultrasonic, X-ray and eddy current inspection techniques were developed at the Canister Laboratory. Ultrasonic inspection is the primary technique used to inspect root defects (joint line hooking and remaining joint), and for cavities, both X-ray and ultrasonic inspection are applied, whereas eddy current inspection is used as a complementary technique for near-surface and surface-breaking cavities.

6.5.1 Ultrasonic inspection technique (UT06)

The previous NDT report (SKBdoc 1179633) describes how the weld originally is inspected from the top of the lid by the phased array ultrasonic inspection techniques (UT03 version 3.0 and UT04 version 1.0) using a 5-MHz linear array with electric scanning at various inspection angles while the welded canister rotates. As a suitable frequency (3.5 MHz) for the inspection of the copper components was determined, it was decided that the same probe specified in Table 6-8 would be used for the friction stir weld.

The ultrasonic inspection channels were defined based on the well-known weld geometry and formation of possible defects in the friction stir weld (Figure 6-43). It was determined that one set of channels should be created with special focus on the root region, where the most common defects are formed, and one set should be created for the remaining main volume of the weld. It was also determined that a minimum of two inspection angles should be applied for the entire inspection volume.

Based on the foregoing factors, the development of the ultrasonic inspection technique was performed by laboratory trials on both side-drilled holes and real defects supported by sound field simulations. The real defects were created by purposely varying different welding parameters; for example, the cavities were created by welding at a temperature that was too low and various root defects were created by either an excessively deep or excessively shallow welding depth. Based on the fact that the root defects can only be detected by ultrasonic inspection, five different inspection angles were defined, and because the root area is rather narrow, the beams were focussed as much on the root area as the lid geometry allowed. The choice of inspection angles (0°, ±12° and ±20°) was based on the signals from the real defects and the expected defect geometry.

For the remaining volume of the weld, which includes the outer region where the cavities can be formed, the lid geometry limits the degree of freedom for possible inspection angles. To cover the entire weld, which is wider closer to the surface, using focussed beams, two ultrasonic channels were created for each inspection angle. Through an analysis of the signals from a number of real cavities and the geometric inspection limitations, the angles +25° and +35°, as well as a 0° inspection channel, were defined. Based on these experiments, the final focal laws, gain and gate settings etc., and the instructions for full-scale inspection, which included data evaluation, were developed. For the inspection performed with the array in contact with a thin water film, the weld is rotated, and the array is fixed to the top of the surface. In Table 6-10, the primary parameters for all inspection channels of the developed technique (UT06 version 1.0) are compiled, and Figures 6-44 and 6-45 shows the combined sound fields obtained from the Civa simulation (SKBdoc 1435212).

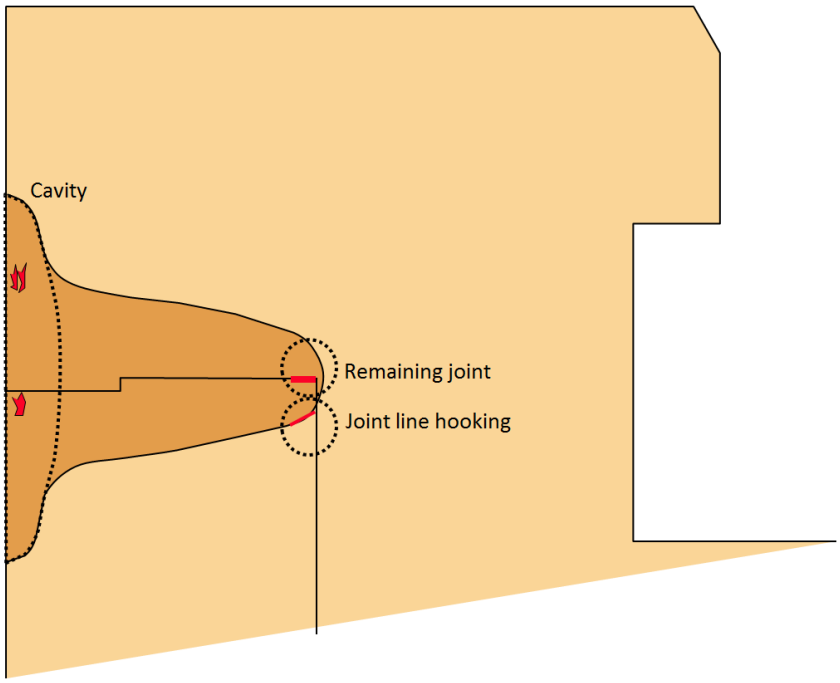

Figure 6-43. *Schematic view of the friction stir weld.*

Table 6-10. Phased array parameters for the ultrasonic inspection of the friction stir weld (UT06).

Inspection channel	Inspection region	Inspection angle [°]	Depth range [mm]	Aperture size [number of elements]	Focus depth [mm]
+20° root	Root	+20	40-65	50	60
+12° root	Root	+12	40-75	50	60
0° root	Root	0	51-76	50	60
-12° root	Root	-12	50-80	40	67
-20° root	Root	-20	55-75	28	67
+35° shallow	Upper part excl. root	+35	30-63	42	47
+35° deep	Lower part	+35	57-88	55	75
+25° shallow	Upper part excl. root	+25	30-62	39	45
+25° deep	Lower part excl. root	+25	57-88	50	75
0° shallow	Entire weld excl. surface	0	30-90	32	60

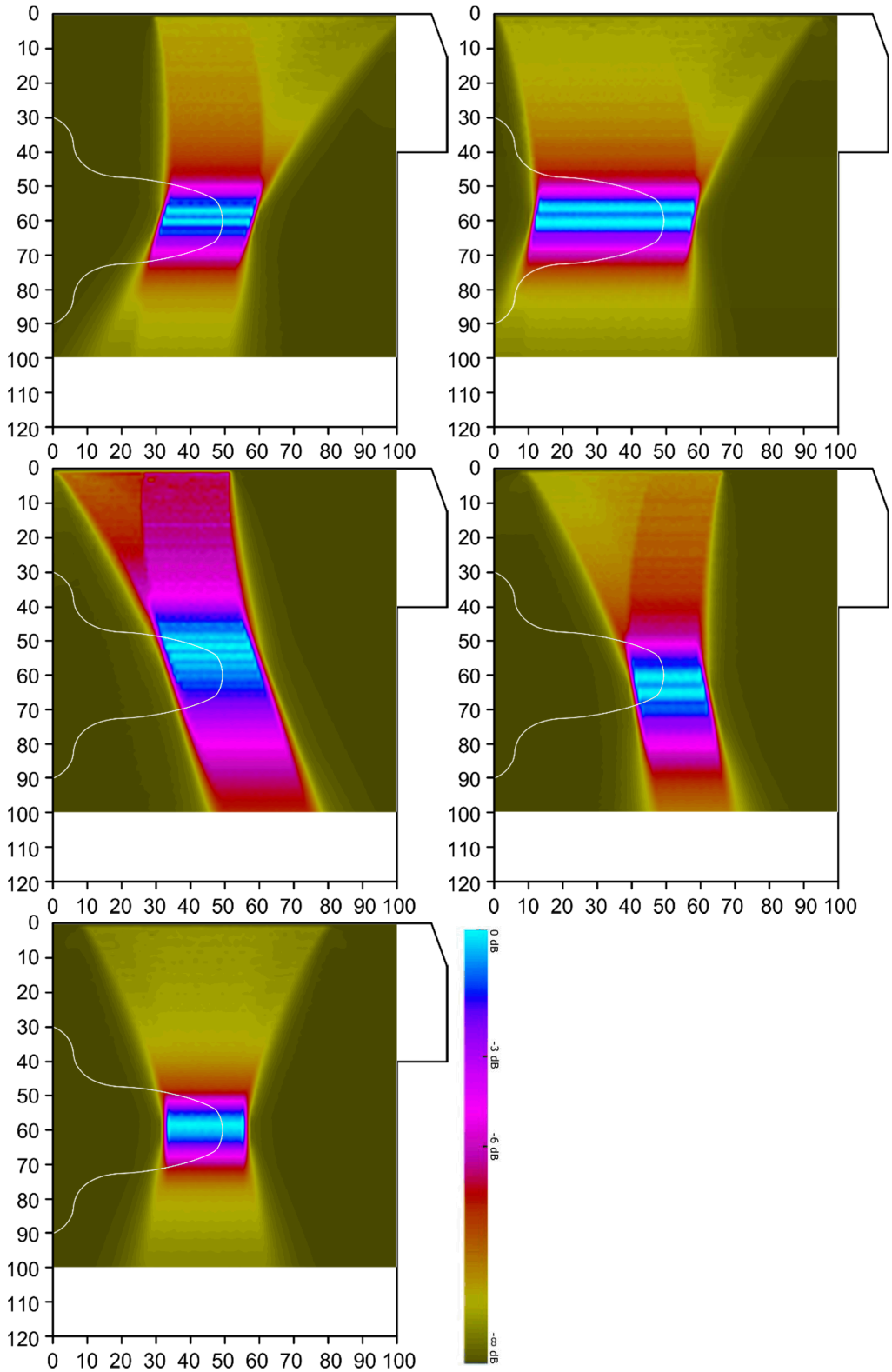

Figure 6-44. *Civa simulation of the sound field for root inspection (Table 6-10). The images show the combined sound fields as follows: top, +20° (left) and +12° (right); middle, -20° (left) and -12° (right); and bottom, 0° inspection.*

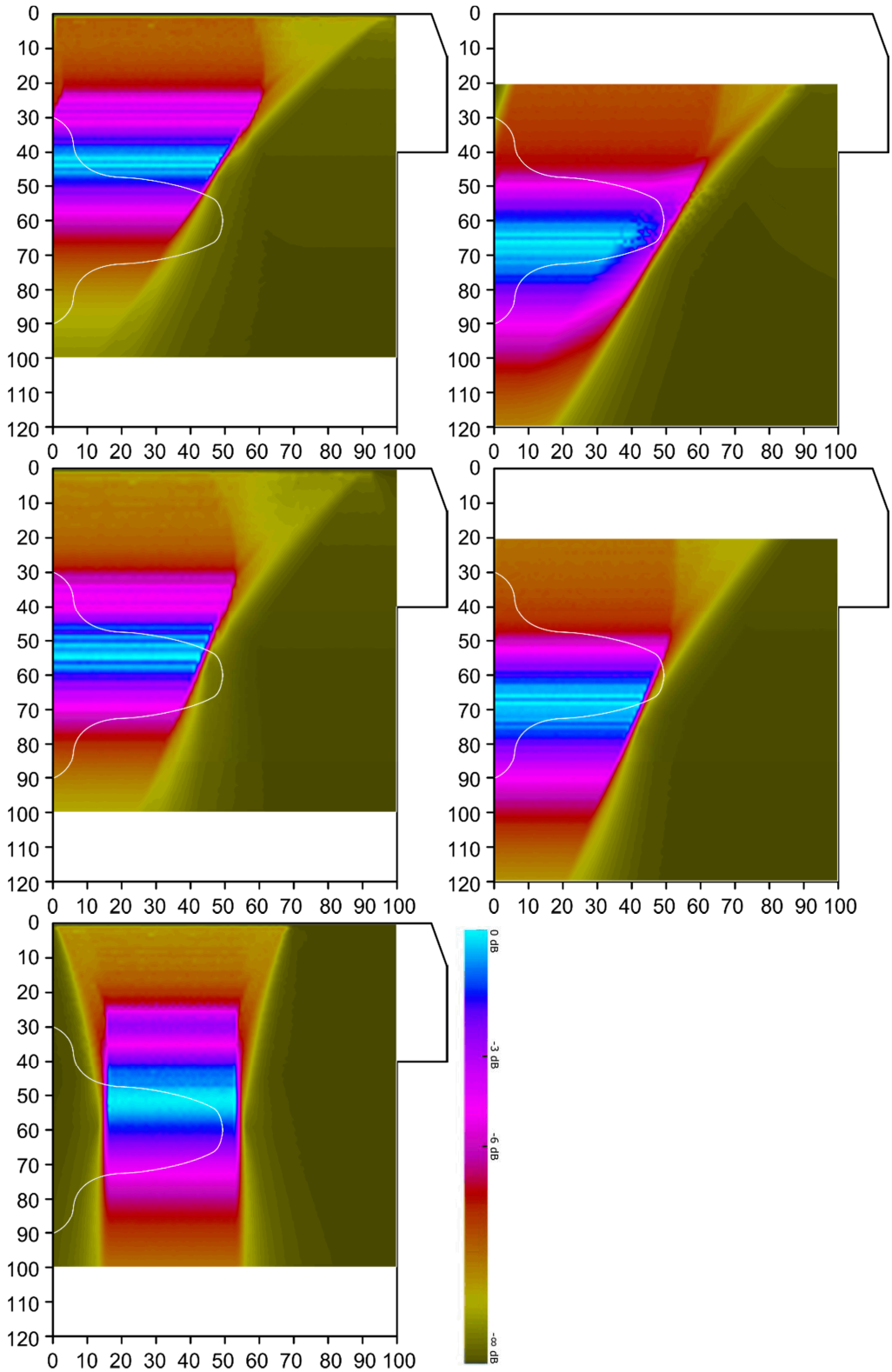

Figure 6-45. *Civa simulation of the sound field for the inspection of the main volume (Table 6-10). The images show the combined sound fields as follows: top, the +35° shallow (left) and +35° deep (right); middle, +25° shallow (left) and +25° deep (right); and bottom, the 0° inspection.*

6.5.2 X-ray inspection technique (RT01)

The previous NDT report (SKBdoc 1179633) describes how the weld originally is inspected using the linear accelerator and detector array, as described in section 6.1.2, at an incidence angle of 35°. The radial propagation is the most critical for defects in the welds, whereas the exact radial position is of minor interest.

Thus, the incidence angle was decreased to reduce the penetrated wall thickness and thereby obtain higher X-ray sensitivity. Due to the geometry of the lid and weld region, an incidence angle of 8° was selected (Figure 6-46) instead. The figure shows that an even lower incidence angle could be applied without any disturbance from the flange near the X-ray source. However, the choice of incidence angle was based on the assumption that the weld might require inspection before machining when the lid flange is 55 mm higher. The inspection is performed in the same manner as previously described (SKBdoc 1179633); by rotating the welded canister slowly while the accelerator transmits a pulsed X-ray beam through the weld, via a collimator, to the detector. The resolution in both directions (0.4 mm) is determined by the collimator opening in the circumferential direction and by averaging eight elements of the detector array in the vertical direction.

Figure 6-46. *Principle drawing showing the X-ray source on the right and the detector on the left.*

6.5.3 Surface inspection techniques

An inspection technique for the machined weld surface is considered complementary to the ultrasonic and X-ray techniques used for the inspection of the bulk volume of the weld. The eddy current method is aimed to detect defects that are either actually breaking the surface or located near the surface. Initial trials were performed using conventional eddy current equipment and probes attached to a primitive semi-automatic raster scanning manipulator, as shown in Figure 6-47. Based on the results of the initial trials, a multi-differential probe Leotest SKB MDF 12 driven at a frequency of 0.9 kHz was selected for subsequent investigations.

A reference copper block with three flat-bottom holes (FBHs) with Ø2 mm and ligament sizes of 0 mm, 1 mm and 2.4 mm were used for the sensitivity setting of the inspection system. Figure 6-48 shows a typical result obtained from the inspection of the reference block and the three Ø2 mm flat-bottom holes. Because the probe is composed of four coils in a square pattern, the indication of a single hole forms a similar square pattern.

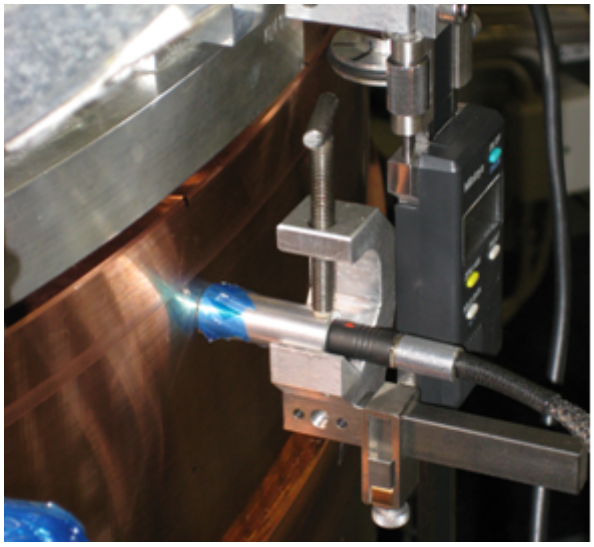

Figure 6-47. *Conventional eddy current single probe, Leotest SKB MDF 12, attached to a primitive semi-automatic raster scanning manipulator used to inspect the envelope surface of a machined FSW weld.*

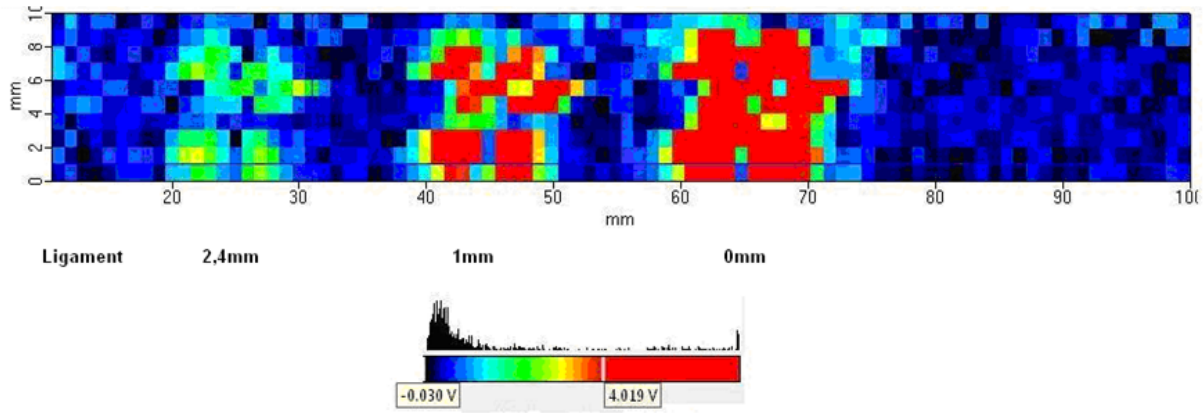

Figure 6-48. *Eddy current inspection results with a conventional single probe, Leotest SKB MDF 12, on a reference copper block with three flat-bottom holes (FBHs) Ø2 mm and ligament sizes of 0, 1 and 2.4 mm. As the probe is composed of four coils in a square pattern, the indication of a single hole forms a similar square pattern.*

An analysis was also made of the relation between the ligament thickness of the holes with different ligaments and the phase shift of the corresponding indications. The assumed linear relation, a typical example of which is shown in Figure 6-49, could be a useful tool for estimating the ligament thickness of an indicated defect.

During the continued evaluation, comparisons of the X-ray and eddy current inspection results for cavity-type defects in an FSW weld were performed. Figure 6-50 shows the typical result obtained from such inspections.

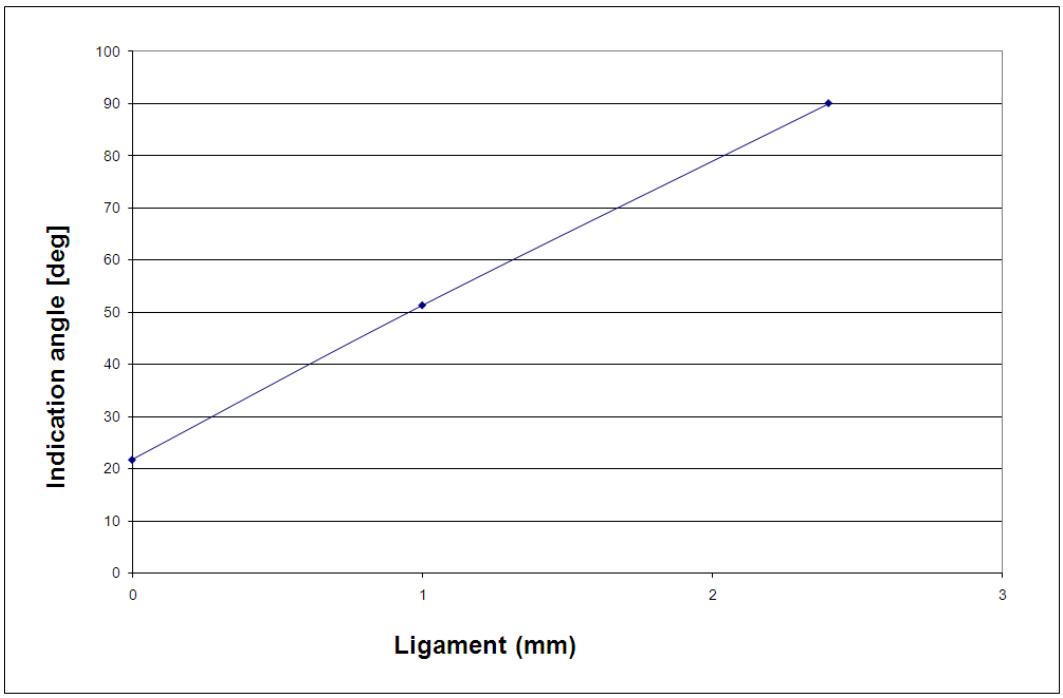

Figure 6-49. *The relation between the ligament thickness of FBHs (Ø2 mm) and the phase shift of the corresponding indication obtained with the Leotest SKB MDF 12 probe.*

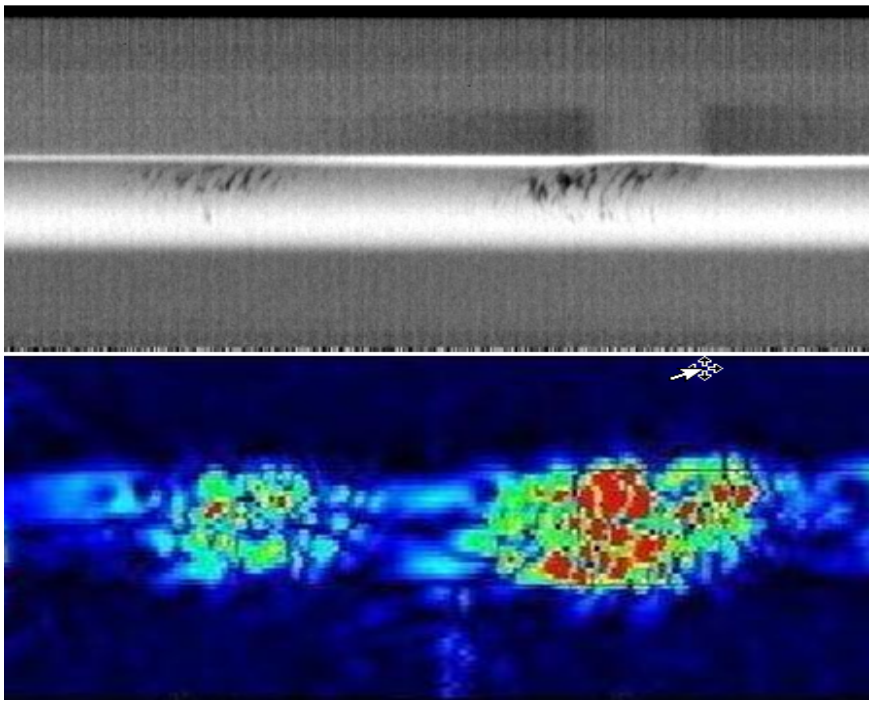

Figure 6-50. *Result from the X-ray (top) and eddy current inspection (bottom) of a section of an FSW-weld containing two regions of cavities.*

Based on the results obtained, an eddy current array instrument (Ectane; see Figure 6-5) and an array probe adapted to testing of copper were specified and procured. The array probe, Eddyfi PESD5043A (KLM194), consists of 32 individual coils arranged in two parallel rows covering the entire width of the welded area in a single pass. The coils are excited in a number of transmit/receive sequences such that weld defects in both the circumferential and axial direction can be detected. The mounted array probe and the arrangement of coils in the array pattern are shown in Figure 6-51.

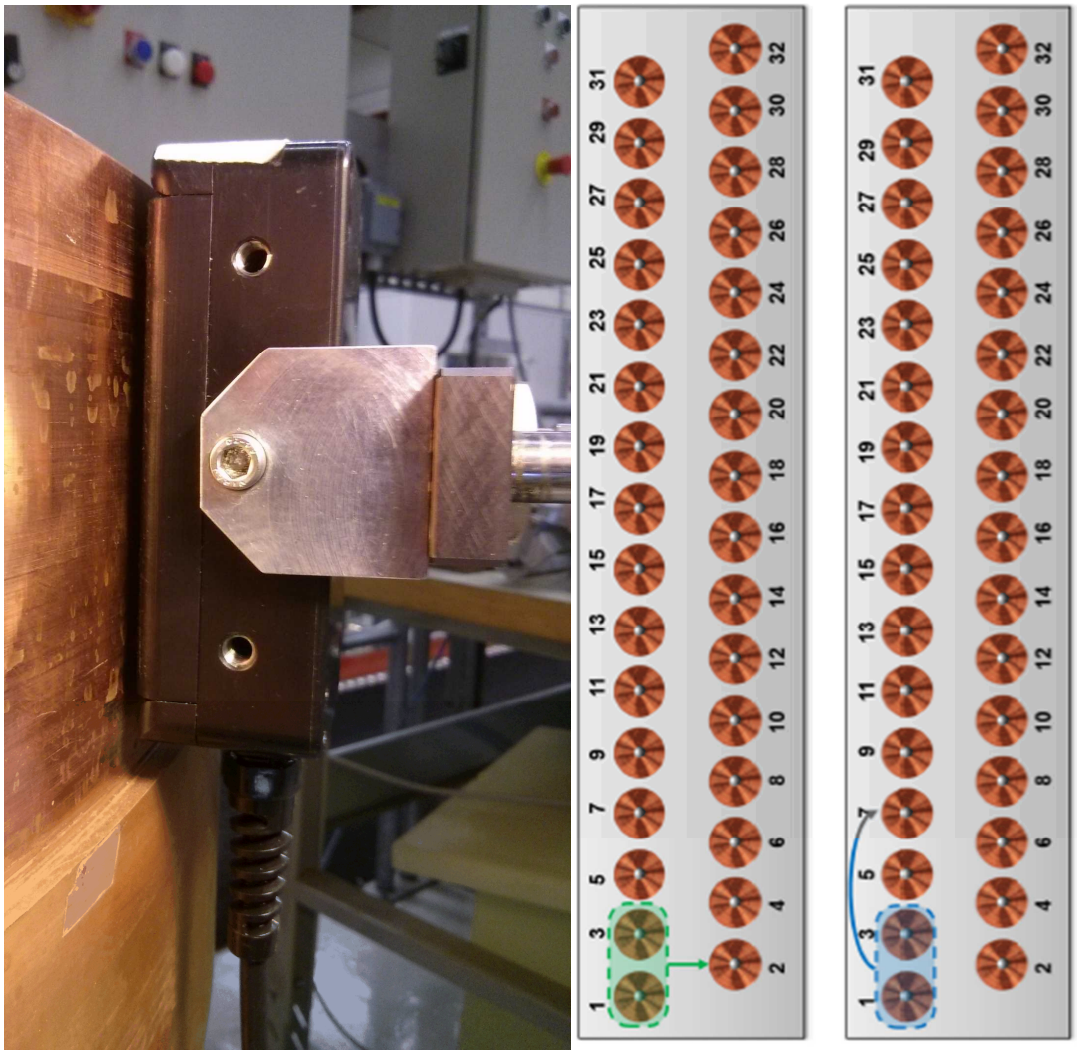

Figure 6-51. *The array probe mounted for inspection (left) and the principal arrangement of the coils in the array pattern. In the middle, the transmitter/receiver configuration with two driver coils and one receiving coil is optimised for defects with a circumferential extension along the weld. On the right, the transmitter/receiver configuration is shown for detection of defects, with an extension transverse to the weld.*

The array probe was evaluated and a draft instruction (ET01) for the inspection of the machined weld surface was developed. The preliminary inspection technique uses two different excitation frequencies, 1.1 kHz and 10 kHz.

As part of the evaluation, the same reference copper block with three flat-bottom holes, which previously had been inspected by the initial single probe approach as shown in Figure 6-47, was also inspected by the array probe, as shown in Figure 6-51. The results, shown in Figure 6-52, indicated that the array probe under evaluation achieved similar sensitivity for defects than that of the evaluated single probe.

An analysis of the relation between the ligament thickness of the holes with different ligaments and the phase shift of the corresponding indications was repeated for the array probe. A relation similar, though not identical, to that obtained with the single probe presented above was obtained with the array probe, as shown in Figure 6-53.

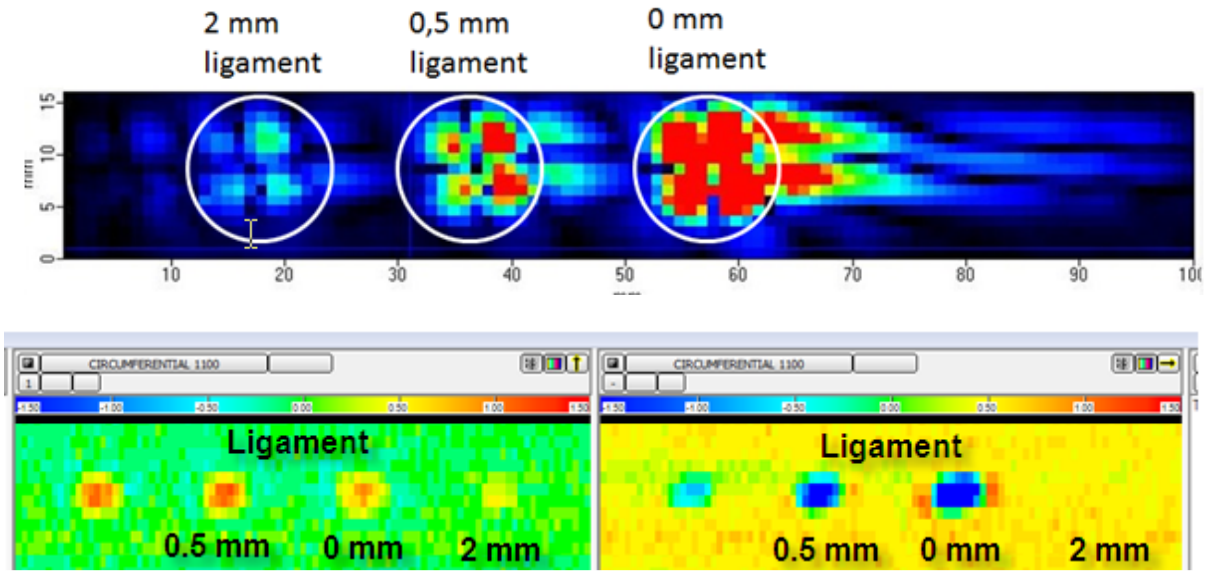

Figure 6-52. *Results from the evaluation and comparison of a single probe and array probe approach on a copper reference block with FBHs (Ø2 mm) with different ligaments. The top image presents (single probe) the absolute signal deflection, while the bottom images present (array probe) the signal deflection in the vertical (left) and horizontal (right) directions in the probe impedance plane.*

Figure 6-53. *The relation between the ligament thickness of the FBHs (Ø2 mm) and the phase shift of the corresponding indication obtained with the Eddyfi array probe PESD5043A (KLM194).*

7 Results and experiences

For a number of years, SKB has performed inspections of both small parts and full-size components in parallel with the development of NDT techniques. Within this context, much experience and results from different types of indications have been obtained, which are summarised in the following sub-sections.

7.1 Cast iron insert

The main work on the cast iron insert was performed on the insert material itself, whereas very limited work has been conducted on the integrated parts (for example the steel tubes and cassette) and components (for example the steel lid and screw).

7.1.1 Ultrasonic inspection techniques

About 40 inserts have been inspected by at least one ultrasonic inspection technique (all with the normal incidence ultrasonic technique and a majority by the TRL technique, UT32). Of these inserts about ten have been inspected by the further developed normal incidence ultrasonic technique, whereas only the last three manufactured PWR inserts (IP23, IP24 and IP25) have been inspected by all three newly developed ultrasonic techniques (UT31, UT33 and UT34). In general, the inspections show that the indications of large defects are limited, whereas indications with low amplitudes and small sizes are more common.

Defect indications

SKBdoc 1179633 indicates that a limited number of indications have been observed by the normal incidence technique, whereas inspection by the TRL technique has resulted in a large amount of indications in BWR inserts (I53-I57). After further analysis of the indications, it was shown that the indications originated from clustered porosity (a large number of distributed pores, each clearly smaller than 1 mm).

As this clustered porosity was not detected by the original normal incidence ultrasonic technique, a number of insert segments were re-inspected by the further developed technique (UT31 version 6.0). The results showed that the sensitivity of the further developed technique was clearly improved and that clustered porosities could be detected. Based on the ultrasonic data, several samples were cut and machined to suitable dimensions for tensile testing. Prior to tensile testing, the samples were examined by computed tomography (CT), and afterwards, the fracture surfaces were examined by fractography (SKBdoc 1352906, 1358335). In Figure 7-1, an example of an ultrasonic indication of clustered porosity is shown, and Figure 7-2 shows the corresponding results obtained from computed tomography and fractography. It can also be observed that the indicated porosities are distributed along the insert length and located in the same region in the inserts, that is within the first few centimetres from the envelope surface and with a 90° separation in the central path between the BWR insert fuel channels (3, 6, 9 and 12 o'clock according to Figure 6-6).

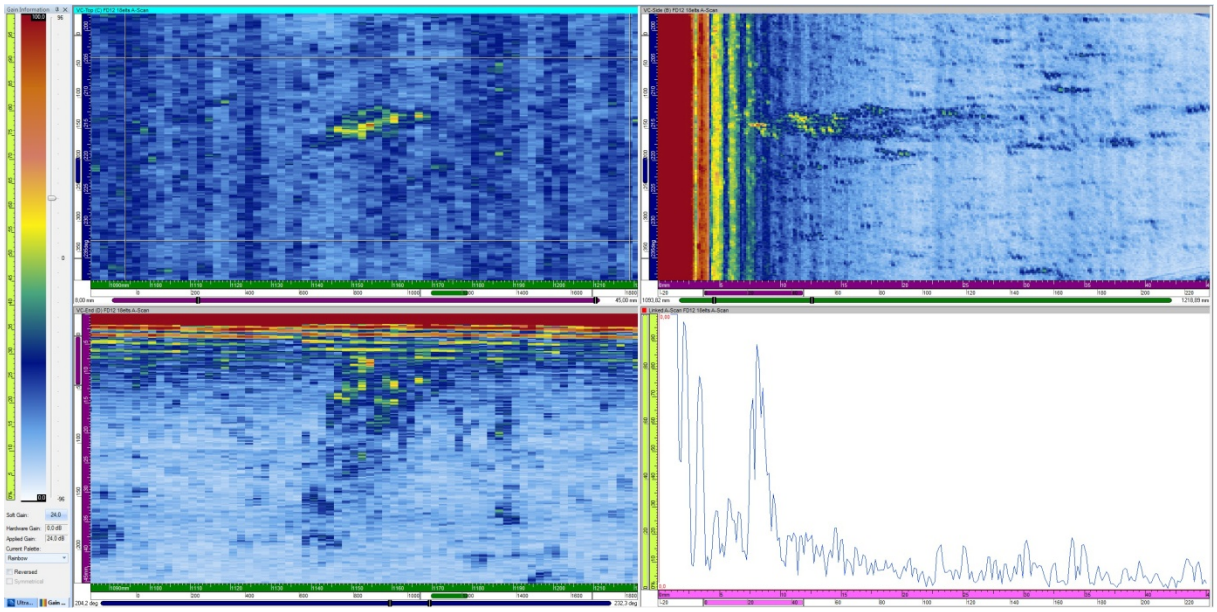

Figure 7-1. *Results from phased array ultrasonic inspection (UT31) of a BWR insert area with porosity are shown as projections in three directions: a C-scan from the envelope surface (top left), a B-scan viewed from the end surface (top right) and a D-scan viewed along the axial direction (bottom left). The ultrasonic signal as a function of depth is shown in the A-scan (bottom right). The indication shows a SNR of ~5 (~14dB).*

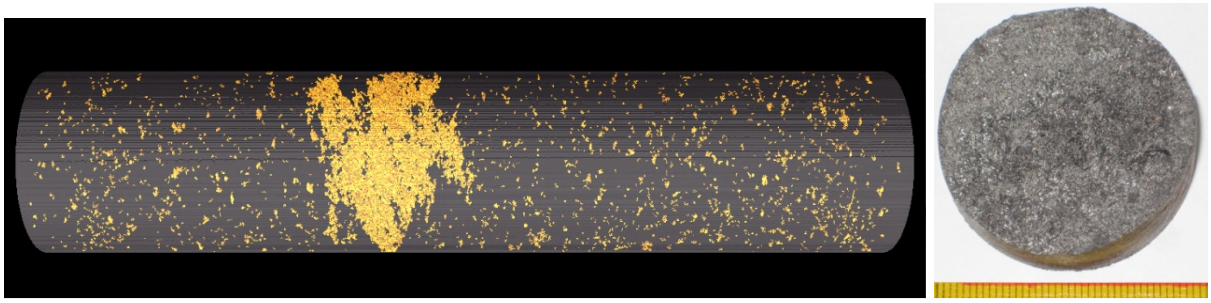

Figure 7-2. *Characterisation of porosity indicated in Figure 7-1. Computed tomography (left) and fracture surface (right) images of a tensile test sample with a diameter of 40 mm.*

In addition to the aforementioned clustered porosities, the number of widespread indications detected by the UT31-technique was limited. While inspecting early manufactured inserts some widespread indications were detected. For example, a few blowholes in the region of the channel tubes were found using the previous technique, as shown in Figure 7-3.

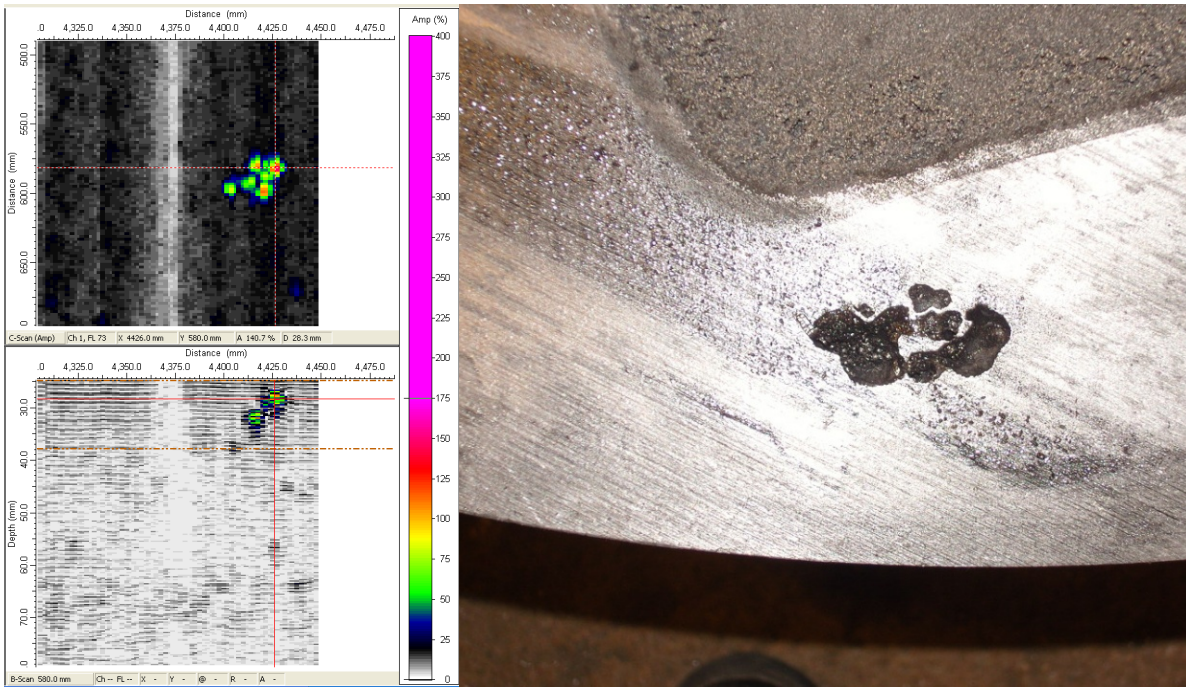

Figure 7-3. *Results from the previous phased array ultrasonic inspection (UT31) of a blowhole. C-scan from the envelope surface (top left), a B-scan viewed along the axial direction (bottom left) and a photograph of the cut insert (right). The indication shows a SNR of ~10 (~20dB).*

The most common indications detected by the UT31 technique show point-like behaviour with low amplitude and limited size, particularly along the length of the insert (Figure 7-4). The point-like, low-amplitude indications are typically smaller in the axial direction than in the circumferential direction. This can be explained due to the sound field, as described in section 6.2.2, is smaller in the axial (active) direction than in the circumferential direction (passive). A number of indications of this type were chosen for further analysis. The analyses were performed in a number of steps. First, the position of the defect indication was marked using an ultrasonic signal from the array, and then a sample that included the assumed defect was cut. The final analysis was then performed in two ways. First, the sample was cut and polished at the position of the assumed defect, and the polished surface was carefully examined. Second, the sample was positioned in a milling machine, and in the identified position of the assumed defect, the sample was machined stepwise (in 0.5-mm steps) and inspected by magnetic particle inspection between all steps.

The results of these careful examinations of ultrasonic indications were disappointing; no defects (>1 mm) could be correlated to any of the ultrasonic indications that was chosen. Because the results of the examinations were unexpected, the entire chain was investigated, and possible reasons for the results obtained were identified. At first, it was believed that the results were due to errors in sample preparation, for example the wrong location of the defect was used or the position of the cut might have been just to the side of the defect. After further analysis of the signals, it was observed that the signal amplitudes were at the same level as those detected from a Ø1 mm SDH, and as mentioned previously, the size in the axial-circumferential plane was small. Thus, the size of the defects was assumed to be on the order of a few millimetres, making them likely to be missed during sample preparation. However, further analyses are required on these types of defect indications. The methodologies for localisation and sample preparation have also to be further developed.

In addition to these point-like individual indications, some inserts showed a large number of similar indications (most of them with low signal amplitudes), indicating, in general, an inhomogeneous material. The final conclusion of these examinations is that that the sensitivity of the UT31 technique is high and that the detected indications can be assumed to correspond to small defects that are a few millimetres in size.

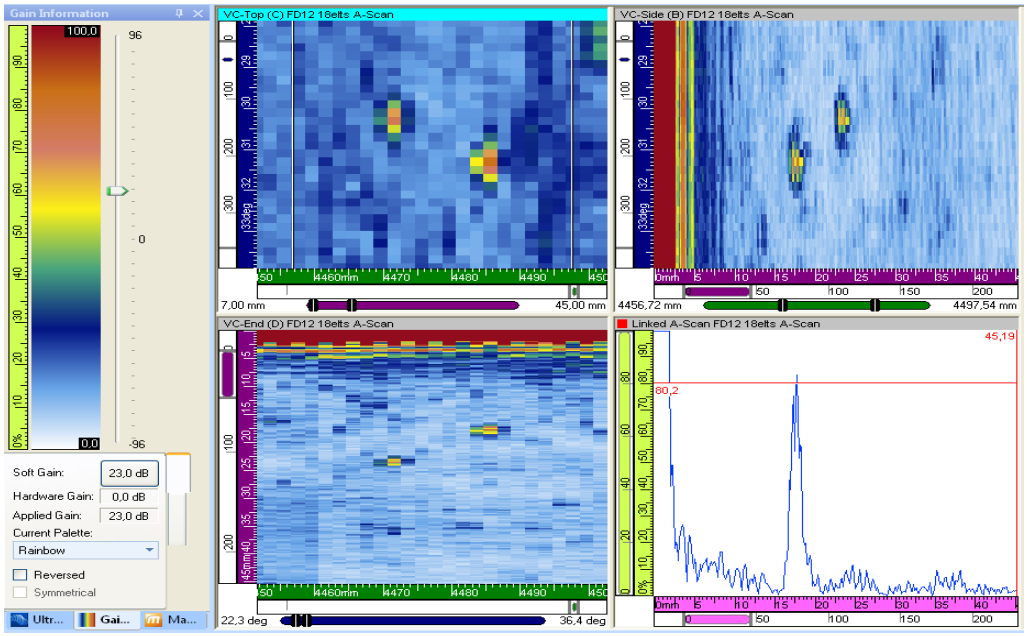

Figure 7-4. *Point-like indication from phased array ultrasonic inspection (UT31). C-scan from the envelope surface (top left), B-scan viewed from the end surface (top right) and D-scan viewed along the axial direction (bottom left). The ultrasonic signal, for the right indication (in the C-scan), as a function of depth is shown in the A-scan (bottom right). The indication shows a SNR of ~8 (~18dB).*

During the development of the inspection technique (UT33) for the volume between the fuel channels in the PWR insert some widespread indications, which exhibits low amplitudes in the pulse echo channels and a total loss of sound in the transmission inspection, were observed in the central part, as shown in Figure 7-5. Due to the low reflected amplitude and the poor ultrasonic transmission properties, the indications were assumed to originate from some type of porosity. This assumption was verified by metallographic examination (Figure 7-6) of one of the indications.

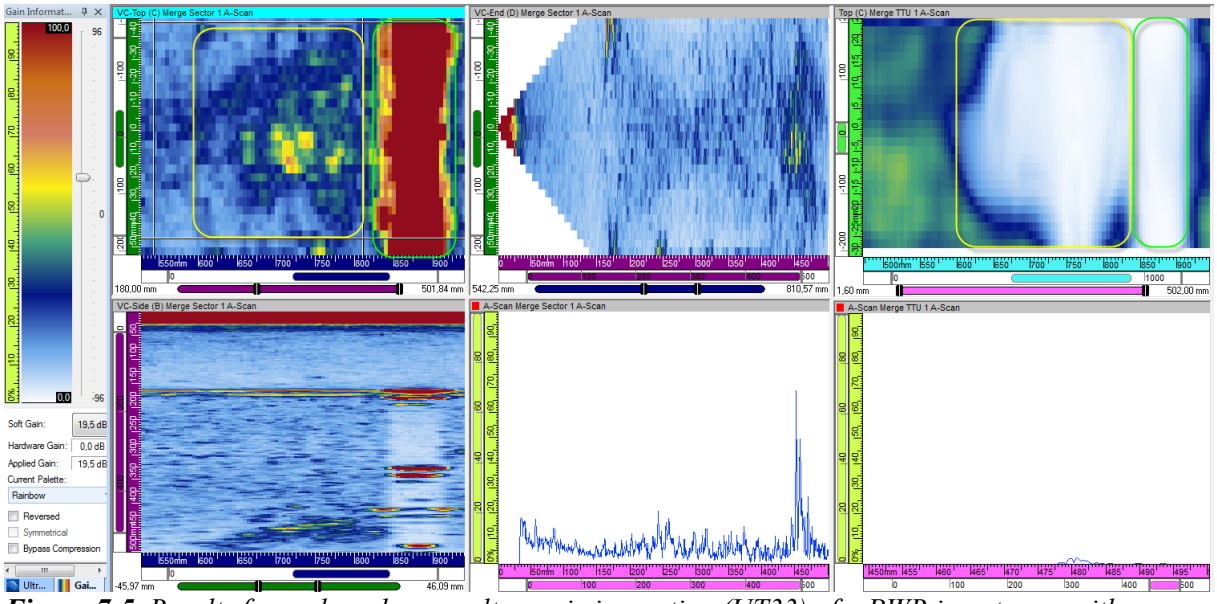

Figure 7-5. *Results from phased array ultrasonic inspection (UT33) of a PWR insert area with porosity. C-scan from the envelope surface (top left), B-scan viewed from the end surface (top middle) and D-scan viewed along the axial direction (bottom left). The ultrasonic signal as a function of depth is shown in the A-scan (bottom middle). The right image shows the loss of signal (white areas) in transmission. The circled areas correspond to porosity (yellow) and a support plate (green). The indication shows a SNR of ~5 (~14dB) in pulse-echo and in transmission >10 (>20dB).*

The new angular shear wave ultrasonic inspection technique (UT34) was only used to inspect three PWR inserts (IP23, IP24 and IP25). The results obtained from these inspections showed only a few indications near the outer corners of the channel tube walls (Figure 7-7) and some indications caused by surface marks (Figure 7-8). For both types of indications, the signal-to-noise ratio was significant. It was also observed that the normal appearance of the inspected volumes was similar to that of the areas surrounding these indications, the general volume being very clean, whereas the region near the outer corners of the channel tube walls contained more noise due to reflections from the uneven interface between the casting and the channel tube walls.

Figure 7-6. *Photograph of the shrinkage pores indicated in Figure 7-5 between the fuel channels in a PWR insert.*

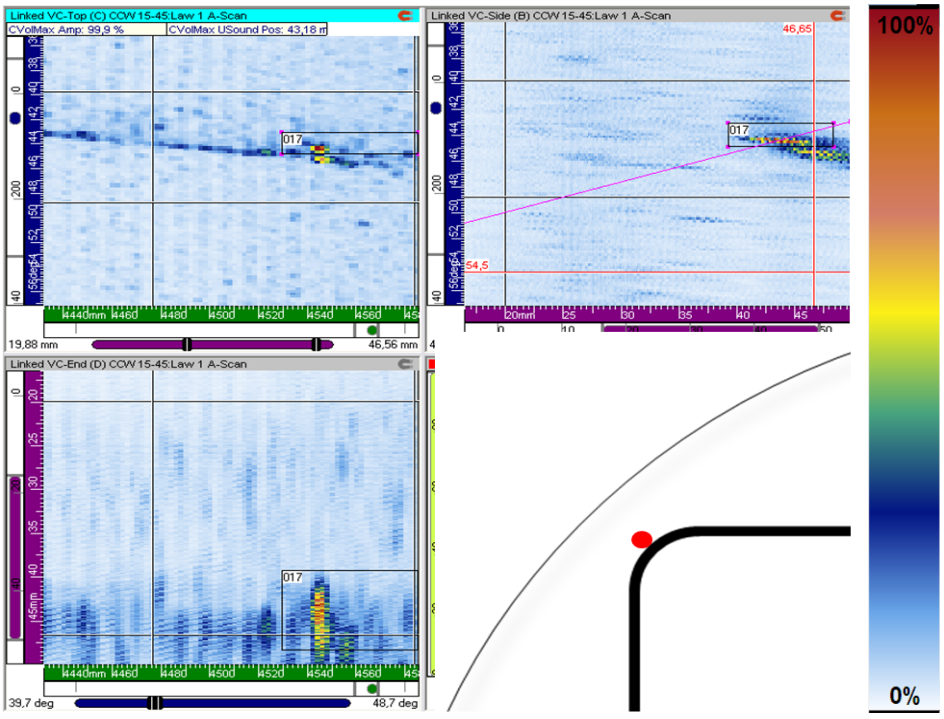

Figure 7-7. *Results from the phased array ultrasonic inspection (UT34), in the circumferential direction, of an indication near the outer corner of the channel tube wall. C-scan from the envelope surface (top left), B-scan viewed from the end surface (top right) and D-scan viewed along the axial direction (bottom left). The sketch (bottom right) shows the position of the indication in the insert. The indication shows a SNR of ~10 (~20dB).*

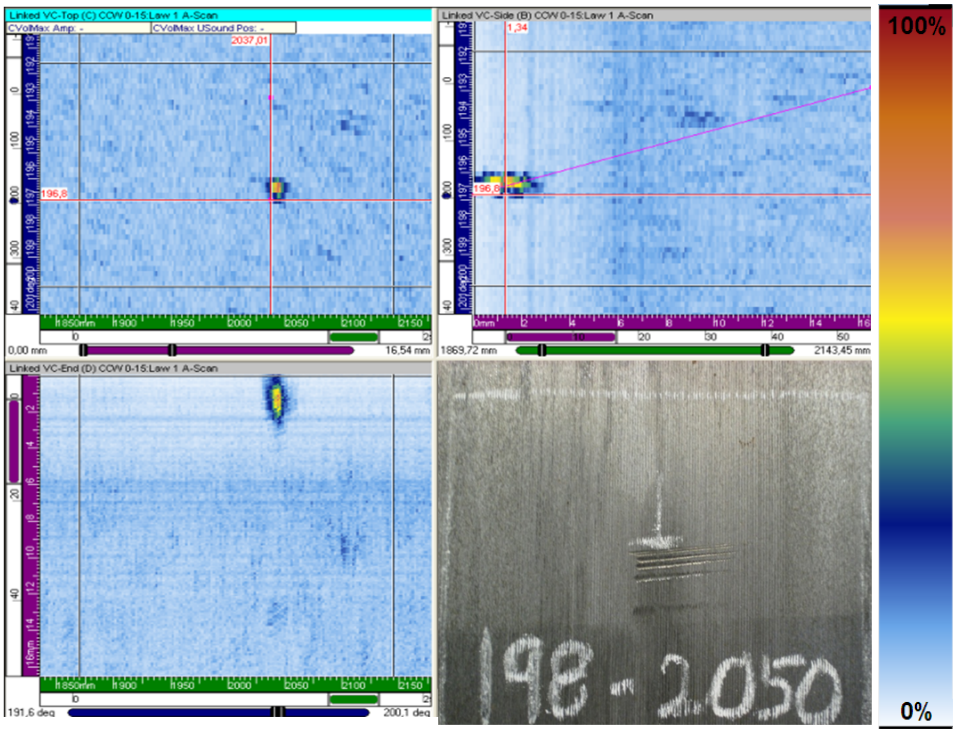

Figure 7-8. *Results from the phased array ultrasonic inspection (UT34) in the circumferential direction of a surface defect indication. C-scan from the envelope surface (top left), B-scan viewed from the end surface (top right) and D-scan viewed along the axial direction (bottom left). To the right, at the bottom, a photograph of the surface marks is shown. The indication shows a SNR of >10 (>20dB).*

Practical application

A number of practical experiences, in addition to the results described above, were gained. For example, it was observed that the surface echoes from the normal incidence inspection (UT31) performed with a water column varied greatly. For several inserts, this variation limited the near-surface resolution from the normal 5 mm to more than 15 mm, which affected this region such that it could not be evaluated with the same sensitivity. Therefore, a study was performed to investigate the effect of the surface roughness, measured as the R_a value, on the surface echo. The results showed that there was no clear correlation between the R_a values and the extension of the surface echoes. However, it was observed that the shape of the surface was more relevant in obtaining a short surface echo. It was discovered that the samples that resulted in long surface echoes exhibited a saw-tooth-shaped surface, whereas the samples that resulted in short surface echoes exhibited a more curved surface, as shown in Figure 7-9. Based on these findings, a number of different milling parameters (tools, cut depth, speed, etc.) were studied, and a new machining procedure (SKBdoc 1432361) was established using a tool that creates a surface that exhibits not only low R_a values but also a particularly smooth surface appearance.

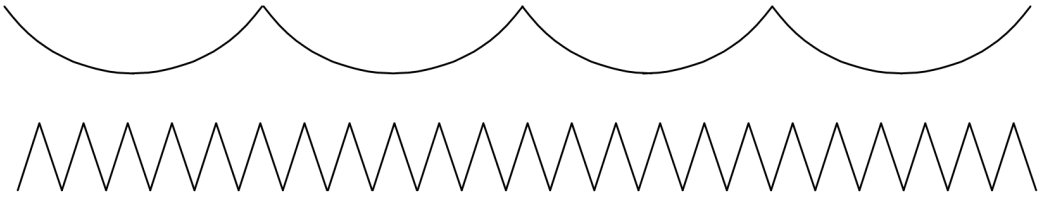

Figure 7-9. *Sketch of a curved surface (top) and a saw-tooth-shaped surface (bottom).*

One of the PWR inserts (IP23) was used to verify the effect of the new machining procedure, and as shown in Figure 7-10, a remarkable improvement was obtained. The left image shows the B-scan obtained from inspecting the original saw-tooth-shaped surface with an accepted R_a value of approximately 3 µm, and the right image shows the B-scan obtained from the inspection of the new smooth surface (R_a-value <2 µm) achieved by the new milling procedure.

The UT31 technique was also used to measure the distance between the insert surface and the outer corner of the fuel channels. From these measurements, a number of results were obtained. One of the most distinct results is that the bonding between the insert material and the channel tubes varies, both between and within the inserts, from complete bonding to an open joint. Additionally, it was observed that the boundary often contained small defects that affected the reflected signal.

The varying degree of bonding between the cast material and the channel tubes complicates the measurement of the edge distance in several ways. First, reflections from inside and outside of the channel tubes arise at different depths, and as the inspection setup is defined these echoes show up in different inspection channels; in this context, the worst case is when the echoes appear at the boundary between two of the inspection channels. Second, it can occasionally be difficult to determine whether the echoes originated from inside or outside of the channel tubes. In Figure 7-11, a clear echo from the boundary between the insert material and the channel tubes can be observed, whereas in Figure 7-12, only a clear echo from inside of the channel tube can be observed near the boundary between two of the inspection channels. By using a different section (at approximately 30 mm instead of at 45 mm) between the shallow and the mid-depth inspection channels, as described in section 6.2.2, the problem associated with using two inspection channels to measure the edge distance can be avoided.

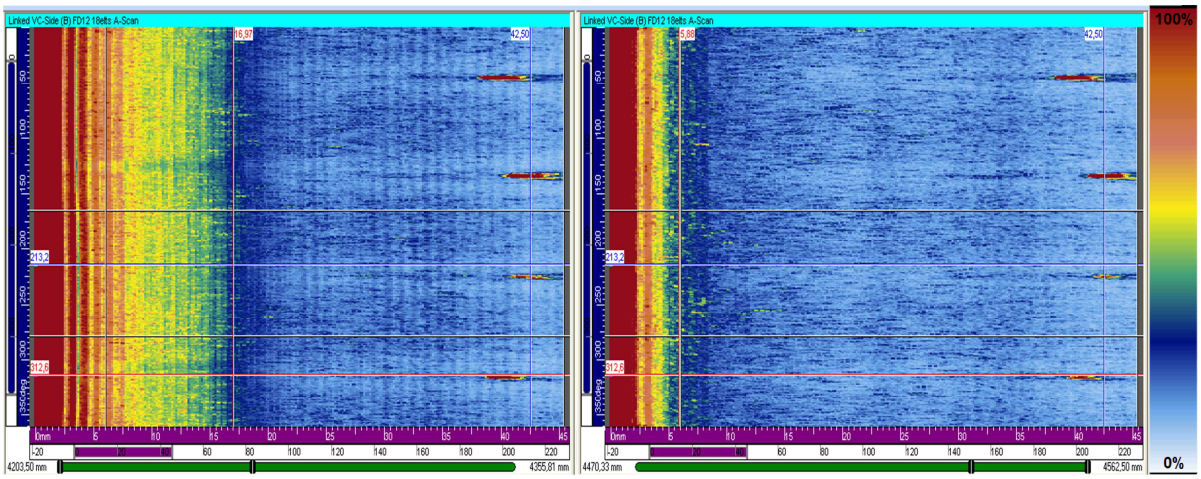

Figure 7-10. *B-scan of the inspection of the PWR insert segments with different surface shapes. On the left, inspection of the original saw-tooth-shaped surface, and on the right, inspection of the new smooth surface.*

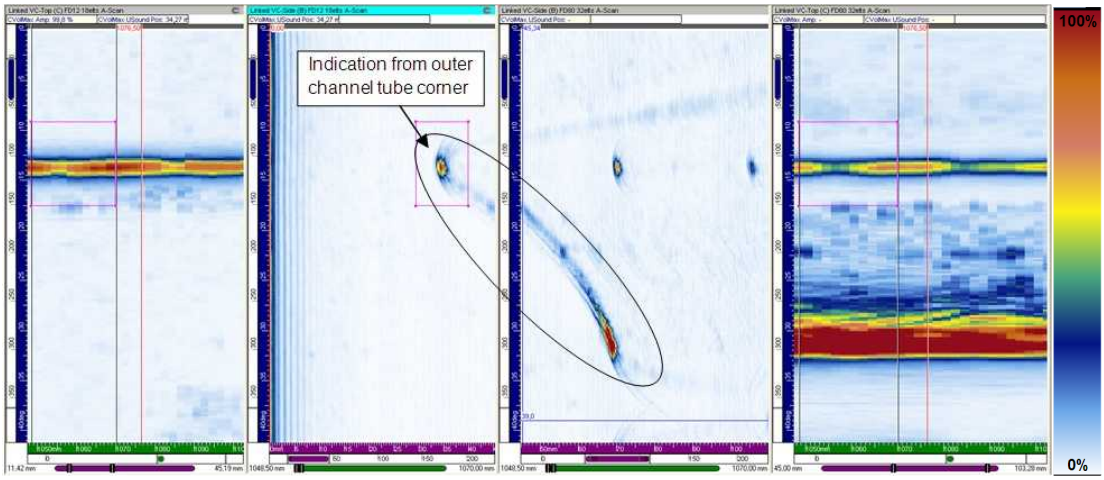

Figure 7-11. *Measurement of the edge distance using the echo from the boundary between the insert material and one channel tube. The two images on the left belong to a depth range of 0-45 mm, and the two images on the right belong to a depth range of 45-110 mm. The outer C-scans are used to choose the measurement region (the pink square), and the B-scans in the middle are used to measure the edge distance.*

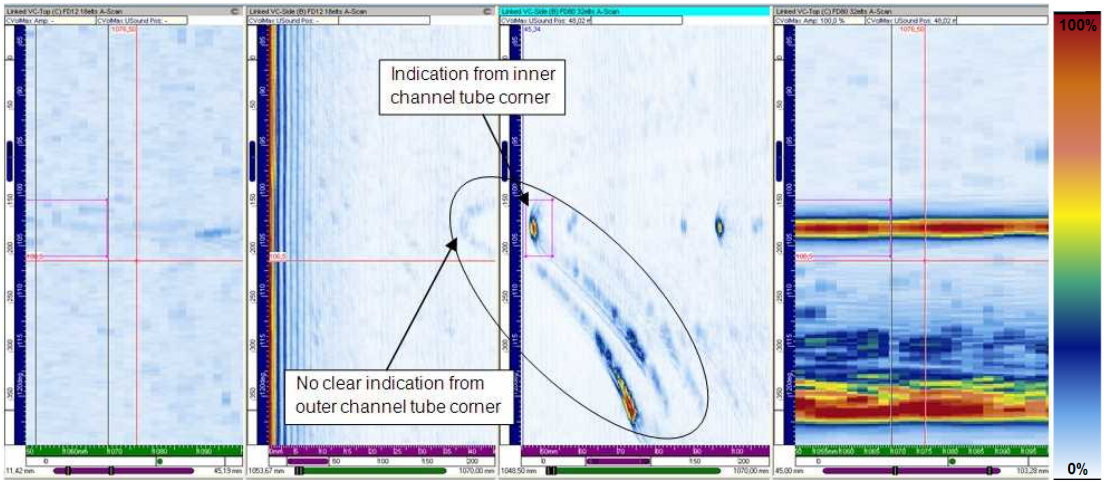

Figure 7-12. *Measurement of the edge distance in a manner similar to that described in Figure 7-11. In this example, there is no echo from the boundary, that is the measurement had to be performed from inside the channel tube, and the measured value had to be compensated for with respect to the channel tube wall thickness.*

For the inspection with the UT31 technique, a flexible local immersion tank (Figure 6-8) designed for use with different types of probes was used, and therefore about six centimetres at the top and bottom of the insert were not covered by the inspection.

Evaluation of signal to noise ratio for artificial defects

During the development of the ultrasonic inspection techniques for the cast iron insert (presented in section 6.2.2) it was identified that the material seemed to be more homogeneous with lower ultrasonic attenuation than expected, and therefore an increased ultrasonic inspection frequency could be applied. To support this assumption, a study was conducted on the response, on the further developed ultrasonic techniques, from artificial defects at different depths in full-size inserts. The analysis was based on pre-collected data and therefore limited numbers of data-points were available. In order to get a quantitative measure in relation to the actual inspection application, the SNR was determined for

each defect based on the measured signal amplitude, and the noise was measured (in the B-scan) at the defect depth.

For the normal incidence ultrasonic inspection technique (UT31), operating at 3.5 MHz, Ø1 mm axial side-drilled holes in the depth range of 5 mm to 185 mm were used. The results presented as a signal to noise ratio diagram in Figure 7-13 in general exhibit high SNR values. As shown in this figure, for some of the hole depths, there are several data points, while the ultrasonic B-scans only show representative signals for a selection of the inspected SDHs. For the near-surface region the SNR is lower; especially for the 5 mm depth. This can be explained by the fact that this specific insert not was machined according to the new specification (presented in previous section); causing a high-amplitude multiple surface echo, clearly seen in the B-scan, giving a much higher noise level at the depth of 5 mm and consequently a lower SNR. For the larger depths of the inspection range a decreasing trend for the SNRs also can be seen. The main interaction with the SDH diameter is caused by the beam in passive direction. This will increase at larger depth (Figure 6-12) and as a consequence the SNR will decrease.

All SDHs (except at 5 mm depth) exhibit SNR values from ten and upwards which are clearly higher than the standard requirements (SNR>2) for reference defects (SS-EN 12680-3:2011).

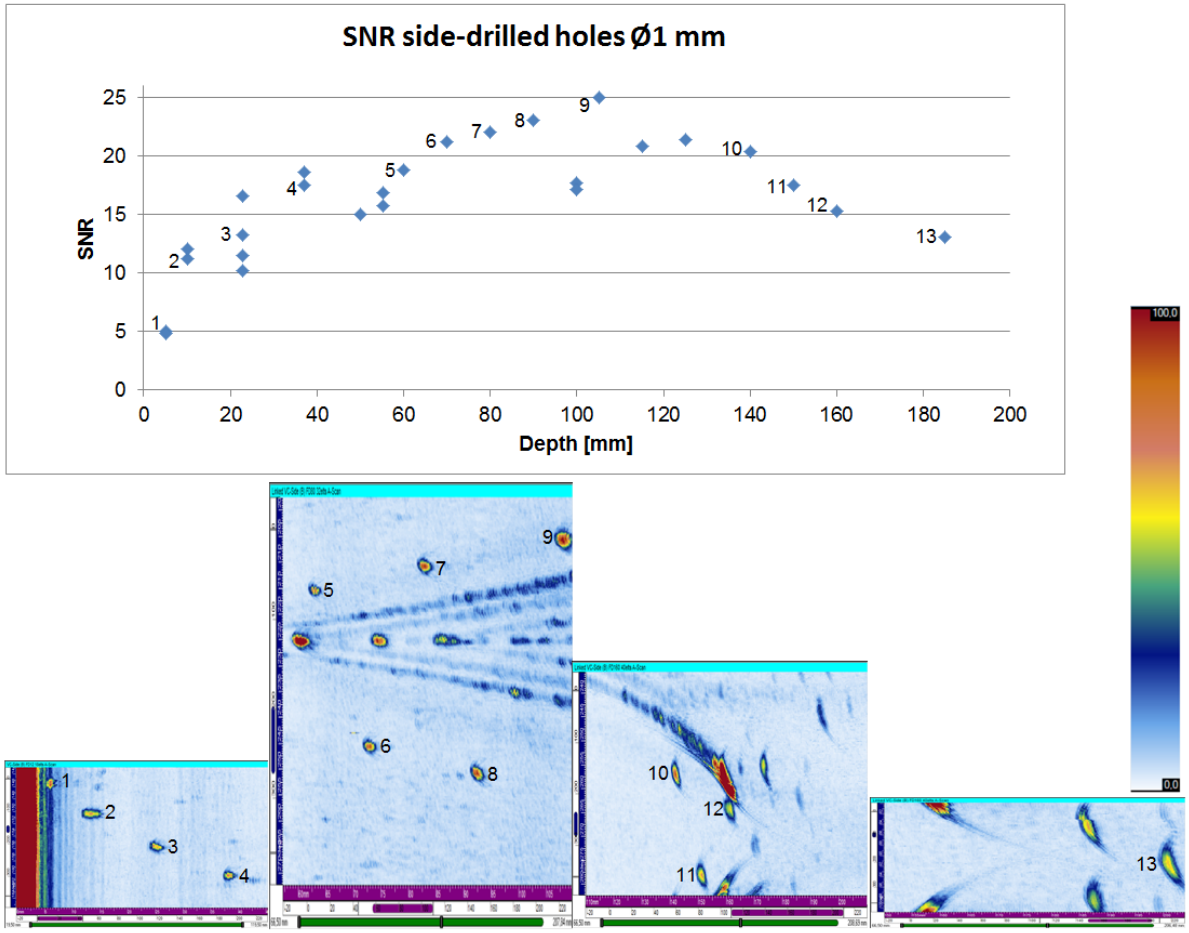

Figure 7-13. *SNR for ultrasonic inspection (UT31) of side-drilled holes (Ø1 mm). The numbered data points in the diagram correspond to the ultrasonic signals in the B-scans showing the maximum amplitude in the circumferential (Y-axis) and radial (X-axis) direction.*

For the angular shear wave ultrasonic inspection technique (UT34), operating at 1.7 MHz, Ø2 mm circumferential side-drilled holes in the depth range of 4 mm to 45 mm were used. The results presented as a signal to noise ratio diagram in Figure 7-14 exhibit high and uniform SNR values along the whole depth. As shown in this figure, for each of the hole depths, there are two data points, while the ultrasonic views (A-, B-, C-, and D-scans) only show one signal for each depth. These SNR values above 15 are clearly higher than the standard requirements (SNR>2) for reference defects (SS-EN 12680-3:2011).

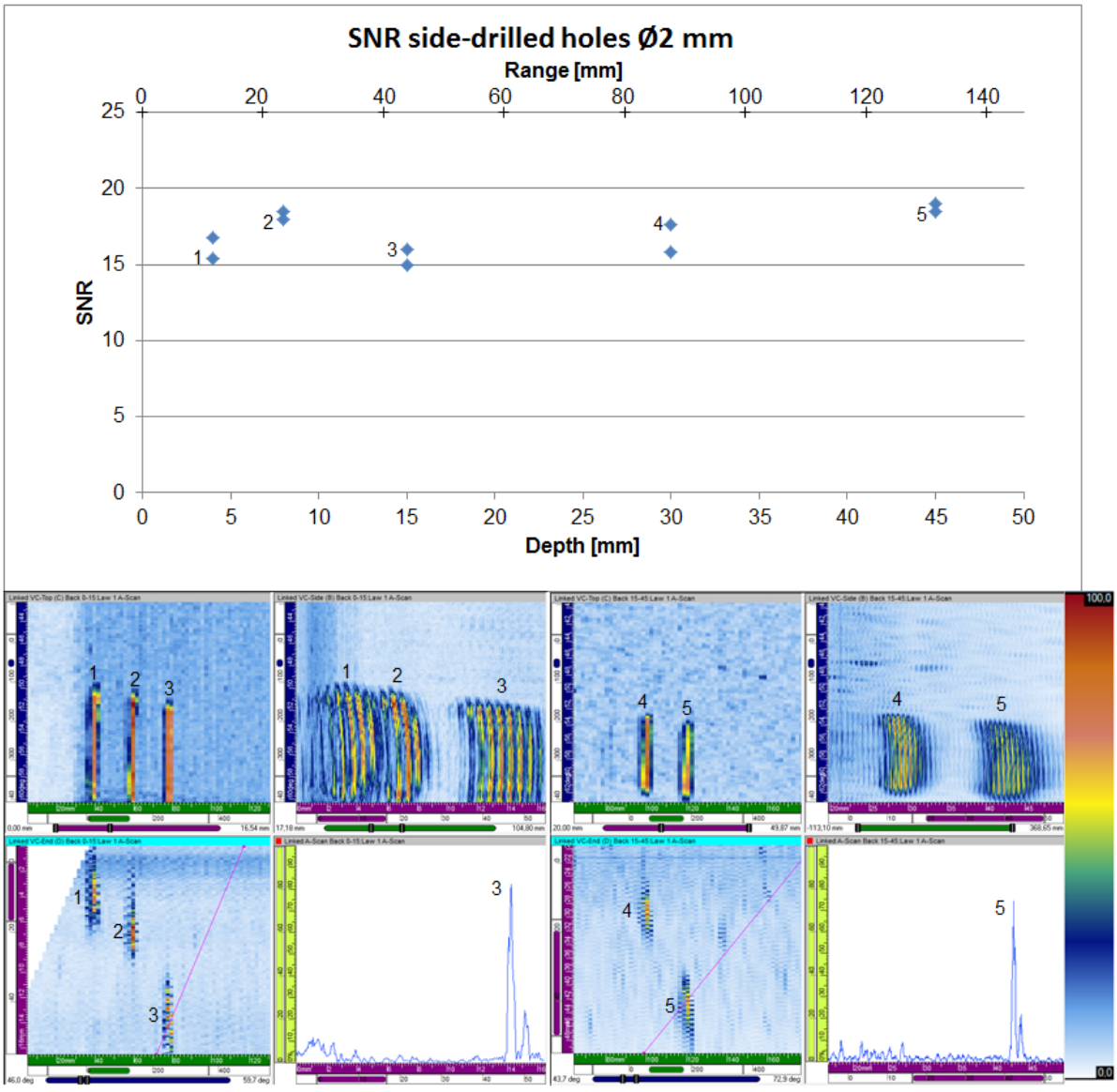

Figure 7-14. *SNR for ultrasonic inspection (UT34) of side-drilled holes (Ø2 mm). The numbered data points in the diagram correspond to the ultrasonic signals in the views. The ultrasonic data are presented for two ultrasonic channels, axial inspection direction towards the bottom for the depth 0-15 mm and 15-50 mm respectively, each showing four ultrasonic views: C-scan (top left), B-scan (top right), D-scan (bottom left) and A-scan (bottom right). The axes are represented by colours as follows: circumferential axis (blue), axial axis (green) and radial (magenta).*

For the ultrasonic inspection technique (UT33), operating at 2 MHz, Ø4 mm axial side-drilled holes in the depth range of 4 mm to 45 mm were used. The results presented as a signal to noise ratio diagram in Figure 7-15 exhibit very high and uniform SNR values along the whole depth. As shown in this figure, for each of the hole depths, there are two data points, while the ultrasonic views (A-, B-, C-, and D-scans) only show one signal for each depth. These SNR values about 30 are very much higher than the standard requirements (SNR>2) for reference defects (SS-EN 12680-3:2011).

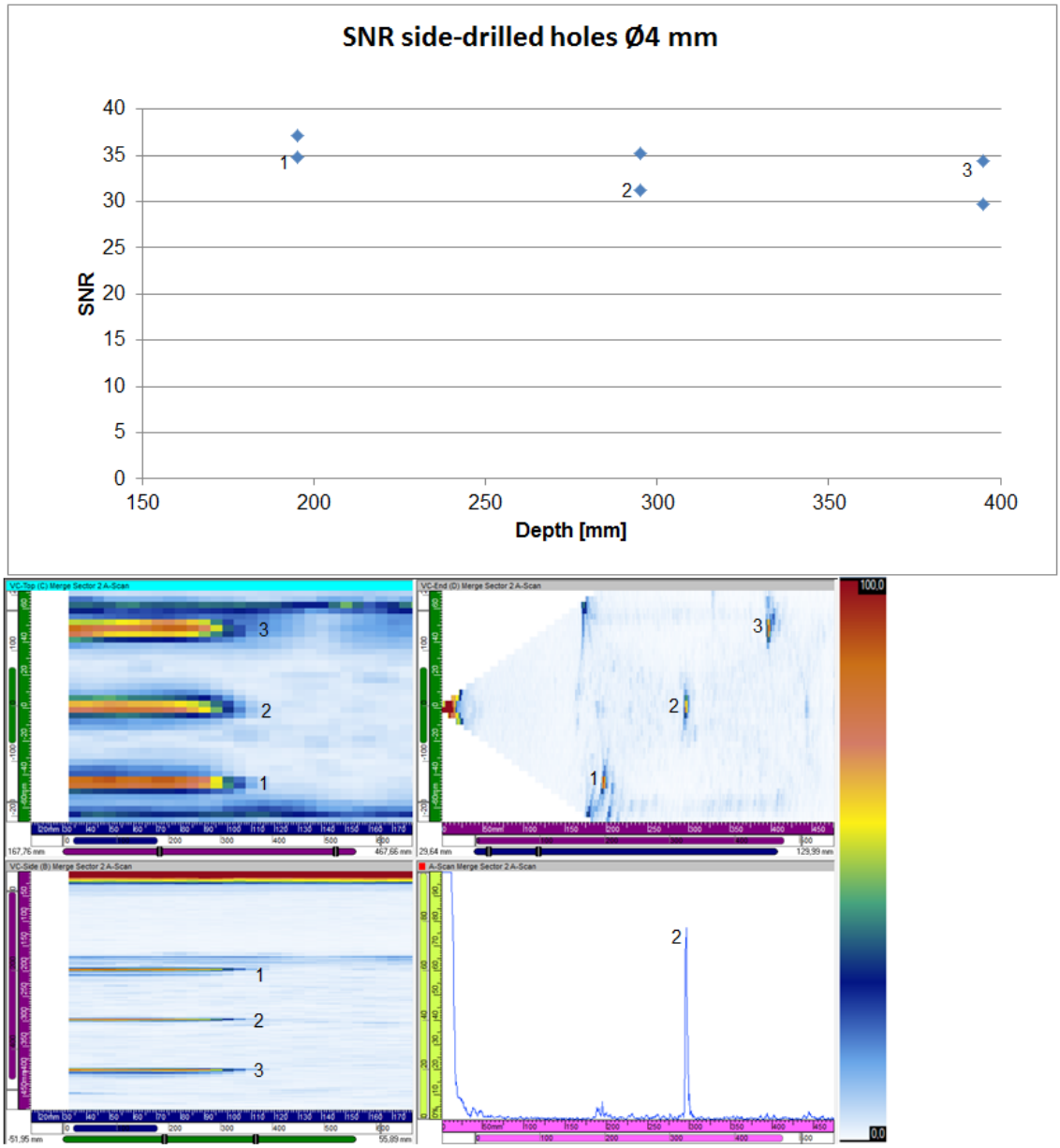

Figure 7-15. *SNR for ultrasonic inspection (UT33) of side-drilled holes (Ø4 mm). The numbered data points in the diagram correspond to the ultrasonic signals in the views. The ultrasonic data are presented in four ultrasonic views: C-scan (top left), D-scan (top right), B-scan (bottom left) and A-scan (bottom right). The axes are represented by colours as follows: circumferential axis (blue), axial axis (green) and radial (magenta).*

The above presented investigations support, by the high and homogeneous SNR along the depth, the assumption that cast iron material exhibit rather low ultrasonic attenuation for the applied ultrasonic frequencies. The only indication of decrease in SNR by depth concerns the normal incidence technique (UT31). However, this is judged to be caused by the large sound field in the passive

direction and its interaction with the SDHs. Additionally, it can be noted that the material exhibit low attenuation for both longitudinal and shear waves.

Summary of experiences

The experience gained from the evaluation of the developed ultrasonic inspection techniques can be summarised as follows:

- At inspections of early produced inserts, the most common indications were either point-like or widespread, such as the clustered porosity described above.
- In some early manufactured inserts, a few high-amplitude defect indications were observed originating from blowholes.
- No indications were observed in the central part of the insert by the UT33 inspection with the developed technique for the newly manufactured PWR inserts. However, in one segment of an early manufactured insert, a porosity cluster was detected.
- No BWR insert was inspected with the new UT33 technique developed for the central part of the inserts.
- At the inspection of the recently manufactured PWR inserts (IP23. IP24 and IP25), only a limited number of small point-like indications (some near the channel tube walls) were detected.
- The boundary between the cast material and the channel tube walls exhibit varying degrees of bonding.
- The attenuation at the applied frequencies for the further developed ultrasonic techniques is low. This results in high SNR for artificial defects and providing possibility for high detectability of real defects.

7.1.2 Surface inspection techniques

As part of the initial acceptance of the delivered insert casting, the supplier performed a magnetic particle inspection of the pre-machined insert surfaces. This manual inspection was conducted by the foundry using an AC yoke and fluorescent magnetic particles. To ensure the detectability for defects with random orientations, the inspection was performed in two orthogonal directions. The inspection was conducted in accordance with the general requirements outlined (SS-EN ISO 9934-1:2001, SS-EN ISO 9934-2:2003, SS-EN ISO 9934-3:2002) and the foundry industry specific requirements (SS-EN 1369:1997). All indications with a length exceeding 1.5 mm were to be recorded and documented together with information regarding the orientation of the indications.

Two typical types of indications at two different types of locations were reported. One type was found located on the envelope surface of the insert. These linear and continuous indications, an example is designated MT-1 below, were all with a maximum length of 4 mm. Another type was located on the end surfaces near and in the connection with the cassette structure, either the channel tubes or the bottom round bars. These indications, examples of which are designated K2 and B1 below, were somewhat larger, although were primarily located close to and along the interface between the casting and cassette structure. All of these three indication examples from magnetic particle inspection, designated MT-1, K2 and B1, were cut and analysed by SEM-EDS (scanning electron microscopy – energy-dispersive X-ray spectroscopy) to obtain information regarding the defects that cause the indications. Subsequent analyses were performed after repetitive removal of the material to determine the actual depths of the defects.

Figure 7-16 shows the 3 mm linear magnetic particle indication MT-1 detected in the circumferential direction on the envelope surface of the insert.

The SEM-EDS analyses of the MT-1 indication showed that the corresponding location showed evidence of micro-porosity in combination with degenerated graphite and a reduced concentration of graphite nodules. It is believed that this indication was primarily caused by the aligned micro-porosity.

The depth of the defect was less than 0.5 mm. The defect showed an intermittent appearance rather than a continuous appearance, similarly to the original indication. As the red arrows in Figure 7-17 indicate a fixed, absolute orientation of the sample, it could be concluded that the orientation of the defect depends on depth.

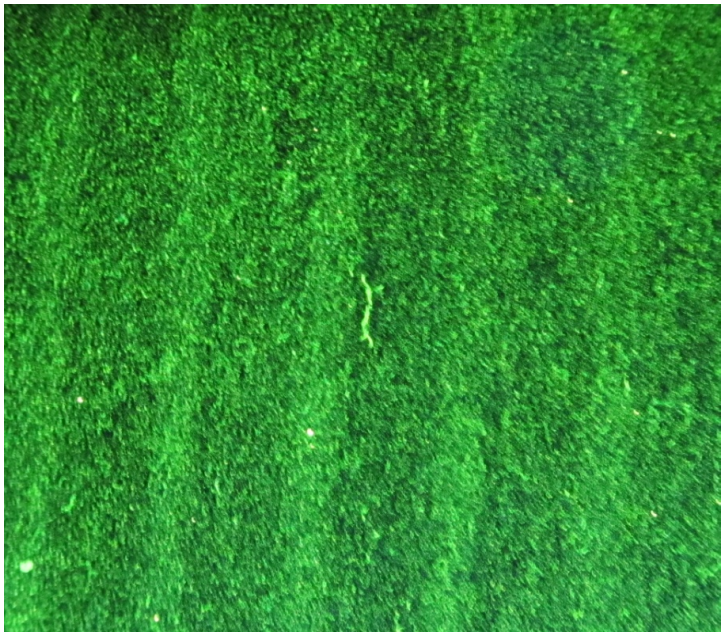

Figure 7-16. *MT-1, a 3-mm linear indication obtained by magnetic particle inspection. The indication detected on the envelope surface of the insert is oriented in the circumferential direction. The five broader, weaker, non-relevant indications along the entire figure in the same vertical direction of the figure are caused by magnetic leakage fields related to the surface finish left by the turning operation.*

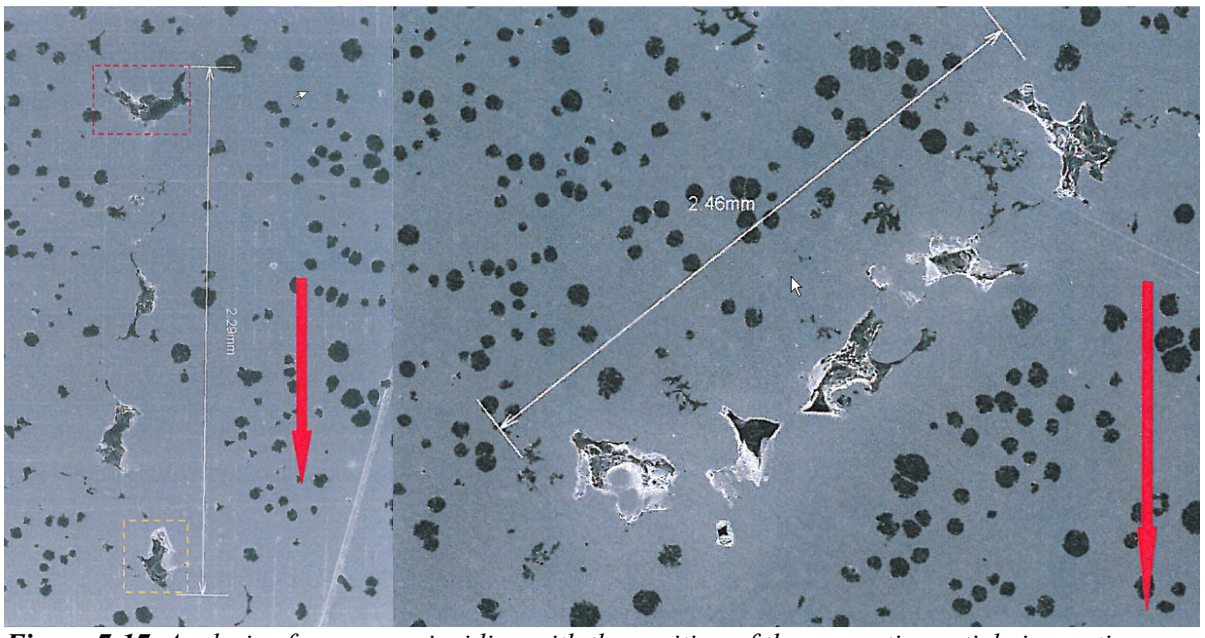

Figure 7-17. *Analysis of an area coinciding with the position of the magnetic particle inspection indication, MT-1, which was detected on the envelope surface of the insert. The red arrow indicates a fixed, absolute orientation of the sample. The analysis indicates the presence of micro-porosity and degenerated graphite. The image on the left shows the defect analysed at the surface, and the image on the right shows the defect analysed at a depth of 0.4 mm. The coloured rectangles denote the locations selected for detailed analysis.*

The linear magnetic particle indication, K2, detected along the interface between casting and channel tube wall, is shown in Figure 7-18.

The analyses of the K2 indication showed the presence of thin, continuous casting defects, which consist of complex magnesium oxides (slag) with a graphite agglomeration, as shown in Figure 7-19. The defect depth could not be determined because it occurred throughout the entire cut-out sample.

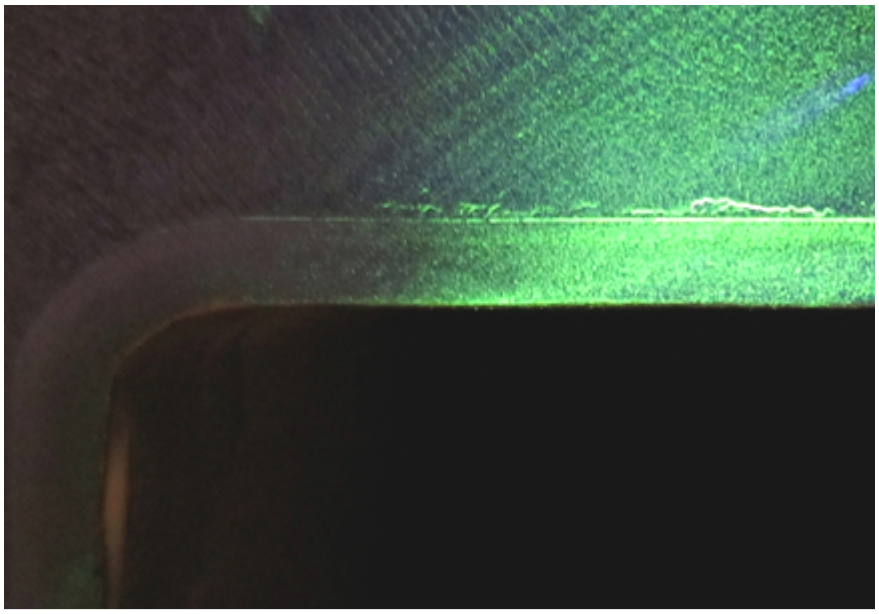

Figure 7-18. K2, *linear indications obtained by magnetic particle inspection of the insert end surface along the interface between the casting and channel tube wall. The thickness of the channel tube steel wall is 12.5 mm.*

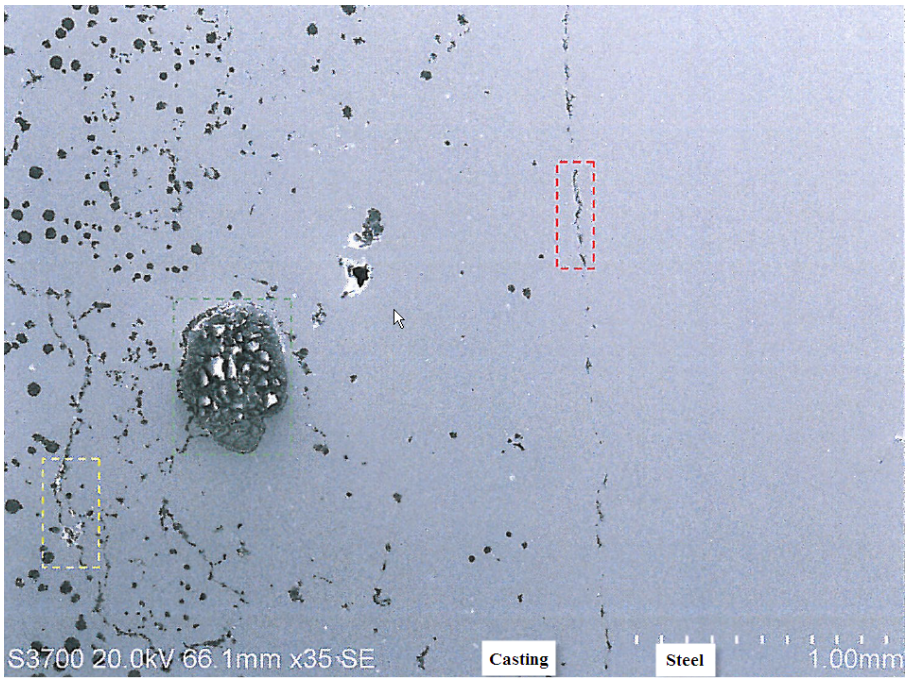

Figure 7-19. *Analysis of an area coinciding with the position of the magnetic particle inspection indication K2, detected in connection and along with the interface between the casting and the channel tube steel wall. The interface is shown in the figure as an intermittent vertical line. The analysis revealed the presence of slag and sand. The coloured rectangles denote the locations selected for detailed analysis.*

The linear magnetic particle indication, B1, detected along the interface between the casting and the round steel bar at the bottom of the cassette is shown in Figure 7-20.

The analyses of the B1 indication showed that the corresponding defect contained slag and sand particles. The defect extended down to a depth of approximately 3.6 centimetres below the inspected surface, which corresponds to the interface between the casting and the steel nut, as shown in Figure 7-21.

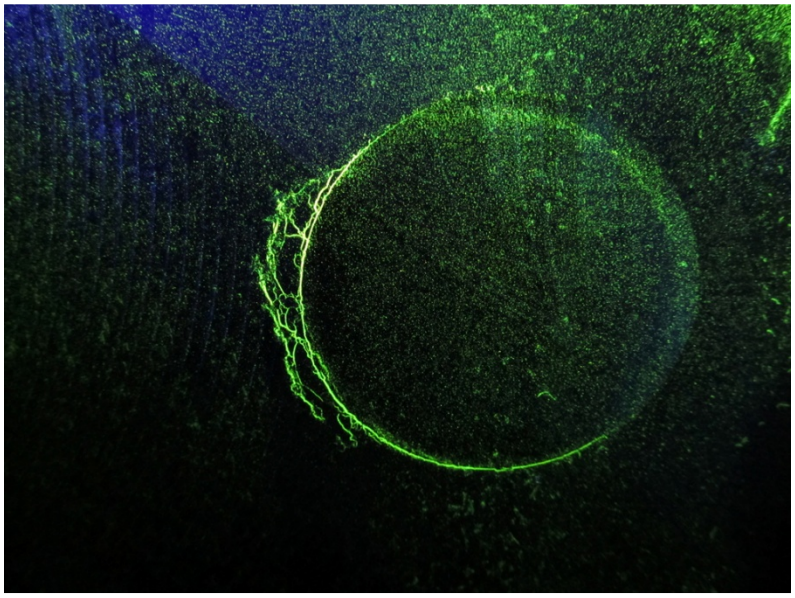

Figure 7-20. *B1, linear indications obtained by magnetic particle inspection of the insert bottom end surface along the interface between the casting and cassette bottom round bar (M48 screw).*

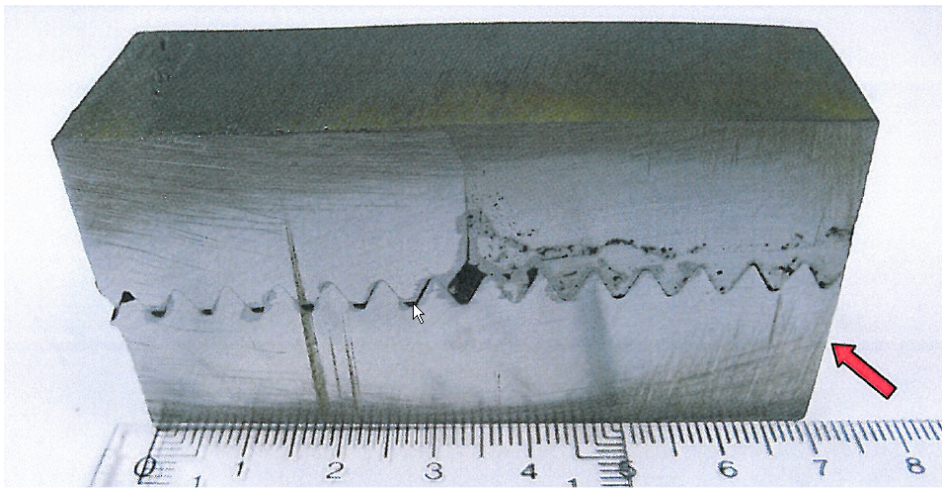

Figure 7-21. *SEM-EDS analysis of an area coinciding with the position of the magnetic particle inspection indication B1 detected in connection and along with the interface between the casting and the cassette bottom round bar. The lower part of the sample depicted is the bar, the upper left part is the cassette bottom nut and the upper right part is the casted material. The analysis revealed the presence of inclusions of slag, which contained Mg, and quartz sand inclusions. The red arrow indicates the bottom surface of the insert inspected by magnetic particle testing.*

7.1.3 Manufacturing of defects

Access to samples containing real defects, which could occur in the final state of insert, is important for several different reasons. From a general point of view, it is necessary to compile information regarding the typical, actual physical and geometrical appearance and extension of defects and to understand the behaviour when such defects are exposed to external mechanical loads.

Artificial defects

For the different NDT techniques, samples that contain real defects are required to be used as reference defects. The reference defects are used to set the defect sensitivity levels and to evaluate the reliability of the technique. In previous projects and as a consequence of limited detailed defect descriptions, artificial defects, such as flat-bottom holes and side-drilled holes, together with surface-breaking EDM notches were used for the ultrasonic and eddy current techniques. During this work, a number of new artificial defects were manufactured, including narrow EDM notches with widths of 0.2 mm. A method for manufacturing non-surface-breaking EDM notches with small ligaments was also developed. Examples of such notches with ligaments are shown in Figure 6-26.

Realistic defects

Defects in the final insert could be connected to the cassette, its sub-parts and the corresponding assembly/welding, casting and/or subsequent machining processes. Because casting defects were judged to be the most important, a pre-study was performed in which small test objects (< 50 kg) with casting defects were manufactured in a controlled manner. Simulations determined suitable casting parameters, and casting tools were designed based on the results. Figure 7-22 shows a CAD model of the casting layout. A few test objects were manufactured and evaluated. Figure 7-23 shows the results obtained from radiographic film and pulse-echo ultrasonic inspection of castings with internal indications, which were believed to originate from defects such as shrinkage pores and/or pore clusters. The objective of future work is to determine whether this approach might be suitable for creating samples with reference defects to set sensitivity levels and validate inspection techniques.

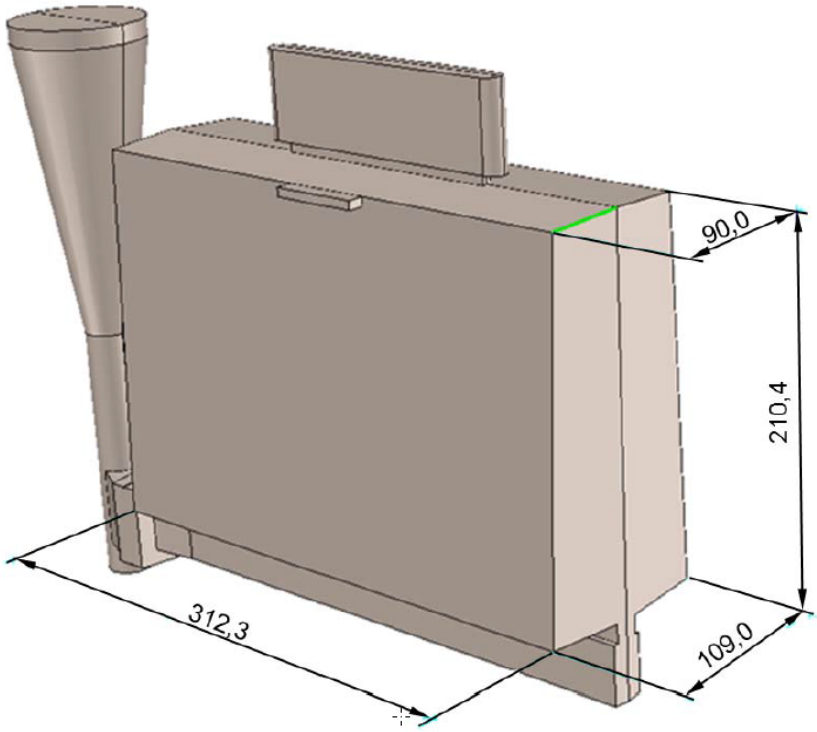

Figure 7-22. *CAD model of the casting layout.*

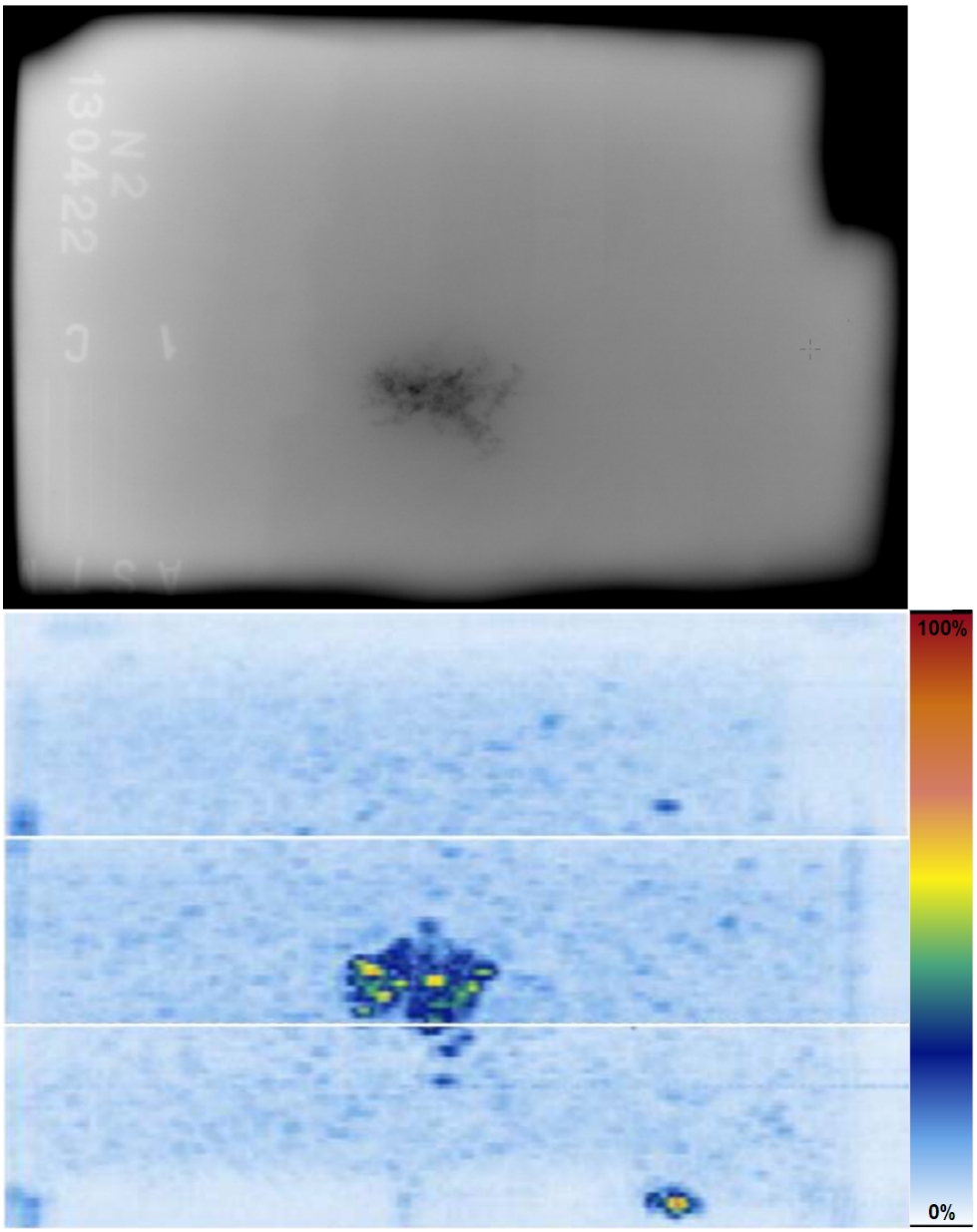

Figure 7-23. *Results from radiographic film (top) and ultrasonic pulse-echo inspection (bottom) of a casting with internal indications, which are believed to originate from defects such as shrinkage and pore clusters. Note: the ultrasonic indication down to the right is a geometrical indication caused by lack of material at the side surface.*

7.2 Copper tube

For a number of years, SKB has performed inspections of both small parts and full-size components in parallel with the development of NDT techniques. Through these efforts, valuable experience and results from some defect indications have been obtained, which are summarised in the following sub-sections.

The main work has been performed on extruded and pierce-and-drawn tubes, whereas limited work has been conducted on earlier stages in the production chain.

7.2.1 Inspection of copper tube ingots

Copper tube ingots are inspected by penetrant testing before delivery, and the available results obtained from that manufacturing stage are limited to the information described in section 6.3.1. However, a penetrant inspection was also performed on the end surfaces of an earlier, in 1998, casted copper tube ingot, during which the excess material at the ends of the ingots, which is susceptible to casting defects, was not removed. The ingot identification was 268-2-1 and is further described in SKBdoc 1175208. The penetrant results show larger indications from, spider-crack defects at the centre of ingots, and several surrounding scattered, smaller indications, as shown in Figures 7-24 and 7-25.

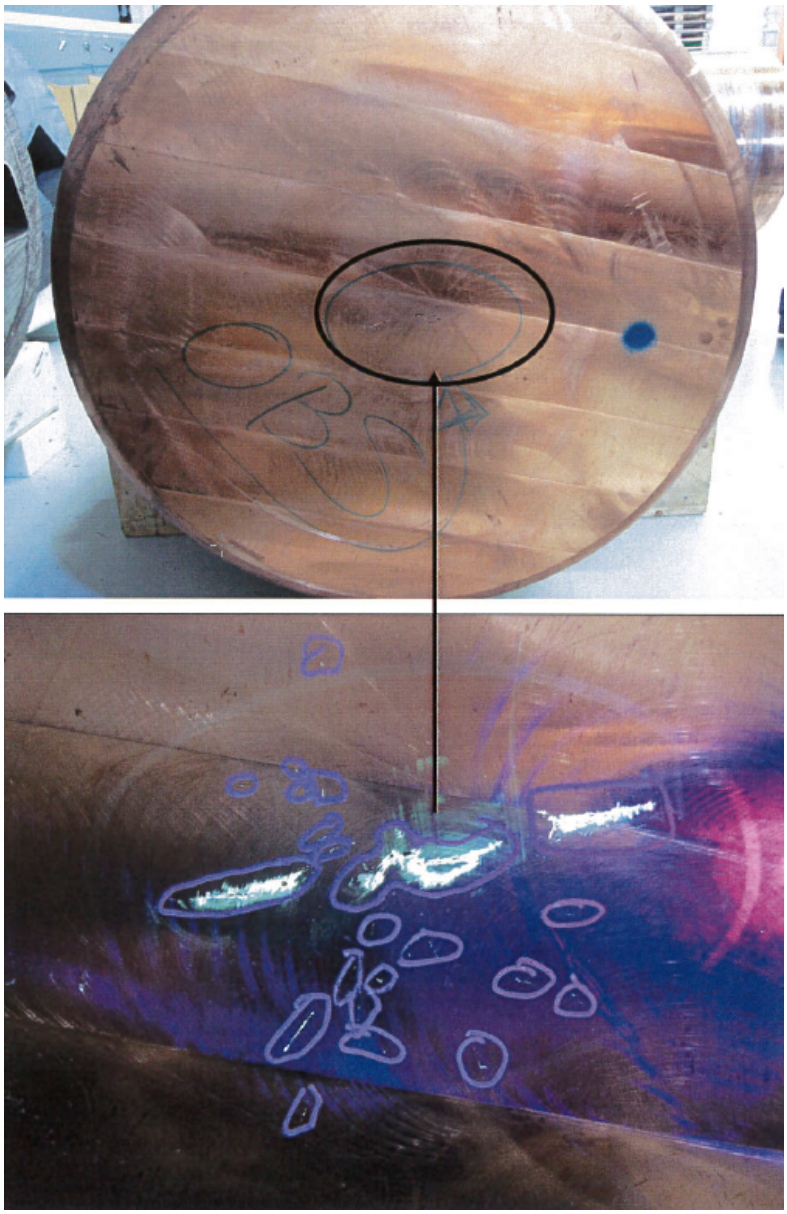

Figure 7-24. *Penetrant inspection results for the copper tube ingot 268-2-1; the excess material at the ends of the ingot, which is susceptible to casting defects, was not removed. The penetrant results showed larger indications from, spider cracks in the centre of the ingot, and several surrounding, scattered, smaller indications. A close-up image of the detected, shrinkage-type defects is shown in Figure 7-25.*

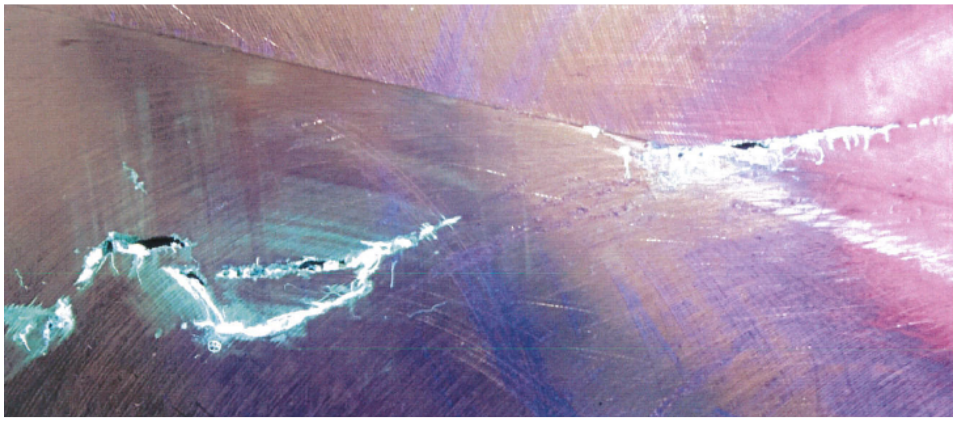

Figure 7-25. *Close-up image of the detected spider-crack defects shown in Figure 7-24.*

7.2.2 Inspection of copper tubes

Until the end of 2013 about 40 tubes had been inspected by ultrasonic inspection, and approximately 10 of these had been inspected by the further developed normal incidence technique (UT11 version 2.0). The results show that the general tube quality is high and that almost no relevant defect indication has been observed. The indications are all caused by surface defects and, with a few exceptions, are related to handling damage, such as indentations and foreign material, as shown in Figure 7-26. These defects have also been detected by informal visual inspection performed in conjunction with ultrasonic inspection as no dedicated surface inspection technique has been developed to date. The only manufacturing defects that have been observed is one surface scratch in an extruded tube and one crack-like defect on the envelope surface of the integrated base of a pierce-and-draw tube, which are shown in Figure 7-27. Both of the defects had a propagation of approximately 5 centimetres along the length of the tube and a depth of a few millimetres.

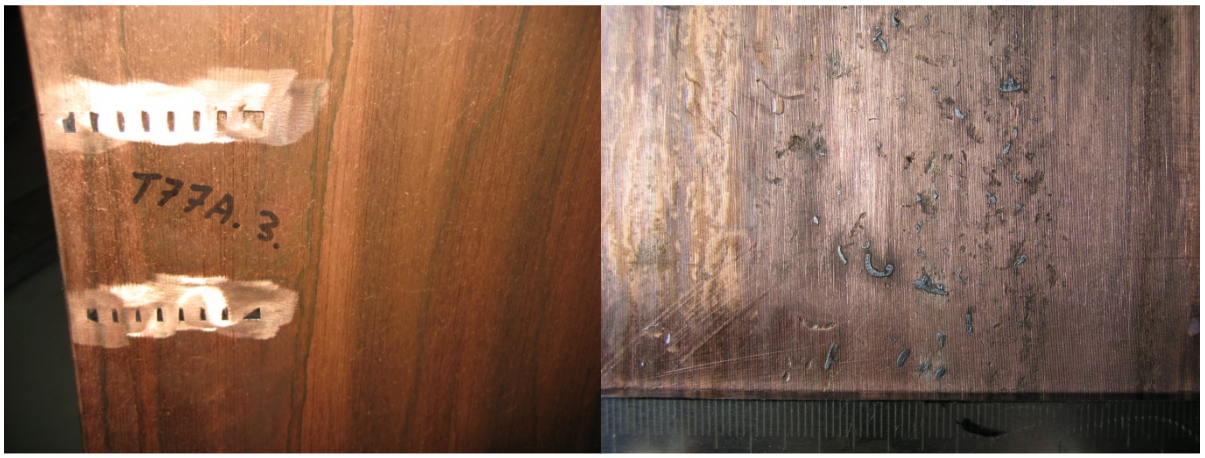

Figure 7-26. *Handling defects manifested as indentations on the inside of tube T77 (left) and foreign material on the outside of tube T43.*

Figure 7-27. *Manufacturing defects in copper tubes. The left image shows an axial scratch (T46) in an extruded tube and the right image shows a crack-like defect in a pierce-and-draw tube (T83).*

SKB (2010) describes how the variations in ultrasonic attenuation, both within and between different tubes, have been observed. Based on this documentation, a number of actions were taken to investigate both the reason for the variations (particularly within tubes) and how the variations can be handled from an inspection point of view. Within the framework of the development of the manufacturing process (SKBdoc 1432038), three copper tubes (T65, T66 and T67) were inspected, both as pre-machined tubes and also during the intermediate manufacturing step when the blocker was formed. The inspection of the blocker was performed with the assumption that the thick (>200 mm) blocker wall would have a coarse grain structure, which would have indicated that inspection results were not attainable. However, during the preparation of the inspection procedure, it was observed that the back wall echoes could be obtained by using any probe, and therefore, it was decided that the same 5-MHz array that, at that time, was used for the normal tube inspection could be used.

Ultrasonic inspection was performed in the manipulator (described in section 6.1.1) on three tubes (T65, T66 and T67), both in the blocker state and as pre-machined tubes. Because the primary purpose of the inspection was to investigate how the ultrasonic attenuation varied within each component and, in particular, whether any deviations were transferred from the blocker to the tube, the focus of the inspection was the back wall echo amplitude. The results from the inspection surprisingly showed that the back wall echo amplitudes were more uniform in all blockers than in the tubes, despite the wall thickness being almost five times greater. In Figure 7-28, the results obtained from the inspection of a blocker and the corresponding tubes are shown. The blocker exhibited a uniform result, except for a few darker areas where scratches or unmachined areas caused a local decrease in the back wall echo amplitude. In contrast to the blocker, the further processed tube exhibited a non-uniform ultrasonic attenuation, where two areas exhibited increased attenuation; one greatly increased (marked in black) and one with a more moderate increased attenuation (marked in red).

From an inspection point of view, as described in section 6.3.2, the ultrasonic inspection frequency was reduced from 5 MHz to 3.5 MHz to make the inspection less sensitive to grain size variations. In section 8.1.2, the effect of different attenuation levels on the inspection sensitivity is described.

Ultrasonic inspection (UT11) has been performed in the same manner and with the same local immersion tank (Figure 6-8) that was used for inspection of inserts, and therefore, approximately 5 centimetres at the top and bottom of the tube were not covered by the inspection. In section 6.3.2 it is mentioned that the ultrasonic inspection is performed at the pre-machined state of the copper tube and that this assess the whole volume to be covered. In Figure 7-29 results from ultrasonic inspection of the depth range 0-20 mm is shown. The results shows that the surface echo, with margin, fade before 5 mm depth (the thickness to be removed in the final machining).

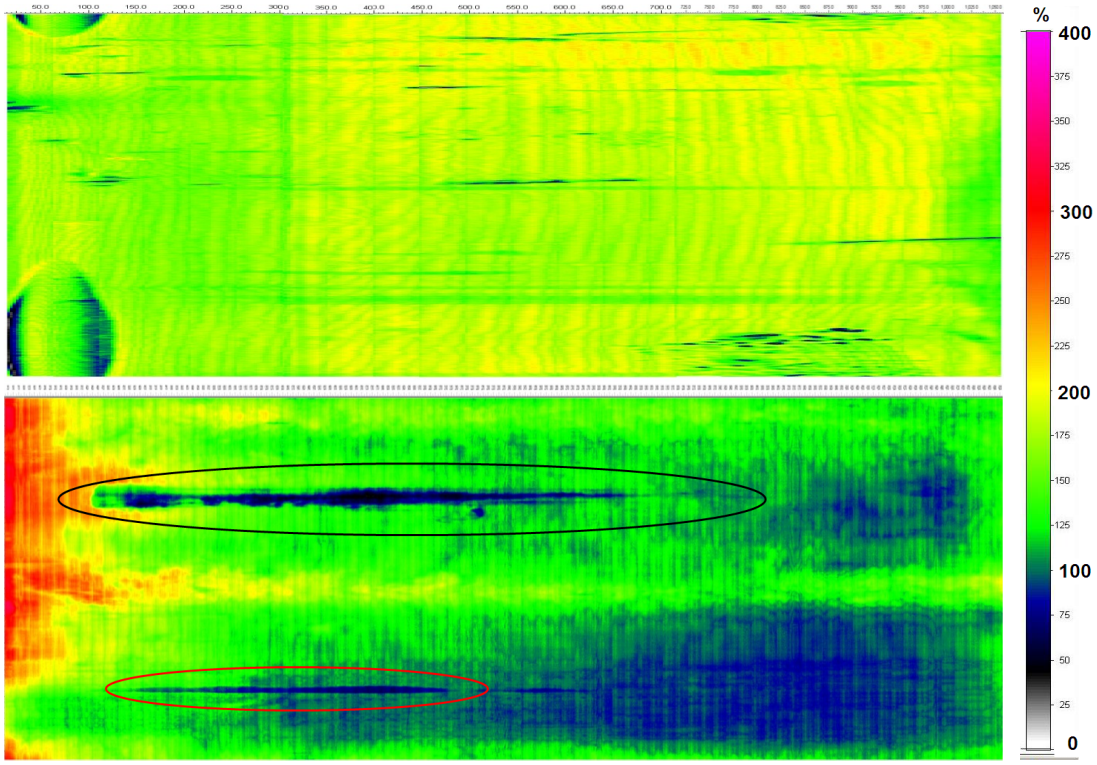

Figure 7-28. *Ultrasonic back wall echo amplitude from tube T66 (vertical axis represents the circumference, and the horizontal axis represents the axial direction). The top image shows the result from the inspection of the blocker, and the bottom image shows the result from the inspection of the pre-machined tube. The circled areas highlight the areas with increased attenuation.*

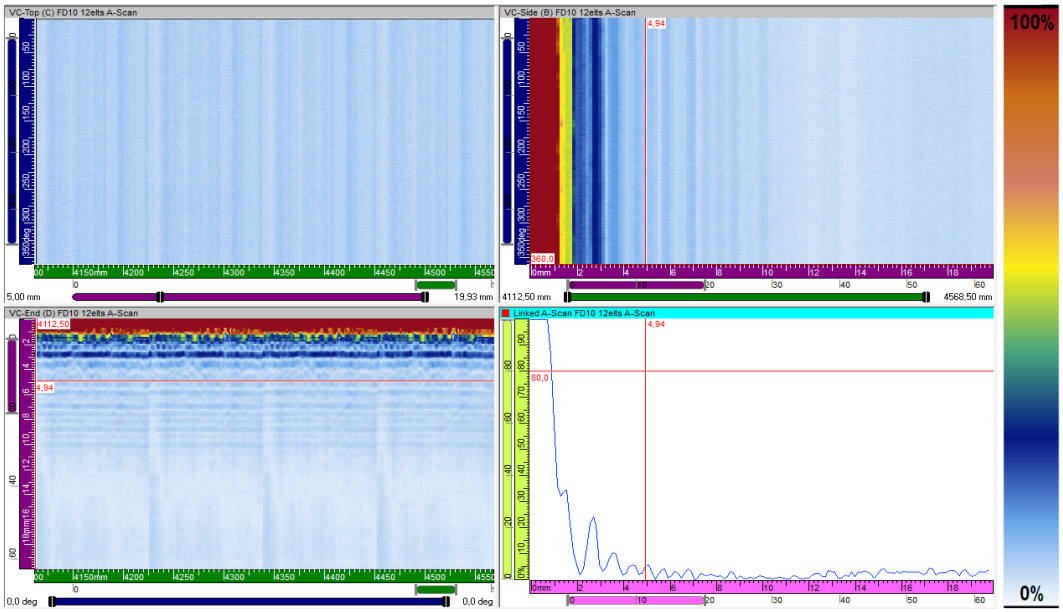

Figure 7-29. *Ultrasonic Results from phased array ultrasonic inspection (UT11) of a copper tube area three directions: C-scan from the envelope surface (top left), B-scan viewed from the end surface (top right) and D-scan viewed along the axial direction (bottom left). The ultrasonic signal as a function of depth is shown in the A-scan (bottom right). The red cursor indicates the 5 mm that will be removed in the final machining and the reporting threshold applied.*

In a manner similar to (but not as significant as) that of the insert inspection (section 7.1.1), it was occasionally observed that the surface roughness and shape affected the resolution near the inspection surface.

7.2.3 Manufacturing of defects

To date, no practical tests have been performed with the goal of manufacturing defects in the copper tubes in a controlled manner. Because the primary cause of defects in the tubes was identified to be the deformation of defects in the used ingot, work will start with an analysis and the development of a way to manufacture defects in the ingot. In parallel, it has been identified that a suitable process for manufacturing small-scale copper test objects with relevant grain structure, which would be used as test objects for the ultrasonic inspection of copper tubes, is needed.

7.3 Copper lid/base

For a number of years, SKB has performed inspections of full-size lids and bases (hereafter referred to as lids) in parallel with the development of NDT techniques. Within this context, valuable experience and results from several indications have been obtained, which are summarised in the following sub-sections.

The primary work has been performed on machined lids, whereas only limited work has been conducted on ingots.

7.3.1 Inspection of copper lid ingots

A number of copper lid ingots were inspected with fluorescent penetrant. The envelope surface remained as casted, as shown in Figure 7-30, whereas the end surfaces of the ingots were machined.

Due to the rough conditions of the envelope surface, the penetrant inspection resulted in a large number of non-significant indications, which created excessive background noise, as shown in Figure 7-31.

On the machined end surfaces of the copper lid ingot, the conditions for performing a relevant penetrant inspection were much better. The indications obtained on these surfaces, except for one small indication (<1 mm), were related to handling defects. An example of such indications is shown in Figure 7-32.

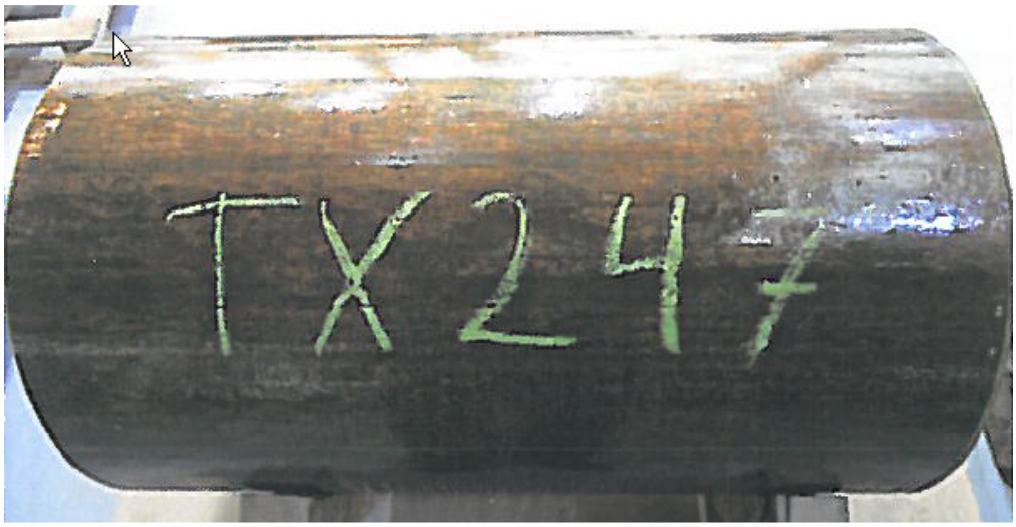

Figure 7-30. *A copper lid ingot prior to fluorescent penetrant inspection with the envelope surface remaining as casted, whereas the end surfaces of the ingots were machined.*

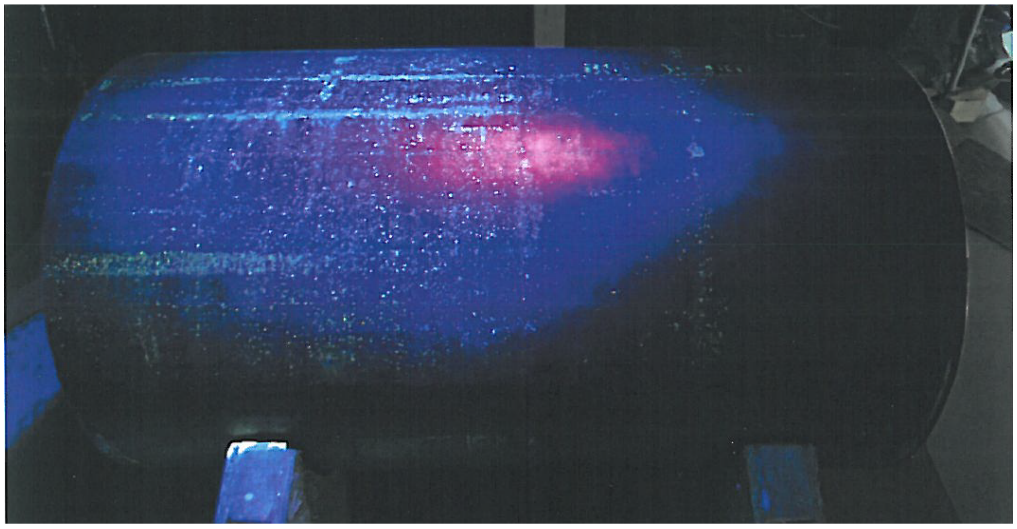

Figure 7-31. *Penetrant inspection results for the envelope surface of a copper lid ingot, which shows a large number of non-significant indications caused by the rough as-cast surface.*

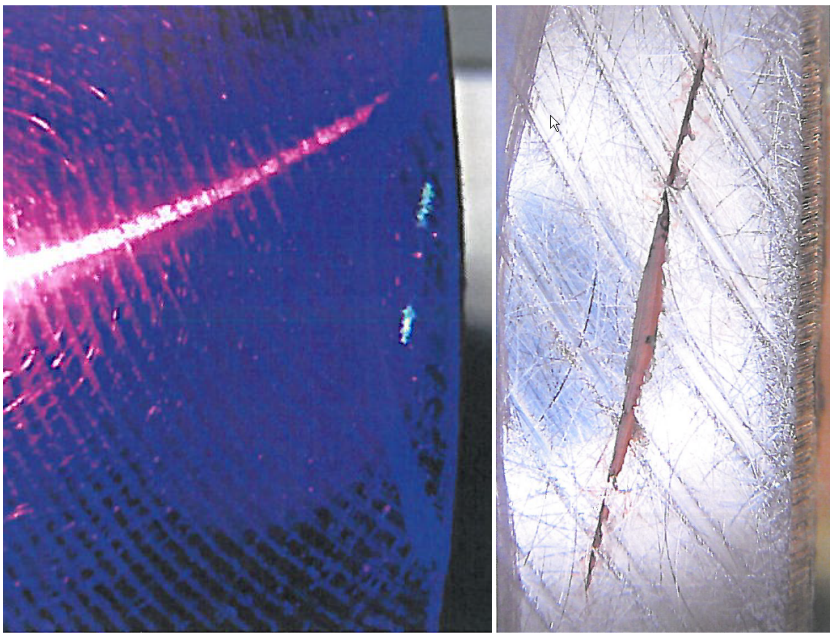

Figure 7-32. *Penetrant inspection results for the end surface of a copper lid ingot showing an indication (left) caused by a sharp handling defect (right).*

7.3.2 Inspection of copper lids

Historically, inspecting copper lids has primarily been performed by ultrasonic inspection; however, due to enhanced knowledge of the formation of defects in lids, the use of dedicated surface inspection techniques has increased. In this section, a summary of the findings is compiled.

Surface inspection technique

A number of copper lids were inspected by fluorescent penetrant inspection in the pre-machined state. On several lids, linear indications were detected on the bottom surface of the lid, that is the inside surface of the lid after sealing of the canister, which were most likely caused by defects of the forging-lap type originated from the forging process. There were numerous indications that were circumferentially oriented, as shown in Figure 7-33.

None of the aforementioned penetrant indications from the forging laps were cut for further metallographic examination. However, on a previously manufactured lid, a forging lap was visually detected and afterwards verified by eddy current inspection. This forging lap was cut, and metallographic examination revealed a defect that extended down to a depth of 8 mm. The metallographic cross-section of the forging lap is shown in Figure 7-34.

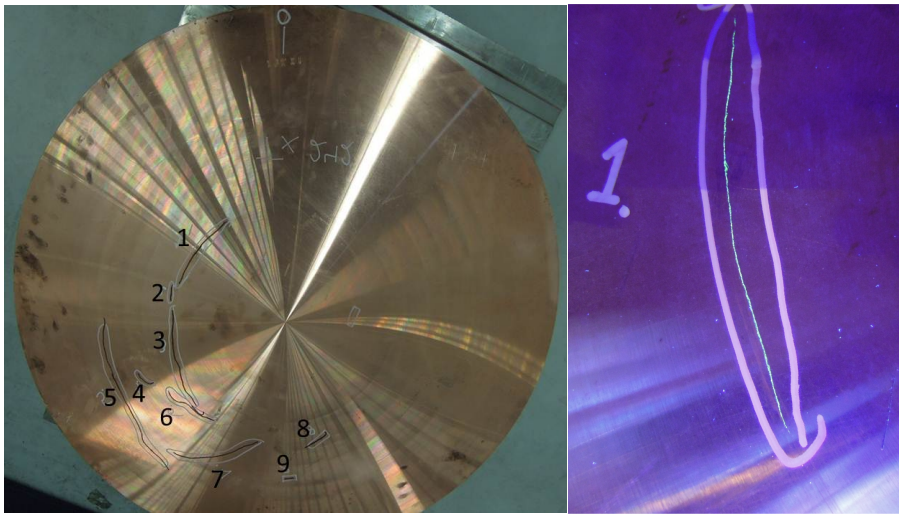

Figure 7-33. *Results from fluorescent penetrant inspection of a lid(TX242) in the pre-machined state. Nine indications were detected on the bottom surface of the lid (left). The indication is circled in white, and the actual penetrant indication is highlighted by a black marker. All indications were linear and more or less circumferentially oriented. A section of indication number 1 is shown in the right image. The linear fluorescent indication is circled in white.*

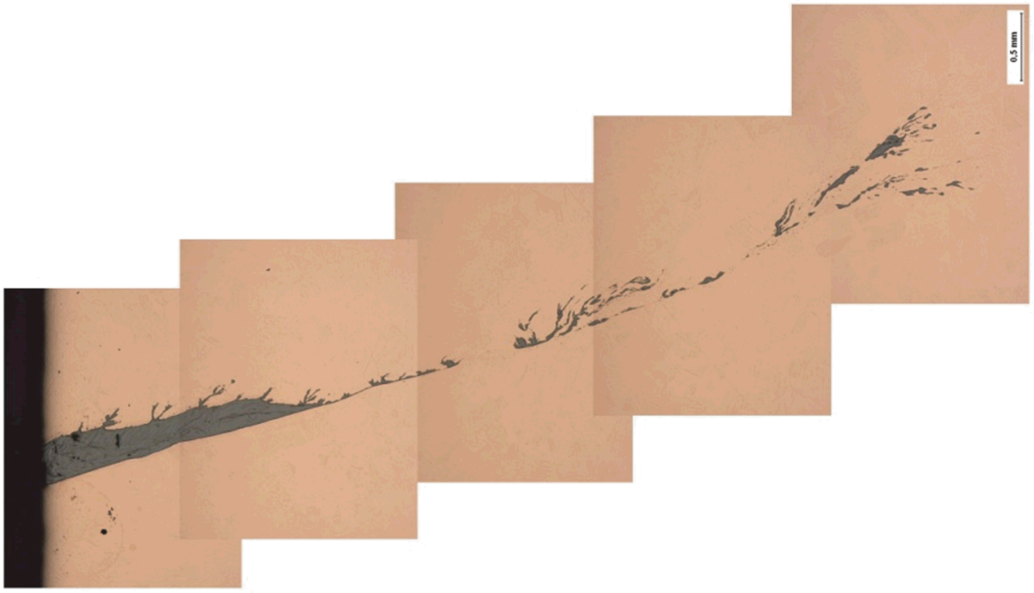

Figure 7-34. *Metallographic cross-section of a forging lap extending from the bottom surface (left). The depth was measured to about 8 mm.*

Ultrasonic inspection technique

Over the years about 60 lids have been inspected by ultrasonic inspection, and about 20 of these lids have been inspected by the further developed technique (UT27). The results show that the general lid quality is rather high, whereas only a few relevant defect indications have been observed. Most of the detected indications are related to the material structure. During the early stages of development of the manufacturing process, large variations were common in ultrasonic attenuation, both within and between different lids. This effect has not been observed over the past few years due to further development of the manufacturing process. However, in several lids, an area measuring up to a few centimetres has been observed with a clear drop in the back wall echo amplitude and without any defect signal response. Based on the results obtained from the ultrasonic inspection of one lid (TX215), a sample was cut, and the etched sample showed that the drop in the back wall echo amplitude was caused by a single large (15 mm) grain, as shown in Figure 7-35.

In addition to the indications caused by variations in the grain structure, only a few of the forging laps described above within the context of the surface inspection technique section have been detected. Figure 7-36 presents an overview of the ultrasonic results obtained in the form of back wall echo reduction from inspection of a lid, in which a number of forging laps were detected by liquid penetrant inspection. As shown in the C-scan in Figure 7-36, not all of the indications detected by the penetrant inspection were detected, and as shown in Figure 7-37, only two of the indications resulted in any ultrasonic reflections. However, it should be noted that ultrasonic inspection is not the primary method for detection of the normally surface-breaking forging laps.

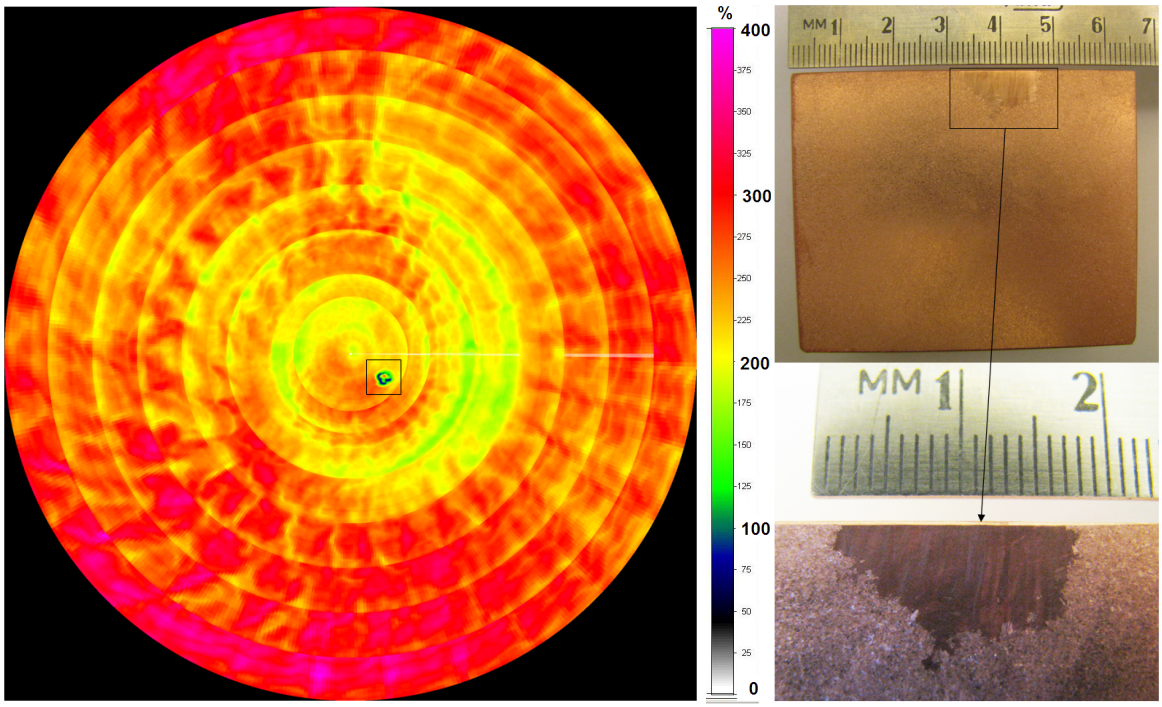

Figure 7-35. *Ultrasonic back wall echo amplitude of the central part of lid TX215 (left) and the corresponding macrograph of the marked indication (right).*

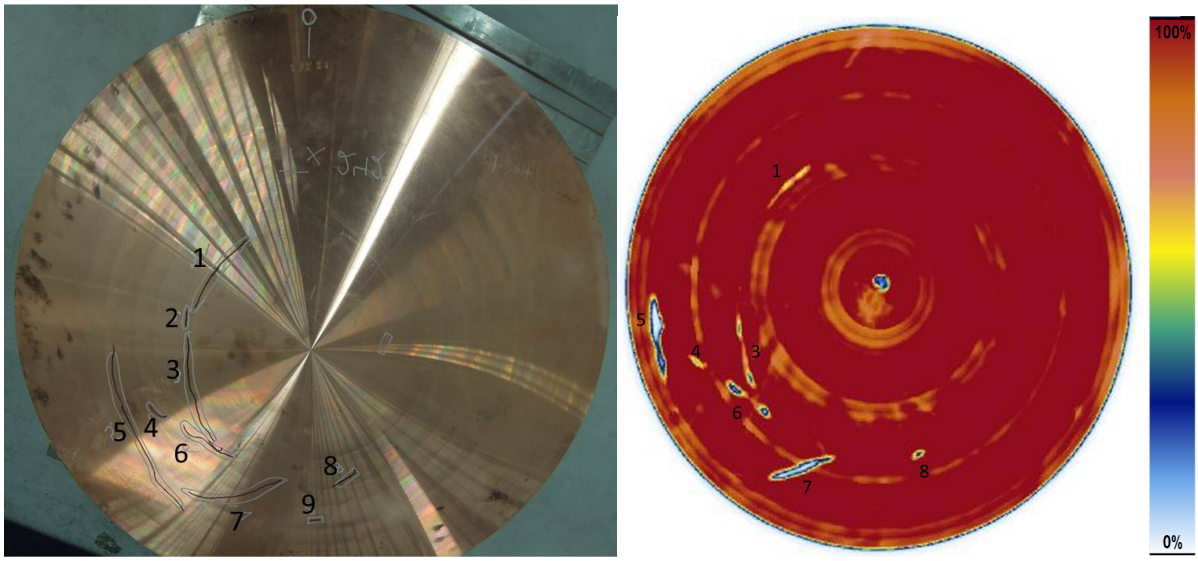

Figure 7-36. *Results from NDT of copper lid TX242. The photograph on the left shows the nine marked indications from the fluorescent penetrant inspection, and the image on the right shows the back wall echo amplitude from the ultrasonic inspection of the central part of the lid with the corresponding indications. The indication in the centre of the lid is assumed to originate from an area with large grains, as described in Figure 7-35.*

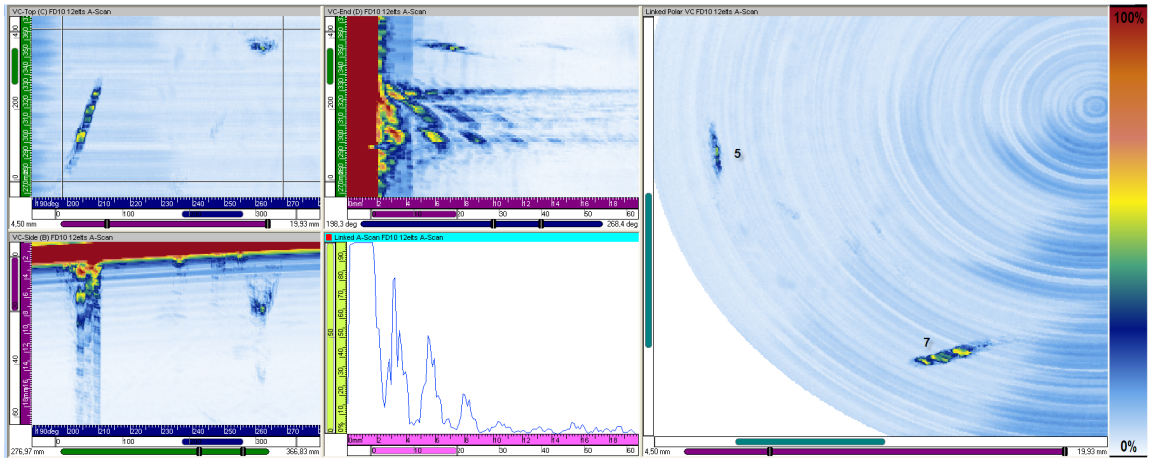

Figure 7-37. *Ultrasonic results from indications 5 and 7 in Figure 7-36. The images on the top left, bottom left, and top middle show the C-scan, B-scan and D-scan, respectively, which correspond with the polar C-scan shown on the right, and the bottom middle image shows the A-scan for the maximum amplitude for indication number 7.*

7.3.3 Manufacturing of defects

To date, no practical test has been conducted in a controlled manner to manufacture defects in copper lids. However, as the manufacturing trials resulted in a number of indicated forging laps that were analysed further, the knowledge of how to manufacture this type of defect is considered to be good. Other defects that were identified are caused by defect deformation in the used ingot, and therefore, work will begin to analyse defect formation in lid ingots.

7.4 Friction stir welding

For a number of years, SKB has performed inspections of both small parts and full-size friction stir welds in parallel with the development of NDT techniques. Within this work, much experience and results from different types of defects have been obtained, which are summarised in the following sub-sections.

7.4.1 Ultrasonic inspection technique

Throughout the years about 100 welds have been inspected by ultrasonic inspection, although only a few of these have been inspected by the optimised technique (UT06). The results show that the presence of larger defects is low in welds performed with normal weld parameters. However, many of the welds created at the Canister Laboratory are produced to test different welding parameters or even with the objective of producing defects for NDT development, and therefore, a rather large number of defects are available. The defects that have been found in friction stir welds can be divided into two groups, near-surface cavities and root defects (joint line hooking and remaining joint).

Based on the findings obtained during the development of the ultrasonic technique and by the experience gathered from the extensive number of inspections performed with previously used techniques, defect formations and their ultrasonic response are considered to be well understood.

The most common root defect is joint line hooking, which is formed by the bending of the vertical joint between the lid and tube that follows the bottom border of the weld. In Figure 7-38, a macrograph shows the characteristics of a joint line hooking and ultrasonic data for a typical indication. The ultrasonic images show an indication for all five inspection angles, ±20°, ±12° and 0°, and it can be observed that the amplitude increases as the inspection angle becomes perpendicular to the defect angle; the highest amplitude is achieved at the inspection angles of -12° and -20°.

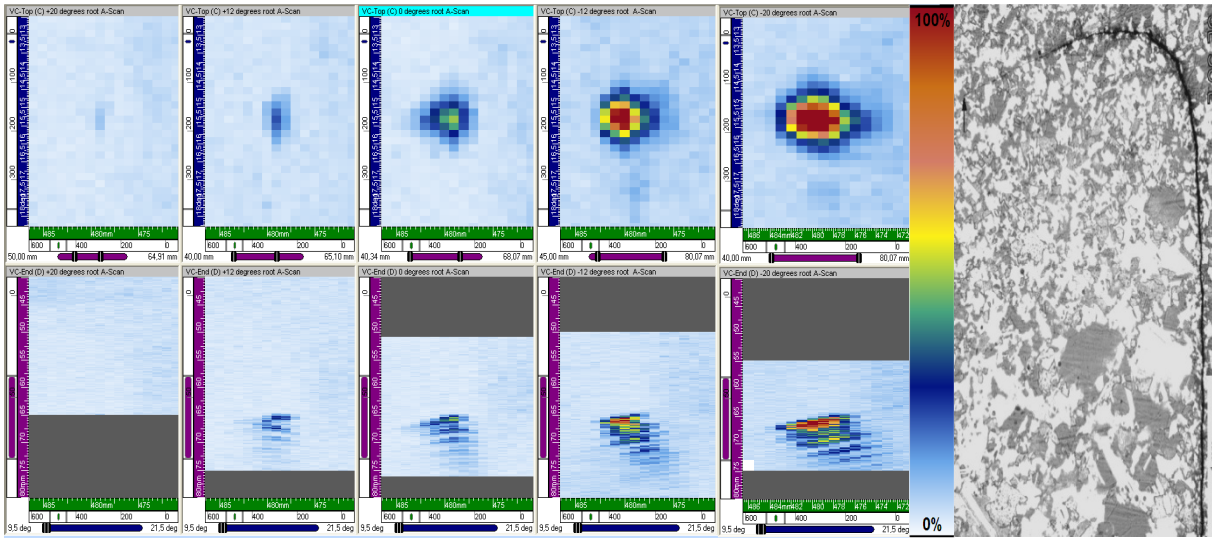

Figure 7-38. *Results from inspection of a joint line hooking. The images on the left show, with the weld surface to the left, the C-scans (top) and B-scans (bottom) for inspection angles of 20°, 12°, 0°, -12° and -20°. In the right image, a macrograph of a joint line hooking is shown.*

The other root defect is the remaining joint that is formed due to a too shallow weld depth, which leaves part of the horizontal joint between the lid and tube un-welded. When it is small (<1 mm), the defect forms an inclined shape, and when the radial size is larger, the defect is horizontal. In Figure 7-39 and Figure 7-40 macrographs of these two variants of the remaining joint together with their corresponding ultrasonic results are shown. For the small inclined remaining joint, it can be observed in Figure 7-39 that the highest amplitude is achieved at an inspection angle of 20°, whereas for the larger defect (~1 mm), similar amplitudes are achieved at all inspection angles (Figure 7-40).

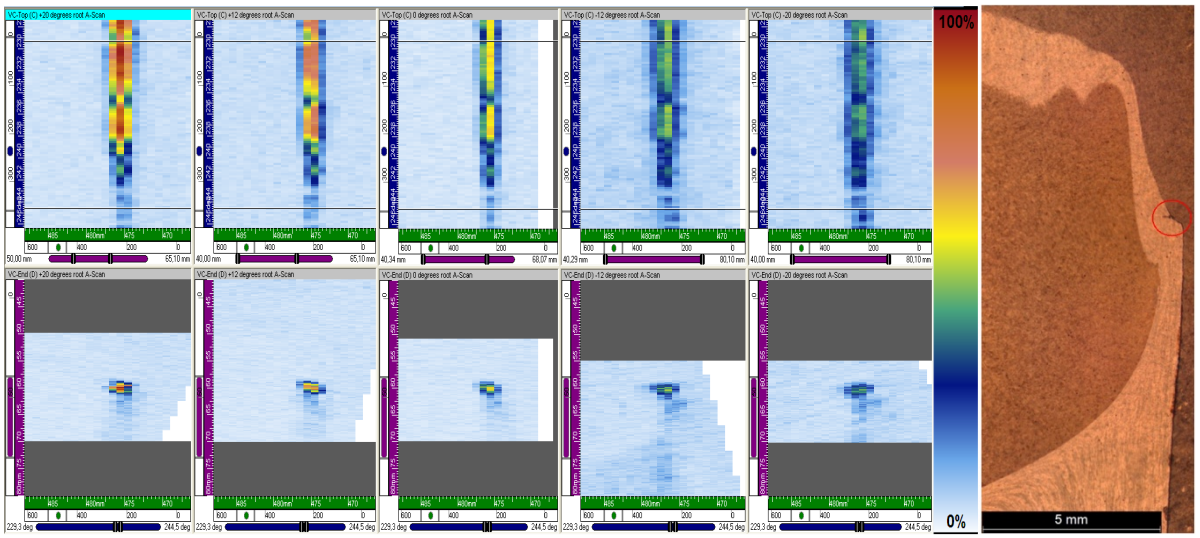

Figure 7-39. *Results from inspection of a minor remaining joint. The images on the left show, with the weld surface to the left, the C-scans (top) and B-scans (bottom) for inspection angles of 20°, 12°, 0°, -12° and -20°. In the right image, a macrograph of a minor remaining joint is shown (circled in red).*

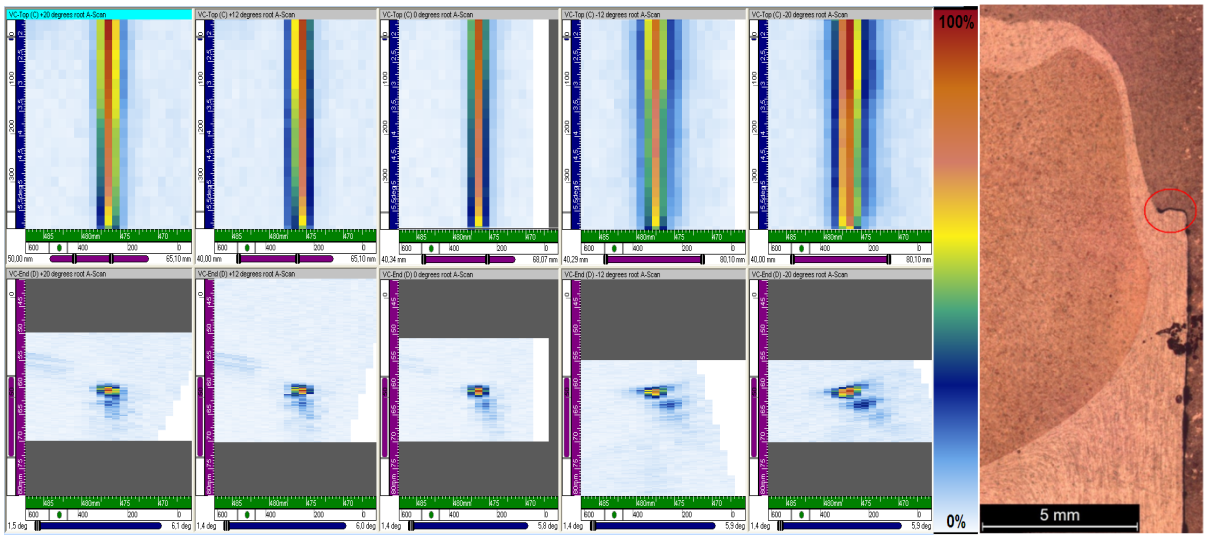

Figure 7-40. *Results from inspection of a remaining joint. The images on the left show, with the weld surface to the left, the C-scans (top) and B-scans (bottom) for inspection angles of 20°, 12°, 0°, -12° and -20°. In the right image, a macrograph of a remaining joint is shown (circled in red).*

Cavities are formed near the weld surface and are inspected primarily at two ultrasonic inspection angles, 25° and 35°. Based on the irregular shape of the detected cavities, it can be assumed that the ultrasonic signals vary, which also has been verified by different experiments. Figure 7-41 shows a macrograph of the characteristics of a cavity and ultrasonic data of a typical indication. The ultrasonic images in Figure 7-41 show the indication for two inspection angles, 25° and 35°, where it can be observed that the highest amplitude in this case is achieved at an inspection angle of 35°.

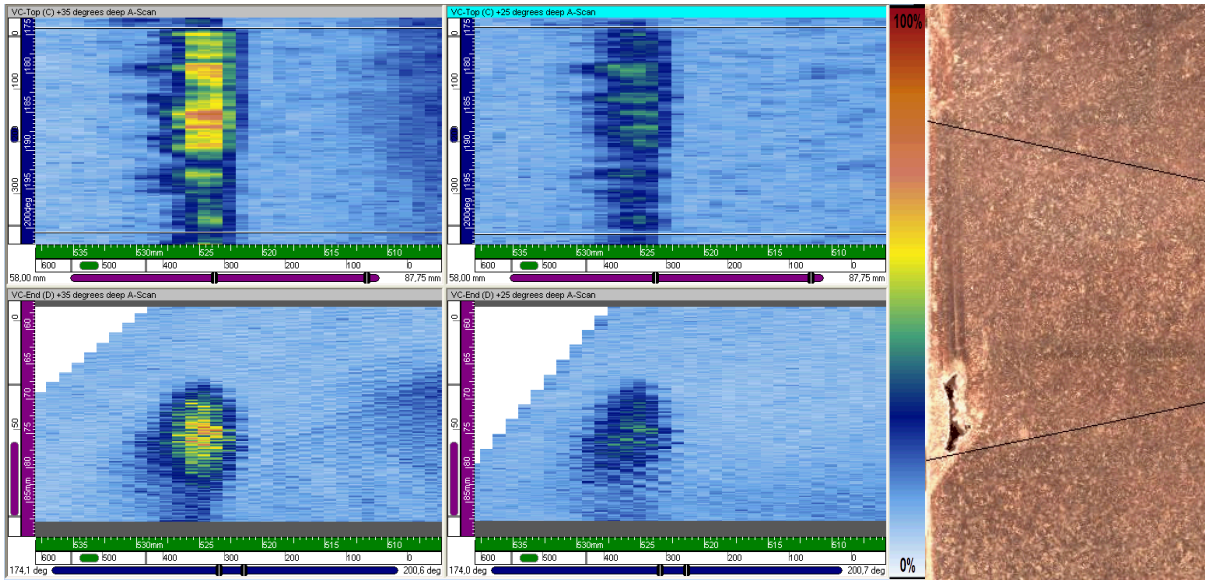

Figure 7-41. *Results from inspection of a row of cavities. The images on the left show, with the weld surface to the left, the C-scans (top) and B-scans (bottom) for inspection angles of 35° (left) and 25° (right). In the right image, a macrograph of a cavity is shown.*

7.4.2 X-ray inspection technique

Throughout the years about 80 welds have been inspected by digital X-rays, and of these, about 20 have in addition been inspected by the further developed X-ray inspection technique (RT01). The results show that no defect has been detected by X-rays in welds created using normal weld parameters. However, many of the welds created at the Canister Laboratory are produced to test different weld parameters or even with the objective of producing defects for NDT development, and therefore, a rather large number of defects are available. In welds, the major type of defect that has been observed by X-ray inspection is the aforementioned cavities; however, in a few welds, parts of broken weld tools have also been detected. In Figure 7-42, X-ray images of cavities and of a remaining part from a broken tool are shown.

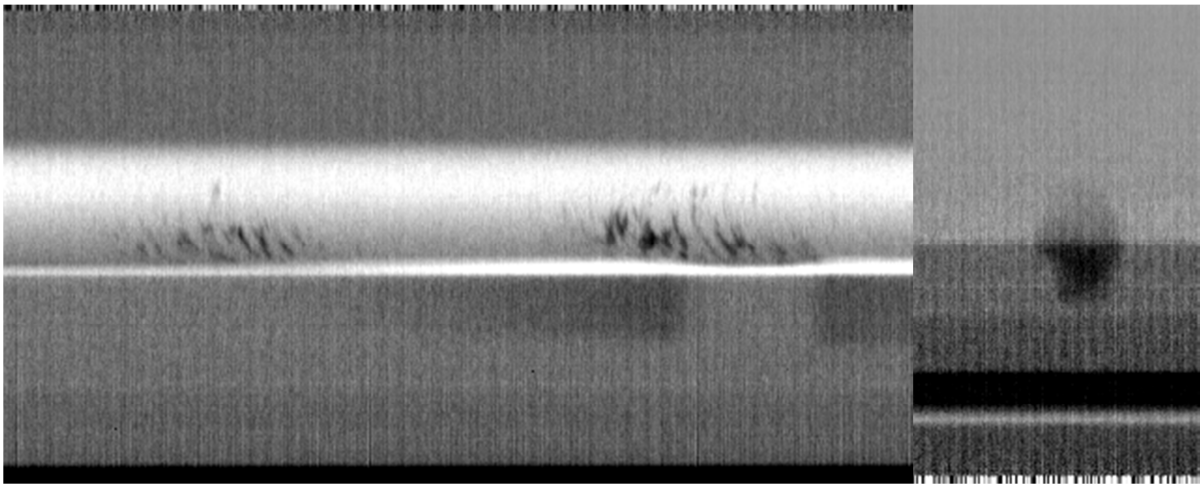

Figure 7-42. *X-ray images of cavities (left) and a broken weld tool (right).*

7.4.3 Surface inspection techniques

A number of welds have been inspected by the initial eddy current inspection technique based on the single Leotest SKB MDF 12 probe and the raster scanning manipulator. However, the performance of the Eddyfi array probe has only been investigated on a few welds. An example of the eddy current inspection results obtained for a cavity-type defect is shown together with the corresponding indications obtained from ultrasonic and X-ray inspection in Figure 7-43.

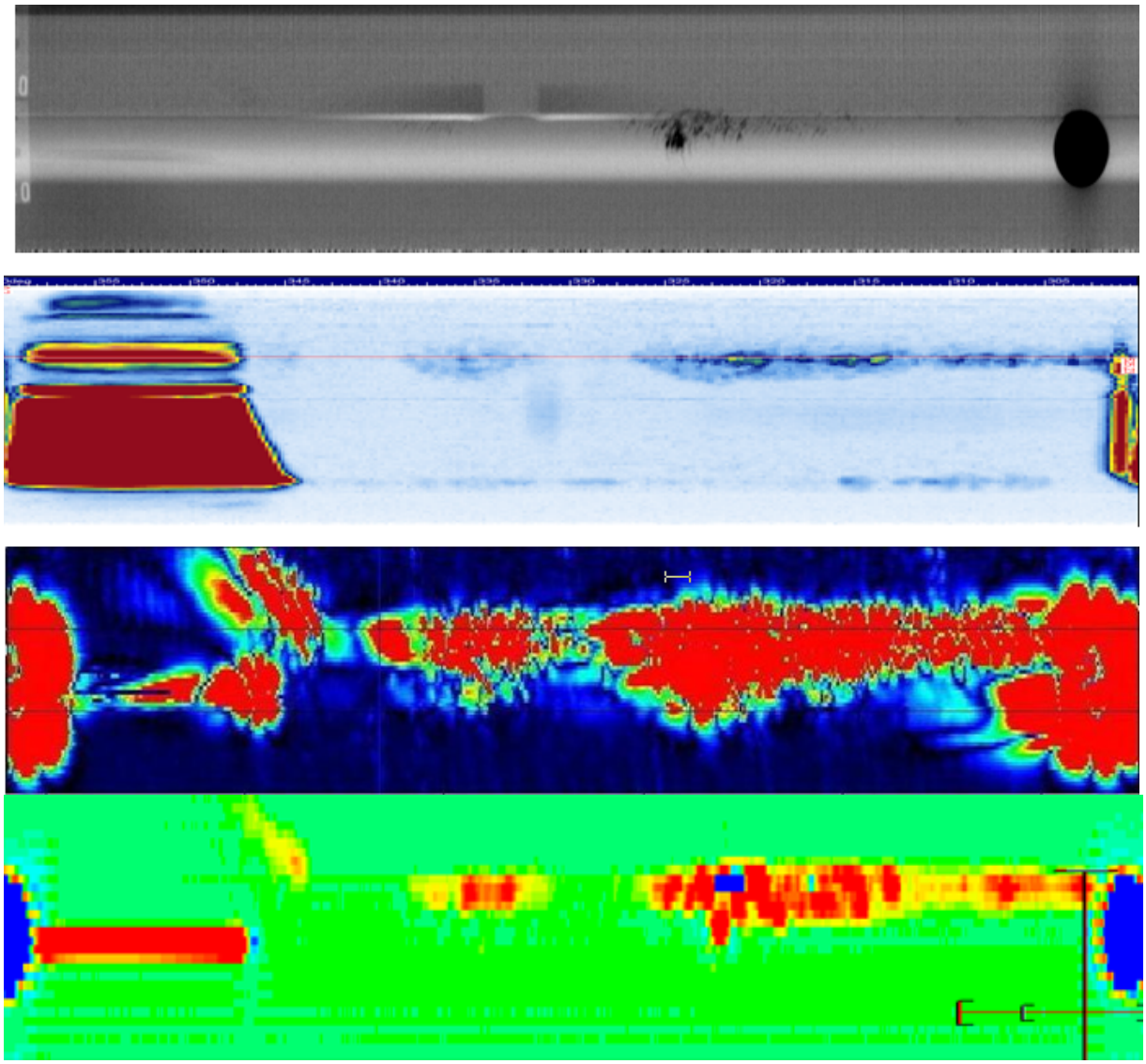

Figure 7-43. *Non-destructive inspection results from a weld with a cavity-type defect. From top to bottom, the following are presented: X-ray, ultrasonic, single probe and array probe eddy current inspection results. The irrelevant indications on the far left were caused by a non-welded section, and those on the far right were caused by a welding tool exit hole that finished the welded section.*

7.4.4 Manufacturing of defects

For many years, SKB has worked to develop the welding process at the Canister Laboratory. Throughout this period, a good knowledge base of defect formation as a function of process parameters has been obtained. Based on this knowledge, it is concluded that welding defects, as specified in section 4.2.4, can be produced in a repeatable manner.

8 NDT reliability

NDT reliability is defined (ASNT 1999) as the degree to which an NDT system (procedure, equipment and personnel) is capable of achieving its purpose regarding detection, characterisation and false calls.

Commonly, the reliability of NDT in the nuclear field is only analysed on a technical basis and only during the stage of the technical justification of methods. During the early stage of NDT development, it was realised that the inspection of the canister components and welds will require a high degree of reliability and that the task clearly differs from normal in-service inspection performed in the nuclear industry. Thus, an NDT reliability project was initiated together with BAM (Federal Institute for Materials Research and Testing) in 2003 with a focus on determining technical reliability via POD curves of the weld inspection. Throughout the years, this reliability project has evolved to cover the technical reliability of inspection techniques for the canister components and also considers human factors in mechanised inspection.

Another motive for initiating reliability studies in this early phase of development is the fact that in parallel to the development of the inspection techniques, NDT is used as a tool in the development of manufacturing and welding processes; thus, the results obtained from inspecting canister components and welds are used as inputs for process development and also as a basis for verifying the level of quality attained.

In the following sub-sections, a summary of the work performed with respect to NDT reliability, both from a technical and a human factor point of view is presented.

8.1 POD studies

From a technical point of view, NDT reliability is normally determined by the probability of detection (POD) and expressed in the form of POD curves. To create POD curves using the signal response approach, a statistical model for data distribution, developed by Berens (1989), is used. Conventional signal response analysis designates the measured response signals as $\hat{a}$ and the crack depth or any other defect dimension related to for the signal strength as a. The crack depth a is considered to be the actual crack depth, that is the true depth, and the measured peak amplitude is a perceived depth (for this reason the designation $\hat{a}$ is used). Values are then plotted against each other in a so-called $\hat{a}$ vs. a diagram. In the next step, linearity between the data is observed in the $\hat{a}$ vs. a log-log diagram, as shown in Figure 8-1.

The POD is then calculated by setting the decision threshold (reporting level) and assuming the scatter of the peak signal measurements to be normally distributed around the model curve (line). Then, the part of the cumulative distribution function that is above the threshold equals the POD for one specific defect size. This procedure is repeated for every defect size in the observed range, and a POD curve is constructed. Figure 8-1 shows a typical result obtained using the $\hat{a}$ versus a scheme as explained above. The indicated vertical line shows the $a_{90/95}$ value, where the lower 95% confidence limit crosses the 90% POD level, which means that in 95 out of 100 repetitions, the POD for this defect size would be above 90%, and it is considered that defects larger than this size can be detected with certainty.

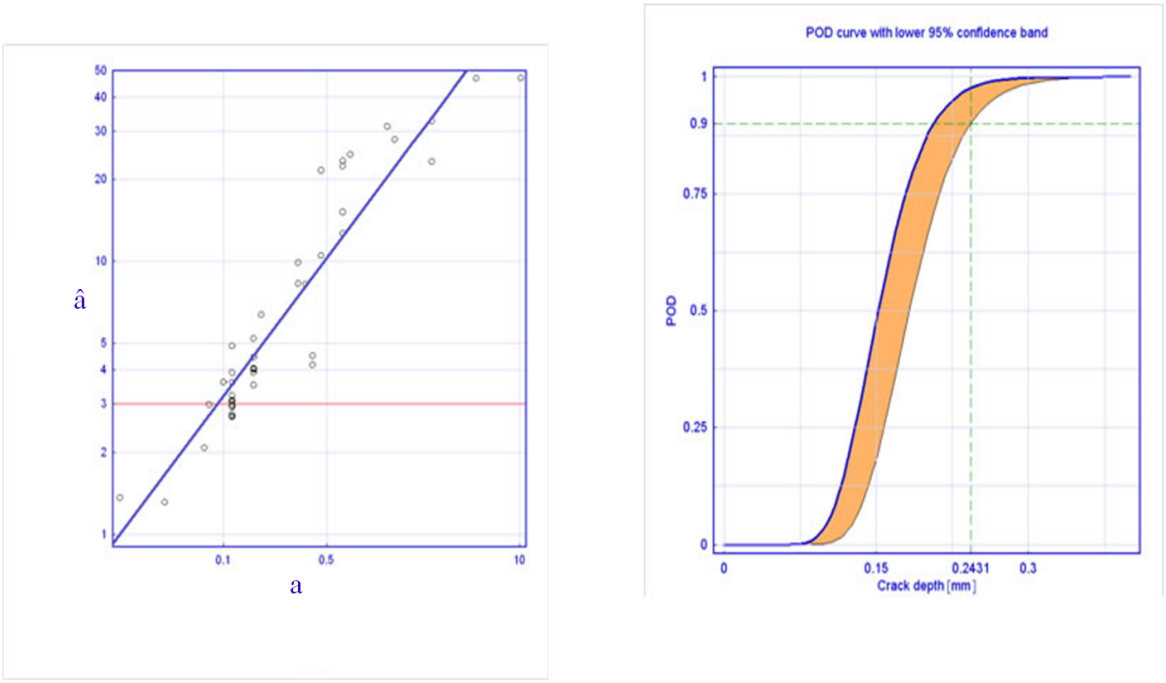

Figure 8-1. *Typical signal response POD â vs. a diagram (left) and the resulting POD curve as a function of defect parameter size (right).*

As described previously, the conventional model expresses the POD as a function of one influential parameter. In most cases, this parameter is considered to be the size of a defect. If there is another influential parameter, one could plot the signal response against the value of that parameter, and if linearity is observed, the POD can be calculated in the same manner. In the case of a small sample size, special care should be taken in interpreting linearity in relation to the signal height and the parameter. In this case, it is helpful to verify the relation with the corresponding physical model.

Furthermore, if there is more than one parameter that affects the POD, one could create several POD diagrams for every parameter and for every combination of parameters. For example, in the case of flat-bottom holes, the amplitude, and as a result the POD is proportional to the square of the diameter and inversely proportional to the depth in the far-field region. In some cases, it becomes practically impossible to perform the necessary number of experiments, particularly as the number of influential parameters increases for example the defect orientation, ultrasonic attenuation. In such cases, a multi-parameter model (SKBdoc 1411328, Pavlovic et al. 2012, Pavlovic 2014) can be applied.

8.1.1 POD calculations for NDT of cast iron inserts

The NDT reliability of the ultrasonic inspection techniques used for the insert described in the canister production report (SKB 2010) was determined by the conventional *â* vs. *a* method and presented in the form of POD curves (SKBdoc 1180132). In this report, it is shown that the sizes of detectable side-drilled holes clearly increase with inspection depth. For example, for the original normal inspection technique, the $a_{90/95}$ value increases from approximately 2 mm at a depth of 50 mm to approximately 8 mm at a depth of 200 mm, and for the original transmission inspection technique, the value increases up to 20 mm in the centre of the insert. In Figure 8-2, this phenomenon is exemplified by POD curves at different depths for the original normal incidence ultrasonic inspection technique.

In addition to the detectability of side-drilled holes, POD curves were also calculated for the ultrasonic inspection of notches by the original angular inspection technique (SKBdoc 1180132). The results showed $a_{90/95}$ values (notch depth) between 2 and 3 mm for surface-breaking notches and between 4 and 9 mm for notches at the outer corners of the channel tubes.

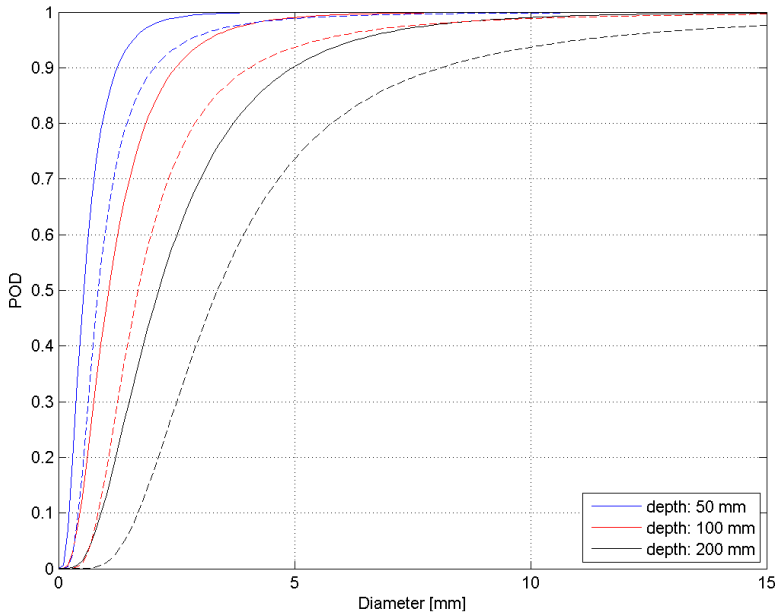

Figure 8-2. *POD curves calculated for side-drilled holes at different depths for the original normal incidence ultrasonic inspection technique.*

Because the ultrasonic techniques were further developed and, as demonstrated by ultrasonic sound field simulations, focussing clearly improved, it is of interest to investigate the hypothesis that the detectability also was improved. In the first step, the normal incidence ultrasonic technique was investigated in a manner similar to that of the original technique. Data were collected by inspection according to the valid instruction, of a section of an insert with a number of side-drilled holes, with diameters of 1-3 mm in size, along the entire inspection range (5-210 mm). The collected amplitudes were then compared with the threshold according to the instruction and sent to BAM for further analysis.

In the first step, the data were re-calculated to the square root of the side-drilled hole diameter to fit the physics of the ultrasound. Based on these data, $\hat{a}$ vs. a diagrams were created, as shown in Figure 8-3 and Figure 8-4. As demonstrated in these diagrams, all amplitude values are above the decision threshold, which for the larger depths is even more distinctive presented in Figure 8-4. The PODs were then calculated first for the square root and then for the diameter of the side-drilled holes, which resulted in $a_{90/95}$ values of approximately Ø0.7 mm for the depth range of 5–45 mm (Figure 8-5).

It should be noted that the creation of the aforementioned POD curves has some limitations. First, the number of data points is lower than what Berens (1989) method recommends, and second, the data set should also contain values below the decision threshold. Because the $\hat{a}$ vs. a diagrams for larger depths (Figure 8-4) show an even greater margin between the side-drilled hole amplitudes and the threshold, it was decided that it not was credible to calculate POD curves for these depths. However, it can be stated, based on the margin between the signals and the threshold levels that the detectability should at least be no worse than that in the shallower region shown in Figure 8-5.

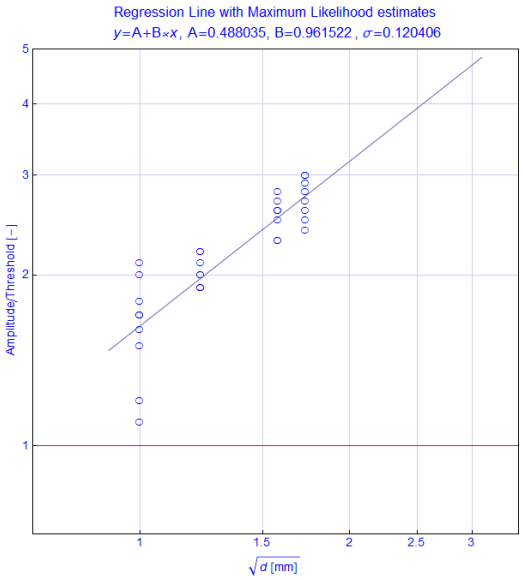

Figure 8-3. *â vs. a curve calculated for side-drilled holes (square root) for the depth range of 5-45 mm using the further developed normal incidence ultrasonic technique.*

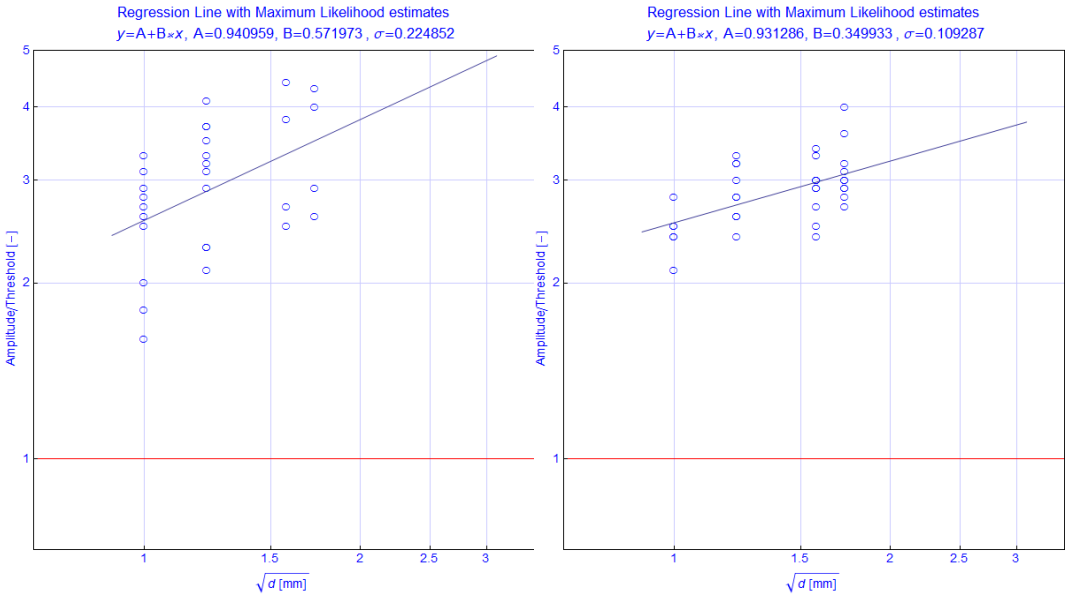

Figure 8-4. *â vs. a curves calculated for side-drilled holes for the depths ranges of 45–110 mm (left) and 110-210 mm (right) using the further developed normal incidence ultrasonic technique.*

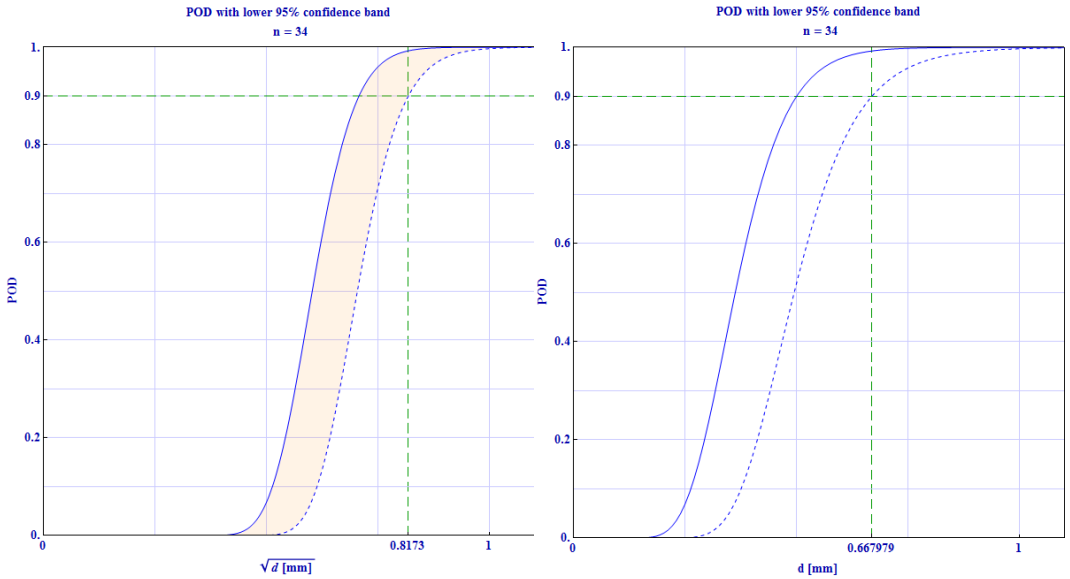

Figure 8-5. *POD curve calculated for side-drilled holes at different depths for the depth range of 5–45 mm using the further developed normal incidence ultrasonic technique. POD as a function of the square root of the diameter (left) and POD as a function of diameter (right).*

For the other further developed ultrasonic techniques (angular and transmission), to date, no new POD curves have been calculated. However, based on the results obtained from the POD calculations of the normal inspection technique and the results obtained from the ultrasonic simulations presented in section 6.2.2, in which a remarkable improvement in the sound fields is presented, a clear improvement in the POD for these techniques is also expected. This improvement is hypothesised to be particularly valid for greater depths for both techniques.

In addition to the ultrasonic inspection techniques, it is assumed that additional inspections will be performed by a type of dedicated surface inspection technique. Eddy current inspection (presented in section 6.2.2.) is one of the techniques evaluated for this application. To investigate the detectability, data were collected (Figure 6-30) on a test object with elliptical EDM notches at a depth range of 1–5 mm with lengths between 3 and 30 mm. The data were evaluated using a threshold corresponding to a signal-to-noise-ratio of 13 dB. To obtain a linear relationship for the data, larger notches were excluded due to their saturated amplitudes. Based on this limited number of data points, an $\hat{a}$ vs. a diagram and a POD curve were created (Figure 8-6). The results showed that the $a_{90/95}$ values for surface-breaking notches corresponded to a length of approximately 5 mm.

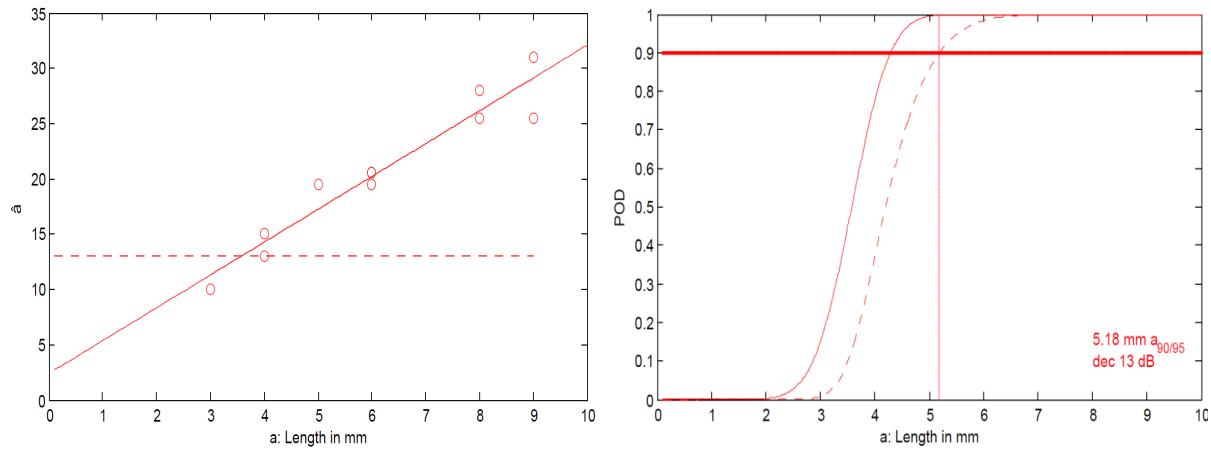

Figure 8-6. *â vs. a curve (left) and POD curve (right) calculated for surface EDM notches for the eddy current inspection technique described in section 6.2.2.*

8.1.2 POD calculations for NDT of copper tubes

The NDT reliability of the ultrasonic inspection techniques for copper tubes, which is described in the canister production report (SKB 2010), was determined by a multi-parameter model and presented in the form of different types of POD curves (SKBdoc 1180131). For example, the POD as a function of the different defect orientations and depths was evaluated. In this report, it is shown that the detectable sizes in the form of flat-bottom holes is clearly dependent on depth, as shown in Figure 8-7, which results in $a_{90/95}$ values that reach up to 4 mm. This result is understandable when it is compared with the ultrasonic simulations shown in Figure 6-37, in which similar sound field behaviour can be observed.

After performing the aforementioned calculations, the inspection techniques were further developed, as described in section 6.3.2, by applying a more optimised and uniformly focussed sound field. Based on this improvement, it is hypothesised that the POD should develop in the same direction, that is lower, more uniform $a_{90/95}$ values along the inspection depth. However, as described in section 6.2.2, non-uniform attenuation was observed in several manufactured tubes, which consequently raises the following question: How does this increased attenuation affect the quality of the inspection?

To answer this question, a study was initiated. The first step in this study was to select suitable tube material where this increased attenuation (in the form of back wall echo amplitude loss) is present. After a survey of the available tube materials, for which ultrasonic inspection indicated high back wall echo amplitude reduction, some parts of the extruded tubes T53 and T58 and the tube T64 manufactured by the pierce-and-draw method were identified. In suitable areas (with high, uniform attenuation) within these tubes, flat-bottom holes with diameters of 1-6 mm were drilled from the inner side of the tubes. For reference, the same set of holes was drilled in a low-attenuating area of tube T53.

The areas of the flat-bottom holes were inspected with the further developed normal incidence ultrasonic technique described in section 6.3.2, and in the first step, the SNR for the flat-bottom holes was analysed. In Figure 8-8, the results show a clear reduction in the SNR for the parts with increased attenuation, and there is a clear difference between tube T64, which exhibited a relative back wall amplitude reduction of almost 17 dB, and tube T58, which exhibited a relative back wall amplitude reduction of approximately 10 dB.

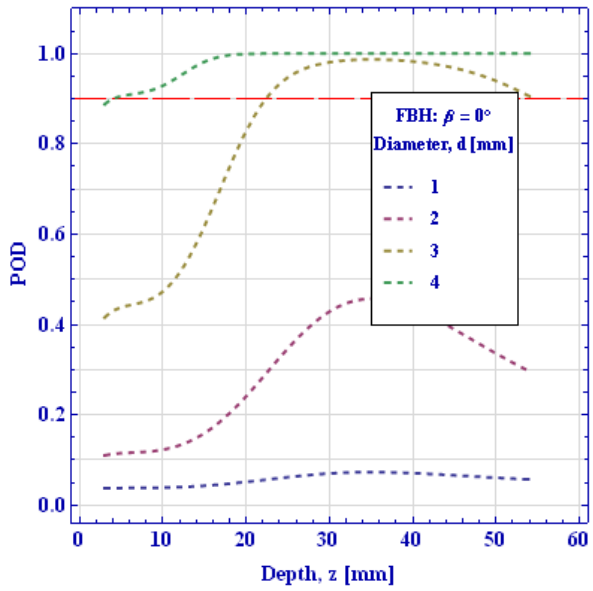

Figure 8-7. *Lower 95% confidence band for FBH vs. depth z for different values of diameter d for the original normal incidence inspection of copper tubes.*

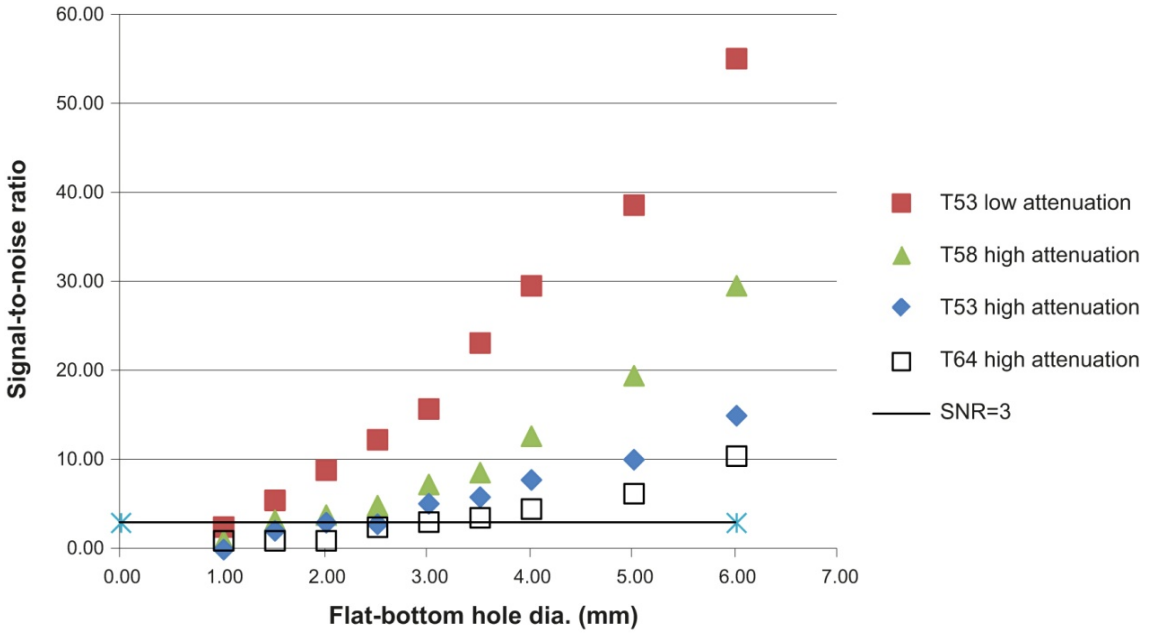

Figure 8-8. *Signal-to-noise ratio (SNR) for flat-bottom holes with different diameters at a depth of 50 millimetres in normal fine-grained extruded material (red) and different levels of higher-attenuation copper tubes (reduction of back wall echo amplitude by 10–17 dB), where the pierced and drawn tube T64 (white) exhibited the lowest SNR.*

Based on the results obtained for this material, a more in-depth study was initiated together with BAM to investigate how different levels of SNR affect detectability. This study, which is described in detail in a separate report (SKBdoc 1411328), was conducted by applying the multi-parameter model; the results were also compared with calculations performed using the $\hat{a}$ vs. a model. The model had to be modified due to the complex physical behaviour of the attenuation in combination with a low-pass filtering of the ultrasonic signal (caused by the grain structure) and the fact that the ultrasonic simulation software used to support the calculations could not handle the TCG corrections applied in the inspection setup.

Figure 8-9 presents the POD curves obtained from the multi-parameter calculations. As expected, the detectable flat-bottom hole sizes clearly increased as the level of attenuation increased. The calculations performed using the $\hat{a}$ vs. a model showed results (Table 8-1) similar to those of the multi-parameter model but with a more distinct increase in $a_{90/95}$ values as a function of increased attenuation. This difference can be explained by the $\hat{a}$ vs. a model: the number of data points (18 per tube material) is far too few to be sufficient. The difference can also be explained by the multi-parameter model, in which the low-pass filtering of the ultrasonic signal is not fully taken into account in the simulations.

Table 8-1. Results from the POD calculations on the different tube materials.

Tube section	Detectable diameter $a_{90/95}$ [mm] from the multi-parameter model	Detectable diameter $a_{90/95}$ [mm] from $\hat{a}$ versus a model	Mean back wall echo amplitude [%]
T53 low	1.66	1.58	43.40
T58 high	2.51	2.72	13.52
T53 high	2.51	3.08	10.82
T64 high	3.41	4.08	6.33

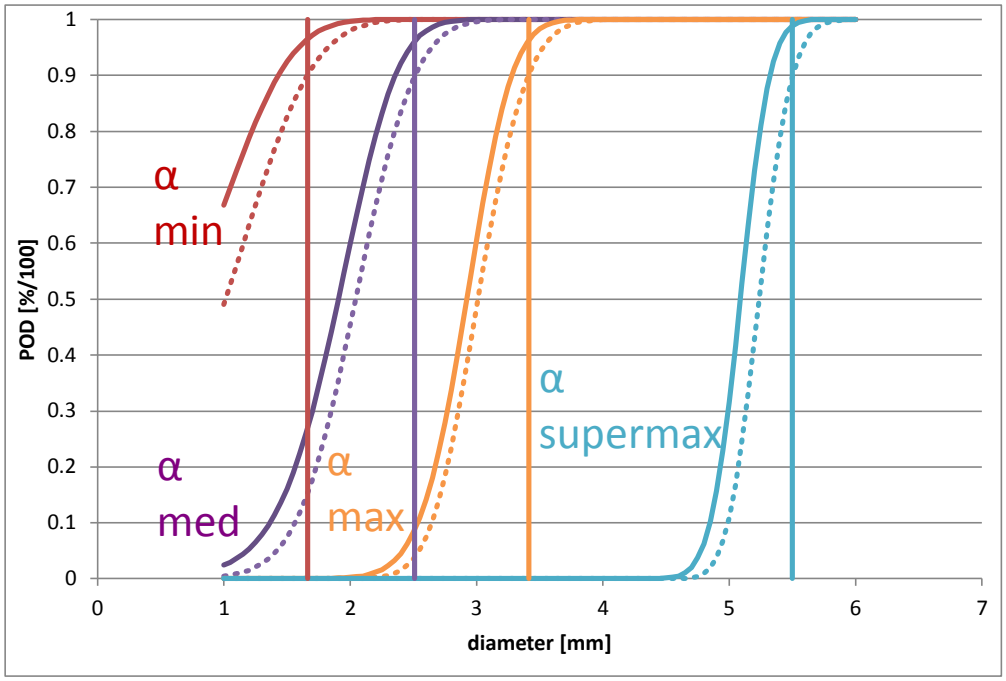

Figure 8-9. *Summary of the calculated POD (as a function of FBH diameter with indicated $a_{90/95}$ values) for tube materials with different levels of attenuation (α). "α min" corresponds to the reference part of tube T53, "α med" refers to the part of tubes T53 and T58 with increased attenuation and "α max" refers to the highest-attenuating tube T64. "α supermax" is a postulated value for even more highly attenuating tube materials.*

After the POD studies, the grain size was measured at three depths (at the centre and 5 mm from the inner and outer surfaces) in samples from each tube segment; based on the measurements, the grain size distribution was calculated (SKBdoc 1417645). The results show a clear difference in grain size and grain size distribution. In Table 8-2, it can be observed that the grain size and the grain size distribution, in the terms of the percentage of grains larger than 350 µm (assumed to greatly affect the ultrasonic attenuation), varied not only between samples but also within samples. This effect is highlighted for sample T53 high, where the outer area exhibits a fine-grained structure and whiles the structure clearly is coarser towards the inner side. In Figure 8-10, the grain size distribution (in 50-µm steps) for each sample is presented.

Table 8-2. Average grain size in different copper tube materials. The numbers in parentheses indicate the percentage of grains larger than 350 µm.

Position	T53 low	T53 high	T58	T64
Outer	76 (0.0)	81 (0.3)	170 (7.0)	124 (2.3)
Centre	79 (1.1)	160 (5.3)	188 (13.7)	214 (15.0)
Inner	83 (0.8)	177 (11.9)	115 (3.7)	177 (10.4)
Average	79 (0.6)	122 (4.1)	156 (8.2)	162 (7.9)

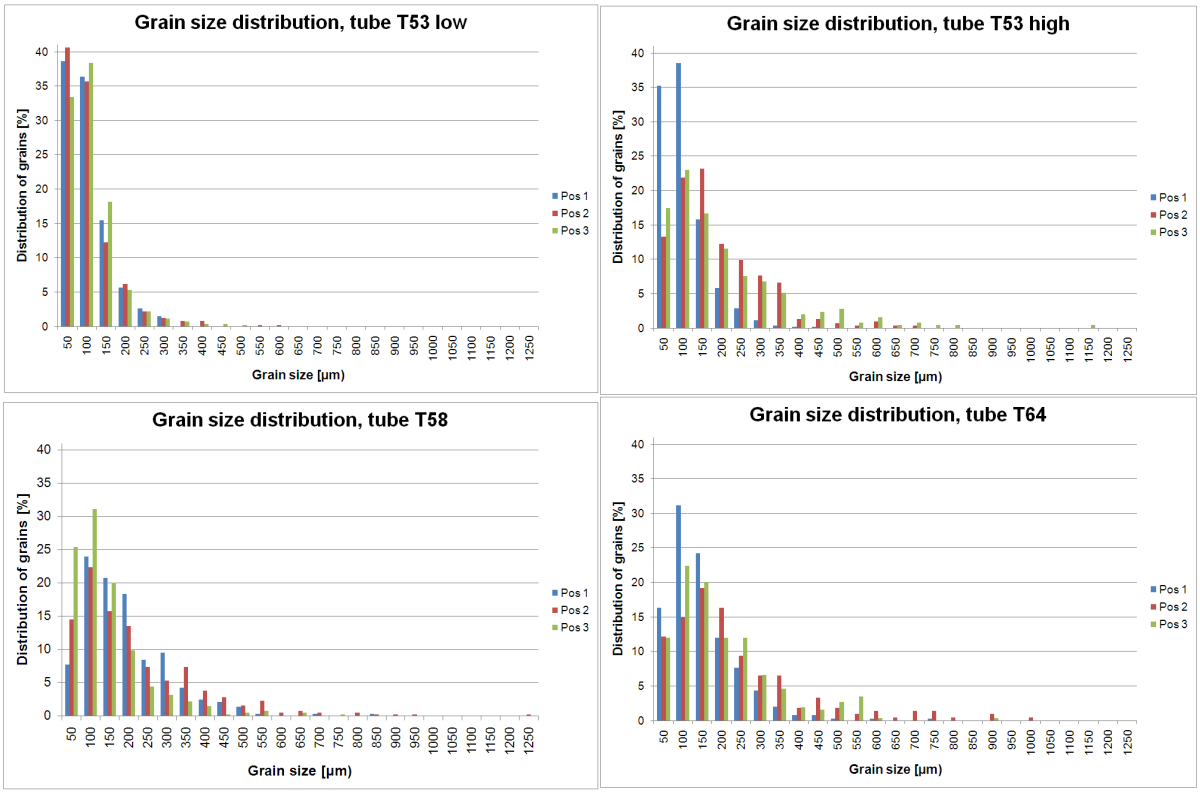

Figure 8-10. *Grain size distributions presented for the tube samples T53 low, T53 high, T58 and T64. The diagrams show the percentage of grains (50-µm segments) for each position: outer (Pos 1), centre (Pos 2) and inner (Pos 3).*

8.1.3 POD calculations for NDT of copper lids and bases

The NDT reliability of the ultrasonic techniques for lid inspection (SKB 2010) is described in the same manner as that for the tube inspection by the multi-parameter model. The results are presented in the form of different types of POD curves (SKBdoc 1180131). In this report, it is shown that the detectable sizes of flat-bottom holes are clearly dependent on depth, as shown in the examples in Figure 8-11, which result in $a_{90/95}$ values between 3 and 5 mm. After these results were further analysed together with the beam simulations presented in Figure 6-37 and Figure 6-42, a clear relationship between the areas where the ultrasound was badly focussed and high POD values was observed.

After the above calculations were performed, the inspection techniques were further developed, as described in section 6.4.2, by using a more optimised and uniformly focussed sound field. Therefore, the hypothesis is that the POD should develop in the same direction, that is lower, more uniform $a_{90/95}$ values should occur along the inspection depth. This hypothesis has, to some extent, been verified by the POD calculations regarding the inspection of the copper tube presented in the previous section. Furthermore, this hypothesis is valid because the inspection of the thin central part of the lid applies the same focal laws as the tube inspection combined with that the lids normally exhibit similar or lower ultrasonic attenuation as the reference tube material. By comparison, the $a_{90/95}$ values for flat-bottom holes improved for diameters of about 3–4 mm to below 2 mm, and it is assessed that a similar improvement is achieved for other inspection areas.

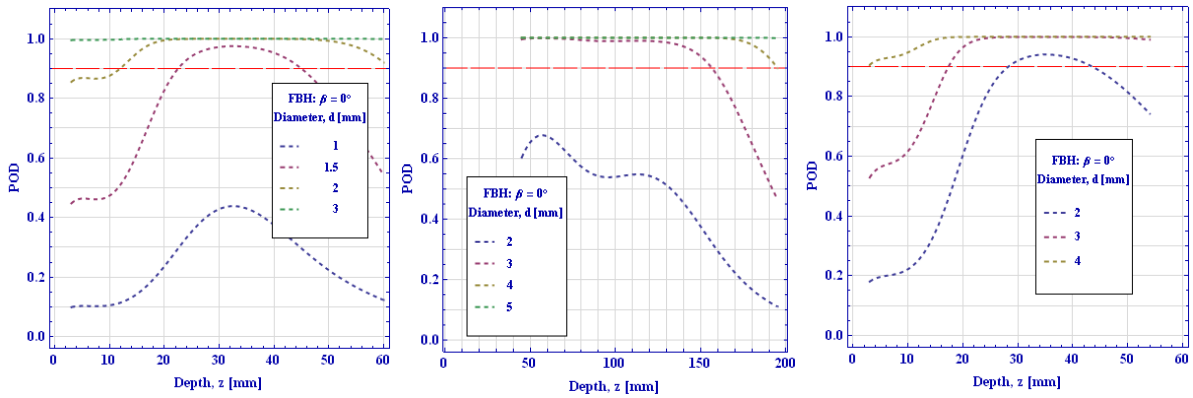

Figure 8-11. *Lower 95% confidence band for FBH vs. depth for different values of diameter for the original ultrasonic inspection of the copper lid. The POD diagrams are presented for the following depth ranges: 5-55 mm (left) and 55-195 mm (middle) of the outer flange, and the whole thickness of the thin central part (right).*

8.1.4 POD calculations for NDT of friction stir welding

The NDT reliability of the inspection techniques for FSWs was the first topic addressed within the NDT reliability project. In this study (SKBdoc 1175235), the reliability of the original inspection techniques (phased array ultrasonic and digital X-ray techniques) described in the canister production report (SKB 2010) was analysed. The analyses were in contrast to the POD calculations for artificial defects with respect to the inspection of canister components conducted using real defects (cavity and joint line hooking).

The digital X-ray inspection technique was analysed to determine its detectability for cavities. For this analysis, the contrast level from the inspection was used as the signal, and a combination of results from computed tomography and metallographic investigations of cut samples were used as the "real" size. The results presented in Figure 8-12 show an $a_{90/95}$ value of 4 mm.

The ultrasonic inspection technique was analysed for its detectability for both cavities and joint line hooking. For the analysis of the POD of the cavities, the ultrasonic amplitude was used as the signal, while the same data set used for metallographic and computed tomography as for the calculations of the X-rays was used as the "real" size. For the analysis of the joint line hooking, the same concept was applied, with the difference being that the real size from the metallographic investigations was used. The results presented in Figure 8-13 for cavities and in Figure 8-14 for joint line hooking show $a_{90/95}$ values of 6.3 mm and 4 mm, respectively. For the joint line hooking, an additional calculation was performed, in which some outliers were excluded; an $a_{90/95}$ value of 3.2 mm was achieved (Figure 8-14).

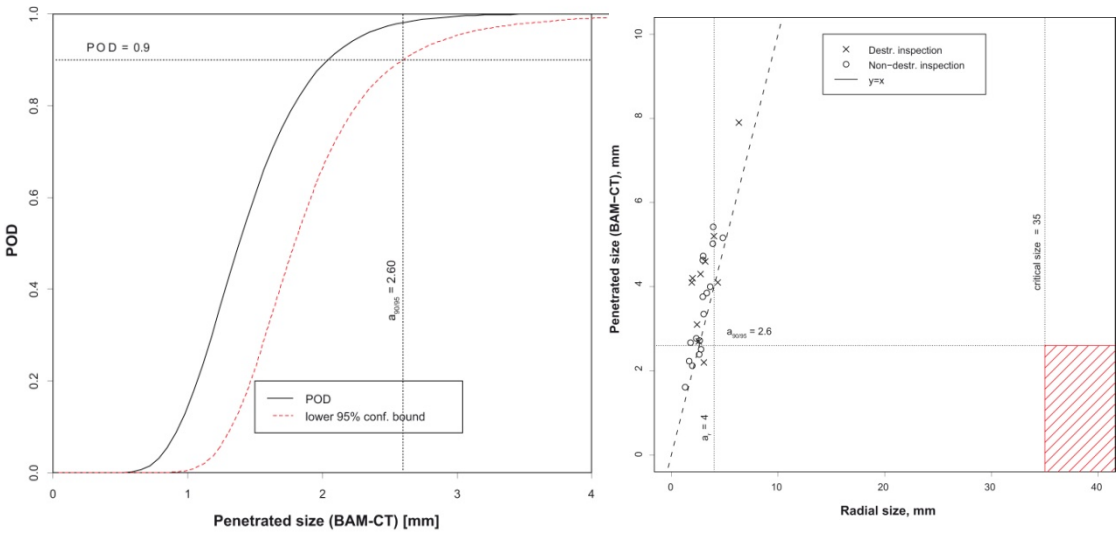

Figure 8-12. *Results from POD calculations on cavities for the original digital X-ray technique. The left image shows the POD vs. the size in the inspection direction (35°), and the right image shows the correlation of the radial size of the defects.*

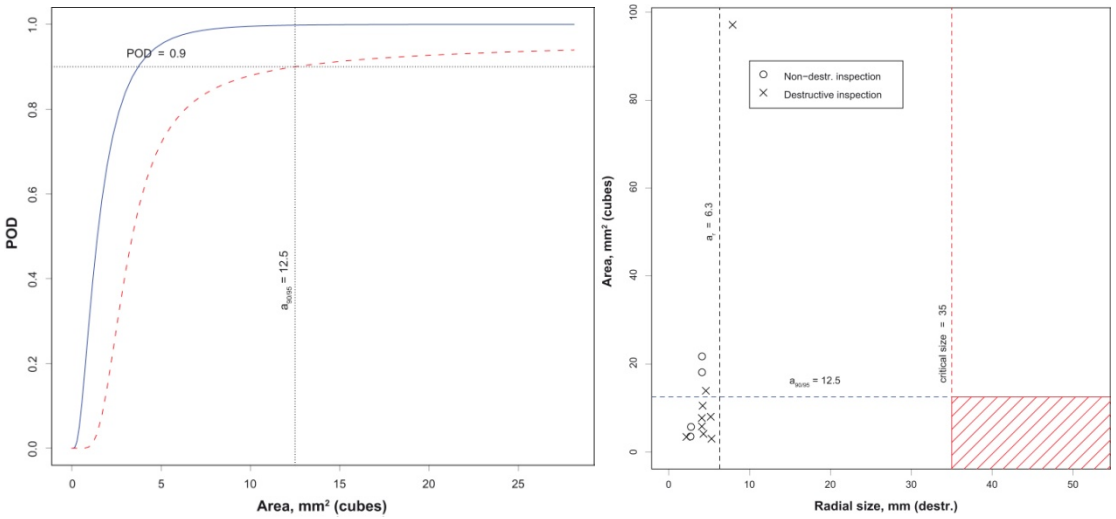

Figure 8-13. *Results from POD calculations on cavities for the original ultrasonic technique. The left image shows the POD vs. the area of the defects, and the right image shows the correlation with the radial size of the defects.*

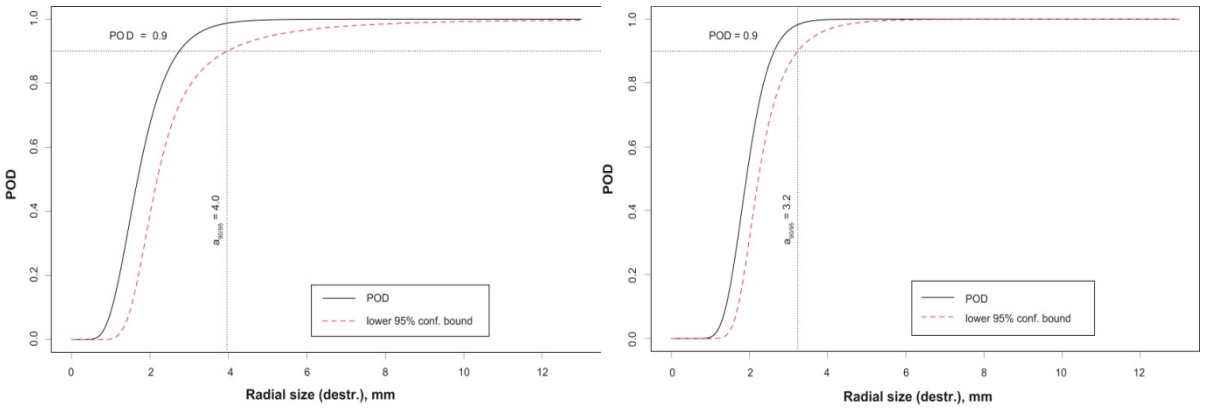

Figure 8-14. *Results from POD calculations on joint line hooking for the original ultrasonic technique. The left curve was calculated using the entire data set, and the right curve was calculated with some outliers excluded.*

No POD calculations were performed for the further developed techniques (ultrasonic, X-rays and eddy current). However, it can be assessed that the detectability of the further developed ultrasonic inspection technique is better due to its more focussed beams and as inspection angles are dedicated to the identified defect geometry. Similarly, it can be assessed that the POD will increase for the optimised X-ray inspection technique, which is due to the smaller inspection angle, which results in a reduced penetrated thickness and thereby a higher SNR for defects along the critical radial direction.

8.1.5 Discussion

In section 8.1.1 to 8.1.4, POD calculations based upon data from inspection of both artificial and real defects are presented. In general it is preferred to perform POD calculations on real defects for final verification of the performance of the inspection technique. However, it has to be noticed that several important factors have to be considered calculating POD based on real defect responses. First, the defect characteristics and critical defect parameters have to be well known. Secondly, the interaction and the linear relationship of the applied NDT technique with these defect parameters need to be specified. Finally, a sufficient amount of well distributed data must be available.

During the phase of NDT development, the use of artificial defects could be beneficial. Reason for this is the fact that these defects are relatively easy to manufacture well distributed both in position and in size. Additionally, a defect characteristic can be selected giving a linear relationship with the response from the applied NDT technique. The objective of POD calculations in the phase of NDT development is to be able to determine the sensitivity of the applied NDT technique using as relevant defect types as reasonable achievable.

In the case of the POD calculations on the canister components presented in section 8.1.1 to 8.1.4, performed by the use of artificial defects such as FBHs and SDHs, it can be assessed that this methodology is reasonable sufficient in this development phase. This assessment is, for example, based on the fact that the majority of the specified insert defects (section 4.2) will probably have an irregular shape giving reflectors with several orientations. In order to verify this assessment the applied NDT techniques have to be analysed with respect to their interaction to both artificial and real defects. These analyses can however not be conducted before the defect specifications and acceptance criteria have been revised further.

8.2 Human factor studies

When discussing human factors in non-destructive testing, the use of manual testing is primarily considered, and when mechanised inspection techniques are applied, most of the human factors are considered to be overcome. Because most inspections performed on canisters will be conducted by mechanised inspection, the following questions are raised: What human factors must be considered when mechanised inspection techniques are applied, and what can be done to prevent human errors from occurring?

Based on the aforementioned questions, it was determined that additional research should be conducted in this field. The initial thought was to explore what had been accomplished in other fields, being prudent in systematically investigating the inspection process. This investigation was carried out by applying Failure Modes and Effects Analyses (FMEA) customised for the mechanical inspection process. These FMEAs were performed in several steps and followed by subsequent human factor studies, which are described in the following sub-sections.

8.2.1 Failure Mode and Effect Analysis (FMEA)

The analysis (SKBdoc 1427252) was conducted in two separate workshops, one dealing with the data evaluation (May 2009) and the other dealing with the data acquisition (May 2011) process of mechanised ultrasonic inspection of canister components. Both workshops were held in Oskarshamn in the presence of 3-4 UT experts. All participants were involved in the development of the techniques and were familiar with the project. The workshops were moderated by two human-factor experts.

The FMEA, conducted with the goal to investigate human factors in the mechanised inspection of canister components, required customisation to fit the purposes of our study. This customisation included identification of potential failures originating from the inspector, organisation or the interaction between the inspector, the organisation, and the technology.

The analysis was performed in the following steps:

1. decomposition of the task into sub-tasks
2. definition of goals for the sub-tasks
3. identification of possible failures/errors
4. consideration of potential causes and effects of failures
5. identification of existing preventive measures/barriers
6. identification of potential preventive measures/barriers
7. assessment of error probability, relevance of effects and detection probability
8. calculation of risk priority.

The workshop began by listing all of the steps performed in data collection and data evaluation, after which, a detailed analysis of each step was performed. After listing potential errors, their causes, consequences and existing and future preventive measures, each of the participants assessed the error probability, relevance of effects and detection probability of each error by assigning a value based on a three-grade scale. The final risk priority was calculated by multiplying the error probability, the relevance of effects and the detection probability.

Data acquisition

As a result of the FMEA of the data acquisition process, possible errors were identified over the entire inspection chain. Errors that could occur during the preparation phase were identified, for example choosing the wrong component or by choosing the wrong or malfunctioning equipment or software. Additionally, it was identified that a number of possible errors could occur during the calibration and while scanning a component. Examples of errors include using the wrong instrument or scanning parameter settings, misinterpretation of reference defects by using the wrong inspection sensitivity and not inspecting the entire component.

In the second stage, the aforementioned errors could result in either the need for re-inspection of the component or, in the worst-case scenario, that the component (or part of it) was not inspected with the desired sensitivity.

Based on these errors, possible preventive measures were identified. For example, several hardware solutions were discussed, such as alarms when equipment malfunctions and automation of both the preparation and inspection using barcodes, where the component, equipment and software and instrument settings are connected. In addition, building an organisation was considered important because up-to-date instructions, computers, setup files and must be responsibly maintained and personnel recurrently trained. Moreover, human redundancy should be considered and special focus should be set on assuring that instructions are clear and easy to follow.

Data evaluation

Within the data evaluation, the FMEA indicated errors during the preparation phase, during the data evaluation and in reporting results. During the preparation phase, typical errors were related to using incorrect settings or incorrect data sets or areas of interest. During data evaluation, typical errors included missing or incorrect characterisation/sizing of indications or misinterpretation of the data. Report-writing errors were related to typing errors or badly described results.

In the second stage, all of the aforementioned errors could result in either incorrectly accepting components with critical defects or incorrectly rejecting acceptable components.

The preventive measures identified were different software solutions such as automatic tools and alarms, use of human redundancy by using independent operators, increased and dedicated operator training and the need for procedures and instructions including decision aids that clearly guide the actions of the operator.

8.2.2 Development of NDT instructions

As stated in the previous FMEA section, instructions for mechanised ultrasonic inspection play an important role, and in this early stage, the focus has been on technical development, not written instructions. Thus, the requirement for a systematic development of instructions from a human point of view was identified.

The foregoing discussion served as the starting point for an extensive study (Bertovic and Ronneteg 2014) with the goal of applying human factor principles in the development of NDT instructions. Moreover, the goal was to optimise the instructions to obtain more reliable, accurate NDT performance and to promote the use of the instructions. The motives for beginning this study at this early stage of technical development are, first the fact that results from the use of preliminary inspection instructions are used to motivate the quality of manufacturing processes as input for the licensee process and, second, because only a handful of canisters will be manufactured and inspected yearly, until the operation of the repository begins in approximately 15 years. Furthermore, during the initial operation phase, good instructions will reduce the risk of a lack of continuity and skill over time; therefore, the need for good instructions is emphasised.

This human factor study was divided into two separate studies:

- development of NDT instructions
- investigation of usability and understanding of instructions.

Development of NDT instructions

The development of NDT instructions was conducted in several iterative stages and within two studies, as shown in Figure 8-15. In these studies, the focus was on data evaluation because in the FMEA, data evaluation was identified as the task that, to the highest degree, relies on the quality of the instructions.

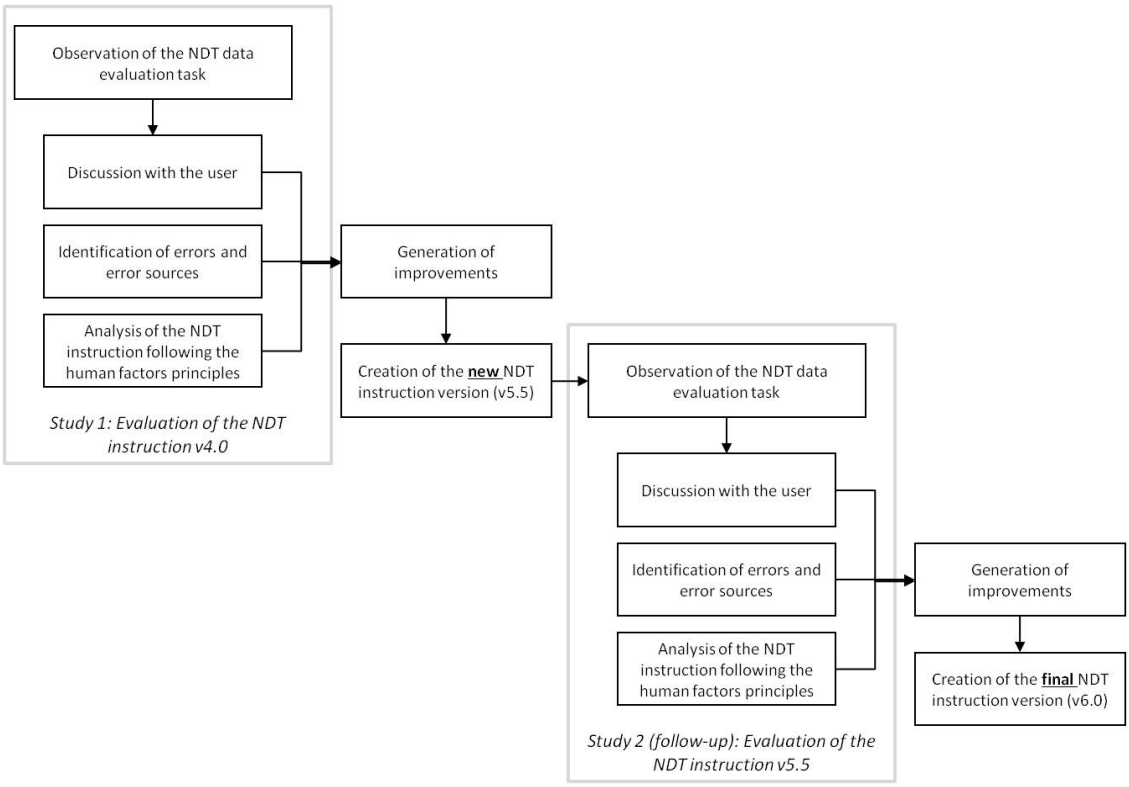

Figure 8-15. *Process chart of the steps taken in the development of the NDT instructions (from version 4.0 to version 5.5 to the final version 6.0) within the scope of the two studies.*

In the first study, four qualified inspectors performed data evaluation following an appropriate NDT instruction.

The objectives of the study were:

- to evaluate the quality of the current instruction by assessing the performance resulting from the use of the specific instruction
- to generate improvements.

During the data evaluation phase, participants were observed with the aid of an eye tracker (Bertovic and Ronneteg 2014), which is a device that follows eye movements and fixations across a computer screen. The eye-tracking data were stored together with all screen recordings, mouse clicks, etc. The collected data (both those regarding the results obtained and those indicating how the data evaluation was performed) and information gathered from the discussions of the participants were analysed and combined with a theoretical analysis of the instruction from the perspective of a human-factor expert. This analysis resulted in a number of suggested changes in the instruction and, consequently, in the creation of a new version of the instruction. The primary changes in this new version were related to how the information was presented (for example changed from being written in a narrative manner to a stepwise manner, highlighting important information and introducing writing consistency).

In the follow-up study, the same methodology was applied to the newly created instruction:

- to determine whether the generated changes improved data evaluation performance
- to generate additional improvements.

The analysis of the results of this follow-up study surprisingly showed only minor improvements in the results obtained from the data evaluation. However, user satisfaction increased. When investigating the cause for the limited improvements, it was realised that important tasks related to the actual performance of the data evaluation had not been updated. This finding, together with all of the obtained results, was taken into account when the "final" NDT instruction was created.

Investigation of the usability and understanding of instructions

To determine whether the aforementioned changes improved the usability of the instruction, a second study was formulated. The goal of this study was to identify the writing patterns that helped users, regardless of their experience, to equally and correctly understand the written material. The underlying assumption was that if the information in the instruction is clearly understood, NDT performance should improve.

The study was performed in two sections, understanding and usability. The studies were performed by a group of 20 participants with different levels of NDT experience (such as technicians familiar with the type of instruction, technicians familiar with other types of mechanised ultrasonic inspections, research personnel, certified inspectors). The eye tracker was used to design and collect necessary information in the study.

In the *understanding section*, participants were asked to answer a number of questions, either by choosing one of the multiple-choice answers on the screen or by writing down an answer on a sheet of paper. Half of the participants used the old instruction (instruction v4.0), and the other half used the latest updated version of the instruction (instruction v6.0). The results showed no significant difference between the two versions of the instructions. However, it was observed that the participants familiar with this type of instruction clearly showed better results, which can be explained by a number of limitations in the methodology used. First, the instruction was written to be followed while working, not to search for information. Second, the number of participants was limited, particularly that of experienced participants. Finally, the concept of understanding is difficult to define and is particularly difficult to investigate quantitatively. However, the study concluded that special care should be taken into account while writing to create instructions that are understood equally by all users.

In the *usability section*, participants were asked a question and then directed to a page where they were required to click on the correct answer using a mouse. The order of presentation of the questions and the corresponding instruction pages were randomised for each participant. Five variables regarding the characteristics of the instruction were investigated as shown in Table 8-3. All 20 participants received 20 questions each, half of which contained characteristics of the old instruction and half of which contained characteristics of the new instruction. After each question, the participants were directed to a page in the instruction and asked to use a mouse to click on the sentence or part of the sentence that contained the correct answer in the shortest amount of time possible.

In the analysis of the results (Figure 8-16), it was observed that the characteristics that yielded clearly improved results (shorter time before the information was found) were highlighting (using notes) and how the information was presented (stepwise presentation with one task per step).

Table 8-3. Analysed characteristics of Instructions v4.0 and v6.0.

Category	Independent variable	Variable levels	
		Style of Instruction v4.0	**Style of Instruction v6.0**
Highlighting	Use of bold	No bold (nB)	With bold (wB)
	Use of notes	No notes (nN)	With notes (wN)
Navigation	Use of titles	No titles (nT)	With titles (wT)
Information presentation	Presentation of task steps	Narrative (N)	Stepwise (S)
	Presentation of actions	Two actions per step (2ApS)	One action per step (1ApS)

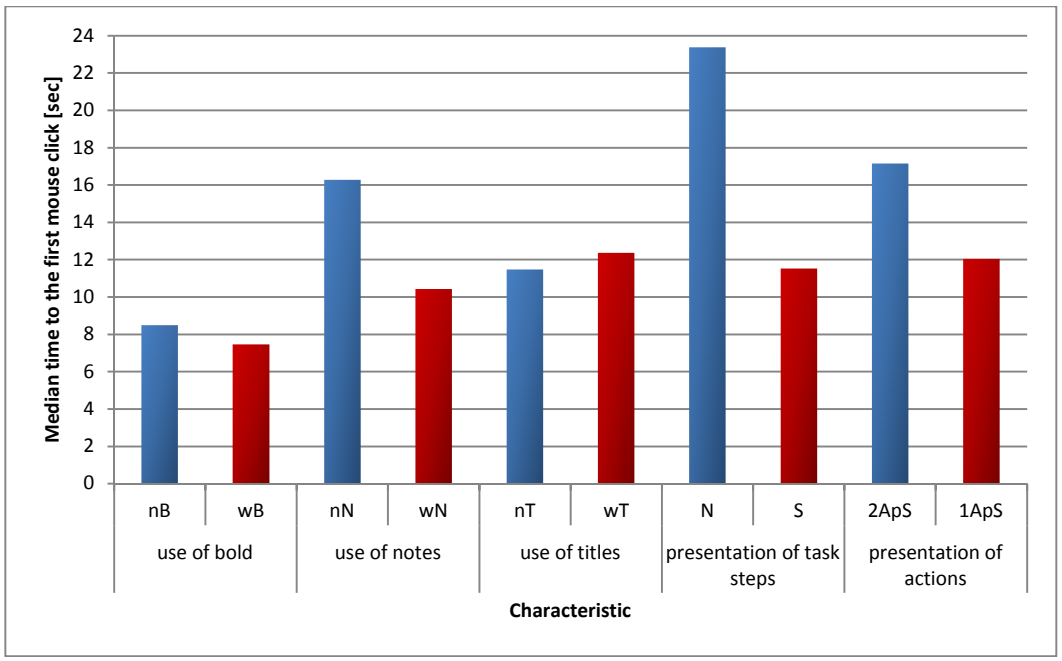

Figure 8-16. *Median time until first mouse click for each analysed characteristic (raw data with missing values).*

8.2.3 Conclusions from the development of NDT instructions

The primary conclusions drawn from the human-factor-guided development of the instructions are summarised as follows:

- The instructions and procedure can be improved by applying human-factor principles to the design. The most important step in developing the instructions or procedures is to consider the user and to develop the instructions together with the users.
- The review of the instructions should be performed through action, not solely through reading.
- Both the instruction content and instruction format play an important role in producing reliable instructions.
- The instruction content is the greatest contributor to the successful completion of an evaluation task. Attention must be given to missing information and to understanding the information.
- Understanding the information can be affected by the information order, information organisation, logic, clarity in writing, and cognitive demands. The frequency of use of the instructions is affected by users' experience with the instructions and task, particularly for individuals with recent experience.
- Efficiency can be improved by highlighting notes and by presenting task steps in a stepwise manner, with only one action per step.

9 Qualification

Non-destructive testing is, in many contexts, considered to be a special process because the effectiveness and quality of the actual inspection performed is impossible to verify afterwards on the inspected component. Overall, it is often impossible to verify that an inspection was performed. Within the area of recurrent non-destructive testing during in-service inspection of nuclear plants, this phenomenon has been addressed by the Swedish authorities over the past 20 years. Regulations for in-service inspection have been issued by authorities (SSMFS 2008:13), interpreted by the concerned parties and put in practice following the recommendations issued by ENIQ (European Network for Inspection Qualification).

The authority states that the existing regulation (SSMFS 2008:13) is not applicable in the non-destructive testing of canister components. This fact, together with the fact that the present qualification scheme is focussed on the in-service inspection, has made it necessary for SKB to consider developing an alternative qualification scheme. However, this scheme should be based on the experiences gained by the present schemes and should also be tailored to the non-recurrent inspections of unique canister components and align with the SKB principles of quality assurance. A proposal for such a scheme has been issued (SKBdoc 1414464) with a definition of the qualification levels and a description of the qualification process, which are briefly presented below.

9.1 Qualification levels

A qualification level is defined for each inspection of a canister component and weld based on how critical the inspection is in ensuring safety during operation and the post-closure safety of the repository. The qualification level that is set for each specific inspection is used to control the scope and focus of the qualification of the specific inspection. Proposals for different qualification levels are defined in Table 9-1.

Table 9-1. Proposed definitions of the different qualification levels.

Level	Category of inspection	Component/weld	Comments
A+	Inspection in a nuclear environment – encapsulation plant.	Sealing weld	The highest qualification level as a result of securing the final properties in a radiation environment that causes increased requirements related to inspection systems and inspection performance. Limited opportunity for complementary inspection.
A	Final inspection in canister factory.	Canister components, base weld.	Ensuring the final properties.
B	Inspection between process steps.	For example, copper ingot	Applied when reduced ability to detect defects in subsequent stages exist. The final component is inspected in a subsequent step.
C	Inspection of remaining components.	Cassette, steel lid, screw	Conventional standard products purchased based on certificates alternative by conventional inspection according to a standard specification.
D	Delivery inspection by supplier.	Canister components	By SKB prescribed supplier inspection. Final inspection to be qualified at the canister factory.

9.2 Qualification process

Below is a brief description of the proposal for a qualification process for non-destructive testing of the KBS-3 canister and the included parts that may apply. The actual description of the qualification process will be provided in conjunction with the submission of the PSAR - Preliminary Safety Analysis Report. According to the proposal, SKB is responsible for the qualification of non-destructive testing at all qualification levels. The qualification is performed by SKB or with the assistance of external resources. Third-party bodies for NDT are involved to varying degrees, depending on the qualification level (Table 9-2). An accredited inspection body (AK) will also be engaged for level C to examine the calculation basis, which includes the scope of inspection for each component. As the scope of inspection is established, SKB conducts the qualification.

Qualification at Level D is conducted solely by SKB.

For all inspections, it is predicted that relevant third-party bodies will have assessed and issued certificates of conformity regarding defect descriptions, strength calculations, established acceptance criteria and, where appropriate, selection of standards. It is also predicted that these bodies shall be approved by SSM (Swedish Radiation Safety Authority) prior to qualification.

Table 9-2. Suggested involvement of third-party organisation for NDT depending on qualification level.

Level	Inspection coverage	Third-party body involvement	Scope of qualification
A+	Inspection of copper lid weld in a nuclear environment – encapsulation plant.	Monitors and assesses, issues certificates.	Personnel, inspection equipment, inspection procedure / instruction, technical justification.
A	Final inspection in canister factory. Copper components, base weld, insert.	Monitors and assesses, issues certificates.	Personnel, inspection equipment, inspection procedure / instruction, technical justification.
B	Inspection between process steps. Applied when reduced ability to detect defects in subsequent stages exist.	Monitors and assesses, issues certificates.	Personnel, inspection equipment, inspection procedure / instruction, technical justification.
C	Inspection of remaining components (steel cassette, steel lid, screw).	Assesses, issues certificates.	Inspection instruction.
D	Delivery inspection by supplier.		By SKB prescribed supplier inspection. Scope assessed case by case.

The proposed qualification process divides the different qualification levels to differentiate the effort put into each element of the process. An overview of the qualification process is provided in appendix 1.

Important elements of the qualification process include technical justification (TJ), test block, qualification of technique, equipment, inspection instruction and personnel. The complexity of each element clearly depends on the qualification level associated with each inspection. The technical justification document is mainly applicable to the two highest levels, A and A+, the purpose of which is to by reasoning support the selection of inspection techniques. The document will be based on the guidelines developed by ENIQ (EC 2010).

In order to further assess the performance and justification of the entire inspection systems it is important to analyse the reliability. This has been the driving force for development of a NDT reliability methodology, presented in chapter 8, which consider complex inspection technologies

including the entire inspection chain, and can be applied as part of the justification of the inspection systems.

Test blocks are used to verify the capability of the techniques in terms of parameters, such as detectability, sensitivity, spatial resolution, and defect discrimination. The test blocks could, depending on the actual component and qualification level of the inspection, contain defects of different types and origins. Real defects are desirable and could, in some cases, be achieved by driving the manufacturing process outside its process window. This would be an option for defects related to friction stir welding, for which the relation between process parameters and defect appearance is well known. For defects related to other components where a prediction of the defect characteristics is more difficult, one option could be to correlate the inspection outcome with the information gained during a destructive cut and examination of the component.

Modelling of components and related defects together with the simulation of the inspection techniques of these geometries and materials will most likely be used in parallel with more conventional test block to enhance the confidence of the inspection results. If real defects, or real defects with an on forehand given size, orientation, location, etc., are cumbersome to achieve, artificial defects might be an option. These artificial defects could be in the shape of notches, flat-bottom or side-drilled holes. For verification of the simulation results in terms of, for example, ultrasonic field artificial defects such as flat-bottom holes and side-drilled holes suitable for the actual inspection setup will be used. As a complement real defects are necessary for verification of the simulated interaction between the ultrasonic field and the defect. This principle for verification will be applied also for other NDT methods.

Whereas the qualification of technique, equipment and inspection instruction will use “open” test blocks, in which all information of the defects will be available, the qualification of personnel will use “blind” test blocks, in which defect information will be unavailable to the inspection personnel undergoing qualification.

10 Assessment of the developed NDT techniques

The focus of NDT work at the Canister Laboratory was initially to develop the actual inspection techniques to be used in future production. Throughout the years, it has also been emphasised that the knowledge of material characteristics, possible defects and geometrical properties is crucial for developing manufacturing and welding processes and inspection techniques. Thus, a large number of components have been inspected, and the results have clearly enhanced the knowledge within these fields. This approach was originally applied to the welding process, however has gradually been implemented for all canister components.

In the same manner in which knowledge of canister components and welds has been enhanced by each manufacturing trial, the acceptance criteria for NDT have also developed over time; thus, at the beginning of NDT development, only limited acceptance criteria were available (section 4.1), while the preliminary acceptance criteria presented in section 4.2, were established first after the completion of NDT development described in this report. This further highlights the fact that NDT development has had to focus on obtaining as much information as possible on canister components and welds to support the development of the corresponding manufacturing processes and to build an understanding of the characteristics of each component. In addition, it should be noted that no acceptance criteria were available for pre-fabricated components such as the steel cassette and copper ingots until this phase of the NDT development was completed, and therefore, work in this field has been limited.

In the following sections, specific discussions related to inspection of each component such as the insert, copper tube, lid and base, and friction stir welds are presented.

10.1 Inspection techniques for inserts

Three ultrasonic inspection techniques have been developed for inspection of the major volume of pre-machined BWR and PWR inserts. The development was conducted by practical trials on real components in combination with sound field simulations. As a complement, several surface inspection techniques for inspecting the final machined inserts were tested. Although most of the insert volume is covered by the techniques developed and/or tested to date some areas have not been fully covered for example the insert top surface and insert bottom. Neither has any NDT been developed for pre-fabricated components and their accessory parts such as the steel lid and steel screw. In addition to the inspections planned for the canister factory, inspections required by component suppliers have been analysed. In the first step, the inspections are quality-assured by SKB approval of the NDT instructions of the suppliers.

10.1.1 Shortcomings in the acceptance criteria

The preliminary acceptance criteria presented in section 4.2.1 are specified based on damage tolerance analyses for possible defects in inserts. These acceptance criteria are calculated for defects with a simplified geometry and characteristics that clearly differ from the irregular shapes of real casting defects. Thus, the acceptance criteria should be considered to primarily set the accepted main dimensions of defects. In addition to the major concern regarding defect geometries, a number of limitations in the acceptance criteria have been identified:

- The casting defects, presently covered by the first issue of the acceptance criteria in a very general form, need to be described in more detail. The types of information that needs to be expanded upon are definitions of:
    - defect boundary relative to the surrounding matrix material
    - defects shape in three dimensions
    - density of clustered defects
    - interaction between different defect types (porosity, shrinkage, slag inclusions, etc), especially the variability needs to be addressed.

- The variability of the critical defect parameters needs to be especially addressed.
- The acceptance criteria for circumferential defects for the inner parts of inserts only show that the largest size of defects that can be accepted is larger than (>) a specified size. This result in an unnecessarily difficult inspection requirement that might be difficult to fulfil.
- No specific acceptance criteria are set for the volumes near the cassette structure, which can result in unnecessary rejections due to the common appearance of discontinuities in the interface between the casting and cassette structure.
- No restrictions are set regarding the requirements behind the steel support plates in the central part of the insert, which can make the inspection requirements impossible to fulfil.
- No acceptance criteria are set regarding the volume for the lifting holes at the top of the insert.

10.1.2 Assessment of developed NDT techniques

The developed and/or tested techniques were analysed and compared with respect to the acceptance criteria specified in section 4.2.1; the following assessments can be made:

- The normal incidence ultrasonic technique (UT31) can be used to determine the edge distance. However, the accuracy of the applied technique remains to be determined.
- Volumetric defects (for example blowholes) in the volume outside the cassette can be detected with high reliability. The assessment is based on the POD calculations presented in section 8.1.1, where the UT31 technique shows $a_{90/95}$ values for side-drilled holes that are less than 1 mm and the acceptance criteria allow for defects with sizes on the centimetre scale.
- Volumetric defects (for example blowholes) in the volume between the channel tubes can be detected. The assessment is based on the fact that the further developed inspection technique, UT33, uses a much more focussed sound field (particularly when inspecting PWR inserts) than the original technique, where the $a_{90/95}$ values were calculated to be between 5 and 20 mm and the acceptance criteria allow for even larger defects. The reliability of this inspection technique still requires verification. Additionally, the aforementioned acceptance criteria behind the steel support plates in the central part of inserts must be defined.
- Axial defects in the volume between the channel tubes can be detected. The assessment is based on:
    - The moderate acceptance criteria indicating that defects with lengths/depths of 144/24 mm (BWR) and 624/104 mm (PWR) at least could be accepted. As these defect sizes are given by limitations in the used calculations, even larger sizes could most probably be accepted.
    - The ultrasonic inspection technique, UT33, applies both pulse-echo and transmission technique to this volume. Ultrasonic simulations and experimental trials on artificial defects show that these defect sizes would be detected, primarily by the transmission technique but also with the pulse-echo technique.
    - The reliability of this inspection technique still requires verification.
- It has been shown that clustered porosity can be detected by the developed UT31 technique. However, the level of porosity that can be detected must still be determined.
- The different tests performed using surface inspection techniques have shown that defects that are clearly smaller than the acceptance criterion (length <16.4 mm) for circumferential defects can be detected. Magnetic particle inspection can detect defects with lengths of a few millimetres, and preliminary POD calculations performed using results obtained from the basic eddy current technique indicate an $a_{90/95}$ value of about 5 mm. The tests performed using the eddy current technique also showed that the inserts exhibit uniform material properties.
- Sand- and slag inclusions can be assumed to exhibit an irregular shape and surface; therefore it is likely that these defects contain reflector surfaces with several orientations. Over a range of depths spanning from the envelope surface down to 45 mm, the entire volume is inspected by ultrasonic techniques in five different directions (0° and ±70° in both the axial and tangential direction). The POD calculations presented in section 8.1.1 show $a_{90/95}$ values that

are clearly less than 1 mm (for side-drilled holes) for the UT31 technique, and the sound field simulations of the UT34 technique presented in section 6.2.2 show high SNRs for all analysed reflectors. Based on these findings, the requirement of detecting defects with propagation in the radial direction at sizes greater than 10 mm can be fulfilled down to a depth of 45 mm. This capability can be further supported by the fact that the acceptance criteria state "larger than" (no calculations were conducted for larger defects) and that the acceptance criterion of the radial size for elliptical defects is also applied for circular defects. Reasonably, larger circular defects could be accepted.

- To detect slag inclusions at a depth range from 45 mm down to the cassette, a similar reasoning to that invoked for the shallower depth range can be used, which is based on the fact that the UT31 inspection technique exhibits similar sensitivity along the entire inspection depth range and that larger defects are acceptable for greater depths (Table 4-11). However, it would be beneficial to the inspection reliability if additional inspection angles would be applied and if the technique would be optimised in terms of the focus in the passive probe direction.
- The volume between the channel tubes was not considered in the development of inspection techniques for circumferential defects because no acceptance criteria relevant to the internal loads (due to rock shearing) were formulated before the development presented in this report was finished.
- It is assessed that the acceptance criteria for axial hot tear defects in connection with the outer corners of the channel tube walls can be fulfilled using the UT31 and UT34 techniques. This assessment is drawn based on the moderate requirement in combination with the sensitivity estimated from the POD calculations and sound field simulations.
- The evaluation of the ultrasonic techniques by full-scale inspections showed that weak indications often occur near the cassette walls, and sound field simulations revealed that some areas are not fully covered by the inspections. Thus, it is recommended that the acceptance criteria (if the damage tolerance analysis allows) for these regions should be more detailed to overcome these limitations with respect to both the insert material properties and the performance of the inspection techniques.
- No inspection technique has been developed to inspect the volume behind the support plates in the volume between the channel tubes.
- No inspection technique has been developed to inspect the volumes for the lifting holes at the top of inserts.
- To verify the expected interaction between the ultrasonic inspection techniques and the defects, it is necessary to enhance knowledge regarding the real characteristics of insert defects.
- To achieve the required reliability for the near-surface region, the ultrasonic techniques require a specific surface roughness. For this specific machining, tools and parameters were defined. In addition, a measurable requirement for the surface roughness needs to be determined.

10.2 Inspection techniques for copper tubes

The ultrasonic inspection technique was developed for inspection of pre-machined copper tubes by performing practical trials on real components in combination with sound field simulations. The need for improvement was based on limitations identified in POD calculations (SKBdoc 1180131). As a complement to volumetric ultrasonic inspection, several surface inspection techniques, for inspection of final machined tubes were tested. It is assessed that these techniques can also be applied for inspection earlier in the copper tube manufacturing chain (that is ingot and blocker). No development of NDT techniques has been conducted for the integrated base in the pierce-and-drawn tubes.

10.2.1 Shortcomings in the acceptance criteria

Acceptance criteria are specified in section 4.2.2 for defects that can occur during the manufacturing of copper tubes, which includes the manufacture of copper ingots and blockers. The acceptance criteria were analysed from an inspection point of view, and the following limitations were identified:

- No requirements were set for acceptable defect sizes on the surfaces of ingots, blockers or copper tubes. This requirement is the most important for application of NDT techniques.
- No specific requirements were set for pierce-and-drawn tubes.
- Knowledge of the characteristics of real defects is very limited because only a few defects have been detected.

10.2.2 Assessment of developed NDT techniques

The developed and/or tested techniques have been analysed, and the results have been compared with the acceptance criteria specified in section 4.2.2; the following assessments can be made:

- The normal incidence ultrasonic technique (UT11) can detect exogenous slag inclusions in the tube. This assessment is based on the POD calculations presented in section 8.1.2, where the UT11 technique showed $a_{90/95}$ values for flat-bottom holes that were on the order of a few millimetres and the fact that possible inclusions would become extended in the axial direction and therefore become clearly larger than in the critical radial direction. However, this assessment must be verified by further trials and will likely require additional inspection angles to achieve the required reliability.
- The detectability of the proposed techniques in copper tubes with various levels of ultrasonic attenuation was investigated (SKBdoc 1411328). The results show that the $a_{90/95}$ value is clearly affected by ultrasonic attenuation and that the investigated tube materials could likely be approved to obtain reliable inspection results. To determine an additional acceptance criterion for the copper tube related to ultrasonic attenuation, further analyses are required.
- The initial tests showed that the blocker material can be inspected by ultrasonic techniques. However, no assessment can be made regarding the detectability of slag inclusions, Therefore further work is required to develop inspection techniques and in order to increase the knowledge of the blocker characteristics full-scale components need to be inspected.
- No NDT development and only limited tests have been conducted for the surface inspection of copper tubes, ingots and blockers. However, experience has been gained from inspecting the surfaces of copper lids, lid ingots and friction stir welds. Because no acceptance criteria have been set for acceptable defect sizes, the possibility of inspection techniques fulfilling the requirements cannot be assessed.

10.3 Inspection techniques for copper lids and bases

The ultrasonic inspection technique was developed for inspection of the pre-machined copper lids (and bases) by performing practical trials on real components in combination with sound field simulations. The improvements were identified based on the limitations identified in POD calculations (SKBdoc 1180131) of the original technique. Another measure that led to an improvement was the re-design of the pre-machined lids to facilitate ultrasonic inspection. As a complement to volumetric ultrasonic inspection, several surface inspection techniques, for inspection of the final machined lids were tested. It is assessed that these techniques can also be applied for inspection of copper ingots.

10.3.1 Shortcomings in the acceptance criteria

Acceptance criteria are specified in section 4.2.3 for defects that can occur in the manufacture of copper lids, which includes that of copper ingots. The acceptance criteria were analysed from an inspection point of view, and the following limitations were identified:

- No acceptance criteria have been set for the acceptable defect sizes on the surfaces of ingots and copper lids. These acceptance criteria are the most important for the application of NDT techniques.
- Knowledge of the characteristics of real defects is limited because only one defect type (forging lap) has been detected.

10.3.2 Assessment of developed NDT techniques

The developed and/or tested techniques were analysed and compared with respect to the acceptance criteria specified in section 4.2.3, and the following assessments can be made:

- The normal incidence ultrasonic technique (UT27) can detect exogenous slag inclusions. The assessment is based on the reliability of the developed technique presented in section 8.1.3, where it is assessed that the UT27 technique could detect defects with sizes on the order of a few millimetres, and the fact that possible inclusions would become extended due to the forging process, parallel to the inspection surfaces, and thereby would be clearly larger than in the critical direction. However, this assessment must be verified by further trials.
- The detectability of the proposed techniques for copper tubes with various ultrasonic degrees of attenuation was investigated (SKBdoc 1411328). The results show that the $a_{90/95}$ value is clearly affected by ultrasonic attenuation and that this factor must also be considered for lid inspection. Thus, further analyses are required to determine an additional acceptance criterion for the copper tube related to ultrasonic attenuation.
- No NDT development has been conducted for the surface inspection of copper lids and ingots. However, experience has been gained from inspecting the surfaces of lids, lid ingots and friction stir welds. Because no acceptance criteria have been set for acceptable defect sizes, the possibility of inspection techniques fulfilling the requirements cannot be assessed.

10.4 Inspection techniques for friction stir welds

To inspect the major weld volumes, techniques based on phased array ultrasonic and digital X-ray techniques were further developed. The development was based on experiences gathered from previous inspections and by performing practical trials on real and artificial defects supported by sound field simulations. For inspection of weld surfaces, the eddy current array technique was developed.

10.4.1 Shortcomings in the acceptance criteria

The acceptance criteria established are sufficient for development of NDT techniques and assessment of the weld quality during welding process development. However, a more detailed description of the defect characteristic will be required for qualification of the NDT techniques.

10.4.2 Assessment of developed NDT techniques

The developed techniques were analysed, and their results were compared with respect to the acceptance criteria specified in section 4.2.4; the following assessments can be made:

- Joint line hooking defects can be detected by the developed ultrasonic technique, which was assessed based on the POD calculations presented in section 8.1.4 which were conducted on the original ultrasonic technique that clearly exhibited a lower sensitivity than that of the newly developed technique. Additionally, a number of metallographic samples were collected based on ultrasonic indications that showed joint line hooking defects with radial extensions measuring less than 2 mm. However, the reliability by calculation of POD curves for the newly developed ultrasonic inspection of this defect type remains to be verified.

- The remaining joint can be detected because the orientation of the defect is favourable for ultrasonic inspection; therefore, the defect acts as a “perfect” reflector. However, the reliability by calculation of POD curves for inspection of this type of defect remains to be verified.
- The cavity defects can be detected by the X-ray inspection technique based on the POD calculations presented in section 8.1.4, particularly by considering that the change in the inspection angle results in a reduced penetrated thickness and thereby a higher SNR for defects along the critical radial direction. Additionally, this assessment is strengthened because the ultrasonic technique was further developed and because eddy current inspection was also applied. However, the reliability determined by the calculation of POD curves for inspection of this type of defect with the different inspection techniques remains to be verified.
- Further development of techniques for sizing defects is necessary.
- The inspection of lid welds will be conducted at the encapsulation plant in a nuclear environment, which will require special application of the NDT techniques, which still remains to be solved.

11 Conclusions

Three ultrasonic phased array techniques for inspection of the major volume of cast iron inserts were developed. The development benefitted from the potential of combining practical trials with sound field simulations. The evaluation of the developed techniques, which was performed based on SNR analyses and POD calculations of artificial defects and metallographic and computed tomography inspection, indicated high inspection sensitivity. Despite this high sensitivity some shortcomings of the developed ultrasonic techniques were identified; additionally, no technique has been developed to inspect the insert bottom. In addition one of the developed ultrasonic techniques was used to measure the insert edge distance.

Several techniques such as eddy current and magnetic particle inspection for inspection of the insert surfaces were tested, and the results showed that the techniques could be further developed and be implemented for inspection of inserts.

Full-size inserts were inspected by the developed ultrasonic techniques, and the results were used as input for the manufacturing process and the evaluation of the inspection techniques. From the inspected inserts, a number of defect indications were examined by metallographic and computed tomography inspection, which enhanced the knowledge of insert defect characteristics. However, more work is required to enhance the knowledge of real defect characteristics.

For copper tubes, the phased array ultrasonic technique was further developed to achieve higher, more uniform sensitivity and to make the technique more robust to variations in grain size. Several full-size copper tubes were inspected by the developed ultrasonic technique, and the results showed that the quality of the tubes was high (no defect indications observed); however, variations in the attenuation still occurred.

A limited amount of work was conducted with respect to the pre-fabricated state (copper ingot and blocker) of copper tubes. However, it was shown that blockers can be inspected by the ultrasonic technique.

No surface inspection technique was applied to any of the stages of copper tube manufacturing (copper ingot, blocker and tube). However, it can be assessed that the eddy current technique developed for friction stir welding can be applied for inspection of the tubes. For ingots and blockers, either the eddy current technique or the conventional penetrant inspection tested for lids can be applied.

The phased array ultrasonic technique for inspection of copper lids and bases was further developed. The development was conducted to achieve higher, more uniform sensitivity and to simplify the inspection technique by re-designing the pre-machined lid. Several full-size copper lids were inspected by the developed ultrasonic technique. The results showed areas with locally large grains in the centre of the lids but no occurrence of internal defects.

Surface inspection was applied to lid ingots and pre-machined lids by penetrant inspection. The results obtained from inspecting several ingots showed that, in general, the quality of the ingots was good with no relevant defect indications. However, inspections of pre-machined copper lids indicated forging laps in several lids, and some of these defects were also detected by ultrasonic inspection. To enable the development of optimal inspection techniques, further analysis of the characteristics of forging laps is necessary.

To inspect friction stir welds, three inspection techniques were developed, phased array ultrasonics, digital X-ray and eddy current. The development was based on the enhanced knowledge of the characteristics of weld defects, which has thus enabled the possibility of developing more sensitive inspection techniques.

Modelling of the components geometry and properties and simulation of the different NDT-techniques physical interaction with the component and postulated defects has been of great value during the development and evaluation of the ultrasonic based techniques. Modelling and simulation is to be considered as a valuable tool for the future development of ultrasonic techniques for all canister components and materials as well as for other techniques utilizing other physical effects like eddy current or magnetic flux. The future qualification phase will also most probably benefit from these types of simulations as a supporting complement to more physical demonstrations of the capability of the NDT-techniques.

Acceptance criteria were defined for the non-destructive testing of the major components and welds. From an inspection point of view, a number of limitations of these criteria were identified. For example, the criteria for insert inspection must be clarified to consider real defect specifications, and the criteria for the internal volume of inserts must be further specified. Regarding the acceptance criteria for copper components, no criteria are specified for the acceptable defect size on the surfaces of ingots, blockers or copper tubes. This information is necessary to develop appropriate inspection techniques and to verify the techniques' reliability.

NDT reliability was introduced as an important tool in the development of the NDT techniques. For example, several shortcomings of the inspection techniques were identified by calculating POD curves, and the multi-parameter methodology was extended to also consider the effect of varying attenuation on the detectability in ultrasonic inspection of copper tubes. Human-factor aspects were also incorporated into the NDT development by introducing FMEA into the inspection process and by conducting a systematic analysis of the development of NDT instructions.

A preliminary qualification process was defined. The process considers the course of action adopted for in-service inspection in the nuclear industry when applicable. However, as the inspection requirements and their application are clearly different from those of in-service inspection, a slightly different approach is proposed. The qualification process not only considers the qualification of the final inspections but also inspections performed on the suppliers' premises and inspections at different manufacturing stages.

References

ASNT, 1999. Topical conference paper summaries book of the American-European workshop on non-destructive inspection reliability, Boulder, Colorado, 21–24 September 1999. Columbus, OH: American Society for Nondestructive Testing.

Berens A P, 1989. NDE reliability data analysis. In Metals handbook. 9th ed. Vol 17, Nondestructive evaluation and quality control. Metals Park, OH: ASM International, 689–701.

Bertovic M, Ronneteg U, 2014. User-centred approach to the development of NDT instructions. SKB R-14-06, Svensk Kärnbränslehantering AB.

Dillström P, Bolinder T, 2010. Damage tolerance analysis of canister inserts for spent nuclear fuel in the case of an earthquake induced rock shear load. SKB TR-10-29, Svensk Kärnbränslehantering AB.

EC, 2010. ENIQ recommended practice 2: strategy and recommended contents for technical justifications. Issue 2. ENIQ report No 39. EUR 24111 EN, European Commission.

Pavlovic M, 2014. Probability of detection as a function of multiple influencing parameters. PhD thesis. Der Universität des Saarlandes, Germany.

Pavlovic M, Takahashi K, Müller C, 2012. Probability of detection as a function of multiple influencing parameters. Insight – Non-Destructive Testing & Condition Monitoring 54, 606–611.

SKB, 2009. Design premises for a KBS-3V repository based on results from the safety assessment SR-Can and some subsequent analyses. SKB TR-09-22, Svensk Kärnbränslehantering AB.

SKB, 2010. Design, production and initial state of the canister. SKB TR-10-14, Svensk Kärnbränslehantering AB.

SKB, 2013. RD&D Programme 2013. Programme for research, development and demonstration of methods for the management and disposal of nuclear waste. SKB TR-13-18, Svensk Kärnbränslehantering AB.

SS-EN 12680-3:2011. Founding – Ultrasonic testing – Part 3: Spheroidal graphite cast iron castings. Stockholm: Swedish Standards Institute.

SS-EN 1369:1997. Gjutning – Magnetpulverprovning. Stockholm: Swedish Standards Institute. (In Swedish.)

SS-EN ISO 9934-1:2001. Oförstörande provning – Magnetpulverprovning – Del 1: Allmänna principer (ISO 9934-1:2001). Stockholm: Swedish Standards Institute. (In Swedish.)

SS-EN ISO 9934-2:2003. Oförstörande provning – Magnetpulverprovning – Del 2: Media för detektion (ISO 9934-2:2002). Stockholm: Swedish Standards Institute. (In Swedish.)

SS-EN ISO 9934-3:2002. Oförstörande provning – Magnetpulverprovning – Del 3: Utrustning (ISO 9934-3:2002). Stockholm: Swedish Standards Institute. (In Swedish.)

SSMFS 2008:13. Strålsäkerhetsmyndighetens föreskrifter om mekaniska anordningar i vissa kärntekniska anläggningar. Stockholm: Strålsäkerhetsmyndigheten. (In Swedish.)

Unpublished documents

SKBdoc id, version	Title	Issuer, year
1175208 ver 5.0	Tillverkning av kapselkomponenter. (In Swedish.)	SKB, 2011
1175235 ver 3.0	NDT Reliability - Data report FSW	SKB, 2009
1179633 ver 3.0	Oförstörande provning av kapselkomponenter och svetsar. (In Swedish.)	SKB, 2011
1180131 ver 1.0	NDT Reliability - Data report copper	SKB, 2009
1180132 ver 1.0	NDT Reliability - Data report insert	SKB, 2009
1203875 ver 2.0	Ritningsförteckning för kapselkomponenter. (In Swedish.)	SKB, 2014
1288292 ver 1.0	Summary of important characteristic parameters for the BWR- and PWR-insert, based on performed strength and damage tolerance analyses	Inspecta Technology, 2014
1352906 ver 2.0	High-energy computed tomography investigation of large tensile test specimens	BAM, 2012
1358335 ver 3.0	Investigation report 20470 issue 3	Swerea Swecast, 2014
1411328 ver 2.0	Attenuation dependent detectability at ultrasonic inspection of copper	SKB, 2014
1411571 ver 1.0	Simulation of the ultrasonic beam shape for optimization of the UT31 procedure	Exova, 2014
1414374 ver 1.0	Kravbild för oförstörande provning av kopparkapselns rör, lock och botten. (In Swedish.)	SKB, 2014
1414464 ver 1.0	Kvalificering av oförstörande provning. (In Swedish.)	SKB, 2014
1414760 ver 1.0	Kravbild för oförstörande provning av segjärnsinsats. (In Swedish.)	SKB, 2014
1415307 ver 1.0	Kravbild för oförstörande provning av kopparkapselns svetsar. (In Swedish.)	SKB, 2014
1417645 ver 1.0	Fördelning av kornstorlek i kopparprover, utgåva 2. (In Swedish.)	Exova, 2013
1427252 ver 1.0	Identifying and managing risks in mechanised NDT: a human factors study	SKB, 2014
1432038 ver 1.0	Manufacturing and testing of copper components	SKB, 2014
1432361 ver 1.0	Manufacturing and testing of nodular cast iron inserts	SKB, 2014
1435212 ver 1.0	Simulation of ultrasonic inspection of friction stir welding	Exova, 2014
1435214 ver 1.0	Simulation of the UT33 ultrasonic inspection of inserts	Exova, 2014
1435653 ver 1.0	Sealing of the canister	SKB, 2014
1437573 ver1.0	Development of angular ultrasonic inspection of cast iron insert by sound field simulations	Exova, 2014

Revision audit trail

Version	Date	Description	Author	Reviewed	Approved
2.0	As first pageheader	Chapter 4 has been updated. In section 7.1.1 a new sub-section "Evaluation of signal to noise ratio for artificial defects" has been added. In the sub-section "Summary of experiences" in section 7.1.1 one bullet has been added. In section 10.1.1 bullet number three has been re-formulated. In section 10.1.2 a new bullet (number 4) has been added and the text in bullet number 6, 7 and 9 has been re-formulated. Two references (Pavlovic M, 2014, SS-EN 12680-3:2011) have been added.	As first pageheader	As first pageheader	As first pageheader
1.0	2014-09-18	New document	Thomas Grybäck Ulf Ronneteg	2014-09-29	2014-09-30

Appendix 1: Qualification process